

https://dspace.org/

Structural dynamics and membrane interaction of the chloride intracellular channel protein, CLIC1

Nathaniel, Christos

2008-03-06T10:36:45Z
http://hdl.handle.net/10539/4561

Downloaded from a DSpace repository. https://dspace.org/

CHAPTER 1: INTRODUCTION

1.1 Biological Membranes

1.1.1 Structure and properties

Biological membranes fulfil vital functions as interfaces between cells and the outside world. Within the cell they also serve as important boundaries of intracellular compartments. Complications and malfunctioning in biological membranes are related to numerous diseases such as cystic fibrosis (Riordan *et al.*, 1989) and Dent's disease (Lloyd *et al.*, 1996). Made up primarily of different lipid forms, namely phospholipids, sphingolipids and glycolipids, membranes also consist of cholesterol and proteins. The ratios of these components vary widely among different cellular compartments and among different species (Voet and Voet, 1995). Lipids are amphipathic molecules consisting of a polar head group and a hydrophobic tail. The polar head reacts readily with water, whereas the tail is poorly soluble in aqueous environments. Phospholipids are the major lipid components of cell membranes, and along with other lipids of biological membranes form bilayers in aqueous media (Voet and Voet, 1995). These bilayers consist of two leaflets, with fatty acid tails apposed in the hydrocarbon interior, and the polar head groups decorating the solvent-exposed surface of each leaflet. Lipid bilayers are held together by noncovalent, hydrophobic packing interactions resembling those stabilizing the native fold of proteins. These include van der Waals contacts between fatty acids and the hydrophobic effect, which maintain the integrity of the membrane. In addition, the polar head groups of lipids may participate in hydrogen bonds with neighbouring lipids and proteins.

The fluid-mosaic model (Singer and Nicolson, 1972) proposes that membrane lipids are arranged in a bilayer to form a fluid, liquid-crystalline array (Figure 1A). This model accounts for the flexibility of membranes and their impermeability to polar compounds. It is further postulated that globular proteins are embedded or floating in the lipid bilayer (Figure 1B). The interior of the lipid bilayer is thought to be in motion and highly fluid. The lipid and protein composition of biological membranes is markedly different on the two sides of the bilayer. In human erythrocyte

A.

B.

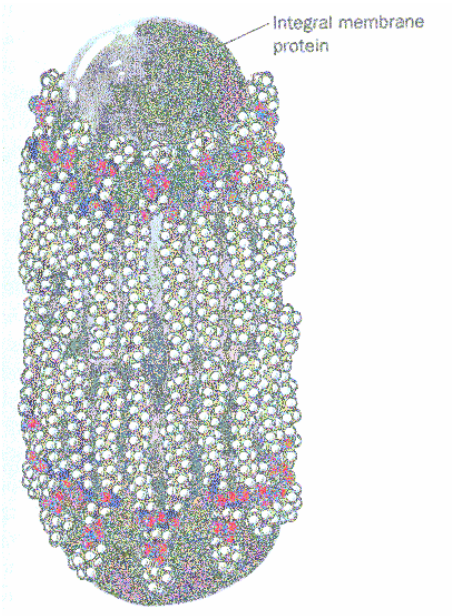


Figure 1: The structure of the lipid bilayer and integral membrane protein.
(A) Structure of a liquid-crystalline phase lipid bilayer consisting of phosphatidylcholine and phosphatidylethanolamine. The non-polar tails are indicated in black while the polar head groups are shown in red. The plane of the bilayer is represented with solid black lines. (B) Shows an integral membrane protein in a lipid bilayer solvated by lipids through hydrophobic interactions between the protein and the lipids' non-polar tails. (modified from Voet and Voet, 1995)

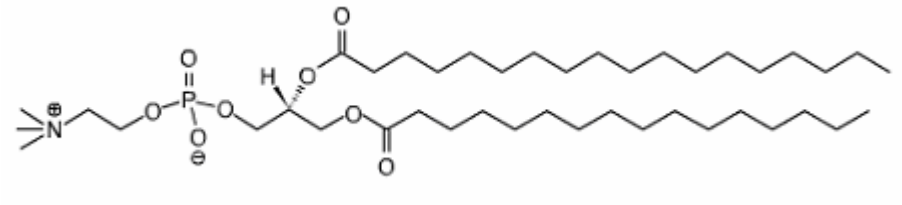
membranes it was found that the outer leaflet was made up of 20% phosphatidylcholine (PC), 5% phosphatidylethanolamine (PE) and 0% phosphatidylserine (PS), while the inner leaflet consisted of 7% PC, 25% PE and 8% PS (Rothman and Lenard, 1977). Lipid distribution also varies greatly between different species. The biological membranes found in *Escherichia coli* for example are made up primarily of PE (65%) with 0% PC, while in the human erythrocyte membrane PE makes up 18% PE and PC 19% (Tanford, 1980). Figure 2 shows the chemical structure of the common lipid components of membranes and shows the arrangement of these lipids in liposomes compared with bilayers.

Cholesterol is a planar, tetracyclic hydrocarbon (sterol) of higher organisms that is not found in most bacteria. It is abundant in the plasma membrane and decreases membrane permeability by strengthening the hydrophobic packing interactions of the constituent lipids. In human erythrocyte membranes cholesterol can make up 26% of total lipid composition (Tanford, 1980).

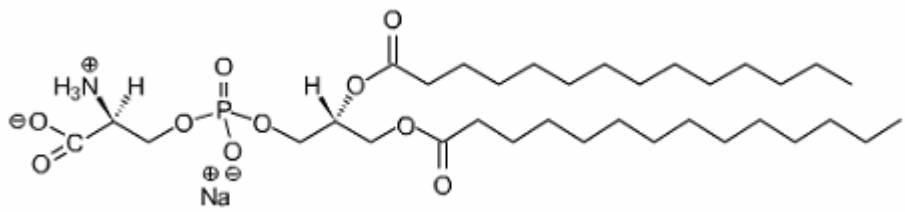
Biological membranes are approximately 30 Å thick and exhibit a characteristic transmembrane potential that arises due to a difference in charge across the membrane. The intracellular side of the membrane is more negatively charged relative to the extracellular side. The membrane also has a surface potential as a result of the electrostatic potential at the interface between the membrane and aqueous environment. Biological membranes have a negative surface potential due to the high percentage of negatively charged phospholipid head components of membranes. This negative surface potential attracts protons from the surrounding aqueous solution, effectively decreasing the pH value at the membrane surface by up to two pH units relative to the surrounding environment (van der Goot *et al.*, 1991). The dielectric constant at the membrane interface ranges from 10 –20 compared with approximately 80 for water (at 25° C). The hydrophobic core of the membrane exhibits a very low dielectric constant of approximately 2, while the value within the core of a folded protein can range from 3 – 5. The differences in dielectric constants of these environments greatly influences the stabilizing forces within a protein.

Transmembrane proteins span the membrane and are therefore exposed to the aqueous milieu of the cytosol and the extracellular fluid, as well as the hydrocarbon interior of

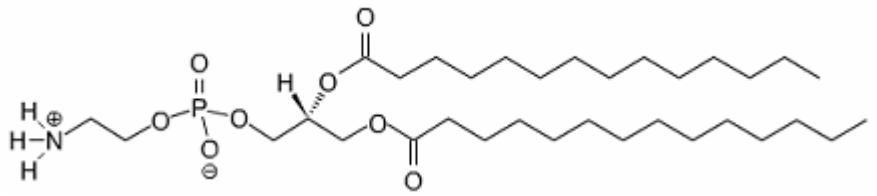
A.



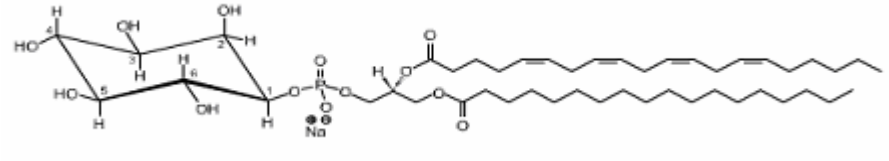
phosphatidylcholine (PC)



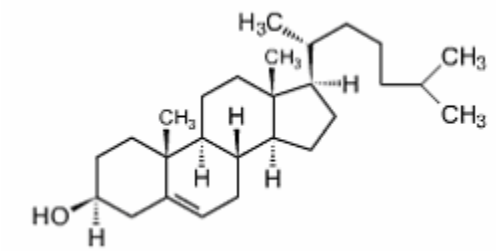
phosphatidylserine (PS)



phosphatidylethanolamine (PE)

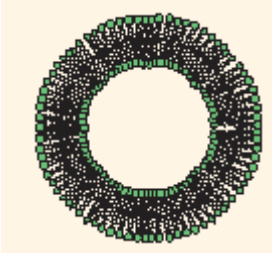


phosphatidylinositol (PI)



cholesterol

B.



C.

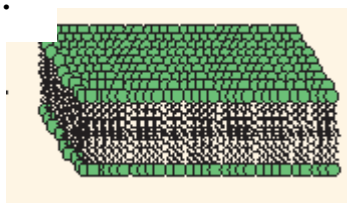


Figure 2: Chemical structure of lipid components and liposome/bilayer structure. The chemical structures of various lipid components are shown in A. The structure of the cross-section of a liposome (B) and lipid bilayer (C) are also shown. Images taken and modified from Avanti Polar Lipids (www.avantilipids.com)

the bilayer. They are adapted to floating in the lipid bilayer, having a hydrophobic "waist" and two hydrophilic, exposed tails. The packing arrangements of the membrane-spanning segments of proteins may result in oligomerisation and the formation of membrane channels or pores. Membrane proteins typically have a less polar surface compared with proteins found in solution. This is due to the fact that membrane proteins are buried within the hydrophobic interior of the membrane. Predominantly hydrophobic residues such as isoleucine, leucine, phenylalanine, valine, methionine and alanine are typically found in membrane spanning segments of proteins (Arkin *et al.,* 1998). Charged amino acids like arginine and lysine are typically found at the membranes cytoplasmic face, while aromatic residues with rigid side chains like tyrosine and tryptophan do not favour the inner hydrophobic environment of the membrane and are typically found near the membrane interface (Landolt-Marticorena *et al.,* 1993; Ulmschneider and Sansom, 2001).

Although 30% of all sequenced genes code for membrane proteins only a small percentage of these protein structures have been resolved at atomic resolution. Of the approximate 3000 unique protein structures that have been solved only around 30 are membrane proteins. This is because of the difficulty of producing 3D crystals suitable for X-ray analysis from detergent solubilised membrane proteins. Furthermore, most of the membrane proteins that have been solved are of bacterial origin because of their easier production, purification and crystallisation. Progress in the 3D crystallisation of animal membrane proteins has been made, however, with the determination of the crystal structure of aquaporin-1 at 2.2 Å resolution (Sui *et al.,* 2001).

1.1.2 Channels and pores

The non-polar cores of biological membranes make them highly impermeable to ionic and polar molecules such as Na^+, K^+, Ca^{2+} and Cl^-. A mechanism to transport these small inorganic ions across membranes exists in the form of channels or pores. The specific arrangement of proteins within the membrane mediates the passive diffusion of the polar molecules across the membrane by creating a hydrophilic pore using the proteins polar groups or opposite charge to the ion being transported. This passage created by the protein lowers the electrostatic energy barrier (~40 kcal/mol) encountered by small ions when moving from a high dielectric environment such as water to the low dielectric environment of the membrane interior, known as the Born electrostatic barrier (Honig *et al.,* 1986). This is achieved by increasing the dielectric

constant of the membrane interior. Channels show selectivity toward ions of appropriate size and charge and only open in response to certain stimuli or conditions (Jentsch, 2001). This is known as channel gating.

Cl^- is the most abundant anion and the predominant permeating species in all organisms (Nilius and Droogmans, 2003). Chloride ion channels are found within the plasma membrane and other internal cell membranes. Their roles are diverse and include secretion and absorption of salt, regulation of membrane potentials, organellar acidification, and cell volume homeostasis (Strange *et al*., 1996). Malfunction of these channels can lead to severe disease states e.g. cystic fibrosis. Therefore, it is important to understand the process by which these transmembrane chloride ion channels are formed and regulated. The best studied and understood family of Cl^- channels is the voltage-dependent CLC family, the crystal structure of which has recently been described (Dutzler *et al.,* 2002). The channel shows two identical pores formed by separate subunits, thus forming a homodimeric membrane protein. Each pore has a selectivity filter, which binds a Cl^- ion, and is formed by electrostatic interactions with α-helix dipoles and by chemical coordination with nitrogen atoms and hydroxyl groups.

1.2 Amphitropic proteins

1.2.1 Overview

Conventionally, integral membrane proteins making up ion channels are ribosomally synthesised and transported to the membrane via the secretory pathway. This pathway consists of three steps: 1) During their ribosomal synthesis, their glycosylation is initiated in the lumen of the endoplasmic reticulum. 2) After ribosomal synthesis is completed, coated vesicles containing the protein bud off from the endoplasmic reticulum and move to the Golgi apparatus where protein processing is complete. 3) Later, coated vesicles containing the mature protein bud off from the Golgi apparatus and fuse to the membrane for which the protein is targeted.

In contrast, some proteins, the so-called amphitropic or dual-form proteins, can exist in either soluble or integral membrane form. These proteins are synthesised as soluble proteins and have the ability to insert into membranes at some stage during their

biological activity (Figure 3). The amphitropic protein may only be signalled to convert from soluble to integral membrane form during a certain stage of the cell cycle or as a response to a change in cellular conditions such as oxidative stress. The regulation of this conversion plays a key role in many biological functions. The exact mechanism and structural changes required for the insertion of amphitropic proteins into membranes remains largely unknown.

1.2.2 Pore-forming toxins

The pore-forming toxins can be classified among amphitropic proteins, because they are soluble proteins, which are driven to insert into membranes and form pores in lipid membranes of a target organism to exert their toxic influence as part of their physiological function. Pore forming toxins are characterised in two main groups: the α-helical toxins that involve α-helix regions to form transmembrane pores and the β-barrel toxins that insert into the membrane by forming a β-barrel composed of β-hairpin structures from each monomer. Colicin A, diphtheria toxin and Cry1 proteins are examples of α-helical toxins, while aerolysin, hemolysin, anthrax protective antigen, insecticidal δ-endotoxin, equinatoxin II and perfringolysin O are examples of β-barrel toxins (see review by Parker and Feil, 2005).

Pore-forming toxins that provide interesting examples of polypeptides that, depending on environmental conditions, can exist in either a water-soluble or a membrane-associated state. None of the pore-forming toxin in the α-helical families show any detectable sequence similarity between them. Despite this, their protein insertion/translocation domains all adopt similar folds consisting of a bundle of alpha helices organised in a layered structure, with some helices completely buried (Figure 4). In all cases, at least one helix of sufficient length to span the membrane can be identified.

Studies performed on the pore-forming domain of colicin A revealed that exposure of the hydrophobic buried helical hairpin lead insertion into membranes and formed the

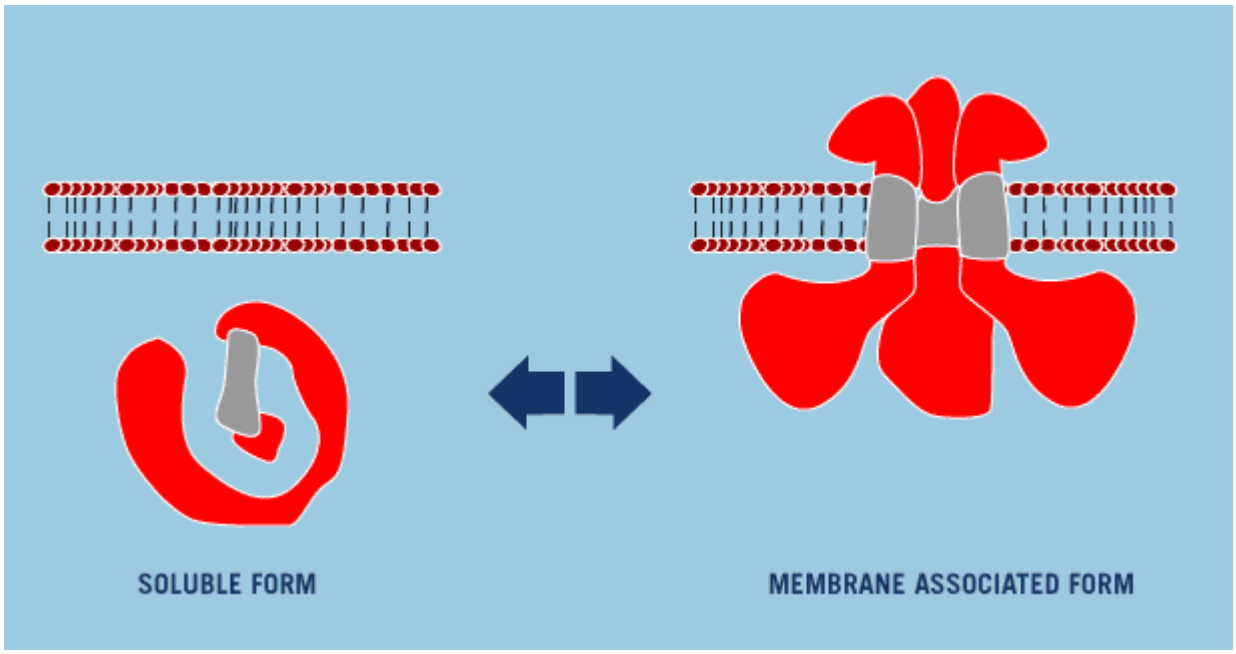


Figure 3: Schematic showing the conversion of amphitropic proteins from soluble to integral membrane form.

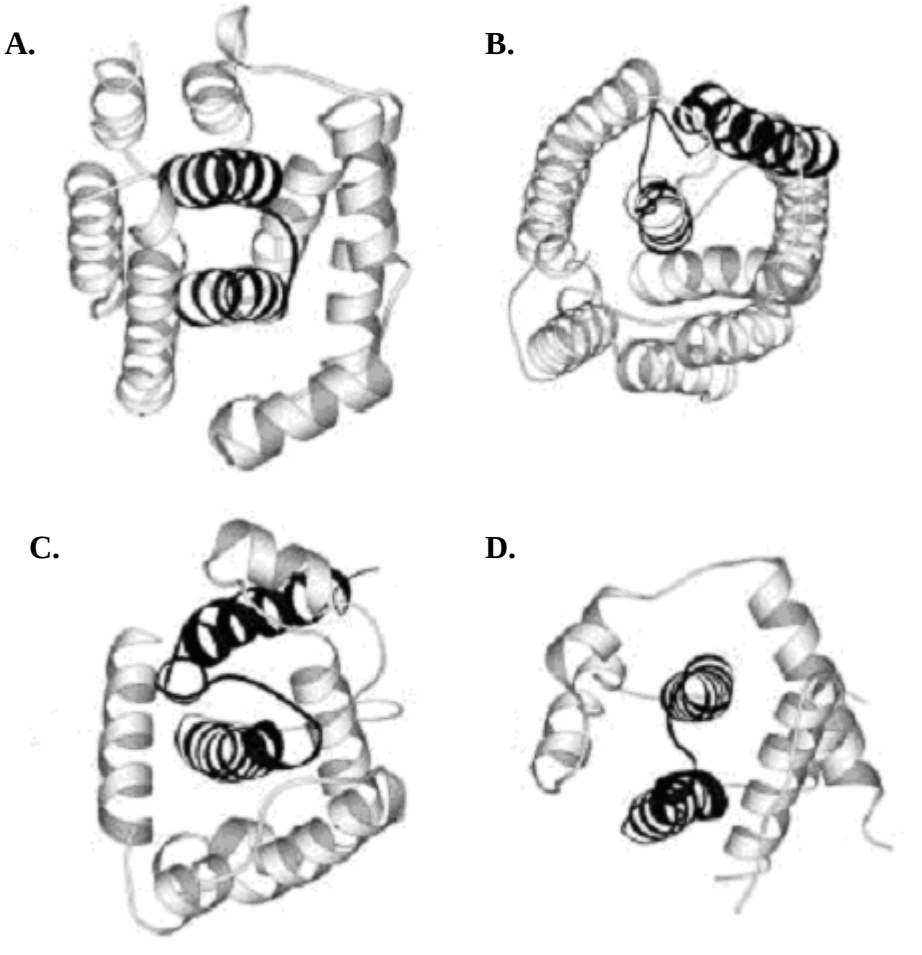


Figure 4: Ribbon representations of amphitropic α-helical proteins highlighting their putative transmembrane regions. Regions thought to represent insertion/translocation domains are shown in dark shade. (A) Colicin A (Parker *et al.*, 1992), (B) insecticidal δ-endotoxin (Li *et al.*, 1991), (C) diphteria toxin (Choe *et al.*, 1992), and (D) Bcl-X_L (Muchmore *et al.*, 1996) are all amphitropic proteins that can exist in water-soluble or integral-membrane form. (Modified from Cromer *et al.*, 2002)

transmembrane channel (Parker *et al.,* 1992). The membrane insertion process for Colicin A has been explained by membrane-pH dependence (Muga *et al.,* 1993). Colicin A was shown to form a molten globule state at low pH, which reduces the energy barrier required in unmasking the hydrophobic hairpin for membrane insertion. Furthermore, low pH neutralises the acidic regions, which renders the face more hydrophobic and hence lowers the energy cost of inserting the helical hairpin into the membrane.

Diphtheria toxin is a 58 kDa polypeptide that is readily cleaved proteolytically into a N-terminal 21 kDa fragment and a C-terminal 37 kDa fragment joined by a disulphide bond. While the C-terminal fragment is responsible for receptor binding, the N-terminal fragment translocates across the endosomal membrane as a result of exposure to the acidic lumen of the endosome (Sandvig and Olsnes, 1980). The oligomerisation state of the functional pore is thought to be dimeric (Choe *et al.,* 1992).

Bacillus thuringiensis produces insecticidal Cry toxin proteins that are active against different insect species. The inactive protoxin is 130 kDa in size and is cleaved by proteases to yield 60 kDa monomeric toxins (Hofmann *et al.,* 1988). After adhereing to cadherin receptors on the host epithelial cell membrane Cry undergoes conformational changes from monomeric structure to a pre-pore oligomeric form that inserts into the membrane (Pardo-Lopez *et al.,* 2006). After membrane insertion there is another conformational change to form the fully functional pore. The conformational changes are triggered by acidic pH causing a molten-globule state that is in a partly unfolded but compact state that is used to overcome the high-energy barrier of membrane insertion (Pardo-Lopez *et al.,* 2006). The model proposed for Cry membrane insertion involves the insertion of two α-helices into the membrane analogous to the handle of an umbrella while the rest of the helices are rearranged on the membrane surface (Gazit *et al.,* 1998).

Equinatoxin II is a 19.7 kDa protein composed of predominantly β-sheet secondary structure when in water-soluble form (Athanasiadis *et al.,* 2001). The pore region of the transmembrane form, however, is thought to be formed by an amphipathic helix

that is exposed as a result of the soluble form interacting with the membrane. The membrane surface causes partial unfolding of the protein, which exposes a buried α-helix that inserts into and traverses the membrane (Ulrih *et al.,* 2004). The protein then oligomerises to form a functional pore. Equinatoxin II has strong dependencies on the solution pH and ionic strength for its conversion from soluble to integral membrane form (Poklar *et al.,* 2001).

Aerolysin is a predominantly β-sheet protein secreted as an inactive water-soluble dimer called proaerolysin. The protoxin must be nicked by proteolysis, which removes a C-terminal fragment and enables the process of channel formation. The active aerolysin is also water-soluble and dimeric. However, unlike the protoxin, it can undergo a concentration-dependent transition to become a heptameric protein which is insertion-competent. The heptamer inserts into the target membrane forming a large open channel that kills the cell. The crystal structure of proaerolysin (Parker *et al.,* 1994) was the first to be determined for a group of toxins termed the hydrophilic (β-sheet) channel-forming protein toxins that include insecticidal δ-endotoxin, α-hemolysin, anthrax protective antigen, and perfringolysin O. All these proteins contain a preponderance of β-sheet and posses the ability to undergo transitions from water-soluble states to higher order oligomeric membrane-bound states. A schematic of typical channel formation by β-sheet amphipathic proteins is shown in figure 5.

The *Bacillus thuringiensis* insecticidal δ-endotoxins have a three-domain structure, with seven amphipathic helices which comprise domain 1 being essential for toxicity. The structure and membrane insertion characteristics of insecticidal δ-endotoxin are similar to Colicin A. Membrane insertion is thought to be pH-dependant (Grochulski *et al.,* 1995) involving the formation of a molten globule state. Oligomerisation occurs once the protein has inserted into the membrane with the α5 helix of each monomer playing a crucial role (Kumar and Aronson, 1999).

Pathogenic *Vibrio cholerae* secrete a 80 kDa pro-toxin cytolysin that assembles into an oligomeric pore on target cell membranes following proteolytic cleavage and interaction with cell surface receptors. Once the cytolysin is activated by

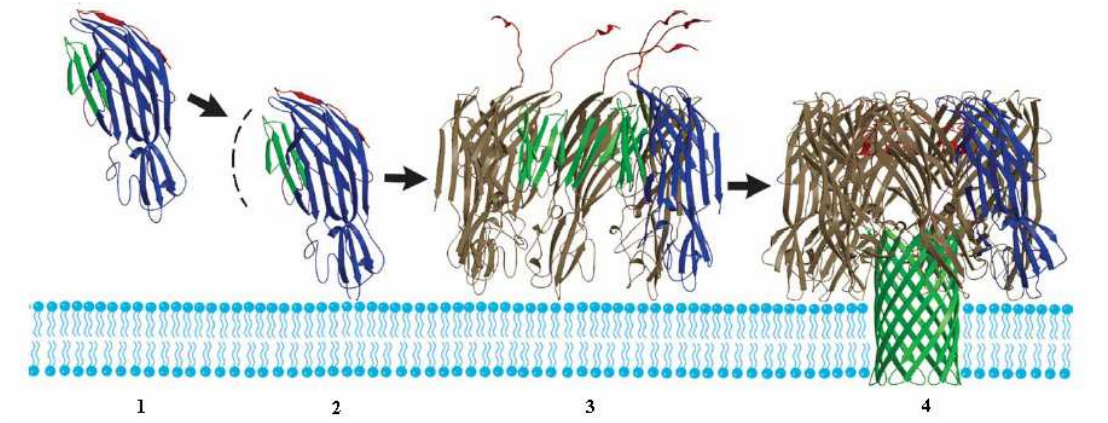


Figure 5: Schematic showing the formation of a β-barrel pore. Example shown is of the entirely β-stranded protein LukF. These proteins are secreted as water-soluble monomers (1), and bind to membranes via hydrophobic interactions (2). The protein then oligomerises at the membrane surface forming a heptameric pre-pore structure (3). Proteases then modify the protein resulting in a irreversible insertion of the pre-stems (green) into the membrane to form a β-barrel pore (modified from Olson and Gouaux, 2002)

proteolytic cleavage it assembles into a heptameric species upon addition of liposomes (Olsen and Gouaux, 2005).

1.2.3 Other dual-form (amphitropic) proteins

The Bcl-2 family of proteins play an important role in regulating programmed cell death or apoptosis. The subfamilies consist of the Bcl-x_L subfamily that inhibit apoptosis and the Bax subfamily that propmote apoptosis. Bcl-x_L is a α-helical protein approximately 21.6 kDa in size, which inserts into membranes by a pH dependent process. The protonation of certain residues at the protein surface by the low pH encountered at the membrane surface is thought to reduce the electrostatic repulsion effects between the protein and the anionic lipids of the membrane (Schendel *et al.*, 1997). Interestingly, the formation of a obligatory molten globule intermediate for proteins that convert from solution to membrane conformations was ruled out for Bcl-x_L by Thuduppathy and Hill (2006). It was proposed that the absence of a molten globule intermediate might have evolved to protect Bcl-x_L from intracellular proteases as it undergoes this conformational change. Recently, a pH-dependent model has been proposed for the solution to membrane conformational change (Figure 6) that consists of three stable conformations: a solution conformation, a conformation similar to the solution conformation but anchored to the membrane by its C-terminal transmembrane domain, and a membrane conformation that is fully associated with the membrane (Thuduppathy *et al.*, 2006). Bax, similar to Bcl-x_L, is a monomeric 21.1 kDa α-helical protein that exists predominantly in the cytosol before before it is triggered to insert into the membrane. Early during apoptosis, Bax translocates from the cytosol to the mitochondria (Suzuki *et al.*, 2000). It is thought that the protein initially forms an intermediate state that is bound to the membrane before oligomerizing to form the active pore structure (Garcia-Sáez *et al.*, 2004).

Signaling of other soluble proteins toward the membrane can occur via receptors on the membrane or by signaling molecules. Annexins are a family of calcium-binding proteins involved in numerous cellular processes including ion channel activity (Cartailler *et al.*, 2000). For this protein, hexamerisation is mediated by calcium binding an intermolecular calcium-binding site (Luecke *et al.*, 1995). Annexin cannot form the functional hexamer until it is signaled to do so by the binding of calcium.

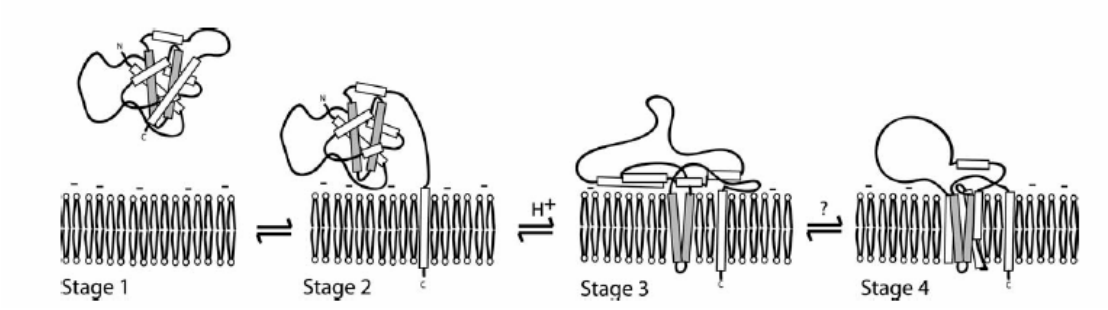


Figure 6: Hypothetical model for the solution to membrane conformational change of Bcl-X_L. Stage 1 shows the protein in soluble form as it is found in the cytosol. The protein is then anchored to the membrane by its C-terminal transmembrane domain (Stage 2). Insertion of the cytosolic domain then occurs via the hydrophobic helical hairpin into the membrane, caused by acidification (Stage 3). The fully inserted membrane conformation is assembled by either oligomer formation or α-helices spanning the length of the membrane. Taken from Thuduppathy *et al.*, (2006)

α-Lactalbumin is another protein that can be classified among amphitropic proteins, because it is a soluble protein, which is driven to interact with membranes to achieve some of its physiological functions. Although α-lactalbumin is well known for its participation in the synthesis of lactose (Gastinel *et al.*, 1999) it is also sectreted as a major protein in breast milk and several functions have been ascribed to it during the neonatal period (Lönnerdal and Lien, 2003). The structure of α-lactalbumin is a mixture of α-helices and β-sheets in the water-soluble form and a persistence of its tertiary structure within the membrane-bound state has been suggested (Cawthern *et al.*, 1996). The formation of a molten globule state prior to membrane insertion has been described (Banuelos and Muga, 1995) as well as the dependence of pH, calcium, lipid membrane curvature and charge on membrane interaction (Chenal *et al.*, 2005).

1.2.4 Membrane insertion

The exact process that amphitropic proteins adopt to convert from water-soluble forms to integral membrane forms varies from protein to protein. The soluble forms, however, all have the characteristic property of having polar, hydrophilic amino acid residues at their surface that can interact favourably with the surrounding aqueous medium, while the integral membrane forms have a less polar surface because they are buried within the hydrophobic interior of the membrane (von Heijne and Gavel, 1988). Inside the membrane the protein loses its flexibility and degrees of freedom and becomes highly immobilised. The change in polarity and reduced dielectric constant within the membrane results in strong van der Waals and electrostatic interactions. The conversion from one form to the other involves structural rearrangements to suit the changing surrounding environment. Often, this structural rearrangement involves the protein essentially turning inside out, exposing buried hydrophobic regions that are driven to interact and insert into the membrane (von Heijne and Blomberg, 1979). The triggers that initiate this structural rearrangement necessary to create a membrane insertion-competent form include factors such as low pH, lipid charge and membrane composition, binding of signalling molecules, proteolysis and redox effects (Epand, 1998; Chenal *et al.*, 2002; Johnson *et al.*, 2003; Yoshida *et al.*, 2004; Chenal *et al.*, 2005). Often, oligomerisation is necessary to form a fully functional pore or channel. This may occur before the protein has inserted into

the membrane interior or after, resulting from the close proximity of two or more transmembrane segments.

The role of electrostatic and hydrophobic interactions in membrane protein insertion is well documented (Chenal *et al.*, 2002). While electrostatic interactions are typically important for the association of proteins with the surface of the membrane (Mosior and Newton, 1995), hydrophobic interactions are dominant for the insertion of transmembrane segments of the protein into the membrane. Low pH at the membrane surface appears to play a role in promoting membrane insertion by either inducing a molten globule state and/or in making a part of the protein more hydrophobic by neutralizing acidic residues. The negatively charged residues, namely aspartate and glutamate, are protonated by the low pH micro-environment, thus neutrilizing them and rendering them more hydrophobic. Hydrophobic interactions are dominant for the insertion of the transmembrane helix into the membrane (Chenal *et al.,* 2002)

The "umbrella" hypothesis of membrane insertion states that the outer helical layers of a protein peel away from the central hairpin like the opening up of an umbrella (Parker and Pattus, 1993). The driving force for the unmasking of the buried hydrophobic hairpin is the formation of a molten globule that is formed as the soluble protein approaches the low pH environment at the membrane surface. The acidic pH at the membrane surface is due to the negative charge of the polar head groups in the lipid bilayer that attract the H^+ ions. The low pH induces the protein to form a molten globule that is thought to be an insertion-competent conformational pre-requisite for membrane insertion (Bychkova *et al.*, 1988). Due to the looser, less compact nature of the molten globule the energy barrier required in unmasking the hydrophobic hairpin for membrane insertion is reduced. However, it has recently been shown that a molten globule state resulting from a low pH environment may not be required for the conformational switch from soluble to integral membrane form (Thuduppathy and Hill, 2006). Other contributions such as the presence of a negatively charged membrane or an electrostatic potential across the membrane may be responsible for destabilizing the solution conformation at low pH.

Once inserted into the membrane, the transmembrane segment is stabilised by side chain interactions with the lipid bilayer interior resulting in the formation of helices and β-barrels. A transmembrane segment can traverse the membrane as a single helix, however, those adopting a β-strand structure need to oligomerise to create a β-barrel for stability.

The general strategy for the conversion of soluble protein forms to integral-membrane forms appears to be that the pore-forming regions are initially folded up on the surfaces of the soluble precursors and are then triggered to extend or refold into membrane-inserted structures. In so doing, the soluble protein form exchanges protein-protein interactions for protein-lipid interactions in a stable new assembly. By inserting a wedge into the membrane, the protein changes the curvature of the membrane and ultimately punctures the bilayer to form a stable pore lining.

1.3 GST family and the thioredoxin fold: new roles in membrane interaction

The thioredoxin fold is a scaffold used by many proteins to carry out a large range of various functions (Martin, 1995). This versatile fold that adopts an βαβαββα arrangement can adapt to provide new functions while retaining its structure and stability (Martin, 1995). Proteins that utilise the thioredoxin fold, grouped as the thioredoxin superfamily, have low sequence similarity and very few strictly conserved residues (Martin, 1995). The overall structural similarity between the thioredoxin folds in all the superfamily members and the similarity in the positioning of their important active-site residues is striking, given their functional differences and low sequence identity. Certain points in the thioredoxin fold can tolerate insertions without disruption of the overall structure, however, large scale conformational changes through redox switching have been observed (Declercq *et al.,* 2001; Littler *et al.,* 2004).

The glutathione transferase (GST) family of proteins utilise the thioredoxin fold and are classified as members of the thioredoxin superfamily. Typically GSTs are

homodimeric in structure with each 25 kDa subunit made up of two domains. Domain 1 or the N-terminal domain consists of the thioredoxin fold while domain 2 or the C-terminal domain is entirely α-helical in structure. These cytosolic GSTs are related by evolution to glutaredoxin by their thioredoxin domain that binds glutathione (GSH) in a topologically conserved location named the G-site. These proteins are a vital component of the cellular detoxification of a large variety of endogenous and exogenous toxins (Sheehan *et al.,* 2001). They detoxify toxins by conjugating them with GSH, the first step in the breakdown and eventual excretion of toxins from the organism via the mercapturate pathway (Armstrong, 1997)). The GST family also consists of members that are monomeric in structure, namely, glutaredoxin-2 (Xia *et al.*, 2001) and the chloride intracellular channel protein, CLIC1 (Harrop *et al.,* 2001).

Although GSTs are well known for their detoxification activity, they have many other functions and activities that include peroxidase activity, prostaglandin synthesis, isomerase activity, regulation of stress kinases, dehalogenation reactions, NO carriers and dehydroascorbate reduction (Reviewed by Oakley, 2005). More new uses for the canonical glutathione transferase fold are still becoming apparent. The bacterial stringent starvation protein SspA (Hansen *et al.,* 2005) and the yeast prion protein Ure2p (Bai *et al.,* 2004) both adopt the glutathione transferase fold but their activities are unrelated to detoxification and the primary function of these GST-like proteins may not even be catalytic.

Another recently discovered use of the cytosolic GST fold is the modulation and formation of membrane ion channels. CLICs are a recently discovered family of proteins that form chloride ion channels (Tonini *et al.,* 2000, Harrop *et al.,* 2001, Berryman *et al.,* 2004; Littler *et al.,* 2005). The first crystal structure determination of the soluble form of a CLIC family member, CLIC1 (Harrop *et al.,* 2001) confirmed that CLICs are members of the glutathione transferase family with high structural similarity to the Omega class GST. Interestingly, Tonini and co-workers (2000) showed that CLIC1 can exist in both soluble and integral membrane form and can integrate into membranes to form functional chloride conducting channels. The structural homology of CLIC1 and Omega GST prompted Dulhunty and co-workers (2001) to investigate whether the human Omega class GST (GSTO1-1) forms or

modulates ion channels, and found that GSTO1-1 did indeed modulate ryanodine receptors (RyR), which are calcium channels in the endoplasmic reticulum of various cells. Of possible relevance to CLICs, the channel modulating activity was dependent on the GST being active and the active site cysteine was shown to be essential (Dulhunty *et al.,* 2001).

Another protein that utilises the thioredoxin fold and is involved in modulating receptors at the membrane is calsequestrin (Wei *et al.,* 2006). This member of the thioredoxin superfamily is the major Ca^{2+} storage protein of muscle and has three repeat thioredoxin fold domains (Wang *et al.,* 1998). These three very negatively charged domains, which are topologically identical with that of *Escherichia coli* thioredoxin, surround a hydrophilic center. Recently it has been shown that calsequestrin can regulate RyR and inhibit Ca^{2+} release (Wei *et al.,* 2006). The thioredoxin fold of some proteins clearly has a role in the regulation of Ca^{2+} in the cell since CLIC2, Omega GST and calsequestrin have all been shown to modulate RyR.

The recently solved structure of a new class of GST, designated Kappa (Ladner *et al.,* 2004), shows an overall topology similar to that of a thioredoxin superfamily member, disulfide bond isomerase (DsbA). This suggests that two distinct superfamilies of GSTs evolved from different thiol-disulfide oxido-reductase progenitors by parallel pathways. This is in contrast to the pathway proposed by Sheehan and co-workers (2001) in which all GSTs diverged from a common ancestor. It was also interestingly noted that an extensive disordered hydrophobic patch on the dimer surface near the active sites of Kappa GST could suggest that the enzyme binds to a membrane surface as part of its function.

1.4 Chloride intracellular channel protein (CLIC) family

The chloride intracellular channel (CLIC) proteins are a group of soluble proteins that have the ability to form functional chloride channels in intracellular membranes (Tonini *et al.,* 2000, Harrop *et al.,* 2001, Berryman *et al.,* 2004; Littler *et al.,* 2005). To date, seven members of the CLIC family have been identified, namely, CLIC1, CLIC2, CLIC3, CLIC4, CLIC5A, p64 (CLIC5B in humans) and parchorin (CLIC6 in

humans). Although most of the CLIC proteins are composed of ~240 residues, p64 and parchorin are longer and consist of an additional amino-terminal domain in conjunction with the typical CLIC module. The CLIC proteins have been implicated in various important roles by controlling cellular chloride ion concentrations. These include cell cycle regulation, apoptosis, signal transduction, bone resorption and kidney function (reviewed by Debska *et al.,* 2001).

The CLIC nomenclature that was first proposed by Heiss and Poustka (1997), based on the channel forming activity observed for the first members, can be misleading since many newer members identified by sequence similarity do not appear to show channel formation. Furthermore, it has recently been suggested that CLICs form non-selective multi-ion pores rather than specific chloride channels (Singh and Ashley, 2006). If this is the case it would have significant implications for the nomenclature.

The founder member of the CLIC family was a 64 kDa protein named p64 (Landry *et al.,* 1993). The protein was isolated from bovine tracheal apical epithelium and the kidney cortex using an indanyloxy acetic acid (IAA) derivative as an affinity ligand, and subsequently identified at a molecular level with its cDNA cloned from a bovine renal cortex cDNA library (Landry *et al.,* 1993). p64 was shown to be 437 amino acids long with a distinct amino-terminal domain that is followed by the 240-residue CLIC module that shares structural similarity to the GST family. The avian homologue of p64, known as p62, plays a role in osteoclast formation (Schlesinger *et al.,* 1997) while the rat homologue of p64 is p64H1 (253 amino acids) and does not contain the additional N-terminal domain found in p64 (Howell *et al.,* 1996). CLIC5B (410 amino acids) is the human homologue of p64, which is a 46 kDa splice variant of CLIC5A (Shanks *et al.,* 2002). The C-terminal 238 amino acids of CLIC5A and CLIC5B are identical. CLIC5A was initially identified as a component of a cytoskeletal complex (Berryman and Bretscher, 2000) and was later found to function as a chloride channel and associate with the cortical actin cytoskeleton (Berryman *et al.,* 2004).

Parchorin is another CLIC protein that is known as a p64 homologue. It was originally identified as a secretory epithelium phosphoprotein in gastric parietal and airway epithelia cells. Its cDNA was first cloned from rabbit choroids plexus

(Nishizawa *et al.,* 2000) and was shown to encode a 637 residue protein. Although parchorin has been shown to relocalise from the cytoplasm of water-secreting cells to the plasma membrane when chloride levels are low (Nishizawa *et al.,* 2000), sequence analysis shows no predicted transmembrane regions. Therefore, it is likely that parchorin only serves as a chloride channel modulator as opposed to actually forming the channel itself. The human homologue of parchorin, based on high sequence homology, is CLIC6 (Freidli *et al.,* 2003). This protein is 704 amino acids in length and has a characteristic 6 residue N-terminal motif that is repeated 15 times (Griffon *et al.,* 2003). Parchorin and its homologues have been implicated in playing a role in the regulation of secretion by modulating chloride ion channels (Griffon *et al.,* 2003).

CLIC2 is a 243 residue, 27.8 kDa protein that is widely distributed in human tissues including heart and skeletal muscle (Board *et al.,* 2004). Board and co-workers (2004) also found that CLIC2 is structurally similar to the Omega class GST (18.6% sequence identity) and CLIC1 (58.8% sequence identity). Based on a molecular model designed for CLIC2 using the CLIC1 crystal structure co-ordinates as a template it was found that the CLIC2 model superimposed well with CLIC1, with the only difference being a loop region between helix 5 and helix 6 of CLIC2 (Board *et al.,* 2004). Although CLIC2 was found to have little catalytic activity with typical glutathione transferase substrates, it was a strong inhibitor of cardiac RyR channels (Board *et al.,* 2004) and, like Omega class GST, may play an important role in intracellular calcium homeostasis.

Of all the CLICs, the MAP kinase-associated CLIC3 have been the least studied, and very little is known about their exact function. Human CLIC3 is predicted to contain 207 residues and localises to the nucleus (Qian *et al.,* 1999). Of all the CLICs it shares the lowest percentage of sequence identity to CLIC1 (49 %) and has a relatively limited hydrophobic domain indicating an improbable direct role in channel formation. It has been proposed that by modulating chloride conductance at the nuclear membrane it activates MAP kinase signal transduction and therefore could play a role in cell growth (Qian *et al.,* 1999).

Two CLIC orthologs have been reported in *Caenorhabditis elegans*, namely, EXC-4 and EXL-1. The EXC-4 (for excretory canal) and EXL (for EXC-4 like) proteins have

been labelled as “CLIC-like” based on sequence similarities and their ability to localise in intracellular membranes (Berry *et al.*, 2003). The *Caenorhabditis elegans* homologue of Omega class GST, termed GST-44, revealed strictly cytoplasmic localisation (Berry *et al.*, 2003).

CLIC4 was the first human CLIC to be identified (Howell *et al.*, 1996), is expressed in a wide variety of tissues and is highly conserved across species (Edwards, 1999). Proteinase K treatment of microsomes containing CLIC4 results in a 27 kDa reduction in size of the protein, leaving a 6 kDa fragment (Duncan *et al.*, 1997). This indicates that the integral membrane form of this protein has a single transmembrane region near the N-terminus running from approximately Cys35 to Val57 (Duncan *et al.*, 1997). The crystal structure of CLIC4 (Littler *et al.*, 2005) shows a two domain, GST-like protein, which is highly homologous to that of soluble CLIC1, as was expected based on the high sequence similarity between the two (67% sequence identity). CLIC4 has been shown to associate with lipid bilayers and at low pH induce the efflux of chloride ions from artificial liposomes in a concentration-dependent manner (Littler *et al.*, 2005). The interaction is enhanced when CLIC4 is oxidised. Unlike CLIC1, however, CLIC4 does not appear to form a dimer when exposed to oxidizing conditions, which is thought *in vivo* to represent an intermediate membrane docking form (Littler *et al.*, 2004). The reason for this has been linked to the fact that CLIC4 does not have a conserved cysteine residue at the same position that CLIC1 does (Cys59) with which an intramolecular disulphide bond can be formed that would stabilise a dimeric form. Recently, a crystal structure of a trimeric form of CLIC4 has been described (Li *et al.*, 2006) that may represent an oligomeric mode with a unique assembly mechanism by which the oligomerisation of CLIC4 can be performed without any intramolecular disulfide bond formation.

It has also been reported that CLIC family members associate with a scaffolding protein that is utilised in the cell to localise signalling proteins to specific areas fascilitating precise cellular function (Shanks *et al.*, 2002). Protein kinase A-anchoring proteins (AKAPs) are a class of scaffolding protein utilised by the cell to anchor the regulatory subunit of type II camp-dependent protein kinase A to specific locations within the cell (Lester and Scott, 1997). Shanks and co-workers (2002) showed that all CLIC family members were able to bind a 133-amino acid domain

within AKAP350 through the last 120 amino acids in the conserved CLIC C-termini. This suggests that CLIC family members could be signalled and controlled by AKAP350, and that cAMP-dependent phosphorylation of CLIC proteins by protein kinase A could regulate their distribution and function. Table 1 summarises the characteristics and properties of all the CLIC family members.

1.5 CLIC1 overview

1.5.1 Distribution and functional role

Human CLIC1 was cloned serendipitously after screening a monocytoid blood cell line for PKC-activated genes (Valenzuela *et al.,* 1997). This protein was found to localise to the nuclear membrane and function as chloride ion channels, and was originally designated NCC27 (for nuclear chloride channel-27) but is now more commonly known as CLIC1. Although CLIC1 has been found mainly in the nucleoplasm and nuclear membrane, it has been reported in a wide variety of different tissues and cells (Valenzuela *et al.,* 2000; Tulk *et al.,* 2002). The interesting observation that CLIC1 occurs in the nucleoplasm and in the nuclear membrane raised questions about how the protein is regulated between these two states. Was CLIC1 acting as a regulatory subunit of a multiprotein chloride ion channel complex or did it form the ion-conducting unit itself? Either way, the fact that CLIC1 is practically ubiquitous in its tissue distribution and well conserved across different species (Valenzuela *et al.,* 2000) indicates it plays a fundemental role in the functioning of the cell. Furthermore, CLIC1 is active from early embryogenesis to adult life.

It has been hypothesised that CLIC1 is involved in regulation of the cell cycle based on electrophysiological studies in Chinese hamster ovary (CHO-K1) cells, which indicated that CLIC1 chloride conductance varied according to the stage of the cell cycle, being expressed only at the plasma membrane of cells in the G2/M phase (Valenzuela *et al.,* 2000). It was also demonstrated that Cl^- ion channels that are known to block CLIC1 led to the arrest of CHO-K1 cells in the G2/M stage of the cell cycle, the same stage at which the ion channel is selectively expressed at the plasma membrane (Valenzuela *et al.,* 2000). CLIC1 has also been implicated in roles as

Table 1 : Comparison of properties of the CLIC family members.

	Molecular mass	**Number of residues**	**pI**	**Localisation**	***In vitro* channel formation /modulation**	**Oligomerisation states known**	**Crystal structure**	**% Sequence ID to CLIC1**
[a]**CLIC1**	26.9 kDa	241	4.85	Nucleoplasm, nuclear membrane, kidney, heart, placental cells	[b]Channel activity	- monomer - dimer	[c]YES	----
[d]**CLIC2**	27.8 kDa	243	5.24	Spleen, lung	[e]RyR modulation	- monomer	NO	58.8
[f]**CLIC3**	23.5 kDa	207	6.34	Nuclear membrane	NONE	- monomer	NO	49
[g]**CLIC4**	33 kDa	253	5.42	ER, neurons, kidney, inner mitochondrial membrane	[h]Channel activity	- monomer - trimer	[i]YES	67
[j]**CLIC5A**	28 kDa	251	5.44	Heart, skeletal muscle	[k]Channel activity	- monomer	NO	63
[l]**CLIC5B (p64 homologue)**	46 kDa	410	4.34	Golgi apparatus	NONE	- monomer	NO	66
[m]**CLIC6 (parchorin homologue)**	65 kDa	704	4.05	Water sectreting cells, endocrine cells	NONE	- monomer - dimer	NO	64

[a]Valenzuela *et al.,* 1997, [b]Tonini *et al.,* 2000; Tulk *et al.,* 2000; Tulk *et al.,* 2002; Warton *et al.,* 2002; Singh and Ashley, 2006, [c]Harrop *et al.,* 2001; Littler *et al.,* 2004, [d]Heiss and Poutska, 1997; [e]Board *et al.,* 2004; [f]Qian *et al.,* 1999; [g]Howell *et al.,* 1996; [h,i]Littler *et al.,* 2005; [j]Berryman and Bretscher, 2000; [k]Berryman *et al.,* 2004; [l]Landry *et al.,* 1993; [m]Nishizawa *et al.,* 2000

diverse as microglia-mediated β-amyloid-induced neurotixicity (Novarino *et al.*, 2004) and sperm function (Myers *et al.*, 2004). Since it was reported that CLIC1 expression is related to macrophage activation, Novarino and co-workers (2004) were prompted to examine the expression and role of CLIC1 in brain macrophages or microglial cells. The inflammatory events mediated by microglial activation contribute to several neurodegenerative processes, including Alzheimer's disease (McGeer and McGeer, 1998; Kalaria, 1999). The finding that CLIC1 is involved in microglial activation led Novarino and co-workers (2004) to suggest that the protein should be considered as a therapeutic target for Alzheimer's disease and, indeed, other inflammatory diseases.

1.5.2 Structure of soluble CLIC1

CLIC1 is 241 residues long and has a molecular mass of 26.9 kDa. The protein is mostly α-helical with only ~ 8% of its secondary structural content being β-strand in its reduced monomeric state. Figure 7 shows the amino acid sequence of CLIC1 with the positioning of the secondary structural elements. Based on the proteins primary sequence it was proposed that CLIC1 could be a member of the GST family (Dulhunty *et al.*, 2000). The determination of the CLIC1 crystal structure by Harrop and co-workers (2001) later confirmed this and the protein was classified as the newest member of the GST family.

CLIC1 in its reduced state was found to be monomeric, making CLIC1 and Grx2 the only members of the GST family that did not have a dimeric quaternary structure. The crystal structure of CLIC1 (Figure 8A) shows a monomeric protein with two domains. The N-terminal domain resembles the thioredoxin fold similar to that found in GSTs. The C-terminal domain is entirely α-helical and most closely resembles the Omega class GST (Figure 8B). Although CLIC1 is structurally similar to the subunit of Omega class GST, they only share 16% sequence identity. A notable structural difference found at the C-domain of CLIC1 is the insertion of a highly negatively charged loop (Pro147-Gln164), which is a distinctive feature of CLIC1. This loop is spatially adjacent to the loop linking the two domains, and may have a role in protein-

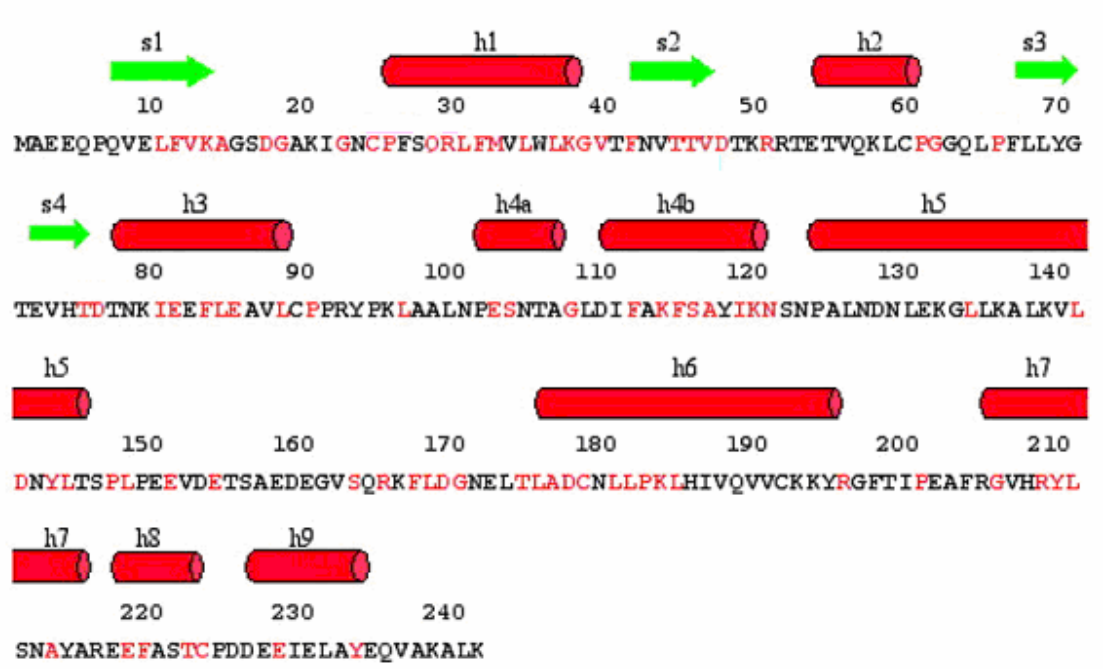


Figure 7: CLIC1 primary sequence showing position of secondary structural elements. Strands are represented by arrows and helices are represented by cylinders. The image was taken and modified from the PDBsum database (Laskowski *et al.*, 1997) using the PDB code: 1k0m (Harrop *et al.*, 2001).

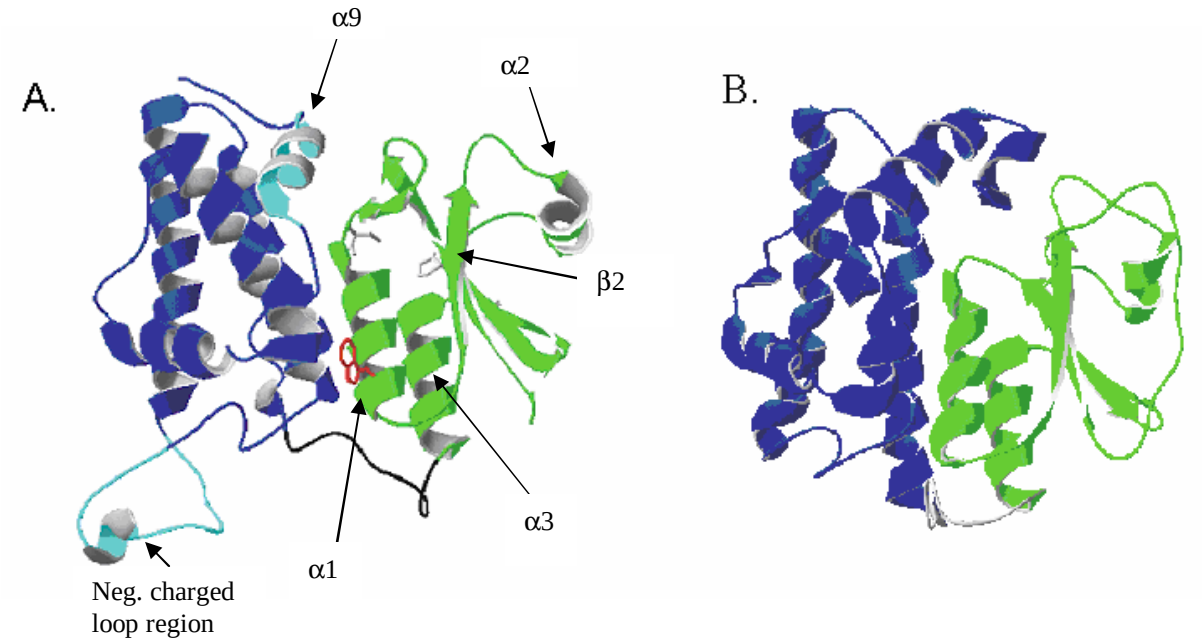


Figure 8: Ribbon representations of the crystal structure of reduced monomeric CLIC1 and Omega class GST. (A) Shows a ribbon representation of CLIC1 highlighting domain 1 (green) and domain 2 (blue). The side chain of the lone tryptophan residue (Trp35) is shown in red and the domain linker is shown in black**.**The regions that are structurally different to Omega class GST are shown in light blue. (B) Shows a ribbon representation of Omega class GST with domain 1 shown in green and domain 2 shown in blue. Images were generated with Swiss PDB viewer (Guex and Peitsch, 1997) using the PDB files 1k0m (Harrop *et al.*, 2001) for CLIC1 and 1eem (Board *et al.*, 2000) for Omega class GST.

protein interactions. In CLIC1 there are seven acidic residues in this region. The C-terminal α9 helix of CLIC1 is also structurally unique and is another hotspot of negative charge. These features may play a key role in membrane insertion of CLICs. CLIC1 has a relatively low pI value of 4.85 (Valenzuela *et al.,* 1997).

The structure reveals a single tryptophan residue (Trp35) located within helix 1 that is partially exposed to solvent and positioned near the domain interface. Eight tyrosine residues are scattered throughout the proteins structure with most residing in the C-terminal domain. Although the protein has 6 cysteine residues, only one (Cys24) is located in the region corresponding to the typical GST active site in domain 1. This single cysteine active site can form a mixed disulphide with glutathione (GSH) and closely resembles the glutaredoxin protein, a member of the thioredoxin superfamily from which GSTs have evolved. The GSH binding properties of CLIC1 are much weaker than those observed for other GSTs, with less extensive interactions occurring between the CLIC1 active site and GSH (Harrop *et al.,* 2001). A covalent complex between oxidised glutathione (GSSG) and CLIC1 has been shown to occur and the structure of CLIC1 with GSSG bound has been crystallised (Harrop *et al.*, 2001). GSSG binding showed only small changes in the protein structure with glutathione covalently attached to Cys24. Like glutaredoxin, the GSH binding site of CLIC1 appears to be designed to ensure the nucleophilicity of the sulfur atom of its lone reactive cysteine (Cys24 in CLIC1) as opposed to the active site of typical GSTs that ensures the nucleophilicity of the sulfur atom of GSH creating a reactive thiolate ion (Wilce and Parker, 1994; Armstrong, 1997). The conserved cysteines at the active site of the CLICs indicates that they may be under redox control, perhaps to target the chloride channel to specific locations in the cell. CLIC1 also has a conserved cysteine (Cys59) located at the end of helix 2, which is not present in other CLIC proteins.

The finding that monomeric CLIC1 undergoes a redox-controlled structural transition to dimeric form (Littler *et al.,* 2004) showed a new structural form of CLIC1 with implications for CLIC1 rearrangement and membrane docking. It was shown by Littler and co-workers (2004) that on oxidation CLIC1 undergoes a reversible transition from monomeric to non-covalent dimeric state due to the formation of an intramolecular disulphide bond (Cys24 – Cys59). The crystal structure of this dimeric

form of CLIC1 reveals a major structural rearrangement occurring in the N-terminal domain, exposing a large hydrophobic surface, which is stabilised *in vitro* by dimerisation (Littler *et al.*, 2004). *In vivo*, this hydrophobic surface may represent the membrane-docking surface. The most apparent structural change between the soluble monomer and oxidised dimer subunits (Figure 9) is relative to the helix 2 region. In the dimer, all the β-strand structures present in the monomeric form have become disordered and the N-terminal domain is entirely α-helical. For the dimeric CLIC1 structure helix 2 is extended by two turns and residues between helix 2 and helix 3 (β-strand 3 and 4 in monomer) form an extended loop and are loosely packed against the C-domain (Littler *et al.*, 2004). The arrangement of the subunits bears no relationship to that seen in GST dimers. Because one of the key residues involved in CLIC1 dimerisation (Cys59) is unique to CLIC1 it is unlikely that a similar oligomerisation or membrane docking mechanism exists for the other CLIC proteins. Although it has recently been shown that CLIC4 can form a trimeric structure in crystals (Figure 10), this oligomerisation mode did not involve any intramolcular disulphide bond formation (Li *et al.*, 2006). The only other CLIC protein known to form a homodimer is CLIC6 (Griffon *et al.*, 2003), although not much is known about its structure or properties.

1.5.3 Conversion of soluble CLIC1 to integral-membrane form

CLIC1 is known to exist in soluble form and as an integral membrane protein. Although high-resolution structural data exists for the resting state of the soluble form of the protein, not much is known about the structure of the integral-membrane form, or the exact mechanism of membrane insertion. Resistance to alkali extraction of CLIC1 when it is in integral membrane form suggests that the protein spans the membrane (Tulk and Edwards, 1998). Because CLIC1 is such a small protein (27 kDa) and the fact that it had an unusual distribution not noted for other eukaryotic ion channel proteins, mostly found in the nucleoplasm but with a small portion inserted in the nuclear envelope, it was unclear whether CLIC1 actually formed channels or just regulated an unidentified ion channel. CLIC1 may be acting as a regulatory subunit of a multiprotein chloride ion channel complex and therefore itself might not represent the ion-conducting unit of the chloride channel complex. Tonini and co-workers (2000) were the first to demonstrate conclusively that CLIC1 is a transmembrane

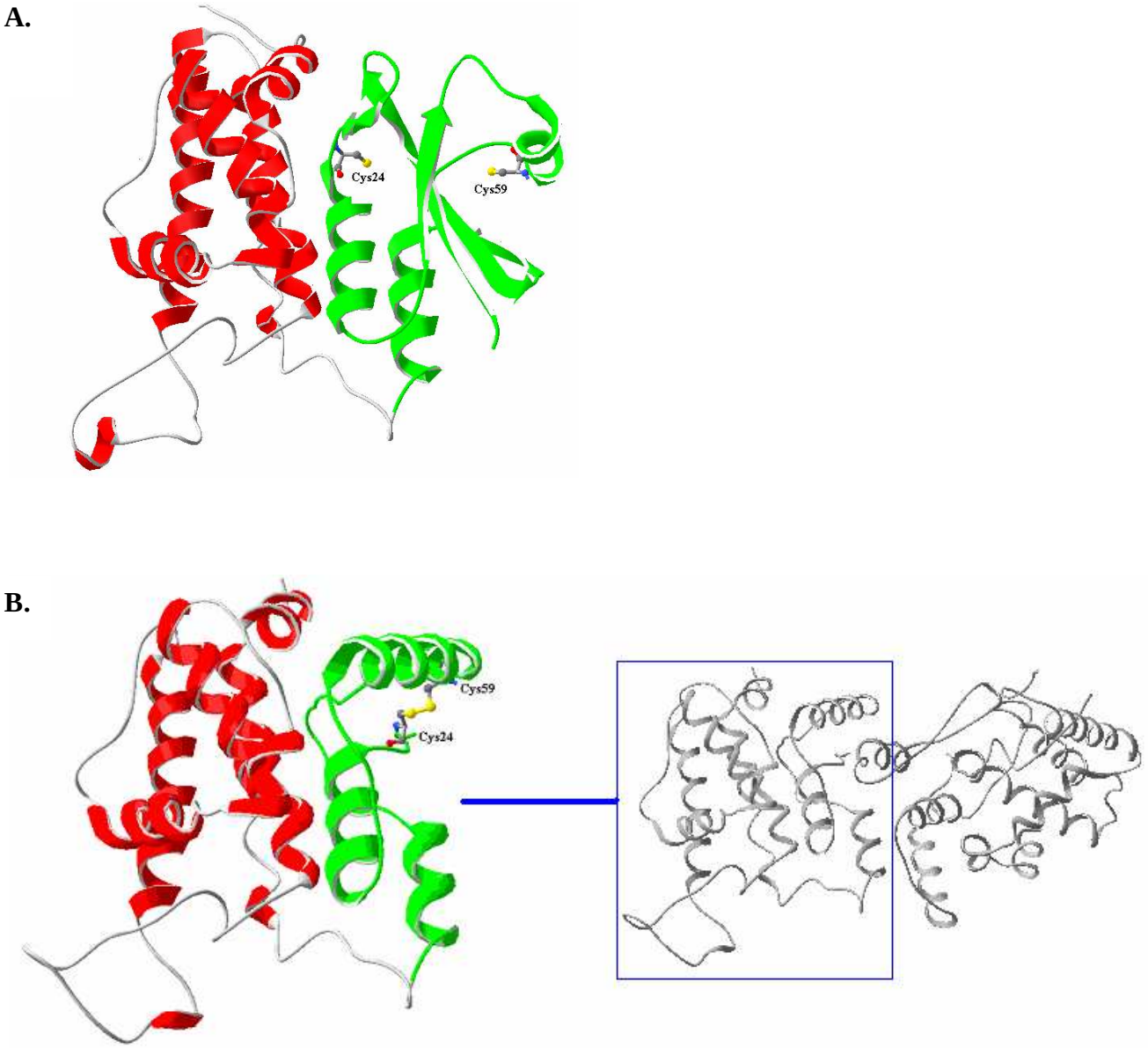


Figure 9: Comparison of CLIC1 monomer and dimer structures. Domain 1 is shown in green and domain 2 in red. (A) A ribbon representation of reduced CLIC1 in the monomeric form showing the side chains of Cys24 and Cys59. (B) A ribbon representation of dimeric CLIC1 (grey) and a subunit of dimeric CLIC1. The disulphide bond formed between Cys24 and Cys59 is shown in yellow. The images were generated with Swiss PDB viewer (Guex and Peitsch, 1997) using the PDB file 1k0m (Harrop *et al.*, 2001) for monomeric CLIC1 and PDB file 1rk4 (Littler *et al.*, 2004) for dimeric CLIC1.

protein that directly forms part of the ion channel and, further, that the N-terminus projects outward and the C-terminus inward. Figure 11 illustrates the orientation of the transmembrane segment of CLIC1.

It was initially demonstrated that purified, solubilised CLIC1 partly co-reconstitutes into asolectin liposomes by detergent dialysis and, therefore, is capable of forming novel, chloride-selective channels in the absence of other subunits or proteins (Tulk *et al.*, 2000). Later it was shown that CLIC1 spontaneously inserts into preformed membranes in the absence of detergent (Tulk *et al.,* 2002; Warton *et al.,* 2002) and that the process of membrane integration is pH-dependent (Warton *et al.,* 2002). The role of lipid composition on CLIC1 membrane insertion was examined by Tulk and co-workers (2002) and showed that CLIC1 cannot insert, or inserts but cannot function as a channel, into phophatidylcholine (PC) liposomes, unless they are supplemented with acidic lipids (e.g. phosphatidylserine), or replaced by liposomes containing 7:3 phosphatidylserine:phosphatidylethanolamine. The channel activity, which is measured using Cl^- efflux assays, is inhibited by indanyloxyacetic acid-94 (IAA), N-ethylmaleimide, and reduced or oxidised glutathione (Tulk *et al.*, 2002). Furthermore, the channel activity was found to be CLIC1 concentration dependent, inactivated by heat, and increased under reducing conditions (Tulk *et al.,* 2002).

Contradictory to this, Warton and co-workers (2002) found that CLIC1 did display chloride conductance in the absence of acidic phospholipids (9:1 PC/cholesterol) and Littler and co-workers (2004) reported that reducing conditions prevent channel activity. It is unclear why the conductance of reconstituted CLIC1 channels differs between studies from different laboratories. Singh and Ashley (2006) speculate that these inconsistencies might be related to the different reconstitution methods:"tip-dipping"(Warton *et al.,* 2002) versus planar bilayers (Tulk *et al.,* 2000; Tulk *et al.*, 2002). The reliability and validity of data produced using planar bilayers has come under some criticism recently (Singh and Ashley, 2006). Furthermore, the use of detergents to release Cl^- in Cl^- efflux studies (e.g. Tulk *et al.,* 2002; Littler *et al.*, 2004) is also controversial. Because most of the Cl^- is only released by detergents, it is probable that very few liposomes contain functional channels, making any results using this method difficult to interpret.

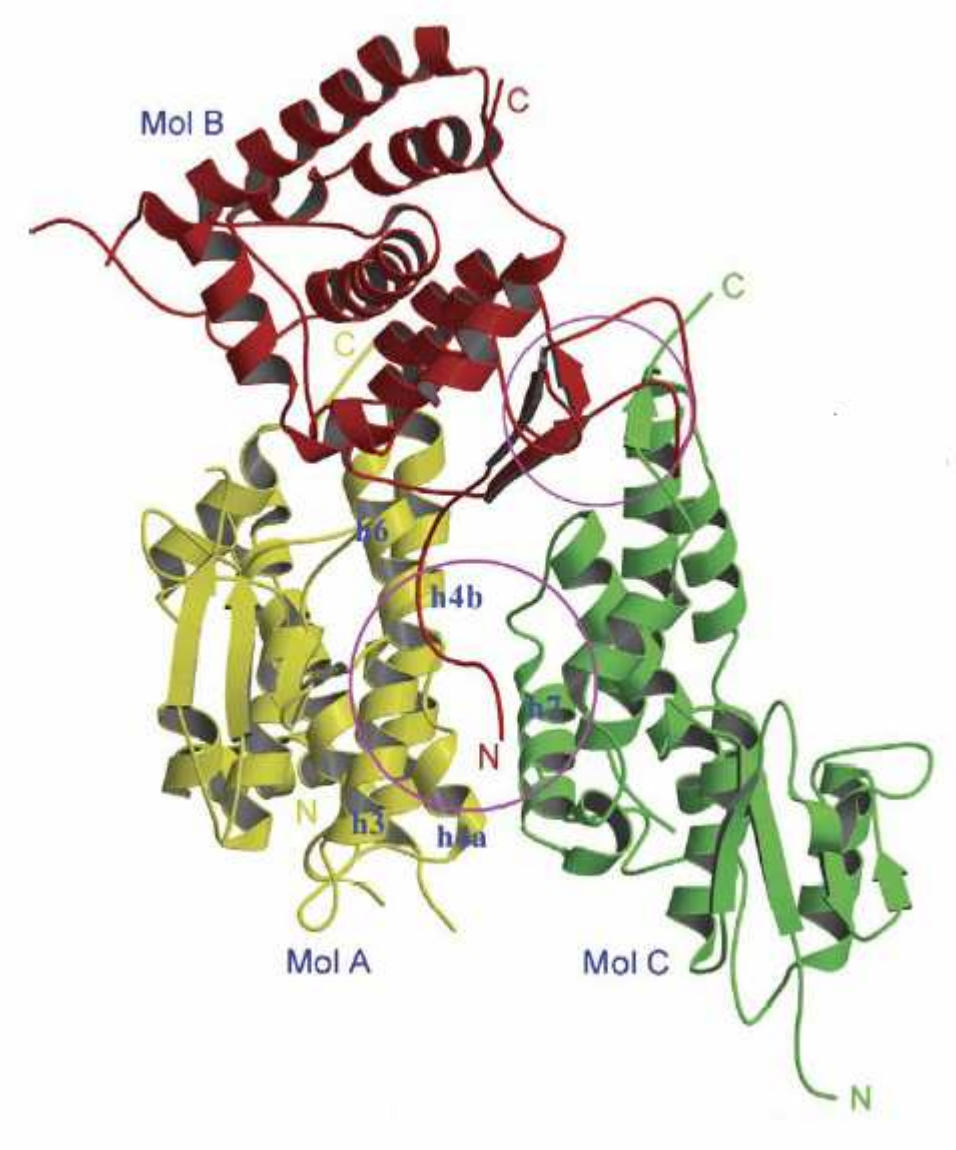


Figure 10: Ribbon representation of the trimeric form of CLIC4. The regions involved in intermolecular contacts are circled. The image was taken from Li *et al.*, 2006.

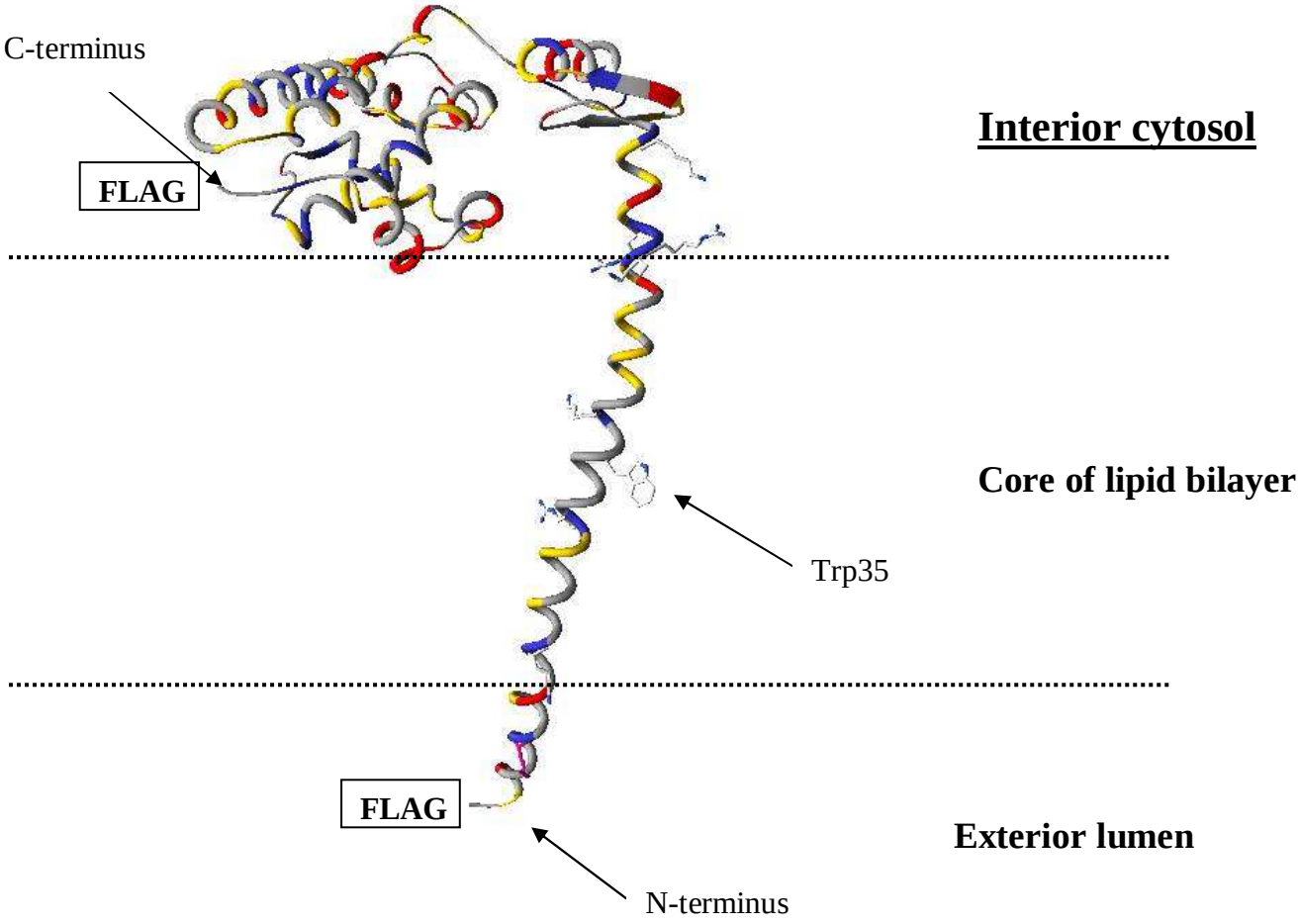


Figure 11: Graphic representation of possible orientation of CLIC1 transmembrane region. The dashed lines represent the plane of the membrane bilayer. Positively charged residues are shown in blue, neutral charge residues in yellow, and negatively charged residues in red. The orientation is based on FLAG-epitope studies performed on CLIC1 (Tonini *et al.*, 2000). The image was generated using Swiss PDB viewer (Guex and Peitsch, 1997) using the PDB file 1k0m (Harrop *et al.*, 2001).

The oxidised CLIC1 dimer maintains its ability to form chloride ion channels in artificial bilayers and vesicles, and mutational studies show both Cys24 and Cys59 are required for channel activity (Littler *et al.,* 2004). Redox regulation of CLIC1 by these cysteine residues was recently investigated (Singh and Ashley, 2006). It was found that although CLIC1 appeared to insert into lipid monolayers regardless of lipid composition, the channel assembly and functioning in planar lipid bilayers required a specific lipid mixture containing 4:1:1 of POPE:POPS:cholesterol. IAA, NEM, oxidised GSH and potassium chloride all dramatically reduced or totally inhibited channel activity, and mutation of Cys24 to an alanine residue also resulted in diminished chloride conductance. CLIC1 under reducing conditions, using either DTT or reduced glutathione, was found to exhibit the highest levels of chloride conductance. It was concluded that oxidizing conditions lead to a closure of the CLIC1 pore possibly via disulphide bond formation involving Cys24 that is located on the extracellular (or luminal) side of membrane CLIC1 subunits, and reducing conditions result in channel opening and conductance (Singh and Ashley, 2004).

Exactly which part of the CLIC1 structure forms the transmembrane helix is unclear. There are two regions of significant hydrophobicity in the CLICs, as judged by hydrophobicity plots. One region is located in the N-terminal domain and comprises helix 1 and β-strand 2, while the second region is located in the C-terminal domain and comprises most of helix 6 and part of the loop preceding it. Although it has been proposed that the C-terminal domain forms the transmembrane portion of the protein (Cromer *et al.,* 2002) based on structural similarities to pore-forming proteins and the unlikeliness of the N-domain that evolved from the thioredoxins to unfold readily, recent consensus seems to suggest that the thioredoxin domain forms the transmembrane region. Sequence analysis reveals a 23 residue segment (from Cys24 to Val46) that is likely to from a transmembrane helix. Experimental support for this hypothesis comes from proteinase K digestion studies using CLIC4 that shows the first 50 residues are protected from proteolysis and therefore inserted into the membrane (Duncan *et al.,* 1997). The polarity of the residues in this predicted transmembrane segment (helix 1 and β-strand 2) also fit the criteria for typical transmembrane helices (Harrop *et al.,* 2001). The hydrophobic surface patch formed

by helix 1 and β-strand 2 are unique to the CLICs and are not hydrophobic in other members of the GST family.

The most direct evidence for the transmembrane segment of CLIC being in the thioredoxin domain comes from *in vivo* studies performed using CLIC-like proteins of the nematode *Caenorhabditis elegans* (Berry *et al.,* 2003; Berry and Hobert, 2006). The study of the EXC-4 CLIC-like protein in the *Caenorhabditis elegans* excretory canal by Berry and co-workers (2003) represented the first time a CLIC protein had been expressed and analysed in an animal system (*in vivo*) and the effects of mutations on protein localisation examined. Using an attached GFP reporter protein, the localisation of various EXC-4 mutants were monitored and it was concluded that the first 55 residues at the N-terminal end were required for membrane insertion since deletion of the β2 strand and a L46P mutation in α1 disrupted membrane insertion (Berry *et al.,* 2003). Furthermore, it was found that the α6 helix in domain 2 does not play a role in membrane localisation. More recent studies by Berry and Hobert (2006) show that a 55 – 70 residue long segment at the N-terminal domain of CLIC proteins from *Caenorhabditis elegans* is a key determinant for membrane localisation and function of invertebrate CLIC proteins. It was also reported that the cysteine residues within this proposed transmembrane region are unnecessary for invertabrate CLIC function (Berry and Hobert, 2006).

Because of the small size of CLIC1 it appears likely that the protein oligomerises to form fully functional channels. Whether this oligomerisation occurs before membrane insertion or after remains unknown. It has been suggested that the CLIC1 ion channel is likely to consist of a tetrameric assembly of subunits (Warton *et al.,* 2002). Following addition of protein to lipid bilayers, small conductance channels with slow kinetics (SCSK) appeared and then underwent a transition to form a high conductance channel with fast kinetics that had four times the conductance of the SCSK (Warton *et al.,* 2002). Singh and Ashley (2006) report, that according to their model, conducting CLIC1 channels must contain a minimum of 4 subunits.

1.6 Objectives

Studies of the conformational dynamics of CLIC1 may provide insight as to how the soluble form of CLIC1 rearranges to form an intracellular channel. Understanding this process at a molecular level would provide information helpful to the development of the treatment of severe diseases caused by malfunction in ion channels. The main objective in this study is to further our understanding of the mechanisms of CLIC1 membrane insertion by studying the changes in structure and stability that soluble CLIC1 undergoes as it approaches and interacts with the membrane. This will give insight into the conformational dynamics involved in the conversion of soluble CLIC1 to the integral membrane form.

This study involves two approaches:

1) Analysis of the structure and stability of CLIC1 in the absence of membrane, investigating the effect of possible signals or triggers that may play a crucial role in the conversion of the soluble form to integral membrane form. The effects of reducing and oxidizing conditions on CLIC1 structure and stability are investigated, as are the effects of pH change. This is of physiological relevance since the movement of soluble CLIC1 in the cytoplasm or nucleoplasm toward the membrane will involve the protein being exposed to a lower pH micro-environment ((McLaughlin 1989, Menestrina *et al.*, 1989, van der Goot *et al.*, 1991).. The effect of this pH change on the structural dynamics of CLIC1 is studied. Furthermore, the role of the primary sequence and unique three-dimensional structure of CLIC1 in membrane insertion is investigated in a bioinformatics-based study that looks at conserved residue features such as hydropathy and charge. Hidden helical propensities and N-capping motifs in the sequence are also reported and the possible implications for transmembrane regions discussed.

2) Analysis of the structure and thermodynamics of CLIC1 interacting with membrane models. Changes in secondary structure, tertiary structure, hydrodynamic volume and thermodynamics when CLIC1 is exposed to membrane-mimicking models are studied. The effect of a variety of conditions (pH, redox, temperature), residue-modifiying agents (NEM), ligands (GSH), and inhibitors (IAA) on CLIC1 membrane interaction are studied. Finally, all this information is used to predict a model for CLIC1 membrane insertion and channel orientation.

CHAPTER 2. EXPERIMENTAL PROCEDURES

2.1 Materials

The *Escherichia coli* pGEX-4T-1 plasmid with the cloned GST-CLIC1 fusion protein was a gift from Dr. S. N. Breit, Centre of Immunology, St. Vincent's hospital, University of New South Wales, Sydney Australia. The restriction enzymes *BamH*1 and *Not*1 were obtained from Roche diagnostics (Basel, Switzerland). Bovine thrombin, 8-analino-1-naphthalene sulphonate (ANS) and indanyloxyacetic acid-94 (IAA-94), N-ethylmaleimide (NEM), NATA, hydrogen peroxide, 5,5'-dithiobis(2-nitrobenzoate) (DTNB), deuterium oxide, trifluoroethanol, pre-liposomes formulation 4, asolectin type IV and sarkosyl were all obtained from Sigma Aldrich (St. Louis, MO, USA). Isopropyl- thio-galactosidase (IPTG) was obtained from Inqaba Biotech (Pretoria, South Africa). Dithiothretol (DTT) was purchased from Whitehead Scientific (Cape Town, South Africa). Reduced glutathione (GSH) was acquired from ICN biomedicals (Aurora, Ohio, USA). SDS-PAGE molecular mass markers were aquired from Amersham Biosciences (Buckinghamshire, UK). Urea was purchased from Merck Laboratory supplies (Darmstadt, Germany). Guanidine hydrochloride was acquired from Roche diagnostics (Basel, Switzerland).

All other chemicals used were of standard analytical grade. Solutions were filtered using 0.22 μM acetate filters from Osmonics.

2.2 Methods

2.2.1 Plasmid verification

The plasmid used as an expression vector was pGEX-4T-1 (Valenzuela *et al.*, 1997) which contains the GST-CLIC1 fusion cDNA insert used for the over-expression of the wildtype CLIC1 protein. The presence of this cDNA insert was confirmed with restriction digestion analysis using the enzymes *Bam*H1 and *Not*1. After incubation with the restriction enzymes for 4 hours at 37°C the DNA was electrophoresed on a 1 % agarose gel containing ethidium bromide. Both single and double digests of the

plasmid were performed. Sequencing was also employed to further verify and confirm the plasmid. The DNA of the CLIC1 insert was sequenced by Inqaba Biotech (Pretoria, South Africa) using the 5' pGEX primer that binds the nucleotides 869 – 891 and the 3' pGEX primer that binds the nucleotides 1041 – 1019.

2.2.2 Over-expression and purification

CLIC1 was purified using an 8 litre batch culture of *Escherichia coli* BL-21 cells transformed with the pGEX-4T-1 plasmid. By adding 100 µl of cells from glycerol stocks to 100 ml 2 X YT media (1.6g yeast, 1g tryptone and 0.5g NaCl) containing 100 µg/ml ampicillin an overnight (16 hours) culture of transformed *Escherichia coli* cells was grown in a rotating incubator at 250 r.p.m and 37°C. The overnight culture was diluted 50 fold with 2 X YT medium containing 100 µg/ml ampicillin and was grown for approximately 6 hours to late log phase ($O.D_{600}$ ~ 1.1). Over-expression of the fusion protein was induced by adding isopropylthiogalactoside (IPTG) to a final concentration of 1 mM. Growth was continued for 4 hours until optimum over-expression was achieved. The cultures were then centrifuged for 15 minutes at 5000 X g at 4°C. The resulting supernatant waspoured off, and the pellets wre resuspended in a minimal volume of resuspension buffer (10 mM Tris-HCl, pH 7.5, 1 mM EDTA, 200 mM NaCl and 0.02 % sodium azide) and frozen at - 20°C overnight to promote cell lysis.

The cells were thawed and lysed on ice by pulse sonicating (0.5 sec on and 0.1 sec off) for 3 x 30 seconds using a Heat Systems sonicator (Ultrasonics Inc.). The crude extract was then centrifuged in a microfuge at 16 000 x g for 30 minutes at 4°C. The resulting supernatant was loaded onto a glutathione-Sepharose column pre-equilibrated with 10 column volumes of 10 mM Tris-HCl, 150 mM NaCl, 1 mM EDTA, 1 mM DTT and 0.02 % sodium azide at pH 8.2. After the column was washed with equilibration buffer, cleavage of CLIC1 from the GST was performed. This was done by adding 3 units of human thrombin in 10 ml thrombin cleavage buffer (200 mM Tris-HCl, 1.5 M NaCl, 25 mM $CaCl_2$, pH 8.4) to the glutahione-Sepharose column where the fusion protein was bound. DTT was also added to the resin and thrombin mixture at a concentration of 0.3 mM. The thrombin was allowed to mix with the resin by agitation for 16 hours at 20° C.

Since CLIC1 was no longer bound to the column by the GST fusion protein the cleaved CLIC1 was recoverable in a mixture containing thrombin. This CLIC1-thrombin mix was collected and ready for separation using DEAE anion exchange chromatography. The GST and any uncleaved fusion protein that remained on the glutathione-Sepharose column was eluted using 10 mM reduced glutathione in 50 mM Tris-HCl, pH 7.5. The CLIC1-thrombin mixture was separated using a DEAE column attached to a Äktaprime purification system (Amersham® Biosciences). The column was pre-equilibrated with 20 mM Tris-HCl, 0.02 % sodium azide, pH 6.5.
Because of the differences in pI of the two proteins (thrombin has a theoretical pI of 8, while CLIC1 has a theoretical pI of 5) it was possible to efficiently separate the proteins based on the fact that at pH 6.5 only CLIC1 will be negatively charged and therefore bind to the positively charged matrix of the DEAE-Sepharose column. Thrombin, which is positively charged at pH 6.5, will pass through the column without binding. The absorbance at 280 nm of the flow through was monitored to ensure CLIC1 was not going straight through the DEAE column and was indeed binding the matrix. With the thrombin component of the mixture not binding the column and coming out with the flow through successful separation was achieved.

The bound CLIC1 was then eluted using high salt concentration buffer (20 mM Tris-HCl, 300 mM NaCl, 0.02 % sodium azide, pH 7.0). Once the protein was recovered its purity and concentration was established, it was concentrated to the desired concentration using a PM-10 membrane at 4° C. The protein sample was then dialysed against 3 changes of storage buffer (50 mM Na_2HPO_4, 1 mM DTT, 0.02 % sodium azide, pH 7.0) to remove the high concentration of sodium chloride present with the protein from the elution off the DEAE-Sepharose column. This dialysis was repeated on a weekly basis to ensure fresh DTT was present in the storage buffer.

2.2.3 SDS-PAGE

The purity and homogeneity of the expressed protein was assessed by SDS-PAGE (Laemmli, 1970). Discontinious gel systems were prepared using a 15 % separating gel (30 % acrylamide, 1 % bisacrylamide, 10 % sodium dodecyl-sulphate (SDS), 10 % ammonium persulphate and 1.5 M Tris-HCl, pH 8.8) and a 4 % stacking gel (30 % acrylamide, 1 % bisacrylamide, 10 % sodium dodecyl-sulphate, 10 % ammonium

persulphate and 0.5 M Tris-HCl, pH 6.8). Before loading to the gel, samples were mixed at a 1:1 ratio with 5 x sample buffer (100 mM β-mercaptoethanol, 20 % (v/v) glycerol, 10 % (w/v) SDS, 0.05 % (w/v) bromophenol blue and 0.5 M Tris-HCl, pH 6.8). Samples were then boiled for 5 minutes to ensure the protein was denatured. 20 µl samples were loaded to the wells and electrophoresed at 120 V for approximately 3 hours. A molecular mass marker containing proteins ranging in size from 14.4 kDa to 116 kDa was also loaded to the gel for calculating the monomeric size of the protein samples. Gels were stained in 2 % (w/v) Coomasie Blue R250 staining solution (13.5 % (v/v) glacial acetic acid and 18.8 % (v/v) ethanol) and and destained using a solution of 40 % (v/v) ethanol and 10 % (v/v) glacial acetic acid until the background of the gel was clear.

2.2.4 Concentration determination

The concentration of CLIC1 was determined spectrophotometrically using the Beer-Lambert law:

$$A=\varepsilon_{\lambda} c l \qquad (1)$$

where A is the absorbance at 280 nm, ε_{λ} is the molar extinction coefficient of the protein at wavelength λ, c is the concentration of the protein and *l* is the pathlength of light through the cuvette. The molar extinction coefficient of CLIC1 was determined by using the extinction coefficients of tryptophan, tyrosine and cysteine residues of the protein (Mach *et al.*, 1995):

$$\begin{aligned} \varepsilon_{(280)}\,(M^{-1}cm^{-1}) &= 5550\Sigma Trp + 1340\Sigma Tyr + 150\Sigma Cys \qquad (2)\\ &= 5550(1) + 1340(8) + 150(6)\\ &= 17170\ M^{-1}cm^{-1} \end{aligned}$$

The absorbance at 280 nm was determined using a Hewlett Packard model 8452A diode array spectrophotometer by fitting a linear regression to a series of 5 serial dilutions. All readings were corrected for buffer absorbance.

2.2.5 SEC-HPLC

The molecular mass of the protein was assessed using a LKB 2150 pump (Pharmacia) at a flow rate of 0.5 ml/min attached to an TSK G2000 SW_{XL} size exclusion column (TOSOHAAS) with a 5 –150 kDa resolution. Samples running through the column

were detected using a JASCO FP-2020 Plus intelligent fluorescence detector. Typically, 5 μM concentrations of protein were loaded to the column followed by de-gassed HPLC buffer (0.1 M Na_2HPO_4, 0.05 % sodium azide) with the salt concentration and pH of the buffer adjusted accordingly. Sensitivity settings for the fluorescence detector were set at 32 for attenuation and 100 for gain.

With a flow rate of 0.5 ml/min and a chart speed of 30 cm/hr the molecular mass of samples was determined based on retention time and using a standard curve prepared from known mass markers.

2.2.6 Preparation and purification of dimeric CLIC1

Dimeric protein was prepared and purified according to the method by Littler and co-workers (2004). Purified monomeric CLIC1 was incubated with hydrogen peroxide in order to expose the protein to oxidizing conditions that have been shown to create a dimeric species of CLIC1 (Littler *et al.*, 2004). 2 ml of monomeric CLIC1 at 60 μM concentration was incubated with 500 μl of 0.8 mM hydrogen peroxide for 1 hour. This results in the formation of mixed CLIC1 species consisting of approximately 67 % dimeric CLIC1 and 33 % monomeric CLIC1. In order to separate the mixed species to obtain a sample of pure dimeric CLIC1, the 2.5 ml mixture was diluted with 3 ml of buffer (50 mM Na_2HPO_4, 0.05 % sodium azide, pH 7.0) and loaded to a Sephacryl S-200 high resolution column with a fractionation range of 5 – 250 kDa. Fractions were collected and their absorbance at 280 nm was determined. Based on the size difference between monomer and dimer, the dimeric species will come off the column before the monomeric species and successful separation can be achieved. Approximately 6 ml of pooled CLIC1 dimer at 8 μM concentration was obtained from a typical purification.

2.2.7 pH adjustment

All monomeric protein from purifications was stored in 50 mM Na_2HPO_4, 1 mM DTT, 0.02 % sodium azide, pH 7.0 and dialyzed against the same buffer with fresh DTT weekly. For experiments at pH 5.5 the same buffer was adjusted by adding orthophosphoric acid until the required pH level was reached. Ten column volumes of this pH 5.5 buffer was then used to equilibrate a 2 ml PD-10 size exclusion column. A

maximum volume of 0.5 ml protein was added to the column and allowed to flow through the column. Fractions were collected in 500 µl volumes and protein was detected by using Protein Assay Dye Reagent Concentrate (BioRad). This brown reagent turns blue when it binds protein and in so doing provides a method to detect protein-containing fractions. The dye was diluted 5-fold with water and 8 µl of each collected fractions was added to test if it contained protein. The protein-containing fractions were then pooled and the protein concentration determined. The lowered pH of the pooled protein was verified by doing a pH measurement using a Crison micropH 2000 electrode.

2.2.8 Liposome and micelle preparation

Two types of liposomes with different lipid compositions were used for experiments:

1) Cholesterol-containing liposomes composed of POPC and DOPG lipids were purchased in a pre-liposome formulation (Sigma). This ready-made liposome preparation only required the addition of 1 ml buffer followed by vortexing for 5 minutes to yield a liposome solution containing multilamellar vesicles (MLV) with total lipid concentration of 16.6 mM. This milky solution was then subjected to sonication in an ultrasonic waterbath for approximately 45 minutes or until the solution was clear. This indicates the formation of small unilammelar vesicles (SUV) that were stored at 4°C for a maximum period of 1 week before use. The size of the liposomes were determined using dynamic light scattering techniques (see section 2.2.12) thus verifying that SUV's had formed.

2) Asolectin vesicles containing no cholesterol were prepared using asolectin type IV (Sigma). 20 mg of asolectin (L-α-phosphatidylcholine) was solubilised in 100 µl of chloroform by vortexing briefly. The solution was then coated onto the sides of a glass test tube by rotation under a stream of nitrogen. The thin film on the test tube was then dryed under vacuum overnight to remove any remaining chloroform from the solution. The lipid film was resuspended in 1 ml buffer containing 50 mM Na_2HPO_4 adjusted to the required pH (either pH 7.0 or pH 5.5). The resulting milky solution was then sonicated using a ultrasonic waterbath for approximately 45 minutes or until the solution turned clear to produce SUV's. The formation of SUV's

by sonication was verified by dynamic light scattering. The asolectin liposomes were stored at 4° C for up to 1 week before use.

Micelles provided an alternative membrane model system to the liposomes and were prepared using an anionic detergent. Sarkosyl (N-laurylsarcosine) is a detergent that forms micelles when at concentrations above 2.3 mM, which is the compounds critical micellar concentration (CMC). A stock solution of 10 % sarkosyl (343 mM) was prepared using a buffer containing 50 mM Na_2HPO_4, 1 mM EDTA adjusted to either pH 7.0 or pH 5.5 depending on the experiment. The solution was stored at 4° C.

2.2.9 Fluorescence studies

Fluorescence is the phenomenon by which a molecule emits radiation or light at a lower energy to which it was absorbed. This emission results from the return of an unpaired electron from the excited to the ground state (Lakowicz, 1983). A mechanism by which the excited molecules can relax back to the ground state is by transferring the excitation energy to the surrounding medium. This will result in areduction or quenching of the fluorescence intensity. Naturally occurring fluorophores are the amino acids tryptophan, tyrosine and phenylalanine found in proteins. Because the quantum yield of tryptophan is more than double that of tyrosine, this residue usually dominates the fluorescence of most proteins. Phenylalanine, on the other hand, has a very small quantum yield and its emission is often negligible (Lakowicz, 1983). Because the indole ring of tryptophan is highly sensitive to solvent polarity this residue can be used as an indicator of changes occurring in the polarity of the surrounding environment and the tertiary structure of the protein.

All fluorescence measurements were conducted using a Perkin-Elmer Luminescence Spectrometer LS50B with FLwinlab v4.00. All experiments were performed at 20°C with excitation and emission slit widths set at 5nm. Readings were taken in a quartz cuvette with a 1 mm path-length containing protein solutions varying in concentration between 2 μM and 5 μM. Data was corrected for the relevant buffer used and spectra were measured as an average of 3 accumulations at a scan speed of 150 nm/min. Spectra were recorded in the wavelength range of 280 nm and 450 nm. Protein was

excited at 280 nm since this resulted in a combined tryptophan and tyrosine excitation and yielded stronger signals compared with excitation at 295 nm, which would only excite the lone tryptophan residue of CLIC1 and thus give a very weak signal.

2.2.10 Far-UV circular dichroism spectroscopy studies

The conformation of proteins and peptides in solution can be analysed by the differential absorption of left- and right-handed circularly polarised light by optically active groups within the protein. Optical activity in proteins arises from disulphide groups, aromatic side chains and the peptide backbone (Woody, 1995). Characteristic absorption bands for disulphide groups and aromatic amino acids are found in the wavelength range of 250-300 nm(near-UV range), while the absorption bands for the peptide backbone is found in between 170-250 nm (far-UV range). Secondary structural elements in protein molecules have distinctive CD spectra in the far-UV region. Proteins with a high α-helical content display characteristic minima at 208 and 222 nm with a strong positive band near 190 nm (Woody, 1995).

All far-UV CD measurements were carried out using a Jasco J-810 spectropolarimeter running Spectra Manager for Windows v1.50 software. Protein at a concentration ranging from 1 μM – 5μM in CLIC1 storage buffer (50 mM Na_2HPO_4, 1 mM DTT, 0.02 % sodium azide) at pH 7.0 or pH 5.5 was used. All spectra were recorded using a 2 mm path-length quartz cuvette at 20° C. An average of 10 scans was taken at a scan speed of 100 nm/min. Data pitch was set at 0.2 nm and the bandwidth used was 1 nm. Typically, ellipticity was measured from 190 nm – 250nm, however, in some cases a high noise to signal ratio made it impossible to record readable spectra below 210 nm. Every attempt was made to reduce noise signal and in some cases required a 10-fold dilution of the buffer. All spectra were corrected for buffer and normalised by calculating the mean residue ellipticity [θ] using the following equation:

$$[\theta] = (100 \times \theta)/cnl \qquad (3)$$

where (θ) is the ellipticity signal in mdeg, c is the protein concentration in mM, n is the number of residues in the protein chain and *l* is the pathlength in cm.

2.2.11 Unfolding and refolding kinetics by manual mixing

Kinetic measurements involve the measurement of a single parameter over time. For fluorescence kinetic studies the change in emission at 345 nm was monitored since this is the wavelength that exhibited a maximum emission for native CLIC1. Kinetic studies using CD involved measuring the change in ellipticity at 222 nm. This is the wavelength that shows a characteristic minimum ellipticity for predominantly α-helical proteins such as CLIC1.

Unfolding kinetic studies were performed by adding a final concentration of 8 M urea to 2 μM CLIC1 and immediately starting the measurement. Measurements were taken over 60 minutes. A manual mixing time of approximately 4 seconds prevented the collection of data within this initial period. Baselines were established for folded protein (no denaturant) and completely unfolded protein (2 μM CLIC1 incubated with 8 M urea for 1 hour). All unfolding traces were fitted using single and double exponential equations by SigmaPlot v 8.0 and the data was analysed for best fit.

Refolding kinetic studies were performed by taking completely unfolded CLIC1 (10 μM CLIC1 incubated with 6 M urea for 1 hour) and diluting the sample 10 fold with buffer. This dilution resulted in a final concentration of 1 μM CLIC1 in 0.6 M urea, and therefore is driven to refold. Measurements were started as soon as the dilution buffer was added. Baselines were established for 1 μM folded protein (in 0.6 M urea) and completely unfolded protein (1 μM CLIC1 incubated with 6 M urea for 1 hour). The refolding kinetic trace was fitted using a single exponential equation by SigmaPlot v 8.0.

2.2.12 Dynamic light scattering

All dynamic light scattering (DLS) experiments were performed using a Malvern Instruments (Worcestershire, UK) Zetasizer Nano-S machine with 90° scattering angle optics. Samples were prepared to a final volume of 1.5 ml and all readings were taken in a square glass cuvette at 20° C. 5 μM CLIC1 concentrations were used for samples containing protein. Depending on the experiment, final concentrations of either 37.3 mM sarkosyl (micelles), 8.3 mM cholesterol-containing liposomes or 12.9 mM asolectin vesicles were used. The refractive index, using a refractometer, and the

absorbance value at 640 nm for each sample were pre-determined. Count rate was set at 43 Kcps and attenuator at 11. Data was analysed and interpreted using Dispersion Technology Software v.4.00. The hydrodynamic size (diameter) of CLIC1 and vesicles/micelles was determined based on an average of 5 runs.

2.2.13 Isothermal titration calorimetry

Isothermal titration calorimetry (ITC) is a powerful tool for measuring thermodynamic parameters of biomolecular interactions. The use of ITC to investigate the thermodynamics of association between proteins and lipid vesicles (liposomes) has been well documented (Ramsay *et al.,* 1986; Plagar and Nelsestuen, 1994; Dimitrova *et al.,* 2000; Dimitrova *et al.,* 2002; Saito *et al.,* 2004). Because ITC allows the direct measurement of the enthalpy of the reaction, the heat effects accompanying the association and insertion of proteins into membranes can be used to gain valuable insight into the nature and strength of the interaction.

All calorimetric studies were conducted using a VP-ITC MicroCalorimeter from MicroCal Incorporated. Raw data obtained from the calorimetric experiments were collected and integrated using ORIGIN software. Baselines were adjusted manually and heat of dilution effects were subtracted from the data. The integrated data were fitted to a variety of binding models and the best fit was selected. Parameters such as Gibbs free energy (ΔG), binding constant (K_a), enthalpy change (ΔH), entropy change (ΔS) and stoichiometry (N) of the binding reaction are then determined. The ΔG of a binding reaction is related to the equilibrium binding constant (K_a) using the equation:

$$\Delta G = -RT\ln K_a \qquad (4)$$

where R is the universal gas constant (1.987 cal/mol/K or 8.314 J/mol/K) and T is the absolute temperature. The free energy change (ΔG) is associated with the enthalpy (ΔH) and entropy (ΔS) by the following equation:

$$\Delta G = \Delta H - T\Delta S \qquad (5)$$

These thermodynamic parameters provide valuable information about the association events of proteins with ligands, inhibitors or vesicles.

ITC was used to obtain a detailed thermodynamic profile of CLIC1 interacting with liposomes and micelles. In all experiments the protein was extensively dialysed at

4º C against 2 litres of storage buffer at the appropriate pH as described in section 2.2.2. Protein concentration was determined spectrophotometrically at 280 nm and corrections due to light scattering effects were taken into account.

For experiments involving CLIC1 and POPC/DOPG/cholesterol liposomes, optimisation of the experimental conditions to produce useable data (signal > 0.2 μcal/sec) included varying the CLIC1 protein concentration in the sample cell from a range of 13 μM – 206 μM, and varying the volume of liposomes (16.6 mM lipid concentration) injected from 5 μl – 15 μl. After sampling a variety of conditions a useable signal was only obtained for 93 μM CLIC1 titrated with 7 μl and 15 μl injections of liposomes at pH 7.0 and pH 5.5, respectively.

Similar conditions as those optimised from the POPC/DOPG/cholesterol liposomes were used for studies involving CLIC1 and asolectin vesicles. Typically, protein at approximately 100 μM concentration was titrated with 7 μl injections of asolectin with a 25.8 mM total lipid concentration.

Micelles were prepared as a 10 % sarkosyl solution in buffer adjusted to either pH 7.0 or pH 5.5. In all experiments performed, the micelles were injected in 4 μl increments into the ITC sample cell containing the protein until complete saturation had occurred. The reference power was set to 15 μcal/sec unless otherwise stated and the initial delay was 60 seconds. The spacing between injections was set to 260 seconds and stirring speed was kept constant at 310 rpm. All experiments were performed at 25º C unless otherwise stated.

For studies involving NEM-modified CLIC1 with micelles, the modified protein was prepared as follows: A final concentration of 66 mM NEM was mixed with 80 μM CLIC1 and allowed to incubate for 10 minutes. The solution was then run through a G-25 size exclusion column using the AKTÄ system to separate the NEM-modified protein from free NEM. The reaction with NEM was followed spectrophotometrically by the decrease in the NEM absorbance maximum at a wavelength of 300 nm, and this provided evidence for the successful separation of NEM-modified CLIC and free NEM.

2.2.14 Deuterium exchange mass spectrometry

Deuterium Exchange Mass Spectroscopy (DXMS) is a recently optimised and specialised technique used for analysing a protein's structural dynamics (For reviews see Woods and Hamuro, 2001; Garcia *et al.*, 2004; Busenlehner and Armstrong, 2005). Because of the idiosyncratic nature of proteins, it is often difficult or even impossible to analyze structural characteristics using current methods alone. DXMS involves using mass spectrometry along with extensive computational analysis to measure deuterium exchange activity for a given protein. Hydrogen exchange is the basis of DXMS and refers to the ability of hydrogen atoms within a protein, specifically amide/backbone protons, to continuously and reversibly interchange with hydrogen in the surrounding solvent (Hvidt and Linderstrom-Lang, 1954). By using a heavier isotope of hydrogen such as deuterium, the increased mass will be incorporated by the protein and can be detected through mass spectrometry (Zhang and Smith, 1993). Thus the rate of exchange can be measured, which provides valuable information about the structural dynamics of the protein. The rate of exchange occurs at a specific rate, which is a function of protein structure and solvent accessibility (Englander and Poulsen, 1969). Since exchange is based on time, more readily accessible areas of the protein will exchange first, while regions buried deep in a hydrophobic region of the protein will exchange much later.

Amide hydrogen exchange techniques are unparalleled in their ability to probe sub-molecular protein dynamics. This information can be used to refine inferences drawn from high resolution structural studies such as x-ray crystallography (Pantazatos *et al.*, 2004; Spraggon *et al.*, 2004), and can provide unique insights when structural information is unavailable for environmental specific conditions (e.g. pH).

All DXMS experiments were performed at the Woods' Laboratory at the University of California San Diego, School of Medicine. The optimised methodologies of this automated high-throughput, high-resolution system termed Deuterium Exchange Mass Spectrometry (DXMS) are well documented (Black *et al.*, 2004; Hamuro *et al.*, 2004; Burns-Hamuro *et al.*, 2005; Del Mar *et al.*, 2005; Derunes *et al.*, 2005; Garcia *et al.*, 2005; Iyer *et al.*, 2005; Wong , *et al.*, 2005; Yang *et al.*, 2005; Begley *et al.*, 2006; Brudler *et al.*, 2006; Derunes *et al.*, 2006; Melnyk *et al.*, 2006).

Tuning of CLIC1 proteolytic fragmentation (digestion optimisation)

Prior to studying the hydrogen-exchanged samples, digestion conditions that produced CLIC1 fragments of optimal size and distribution for exchange analysis were established. CLIC1 protein samples were exposed to 0.5M, 1M, 2M and 4M GuHCL in order to establish the most optimal concentration of denaturant to be used in the quench solution. Samples contained 1 part protein, 3 parts buffer (150 mM NaCl, 8.3 mM Tris, pH 7.2) and 6 parts quench solution. All samples were prepared in triplicate.

Optimal pepsin digestion for CLIC1 was obtained using a 1M final concentration of GuHCL in 0.8 % (v/v) formic acid and a digestion duration of 20 seconds over immobilised pepsin. For the pH 7.0 CLIC1 sample 174 peptides suitable for DXMS analysis were generated and covered the entire amino acid sequence of the protein. The pH 5.5 sample generated 160 peptides with 100% coverage of the amino acid sequence.

Deuterium exchange experiments

Once the optimal conditions for digestion were determined and adequate peptide maps generated, preparation for on-exchange experiments took place. Figure 12 shows a schematic for the preparation of deuterium exchange. Deuterated samples were prepared at 0 °C by diluting 15 µl of CLIC1 with 45 µl of deuterated buffer (10 mM HEPES, pD 7.0 or 5.5, 150 mM NaCl), followed by "on-exchange" incubation for varying times prior to quenching in 90 µl of 0.8 % formic acid, 1 M GuHCL, 0 °C. Incubation times for the CLIC1 pH 7.0 samples were 10, 30, 100, 300, 1000 and 3000 seconds. For the CLIC1 pH 5.5 samples the same time points were used but also included the extended time points of 9000, 30000 and 90000 seconds because of the slower exchange rate at the lower pH. Samples with a final volume of 150 µl containing 0.50 mg/ml CLIC1 (pH 7.0) or 0.34 mg/ml CLIC1 (pH 5.5) were then subjected to DXMS processing as above, along with control samples of non-deuterated and fully-deuterated CLIC1 (incubated in 0.5 % formic acid in 95 % deuterium overnight at 22 °C). Corrections for back-exchange were made employing the methods of Zhang & Smith (1993). Figure 13 shows an outline and summary of the procedures used for DXMS.

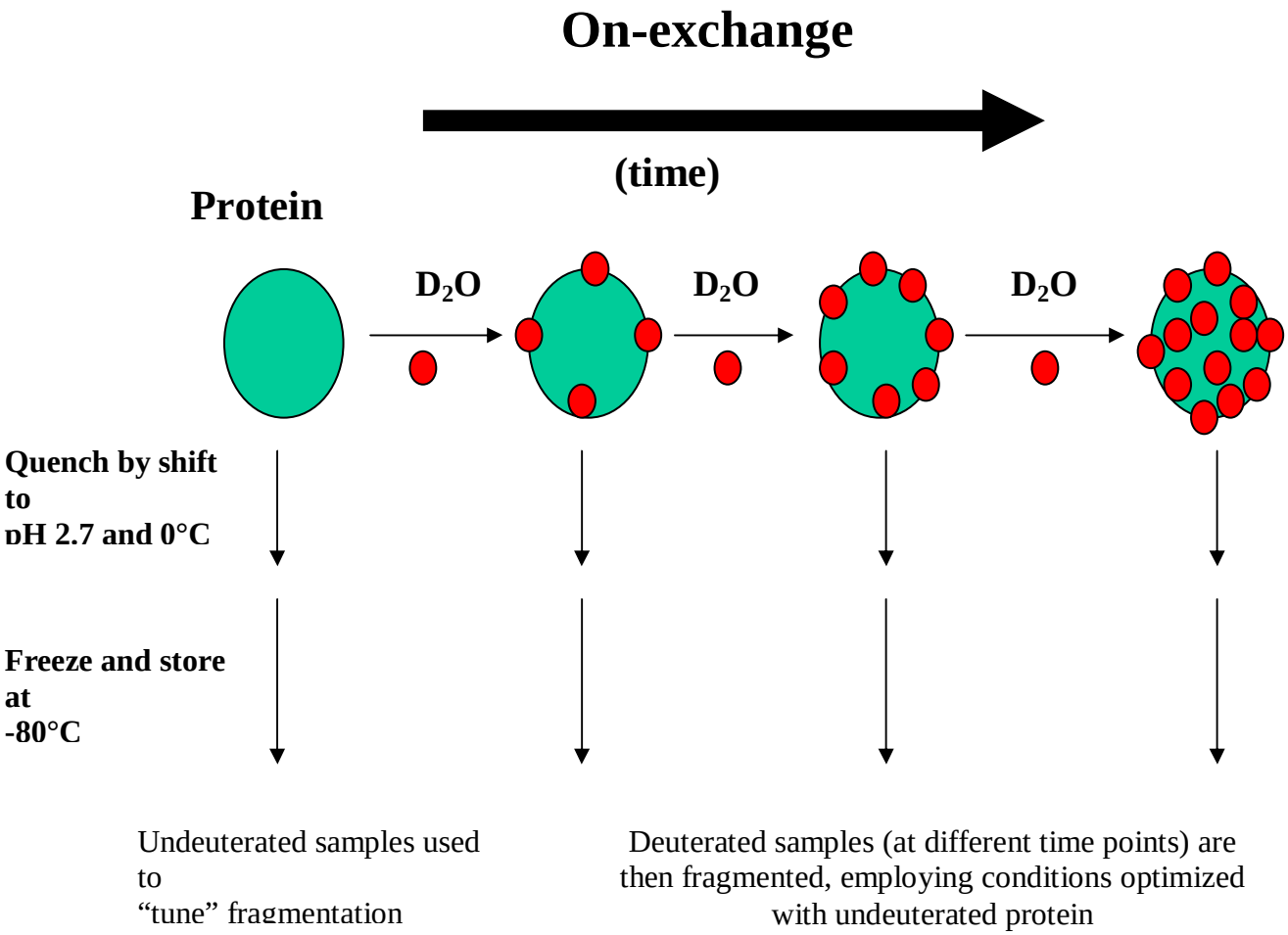


Figure 12: Graphic showing deuterium "on-exchange" with protein.

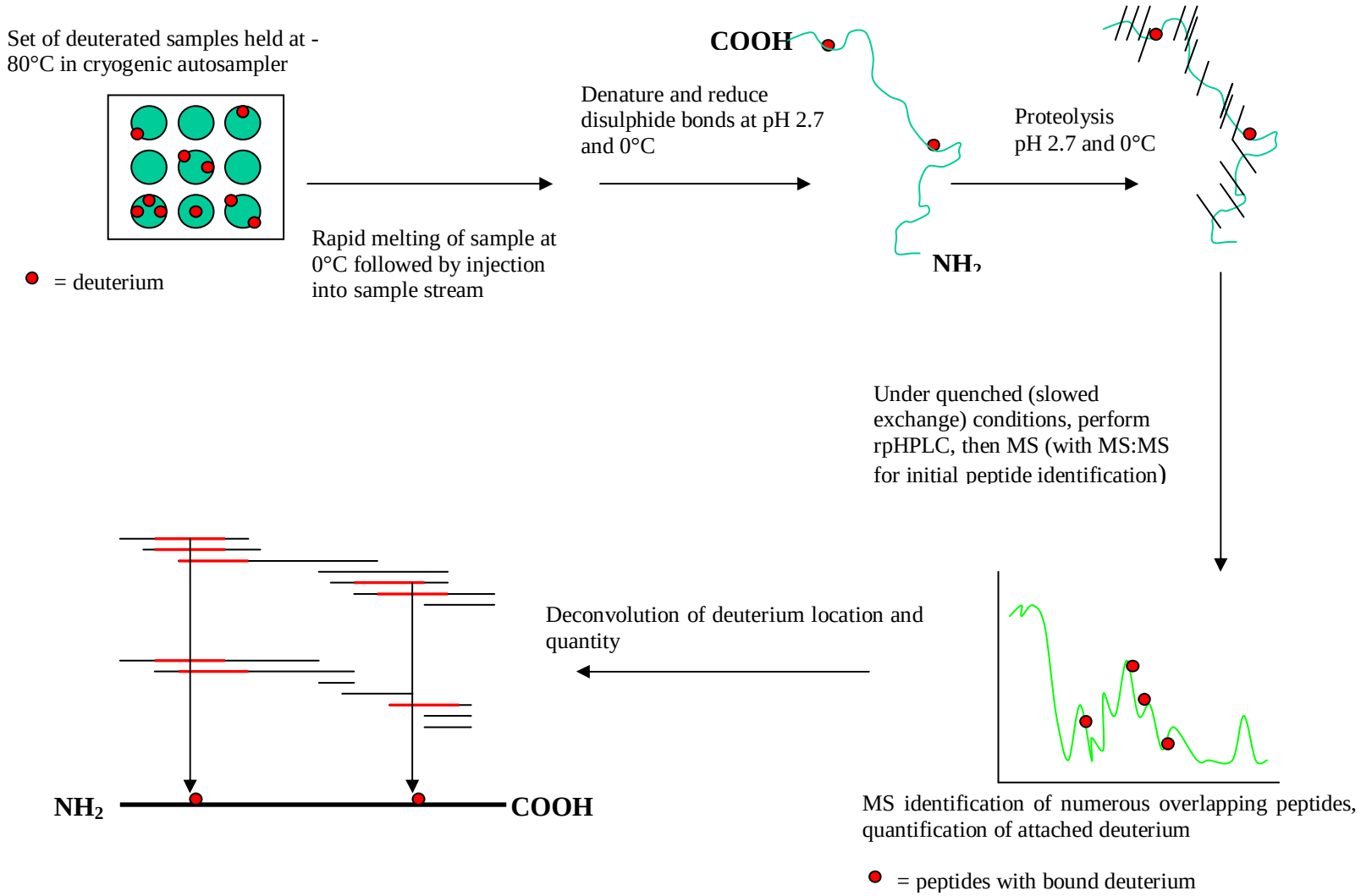


Figure 13: Flow diagram showing the procedure for protein structure analysis using hydrogen exchange mass spectrometry.

General operational procedure

A 30 µl hydrogen-exchanged protein solution was quenched by shifting the pH to 2.3 and the temperature to 0 °C with 60 µl of 0.8 % formic acid with various concentrations of GuHCL (0.5 – 4 M). At 0 °C, a final volume of 100 µl quenched solution containing 0.8 mg/ml CLIC1 (pH 7.0) or 0.5 mg/ml CLIC1 (pH 5.5) was passed over a 66 µl solid-phase pepsin column with 0.05 % trifluoroacetic acid (TFA) at 200 µl/min for two minutes with collection of proteolytic products by a C18 column. Subsequently, the C18 column was eluted with a linear acetonitrile gradient (10% - 50%). Mass spectrometric analyses were carried out with a Finnigan LCQ mass spectrometer with capillary temperature at 200 °C. The sequences of pepsin-generated peptides were determined by acquisition and analysis of data dependent MS / MS data sets obtained from quenched, undeuterated protein, and isotopic envelope centroids of peptides from deuterated samples were determined from raw LCMS1 data, employing specialised DXMS data reduction software developed in collaboration with Sierra Analytics, LLC, Modesto, CA.

Computational analysis

Once all the samples were run, computational analysis using a variety of programs was undertaken to transform the raw mass spectrometry data into useful information about the protein. After obtaining the proteins amino acid sequence in FASTA format, a SEQUEST file was generated. These files identified the protein in the raw mass spectrometer data. A SEQUEST file determined the amino acid sequence and thus the peptide that corresponds to the mass spectrum being analysed. Once peptides from the raw mass spectrometry data were identified they were evaluated for accuracy. A template or pool was created by combining all the peptides identified by SEQUEST.

The quality of the peptides were examined and scored based on how they compared to the theoretical data and specific criteria (Figure 14). Scoring was performed as follows:

Score 0 – Correct peptide, good quality, perfect match to predicted graph, normalisation greater than 30 for charge state +1.

Score 1 – Correct peptide, poor quality, matches the predicted graph somewhat, lower normalisation level than quality 0.

Score 2 – Incorrect peptide, good quality, distinct pattern yet does not match the predicted graph

Score 3 – incorrect peptide, poor quality, no pattern can be found, low normalisation level, inaccurate results.

Particular values that were checked for quality control were retention time, m/z range, centroid and mapping score. Only peptides scoring a 0 or 1 were used for final analysis. Peptides scoring a 2 were double-checked for misidentification. Collision checks were also performed. A collision occurs when the same peptide is applied to multiple different sequences. Often a peak will appear to match the data but is actually an entirely different peptide. This is an easy mistake to make since fragments from different sequences may have the same weight or similar weight as another fragment. Once collisions were identified, they were checked for accuracy or removed from the experiment entirely.

Sub-localisation of deuterium, as described by Burns-Hamuro and co-workers (2005), was performed to indicate the possible location of deuterium within a peptide. This was done by analysing the peptide maps and looking at overlapping peptides. When two or more analogous peptides occurred, sub-localisation of deuterium was possible by subtraction. For example, if the deuterium incorporation of segment 1-7 and 1-9 at a given time point was known, the subtraction of the two gave the deuterium incorporation in the segment 8-9. If a sequence segment was determined by more than two peptides, the average deuterium incorporation was calculated.

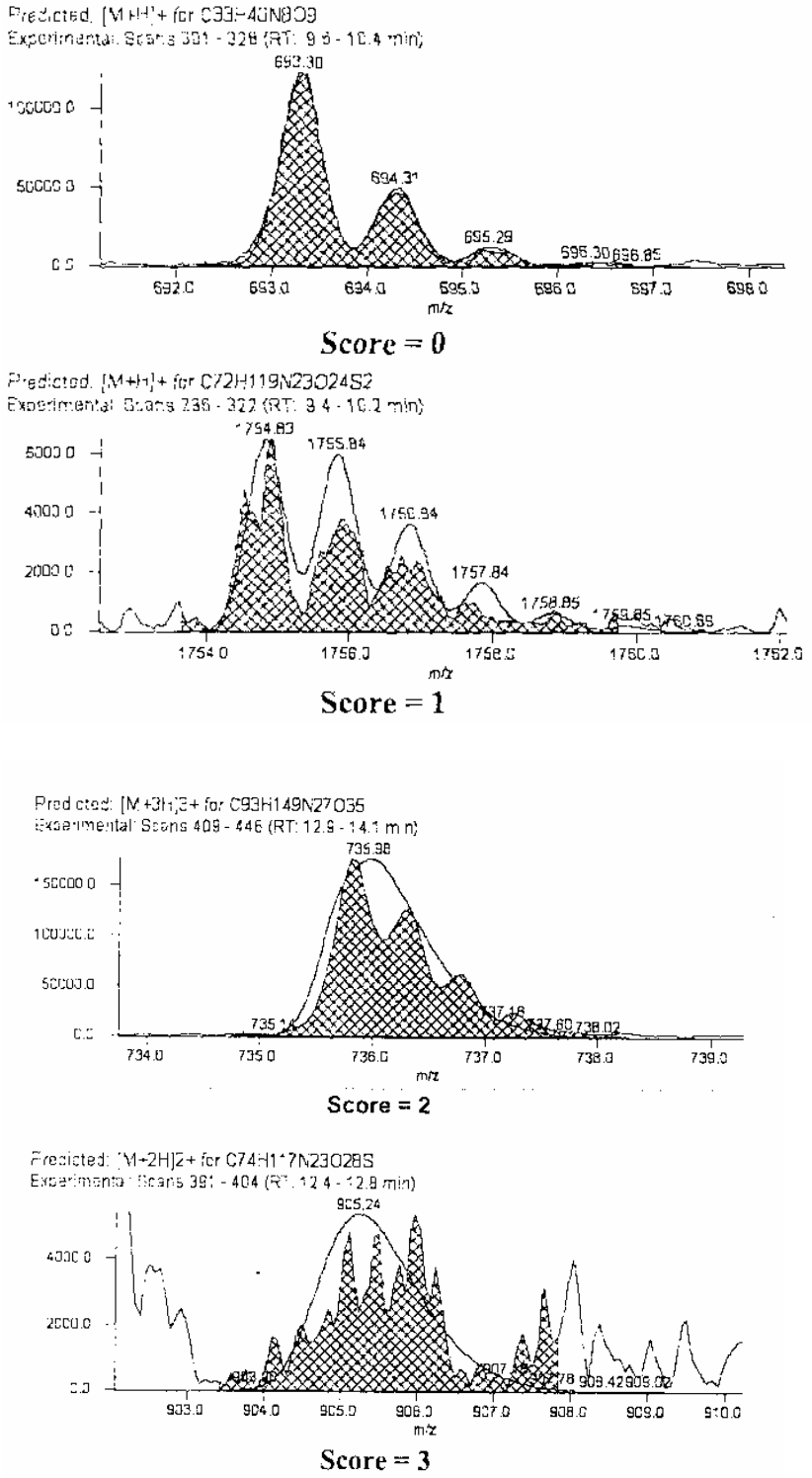


Figure 14: Examples of peptide scoring based on peptide isotope graphs. The theoretical data based on the protein sequence for each specific peptide is shown as an outline. The graph with the shaded area represents the data obtained from the mass spectrometer and scoring is performed based on how well the experimental data fits the theoretical data. Images taken from DXMS instructional manual for collaborators prepared by Woods and co-workers (2005).

CHAPTER 3. RESULTS

3.1 Plasmid Verification

The open reading frame encoding CLIC1 was cloned into the pGEX-4T-1 plasmid (approximately 6000 bp length) that contains a lac operon and therefore confers ampicillin resistance. CLIC1 was expressed as a GST fusion protein that was fused together by a thrombin cleavage site. The fusion protein (approximately 1000 bp length) is flanked on either side by restriction sites *Bam*H1 and *Not*1. The pGEX-4T-1 plasmid containing the open reading frame encoding CLIC1 (Figure 15) was transformed into *Escherichia coli* BL21 cells and DNA from these cells was used for restriction digestion analysis. The restriction enzymes *Bam*H1 and *Not*1 were used to verify the transformation was successful.

Although the results from the restriction digestion analysis (Figure 16) imply that the transformation into BL21 cells was successful (based on the double digest bands being different from the linearised bands), the plasmid was further verified by sequencing. The insert was sequenced at Inqaba Biotech, Pretoria South Africa and the results indicated the correct CLIC1 sequence adjoined to the GST protein (see Appendix, Figure A). The sequencing also showed the additional glycine and serine residues at the amino terminus of CLIC1 as a result of the engineered thrombin cleavage site between CLIC1 and GST that was noted by Harrop and co-workers (2001).

3.2 Protein Over-expression and Purification

Induction studies indicated optimal protein over-expression to occur with 1 mM IPTG added at late log phase (OD_{600} = 1.1) and allowed to grow for a further 5 hours at 37ºC. Cells were then lysed by freezing overnight and sonicating. After centrifugation, the majority of CLIC1 fusion protein was found in the supernatant. The size of the fusion protein was 55.7 kDa according to SDS-PAGE gel analysis (Figure 17), which correlates well with the estimated theoretical mass of 52.4 kDa calculated from the amino acid sequence.

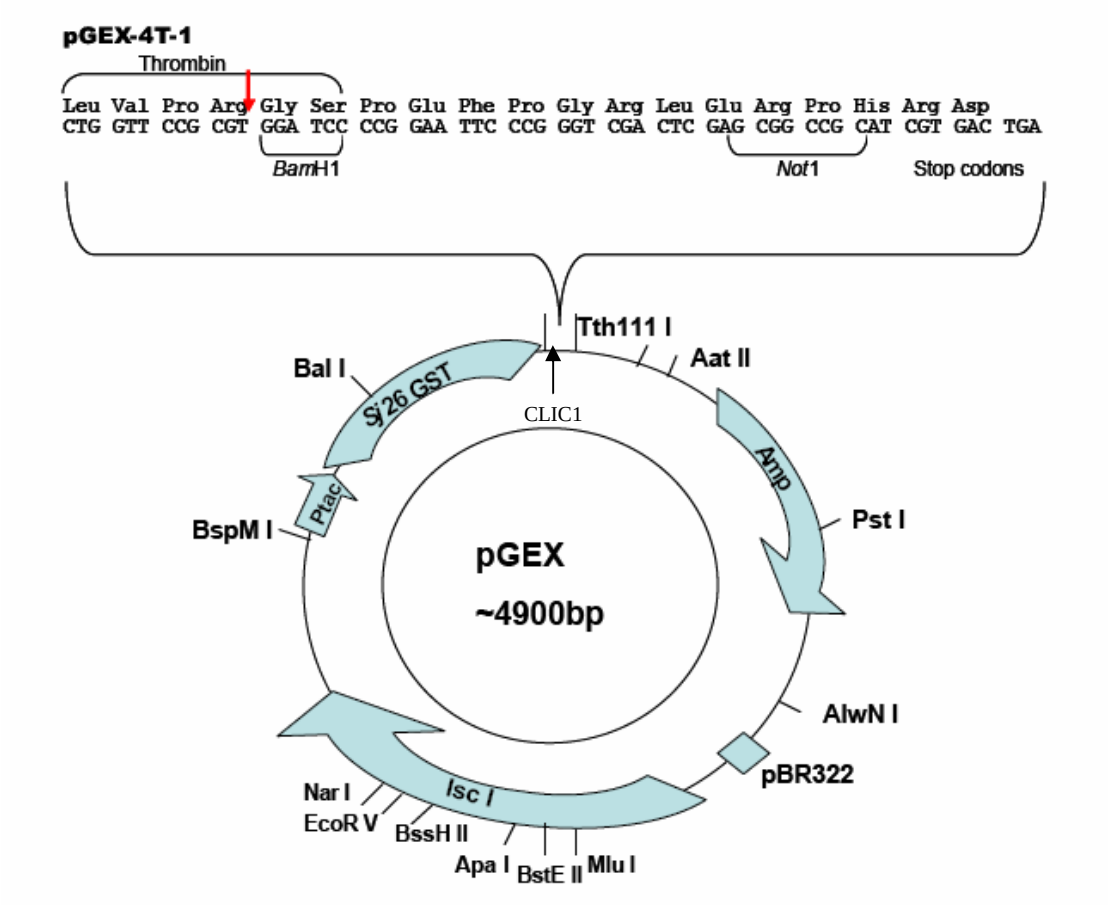


Figure 15: Restriction map of pGEX-4T-1 plasmid encoding CLIC1
A schematic of the plasmid encoding the GST fusion protein (modified from Valenzuela *et al.*, 1997). The thrombin cleavage site joining CLIC1 and GST is indicated in the insert above the plasmid. The restriction sites, *Bam*H1 and *Not*1, flanking the CLIC1 cDNA are also shown.

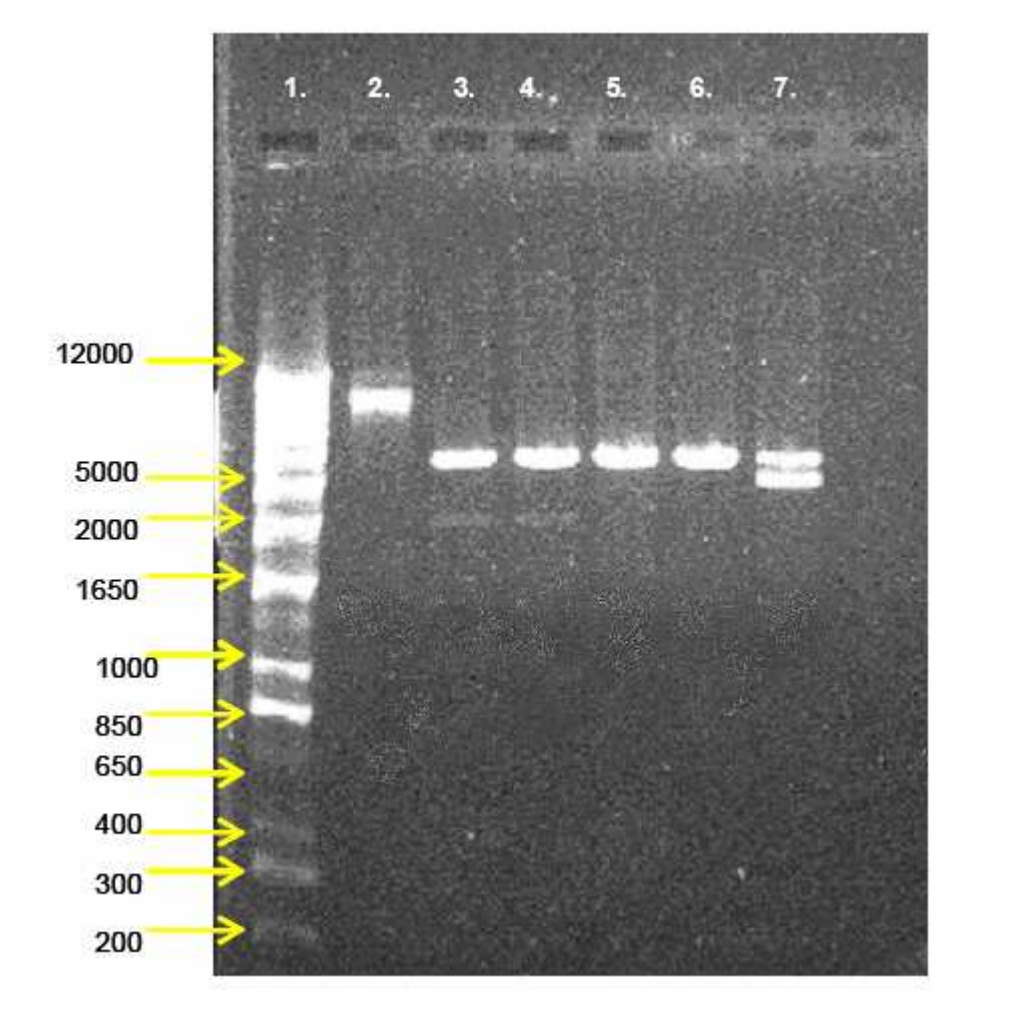
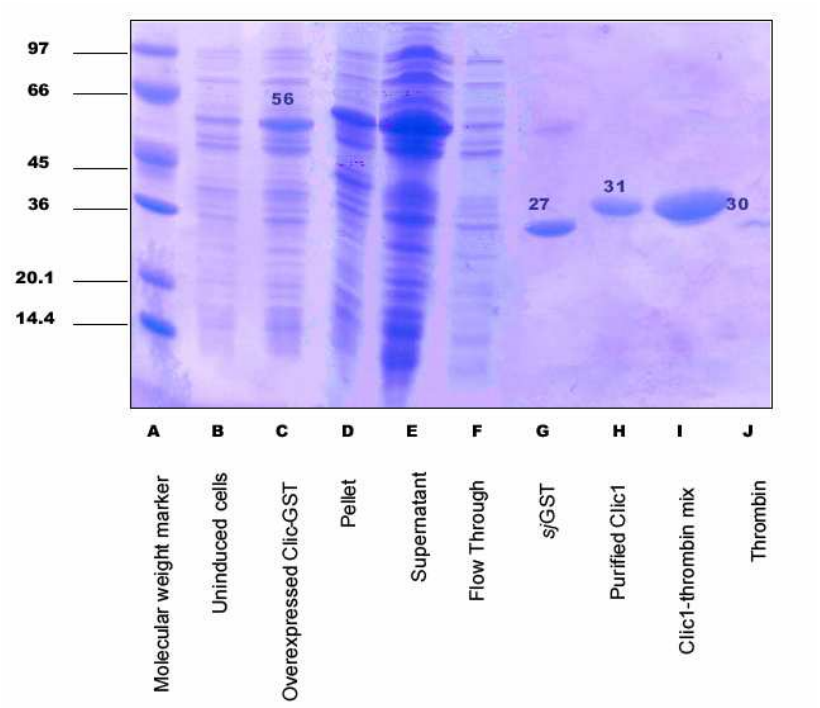


Figure 16: Restriction digestion analysis
The 1% agarose gel stained with ethidium bromide showing the restriction digestion of the pGEX-4T-1 plasmid. Lane 1 shows the DNA marker with sizes ranging from 0.2 kb to 12 kb. Lane 2 shows uncut plasmid. Lanes 3 and 4 show plasmid linearised with *Bam*H1 resulting in a 6 kb band. Lanes 5 and 6 show plasmid linearised with *Not*1 also resulting in a 6 kb band. Lane 7 represents the double digest using both restriction enzymes. The 5 kb band is indicative of the remainder of the plasmid, however, the expected 1.2 kb band for CLIC1 DNA is not visible. Some uncut plasmid is also evident in this lane.

A.



B.

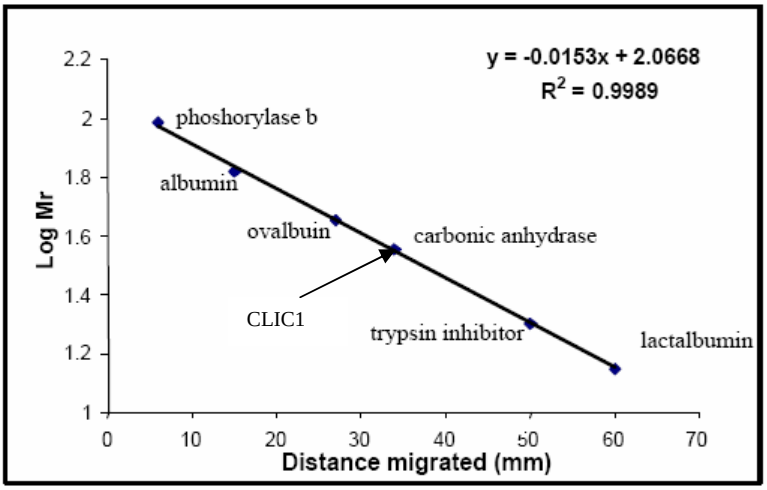


Figure 17: SDS-PAGE analysis of CLIC1 purification
(A). 15% polyacrylamide SDS-PAGE gel stained with Coomassie Brilliant Blue showing representative steps of CLIC1 purification. All samples were diluted two-fold with 5 x sample buffer before loading onto the gel.
(B). SDS-PAGE calibration curve showing the distances migrated by the standard marker proteins

The soluble GST-fusion protein was collected from the supernatant and loaded onto a glutathione-Sepharose column . Lane F in Figure 17 represents the flow through off this column and indicates that the fusion protein bound the column. Cleavage of CLIC1 from GST was successfully accomplished using thrombin, and the CLIC1-thrombin mix was collected. Lane G of Figure 17 shows the band correlating to the 26.5 kDa size of sj26GST after it was eluted from the column with glutathione. Tulk and co-workers (2002) determined the size of sj26GST to be 27 kDa. The fact that there was a negligible amount of protein correlating to the 56 kDa size of the fusion protein indicates that successful cleavage of CLIC1 from GST had taken place.

The collected CLIC1-thrombin mix was then loaded onto a DEAE-Sepharose column to separate CLIC1 and thrombin. Lane J of Figure 17 shows the thrombin that was collected from the flow through. The band correlates to the theoretical molecular mass of approximately 29.7 kDa for thrombin.

CLIC1 remained bound to the DEAE-Sepharose column despite attempts to elute it with acidic buffer with pH values as low as 4.0. Alternate means to elute the protein were necessary since dropping the pH lower than this value would probably irreversibly damage the protein. Elevated salt concentration (300 mM NaCl, pH 7) proved to be an efficient method for eluting CLIC1 (Figure 18). Lane H of Figure 22 shows purified CLIC1 as it was eluted from the DEAE-column. The protein migrated a distance on the SDS-PAGE gel that corresponded to a size of 30.6 kDa, which correlates well with the size of 31 kDa for CLIC1 obtained by Berryman and Bretscher (2000) using SDS-PAGE. It appears that the migration of CLIC1 on polyacrylamide gel is slightly impeded, giving an apparent molecular mass that is slightly larger than predicted. This trend seems to be characteristic of the CLIC family of proteins and may be due to the relatively high acidic nature and low pI of CLICs causing a reduced SDS:protein ratio (Tulk and Edwards, 1998; Edwards, 1999; Berryman and Bretscher, 2000; Nishizawa *et al.,* 2000; Tulk *et al.,* 2000; Board *et al.*, 2004).

Protein yields were approximately 17 mg of purified CLIC1 per litre of culture. A typical purification involving 4 x 2 litre cultures therefore yielded approximately 136 mg of purified CLIC1. This indicates a refinement and optimisation of CLIC1 over-

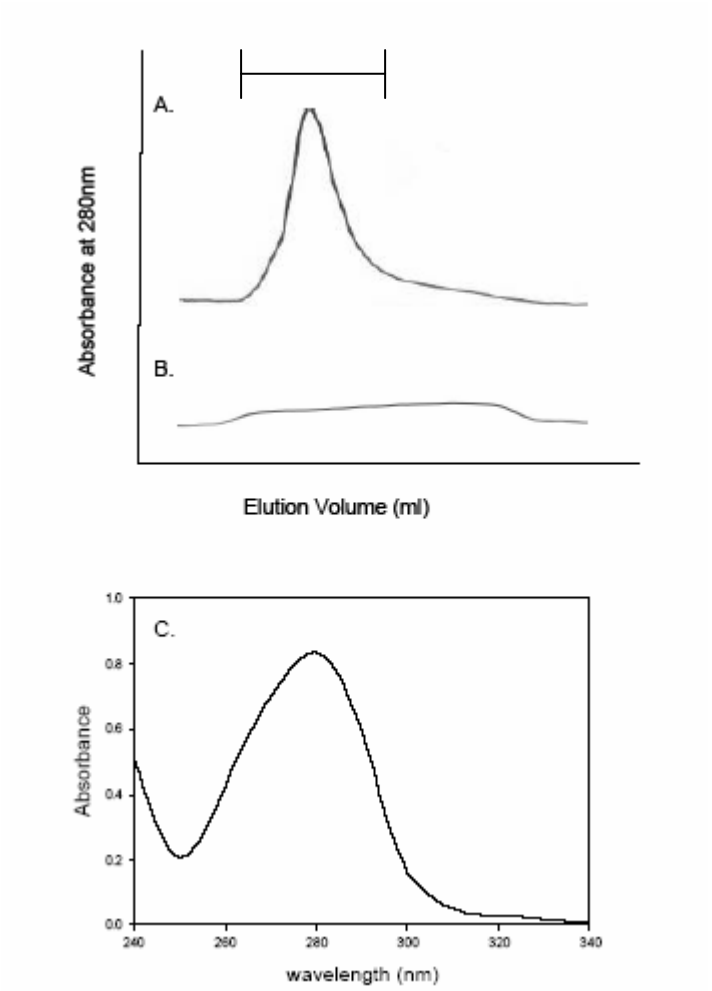


Figure 18: DEAE Sepharose anion exchange column elutions
(A). CLIC1 recovered from the column by elution using high salt concentration buffer (20 mM Tris-HCl, 300mM NaCl, pH 7). The peak area represents 20 ml of eluted CLIC1 and the bar indicates the fractions that were pooled.
(B). Elution of thrombin indicating the successful separation from CLIC1 at pH 6.5.
(C). Purified CLIC1 absorbance spectrum. The absorbance peak at 280 nm had a value of 0.85 that correlates to a protein concentration of 50 μM. No DNA contamination or protein aggregation was evident.

expression and purification based on the protocol by Tulk and co-workers (2000) that only yielded 5 mg of protein per litre of culture.

3.3 REDOX effects on CLIC1

3.3.1 REDOX effects on CLIC1 structure

Upon oxidation, CLIC1 undergoes a transition from monomeric to non-covalent dimer state (Littler *et al.*, 2004). Oxidizing conditions were achieved by addition of H_2O_2 and the resulting dimer was purified as described in the materials and methods (section 2.2.6). Monomeric CLIC1 forms a mixture of monomeric and dimeric species upon addition of hydrogen peroxide. Hydrogen peroxide (0.8 mM) was added to purified monomeric CLIC1 (60 µM) and allowed to incubate for an hour. In order to separate monomer and dimer the mixture was then loaded to a Sephacryl S-200 HR size-exclusion column equilibrated with 50 mM sodium phosphate buffer pH 7.0. Detection at A_{280} showed the dimer coming off in early fractions followed by monomer in later fractions. The dimer fractions were pooled and concentrated yielding 0.8 mg of purified dimeric CLIC1. SE-HPLC showed dimeric CLIC1 to be approximately double the size of the monomeric form (Figure 19). Dimer showed a size of 63.4 kDa compared to 31.1 kDa for monomer in 0.5 M salt. This H_2O_2-induced dimer was the representative used for the oxidised form of CLIC1 in this study. Reduced CLIC1 was obtained by dialysis against buffer containing 1 mM DTT, while non-reduced CLIC1 was dialyzed against buffer containing no reducing agents (50 mM sodium Phosphate, pH 7.0).

Fluorescence spectral properties of the different CLIC1 forms were studied in order to probe any tertiary structural changes that may have occurred. Fluorescence spectroscopy is a powerful tool for obtaining information about the environment of tyrosine, and more specifically, tryptophan residues that are present in proteins. Excitation carried out at 295 nm resulted in the lone tryptophan (Trp35) positioned near the domain interface to be selectively excited. However, because of the low quantum yield produced by exciting a single tryptophan residue, a weak signal was produced. For this reason the protein was excited at 280 nm, which excites both tyrosine and tryptophan residues, resulting in a stronger signal and a

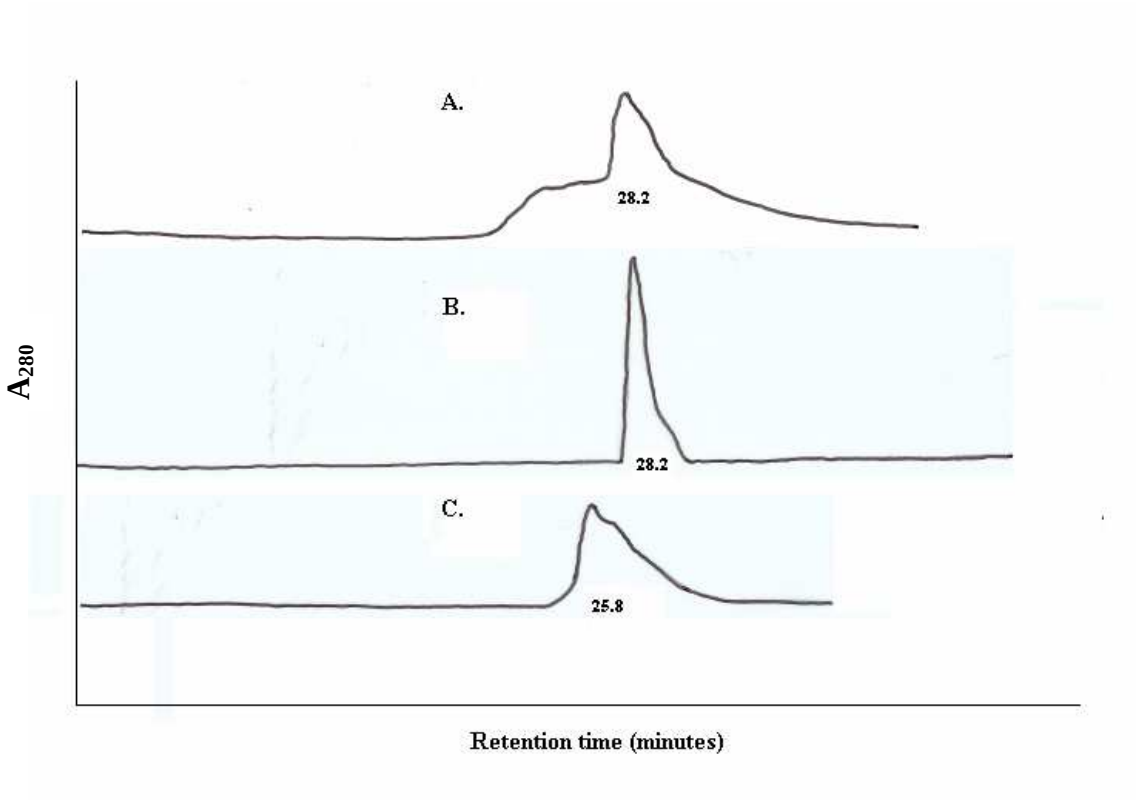


Figure 19: SEC-HPLC elution profiles of CLIC1 forms

A. Non-reduced CLIC1 eluting after 28.2 minutes and corresponding to a size of 31.1 kDa. Also note the shoulder corresponding to 63.4 kDa that may represent some dimeric species formation under non-reducing conditions
B. Reduced CLIC1 eluting after 28.2 minutes and corresponding to a size of 31.1 kDa.
C. Oxidised dimeric CLIC1 eluting after 25.8 minutes and corresponding to a size of 63.4 kDa.

more global reflection of CLIC1 tertiary structure. Furthermore, in the native state the tyrosine residues are in close enough proximity to the tryptophan for fluorescence resonance energy transfer to occur (Lakowitz, 1999).

The emission maximum obtained for reduced CLIC1 in its native form was at 345 nm (Figure 20A). This indicates that the tryptophan is fairly exposed to solvent and correlates well with what we observe in the crystal structure. The fluorescence spectrum for unfolded CLIC1 (denatured using 8 M urea) shows a slight red shift in emission maximum to higher wavelength (347 nm). This indicates that the tryptophan has become fully exposed to the polar solvent upon unfolding. In the unfolded CLIC1 spectrum one can also notice the shoulder at 310 nm indicative of the tyrosines contribution becoming evident as the energy transfer between tyrosine and tryptophan become uncoupled. Fluorescense intensity has decreased approximately 30% in unfolded CLIC1 compared to native protein. This may be due to fluorescence quenching occurring from charged residues coming closer to the tryptophan residue in the unfolded state.

Fluorescence spectra for non-reduced and oxidised CLIC1 show very similar emission maxima compared with reduced CLIC1 (Figure 20B). The non-reduced form shows a slight blue-shift to lower wavelength (344 nm) compared to reduced and oxidised forms that peak at 345 nm. For the oxidised (dimeric) protein a peculiar drop in fluorescence intensity is noticeable. This is probably due to the hydrogen peroxide (H_2O_2) oxidizing the indole ring of the tryptophan reporter, thus decreasing the fluorescence of the residue (Lundbland, 1995). In order to verify that this was the case, the effect of H_2O_2 on N-acetyl-tryptophanamide (NATA) was investigated. Time-drive fluorescence studies using 2 μM NATA were performed, and the effect of H_2O_2 at two different concentrations was established (Figure 21). An immediate (within manual mixing time) drop in fluorescence intensity was apparent when 2 mM H_2O_2 was added to 2 μM NATA. This indicates that H_2O_2 at this concentration has an effect on tryptophan fluorescence intensity. When a lower concentration of H_2O_2 (0.05 mM) was used the effect was much less pronounced.

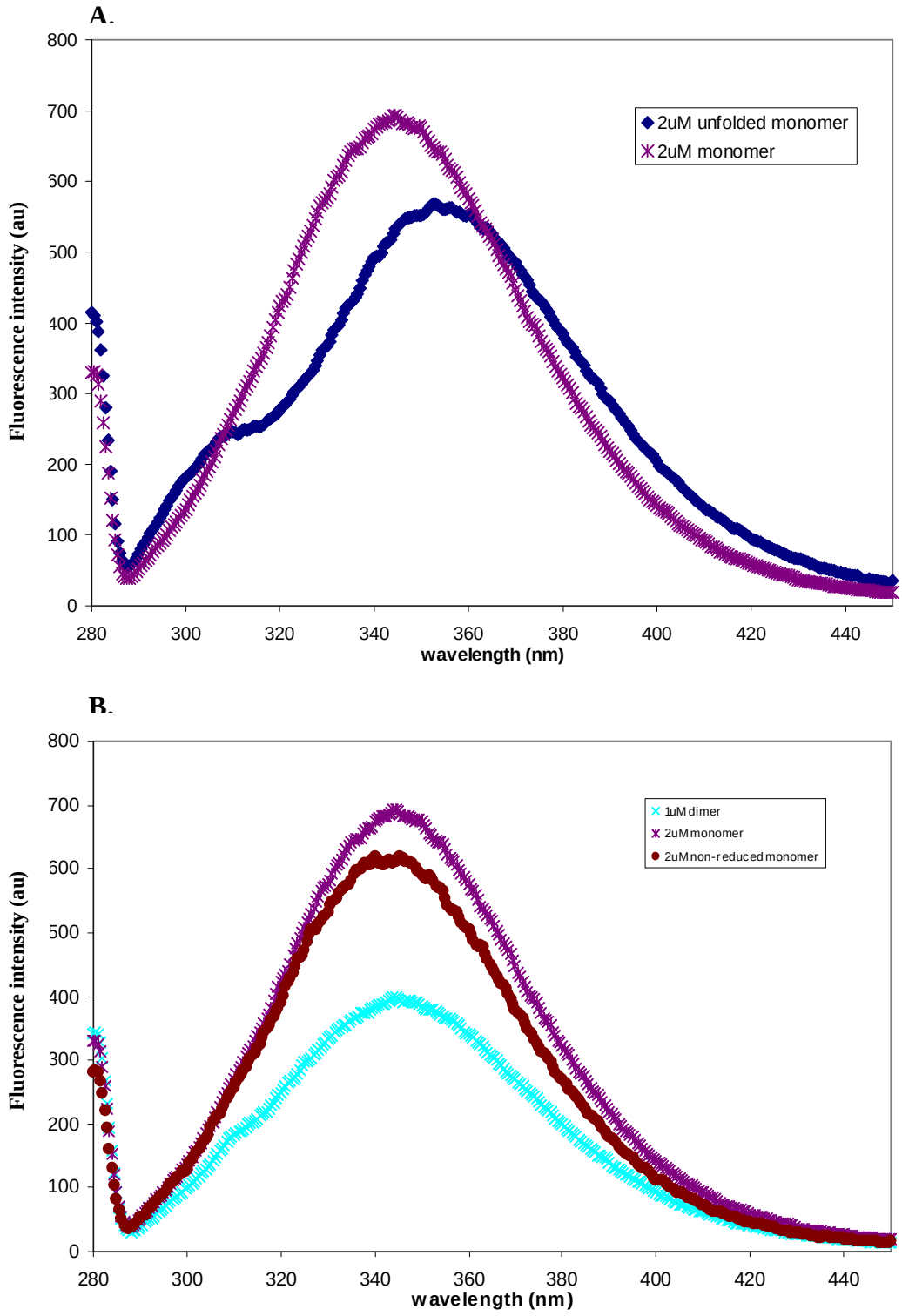
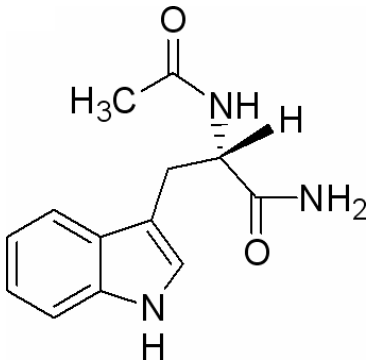


Figure 20: Fluorescence spectra of CLIC1 forms at pH 7.0

A. Fluorescence spectra for 2µM reduced monomeric CLIC1 in native (purple) and denatured (blue) form. All samples were excited at 280 nm. Folded protein emits at 345 nm while unfolded protein emits at 356 nm and exhibits quenched intrinsic fluorescence

B. Fluorescence spectra for native forms of reduced monomer (purple), non-reduced monomer (brown) and oxidised dimer (light blue). Sample concentrations were adjusted to yield 2µM tryptophan concentrations.

A.



B.

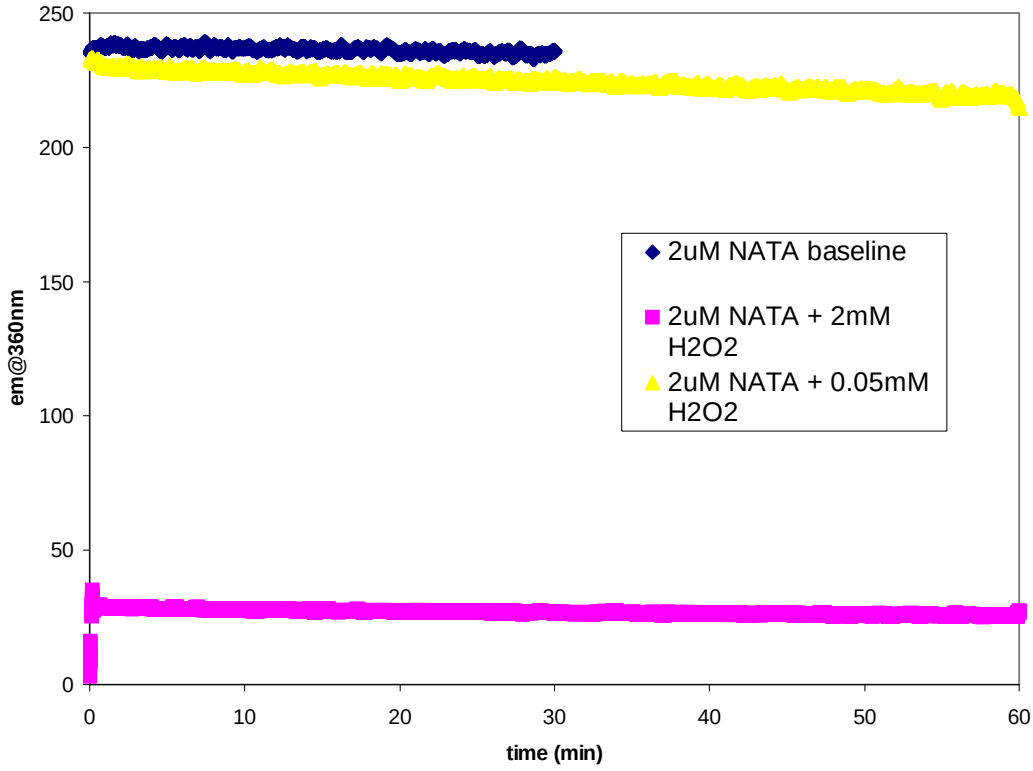


Figure 21: Effect of hydrogen peroxide on tryptophan fluorescence emission using NATA

A. The chemical structure of NATA
B. Fluorescence emission of 2µM NATA (blue) at 360 nm was measured over time and served as a baseline. The effect of adding 2 mM hydrogen peroxide (pink) and 0.05 mM hydrogen peroxide (yellow) to 2 µM NATA was monitored over 1 hour.

Circular dichroism spectroscopy was used as a probe for secondary structure. Ellipticity over the far-UV range (190 nm – 250 nm) was measured and the resulting spectral pattern analysed. The spectra obtained for 2 μM reduced monomer and non-reduced monomer where identical to that for the equivalent concentration (1 μM) of oxidised dimeric form, indicating no difference in secondary structural content between the different CLIC1 forms (Figure 22). All spectral patterns were typical for alpha helical proteins, displaying characteristic minima at 222 nm and 208 nm (Woody, 1995).

3.3.2 REDOX effects on CLIC1 stability

The unfolding kinetics of reduced monomer, non-reduced monomer, and oxidised dimer were investigated using fluorescence and CD spectroscopy. For fluorescence unfolding kinetics the emmision at 345 nm was monitored over time. Baselines for native and completely unfolded proteins were established. The kinetics of unfolding were monitored by adding urea (final concentration of 8 M) to protein.

The monomer unfolding trace fitted best to a single exponential equation suggesting a single unfolding phase with a time constant of 17.4 minutes (Figure 23A). The non-reduced monomer unfolding trace also fitted to a single exponential equation with a lower time constant of 16.4 minutes (Figure 23B). The dimer on the other hand was fitted to a double exponential equation indicating the formation of an unfolding intermediate and a 3 state unfolding pattern (Figure 23C). The time constants obtained were 30 seconds for the initial unfolding event and 10 minutes for the other. The dimeric form appeared to be unfolding much quicker than the monomeric forms. This may be due to the hydrogen peroxide (which is needed to create the dimer from monomer) disrupting the stability of the protein. The dimeric form may, however, unfold quicker because of it being more susceptible to structural alterations as part of its function *in vivo* (i.e. membrane insertion).

For CD the ellipticity at 222 nm was monitored over time. The unfolding kinetic trace indicates a very quick unfolding of the dimer (Figure 24) with a proportion of the unfolding event occurring during the manual mixing time (approx. 5 seconds). It is

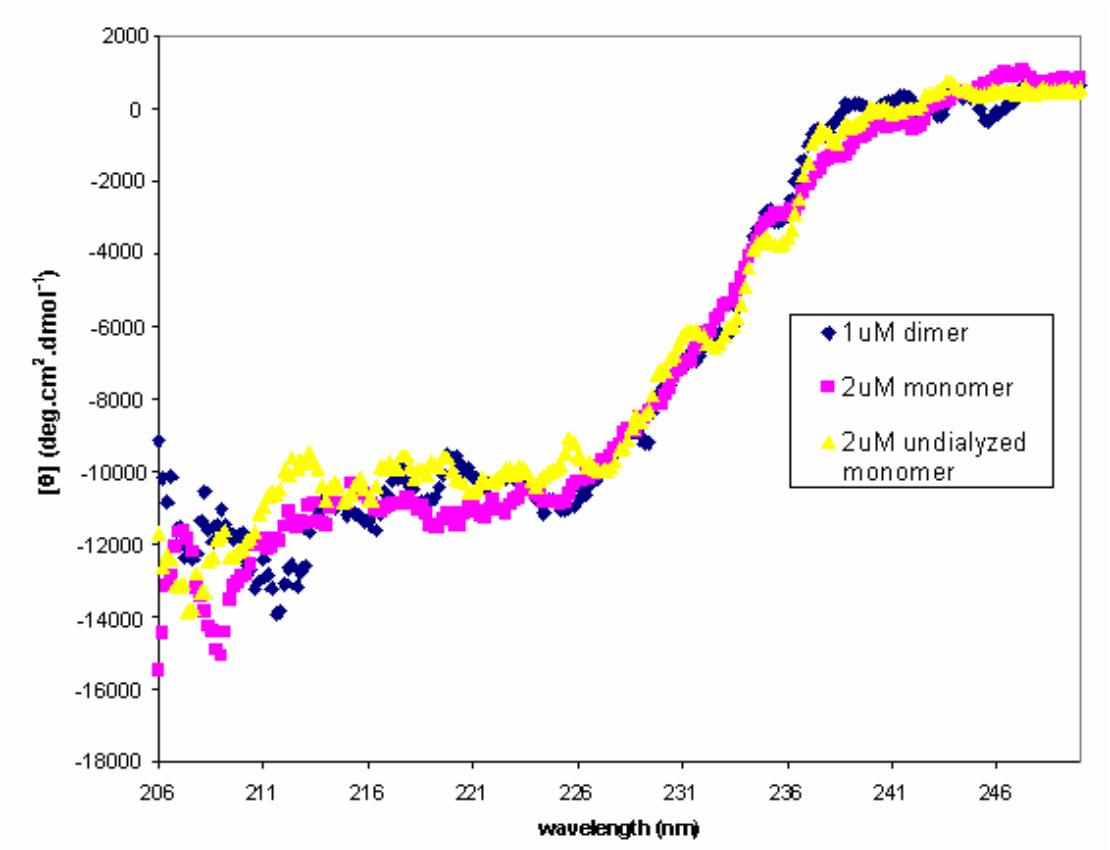


Figure 22: Far-UV Circular Dichroism spectra of CLIC1 forms
Overlay of 2 µM reduced monomer (pink), 2 µM non-reduced monomer (yellow) and 1 µM oxidised dimer (blue). Spectra were corrected for the buffer blank and show an average of 10 accumulations at 100 nm/min.

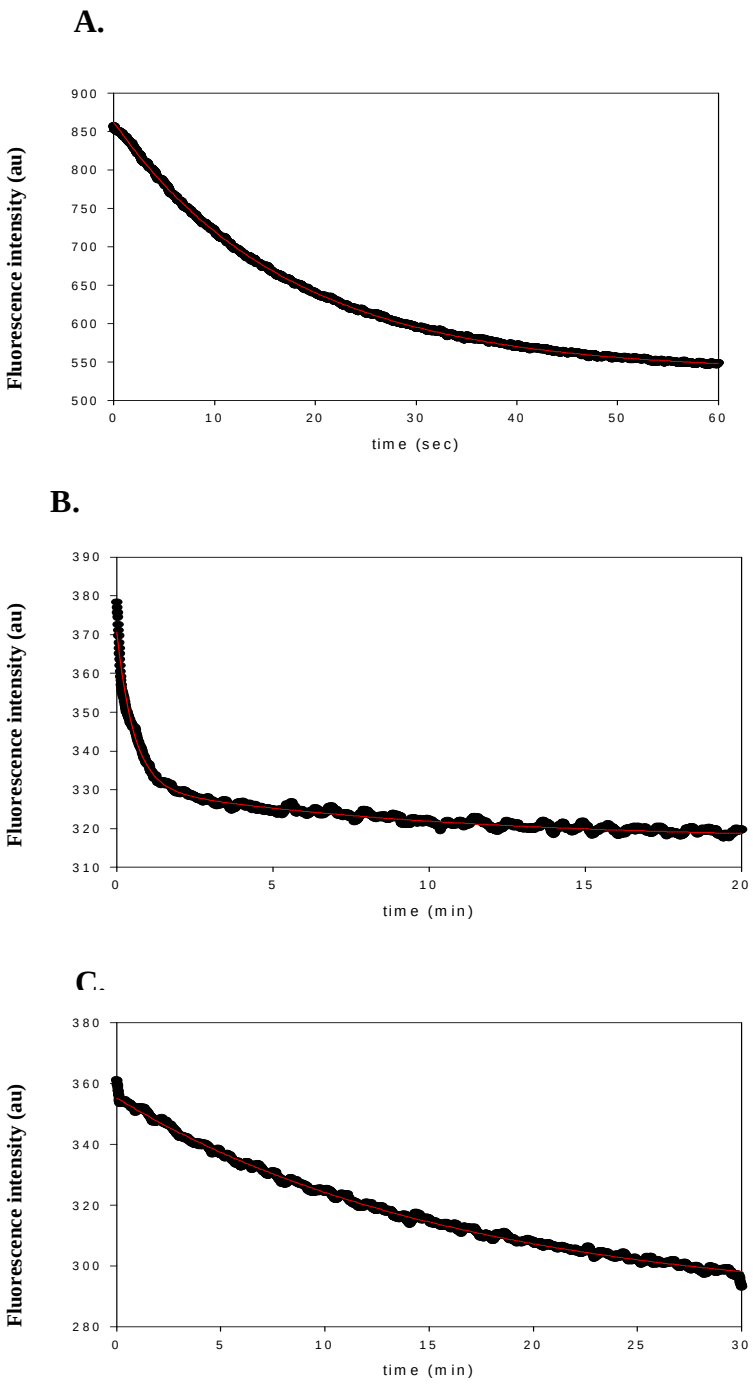


Figure 23: Unfolding kinetic traces of CLIC1 forms monitored using fluorescence

Urea at 8 M concentration was added to the protein samples and the change in fluorescence emission at 345 nm was monitored over time. Samples were excited at 280 nm. Baselines for folded and unfolded protein were established to ensure the unfolding reaction had run to completion.

A. 2 μM reduced CLIC1 unfolding fitted to a single exponential equation suggesting a single unfolding phase with a time constant of 17.4 min.
B. 1 μM oxidised dimer fitted to a double exponential equation indicating the formation of an unfolding intermediate and a 3 state unfolding pattern. Thhe time constants obtained were 30 sec for the initial unfolding event and 10 min for the other.
C. 2 μM non-reduced monomer unfolding trace fitted to a single exponential equation with a time constant of 16.4 min.

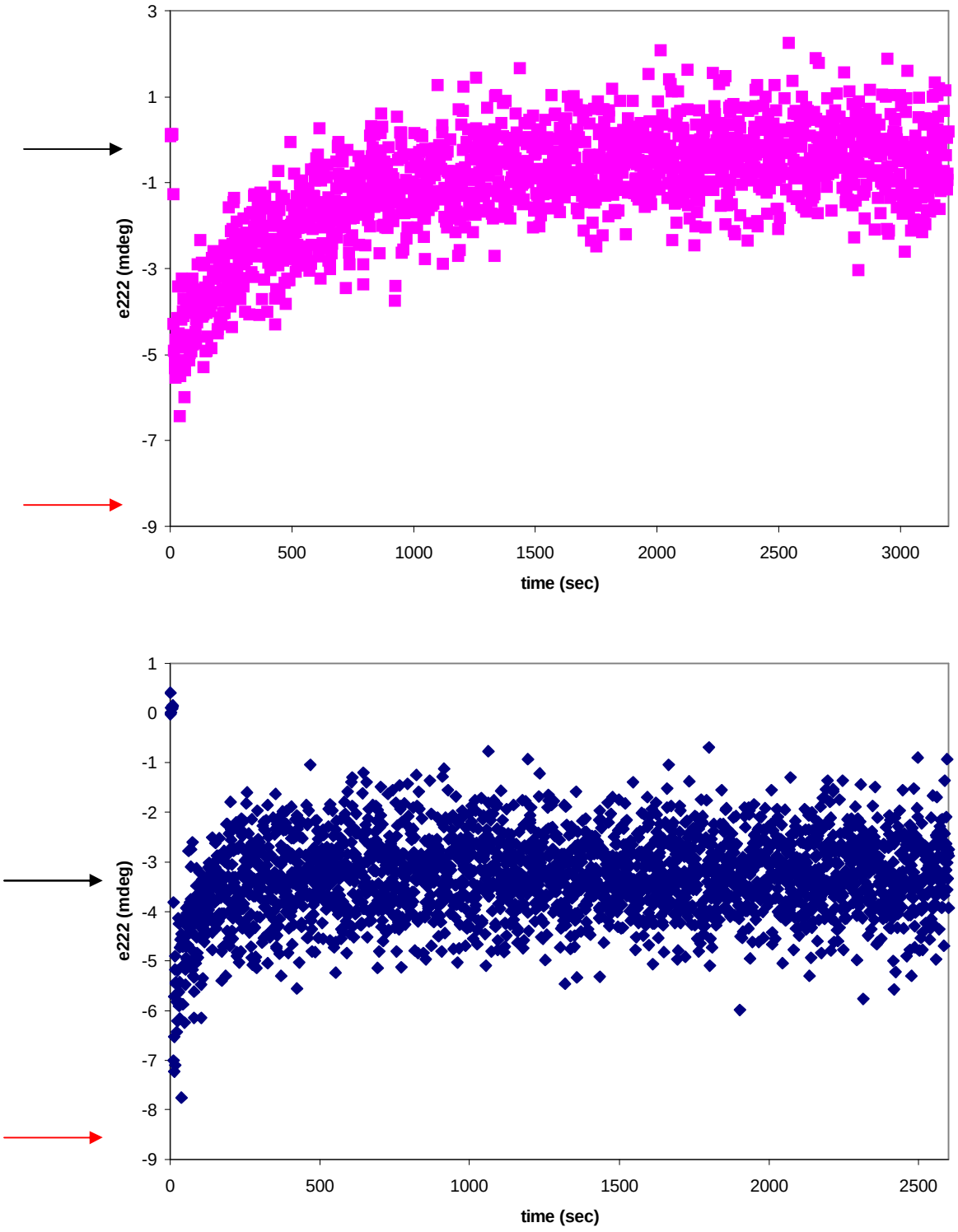


Figure 24: Unfolding kinetics of CLIC1 monomer and dimer using far-UV circular dichroism

Urea at 8 M concentrations was added to protein samples and the change in ellipticity at 222 nm was monitored over time. Baselines for folded (red arrow) and unfolded (black arrow) protein were established in order to ensure the unfolding reaction ran to completion.

A. 2 µM reduced monomer took approximately 26.7 min to completely unfold. Non-reduced monomer exhibited identical unfolding patterns.
B. 1 µM oxidised dimer took approximately 4.1 min to completely unfold. The majority of the unfolding event occurred within the dead time (approx. 5 sec).

unclear whether the quick unfolding of the dimer is due to effects from the hydrogen peroxide method of dimer formation or reduced stability.

Refolding kinetics experiments were performed by diluting unfolded protein (10 μM CLIC1 in 6 M urea) ten times to give folded protein (1 μM CLIC1 in 0.6 M urea). This change was monitored using fluorescence emission at 345 nm. Baselines for folded and unfolded protein were established and all protein samples were excited at 280 nm. Refolding kinetic studies showed reduced CLIC1 to refold in approximately 400 seconds (Figure 25). The early events of refolding occurred too quickly to monitor using manual mixing, however. The refolding kinetics study indicates that the CLIC1 unfolding process is completely reversible since the kinetic trace reached the native CLIC1 baseline.

The stabilizing effect of salt on the different CLIC1 forms was assessed by analysis of the proteins hydrodynamic volume using size exclusion high performance liquid chromatography (SE-HPLC). SE-HPLC was used initially to confirm the purity of reduced CLIC1 after the purification procedure, and to determine its hydrodynamic volume. The column was equilibrated with buffer containing 0.1 M sodium phosphate, 0.5 M sodium sulphate, 0.05 % sodium azide, pH 6.5. A sample of 5 μM reduced CLIC1 (in 50 mM sodium phosphate buffer at pH 7.0) was loaded to the column and yielded a single peak indicating a single species and therefore confirming the purity of the sample (Figure 26A). Analysis of the retention time to elute reduced CLIC1 showed the size to correspond to 31.1 kDa (Figure 26B). This corresponds well to previous SE-HPLC experiments performed on CLIC1 that showed a size of 30 kDa for the monomeric protein (Littler *et al.*, 2004).

Figure 19 shows the HPLC profiles of the different CLIC1 forms. Purified dimer showed a molecular size of 63.4 kDa compared to 31.1 kDa for monomer in buffer containing 0.5 M sodium sulphate. Non-reduced monomer had the same size as reduced monomer (31.1 kDa) but also had a small shoulder corresponding to 63.4 kDa that could be indicative of some dimeric species being formed when the monomer is not dialysed against fresh DTT.

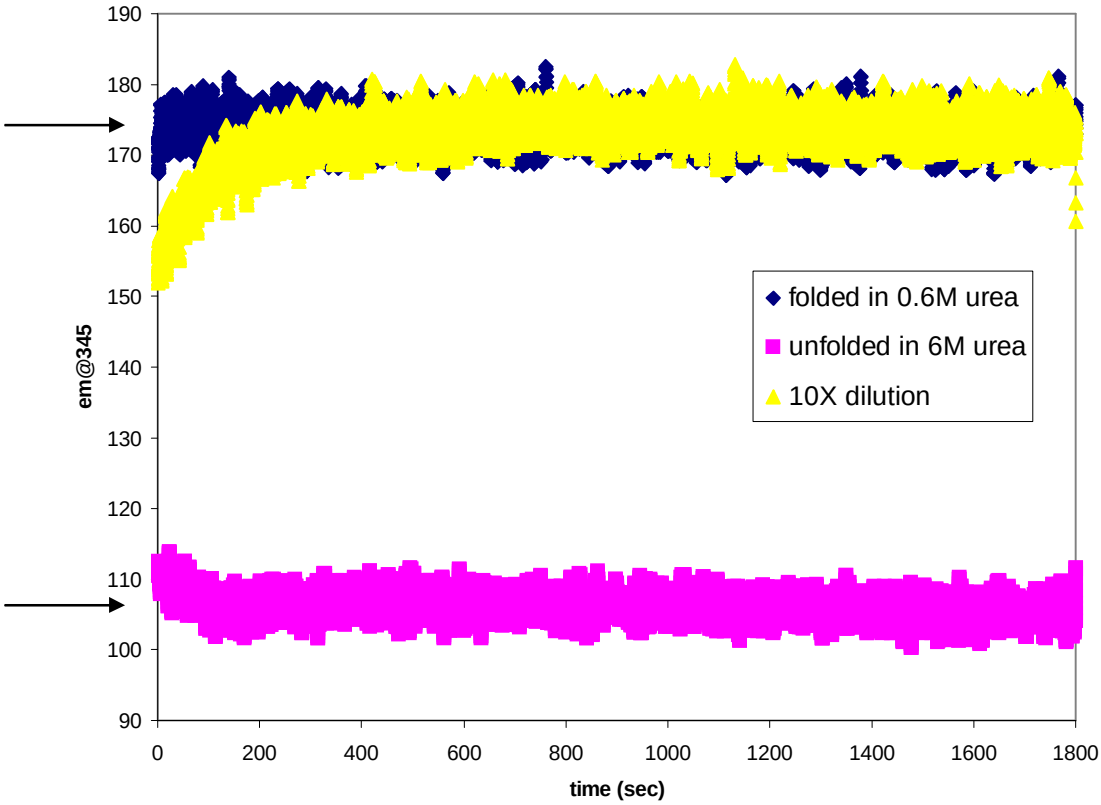
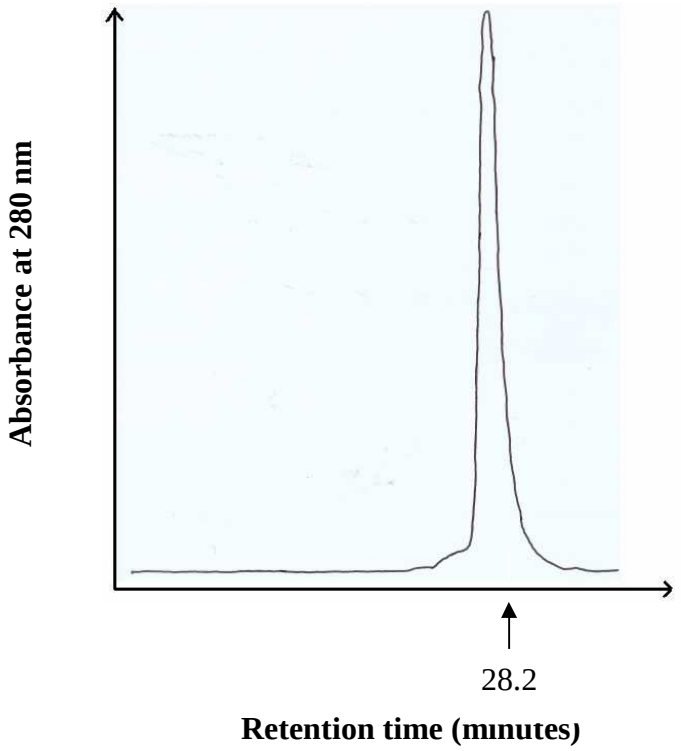


Figure 25: Refolding kinetics of reduced CLIC1 monitored by fluorescence

Ten µM CLIC1 unfolded using 6 M urea was diluted 10 fold resulting in 1 µM CLIC1 in 0.6 M urea (folded conditions) to monitor refolding. Emission at 345 nm was monitored over time. The majority of the refolding event occurred within the time taken for manual mixing (approx. 5 sec). The entire refolding event was complete in 6.5 min as observed by the refolding kinetic trace (yellow) reaching the native protein baseline (blue). The pink trace represents the trace for unfolded CLIC1. Baselines are indicated with the arrows.

A.



B.

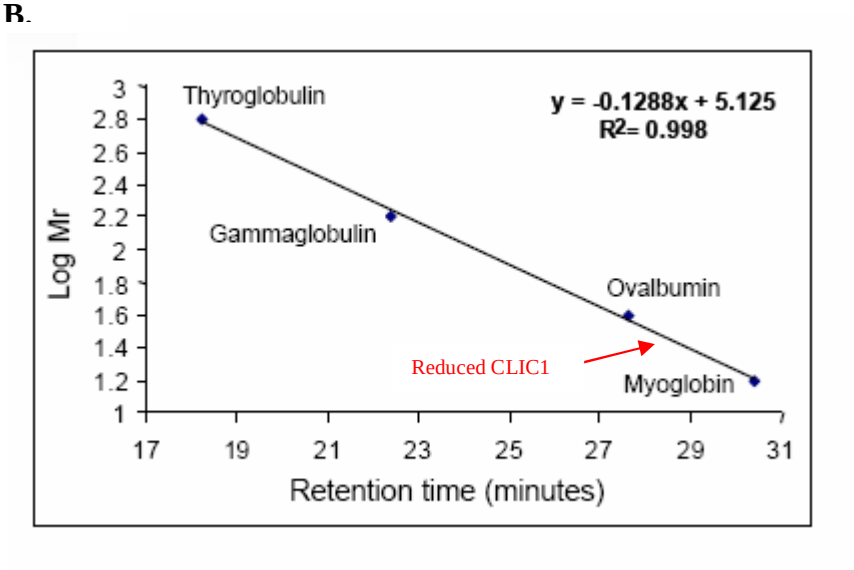


Figure 26: SE-HPLC of reduced CLIC1

A. SE-HPLC elution profile of 5 µM reduced CLIC1 in the presence of 0.5 M sodium sulphate; 0.1 M sodium phosphate; 0.05 % sodium azide buffer pH 7.0. The protein eluted after 28.2 minutes at a flow rate of 0.5 ml/min and chart speed of 30cm/hour.

B. Calibration curve using standard proteins Thyroglobulin (670 kDa), Gammaglobulin (158 kDa), Ovalbumin (44 kDa) and Myoglobin (17 kDa). The molecular mass of reduced CLIC1 was determined to be 31.1 kDa.

Sodium sulphate (0.1 M – 0.5 M) was used to study the effect of increasing salt concentrations on the different CLIC1 forms (Table 2). The size of the dimer did not appear to be significantly altered in differing salt concentrations. The size of the dimer was determined to be 63.4 kDa, 59.7 kDa and 71.36 kDa in 0.5 M, 0.3M and 0.1M sodium sulphate, respectively.

3.4 Effect of pH on CLIC1

3.4.1 Effect of pH on CLIC1 Structure

For this study the two pH values compared were pH 7.0 (neutral pH of cytoplasm) and pH 5.5 (acidic pH representative of that near the membrane surface). For CLIC1, a mechanism for the solution-to-membrane conformational change is not known beyond the requirement for lipid vesicles and acidic conditions. Therefore, it is necessary to investigate what changes are occurring to this protein under acidic conditions in the absence of lipid vesicles. Specifically testing whether lowering the pH induces a change in the tertiary structure, secondary structure or the structural dynamics of the protein.

Fluorescence spectra obtained by exciting 5 μM CLIC1 at 280 nm showed a slight difference in emission maximum wavelength and a significant difference in intensity for CLIC1 at different pH values (Figure 27A). For CLIC1 at pH 7.0 the emission maximum was at 345 nm while for the sample at pH 5.5 it was 347 nm. This slight red shift indicates that the tryptophan has become slightly more exposed to solvent at the lower pH. A slightly higher fluorescence intensity was also observed for CLIC1 at pH 5.5. To determine whether pH had an effect on the secondary structural content of CLIC1 far-UV CD was used to analyse the protein at pH 7.0 and pH 5.5. The spectra obtained in the range from 250 nm – 200 nm were similar showing no significant change in spectral patterns (Figure 27B). Ellipticity values at 208 nm and 222 nm showed approximately 20 % and 27 % change, respectively.

Table 2: Effect of salt concentration on the hydrodynamic sizes of the CLIC1 forms. The size of reduced and non-reduced monomers was greatly affected by different sodium sulphate concentrations. Higher salt concentrations appear to stablize the monomeric forms resulting in a more compact structure. The hydrodynamic size of the dimeric form is not significantly affected by increasing salt concentrations.

	0.5 M salt	**0.3 M salt**	**0.1 M salt**
Monomer (reduced)	31.1 kDa	52.6 kDa	67.5 kDa
Monomer (non-reduced)	31.1 kDa	52.9 kDa	68.1 kDa
Dimer	63.4 kDa	59.7 kDa	71.36 kDa

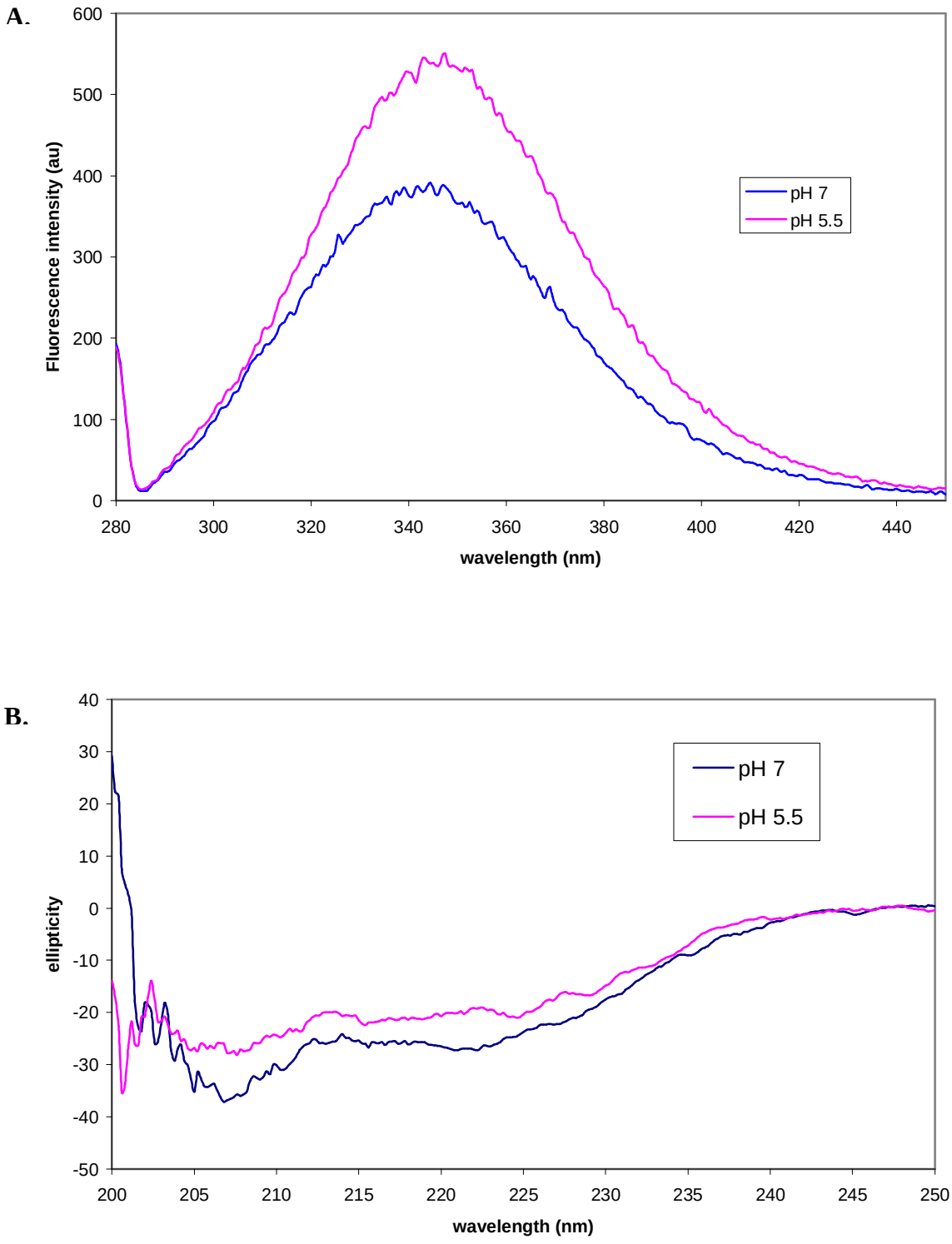


Figure 27: Fluorescence and Far-UV CD spectra for CLIC1 at pH 7.0 and pH 5.5

A. Fluorescence spectra obtained by exciting 5 μM protein samples at 280 nm. At pH 7.0 (blue) emission maximum was at 345 nm, while for pH 5.5 (pink) a slight red shift to 347 nm is evident. Slit width was set to 4 nm.

B. Far-UV CD spectra of 5 μM protein samples at pH 7.0 and pH 5.5 were similar, both displaying characteristic peaks at 222 nm and 208 nm for mostly α-helical secondary structure.

3.4.2 Effect of pH on CLIC1 structural dynamics using hydrogen-deuterium exchange mass spectrometry

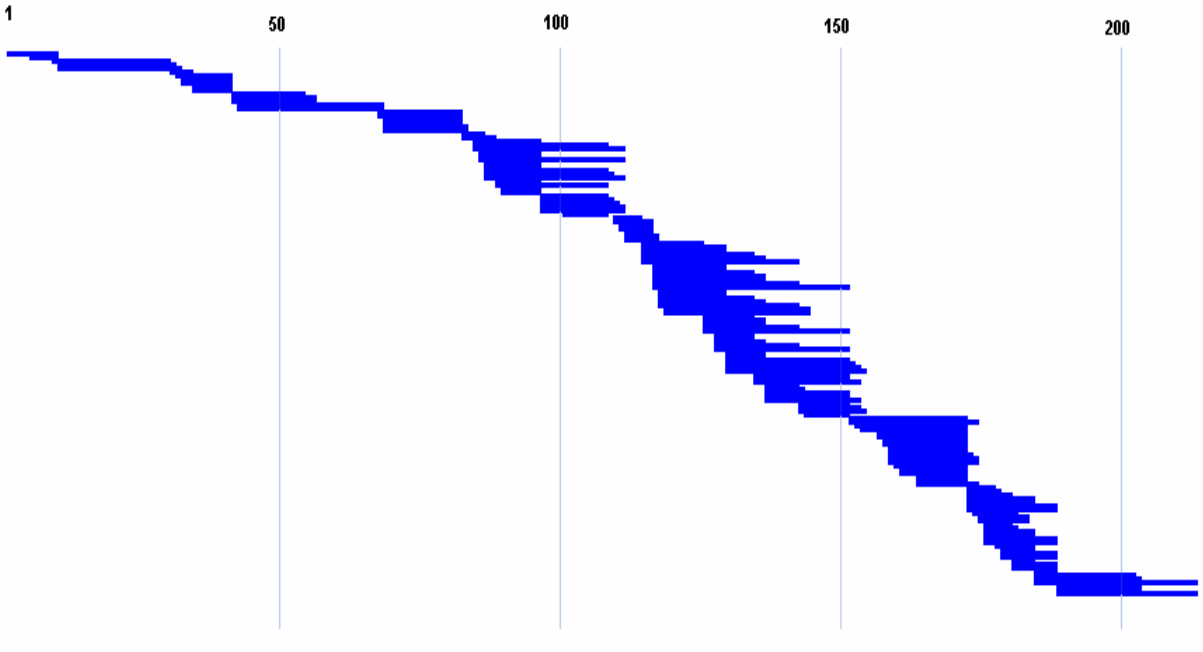
3.4.2.1 Optimisation of CLIC1 proteolytic fragmentation

Prior to studying the hydrogen-exchanged samples, digestion conditions that produced CLIC1 fragments of optimal size and distribution for exchange analysis were established. Optimal pepsin digestion for CLIC1 was obtained using a 1M final concentration of GuHCL in 0.8 % (v/v) formic acid and a digestion duration of 20 seconds over immobilised pepsin. For the pH 7.0 CLIC1 sample 174 peptides suitable for DXMS analysis were generated and covered the entire amino acid sequence of the protein (Figure 28A). The pH 5.5 sample generated 160 peptides with 100% coverage of the amino acid sequence (Figure 28B).

3.4.2.2 Deuterium on-exchange of CLIC1 at pH 7.0

Correct identification of peptides using deuterium exchange data reduction software ensured that the pool of peptides used for structural analysis were of high quality. Sub-localisation of the deuteration levels of CLIC1 peptides was performed by analysing over-lapping peptides and manually fine-tuning deuterium distribution using methods explained in section 2.2.14. Figure 29 shows the sub-localisation for peptides at 10 second and 100 second time points, while figure 30 represents the 1000 second and 3000 second time points. Overall deuteration levels were mapped on to the peptide map and colour coded based on deuteration rates (Figure 31). Combined analysis of the deuterium accumulation graphs, fast exchanging time point (10 sec), and slow exchanging time point (3000 sec) revealed regions of the protein that were buried or stable and regions that were exposed or flexible. Analysis of the deuterium exchange percentage at the first time point indicates which regions are immediately exposed to the deuterium in solution. Any peptides showing greater than 30% deuterium exchange within 10 seconds indicate that the corresponding regions are either highly exposed to solvent, unstable and/or very flexible.

A.



B.

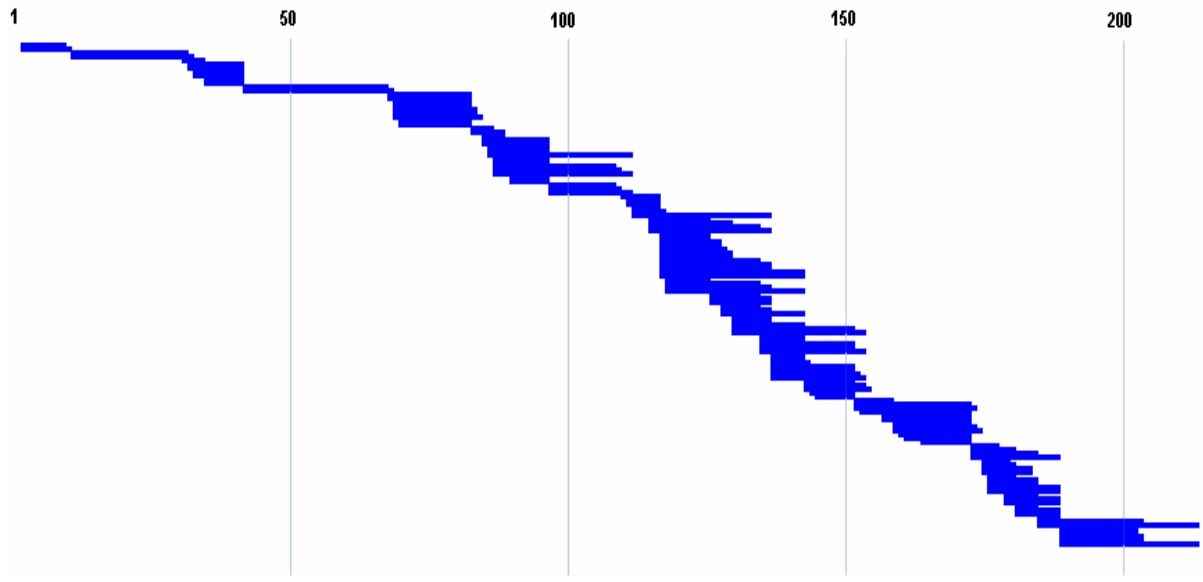
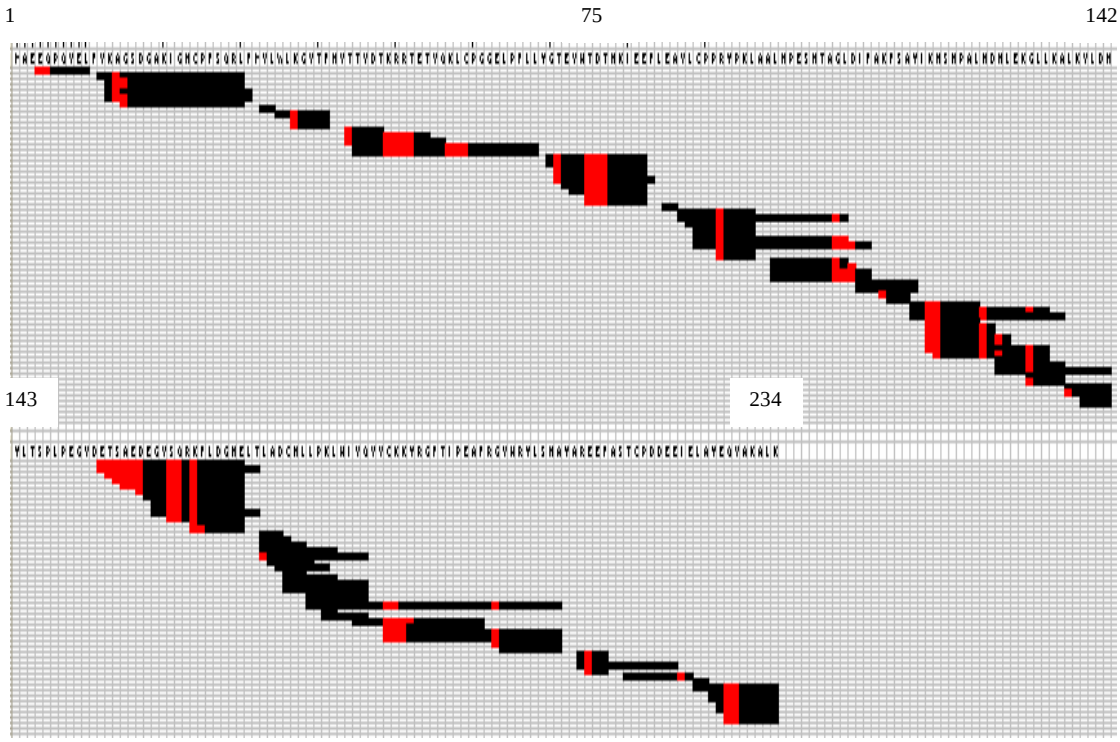


Figure 28: Pepsin fragmentation maps for CLIC1 at pH 7.0 and pH 5.5
Pepsin digest coverage maps obtained for CLIC1 at pH 7.0 (A) and pH 5.5 (B). Each line represents a peptide fragment that was identified from pepsin fragmentation and used for DXMS analysis.

A.



B.

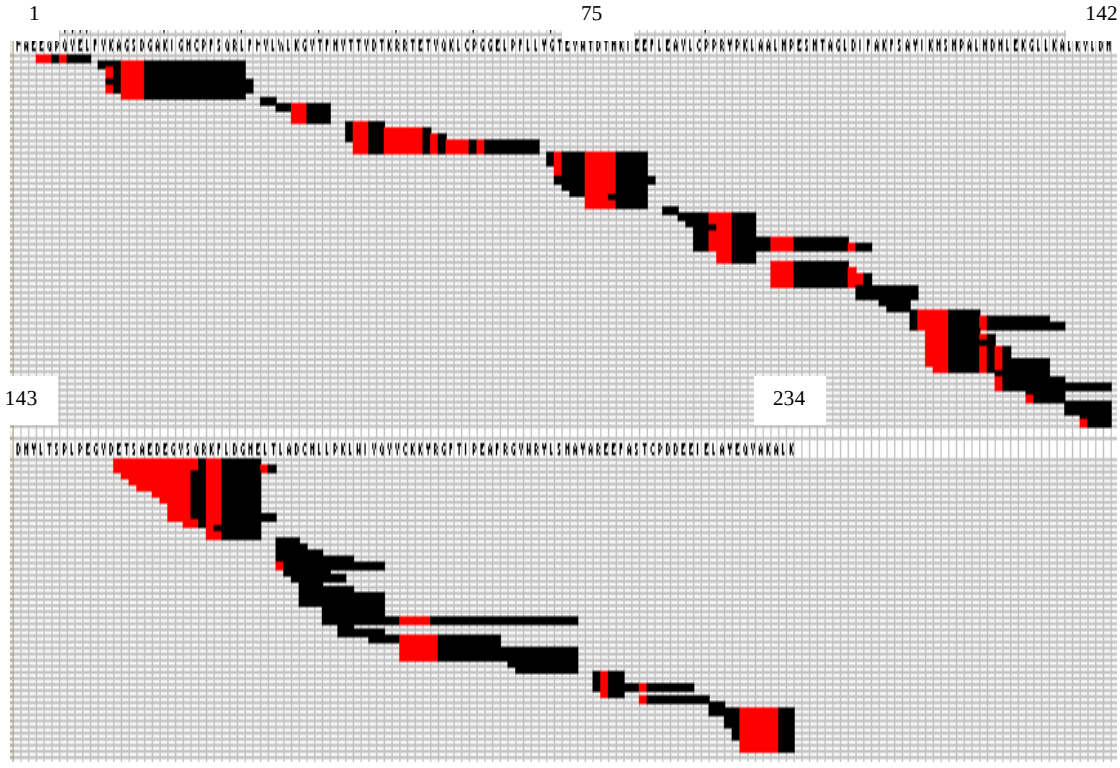


Figure 29: Sub-localisation of the deuterium levels of CLIC1 at pH 7.0 after on-exchange at 0° C. Sub-localisation refers to the prediction of deuterium position within peptide fragments. Manual adjustment of deuterium (red) position within a peptide fragment (black) is based on analysis of overlapping peptides. Deuterium position is manually adjusted to align with overlapping peptides. Sub-localisation of deuterium exchange at (A) 10 seconds and (B) 100 seconds are shown.

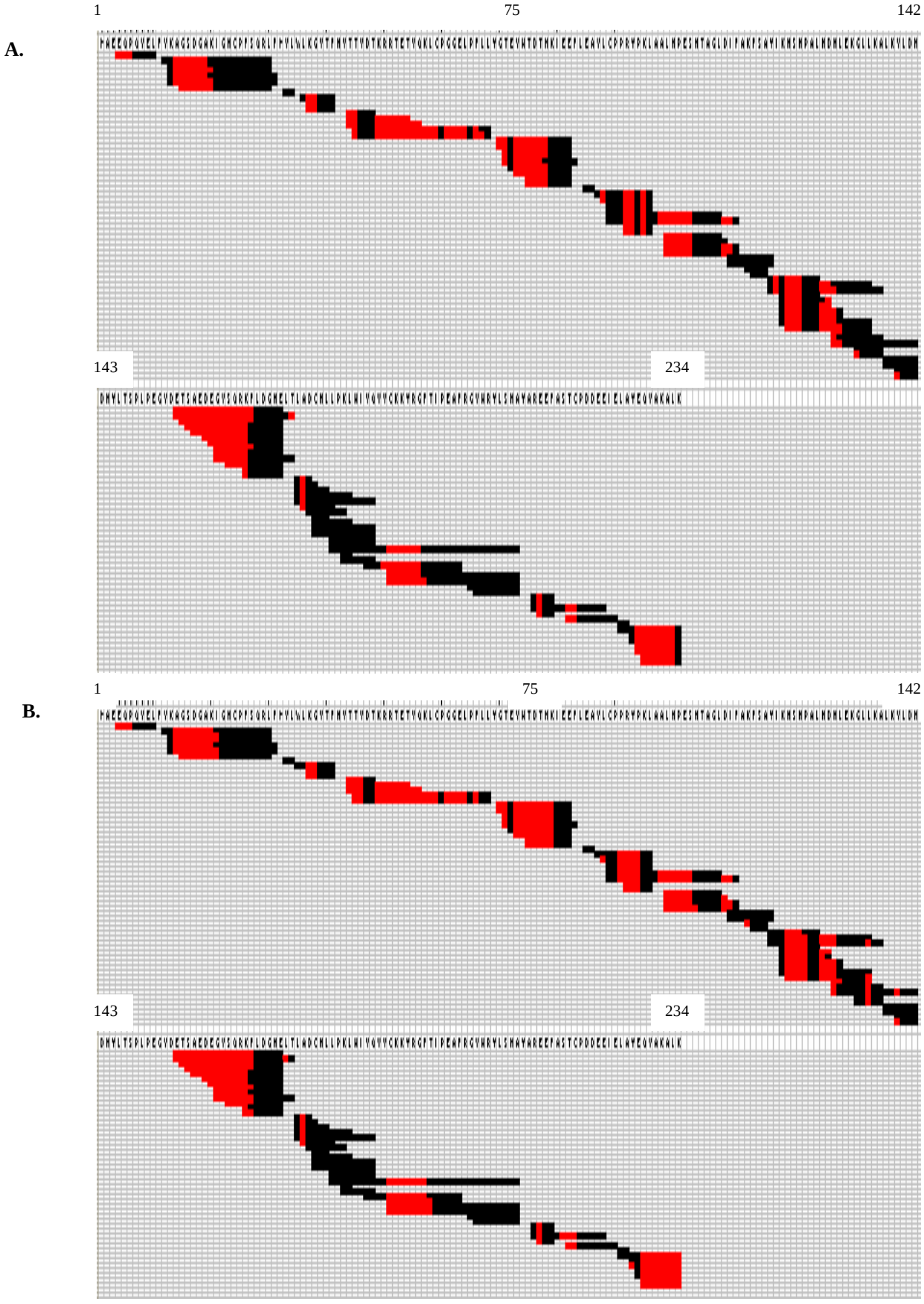


Figure 30: **Sub-localisation of the deuterium levels of CLIC1 at pH 7.0 after on-exchange at 0° C.** Sub-localisation refers to the prediction of deuterium position within peptide fragments. Manual adjustment of deuterium (red) position within a peptide fragment (black) is based on analysis of overlapping peptides. Deuterium position is manually adjusted to align with overlapping peptides. Sub-localisation of deuterium exchange at (A) 1000 seconds and (B) 3000 seconds are shown.

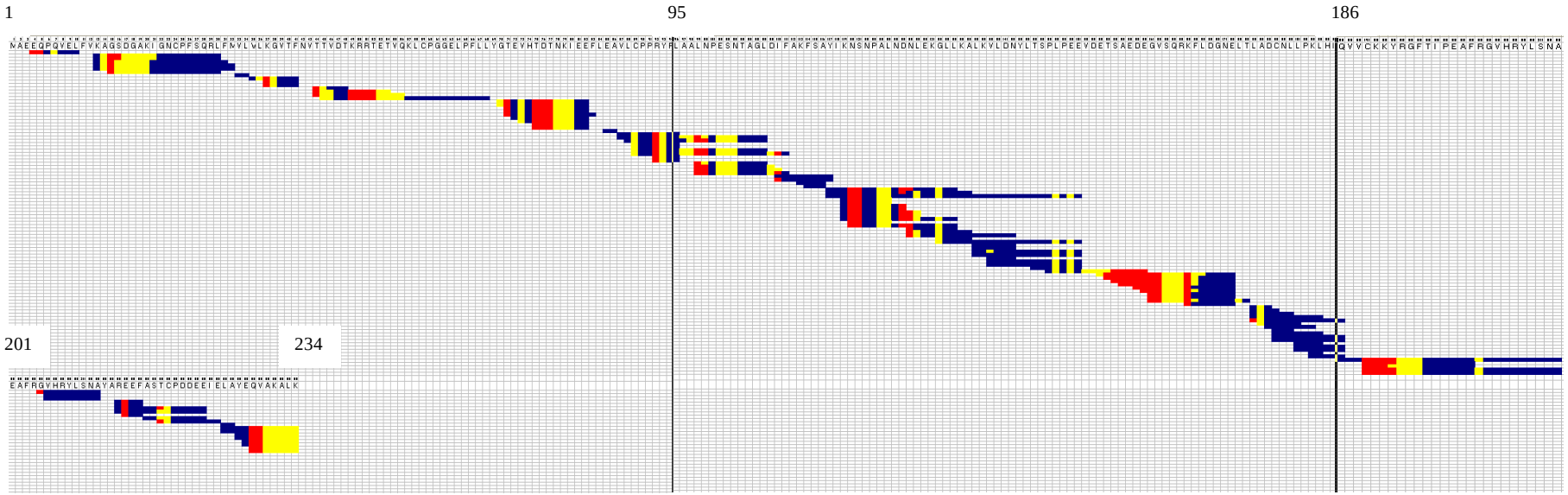


Figure 31: Overall deuteration levels of CLIC1 at pH 7.0 after on-exchange at 0° C.
Blue indicates 0 – 33% deuteration, yellow 33 – 66%, and red 66 – 100% deuteration.

Figure 32 shows a bar graph highlighting the rapid exchanging regions of the protein at pH 7.0.

Accumulation graphs revealed regions that exhibited rapid exchange within the first time point employed or a steep accumulation over all the time points (Figure 33). Residues 152 – 172, corresponding to the negatively charged loop/foot region in domain 2, were noted as having very rapid exchange rates (51 % deuteration within 10 sec) indicating that this region is the most flexible / solvent exposed region of the protein, as expected from the crystal structure (Harrop *et al.,* 2001). High exchange within 10 seconds was also noted for peptide 43 – 64 (59 % deuteration) that corresponds to the region connecting β2 with α2 where, interestingly, a conserved positively charged motif is found. Residues 69 – 82 showed 37 % deuteration within the shortest time point employed. These solvent accessible, mobile regions correspond to the β3-β4-α3 motif of the thioredoxin-fold of CLIC1. Other regions showing high levels of flexibility corresponded to the domain linker region (residue 89 – 96) and the α9 helix (residue 236 – 241) at the C-terminal end. Within domain 2 the only other peptides showing high levels of deuteration (38 %) within the first time point were residues 117 –129 corresponding to helix 5.

Regions showing no deuterium incorporation throughout the entire experiment were identified and representative accumulation graphs are shown in Figure 34. Figure 35 shows ribbon diagrams of CLIC1 deuteration at three different time points. It was interesting to note that the only regions showing complete protection from deuterium exchange throughout the entire experiment (up to 3000 seconds) in domain 1 are short sections of α1 (residue 31 –34) and α3 (residue 83 –88), although these are very short peptides and there is no overlap so they are more susceptible to misidentifications. The majority of domain 2 appears to be stable with peptides 111 – 116 (helix 4), 135-151 (helix 5), 175 – 183 (helix 6), and 203 – 213 (helix 7) showing little or no deuterium exchange even after 3000 seconds.

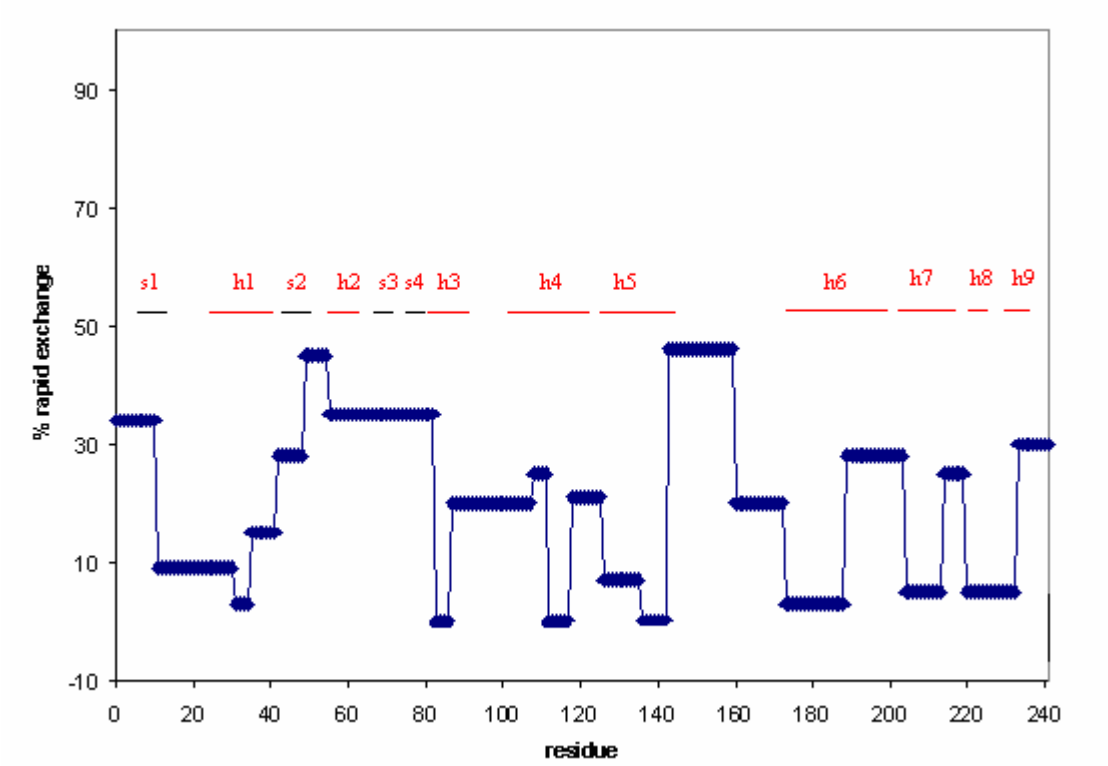
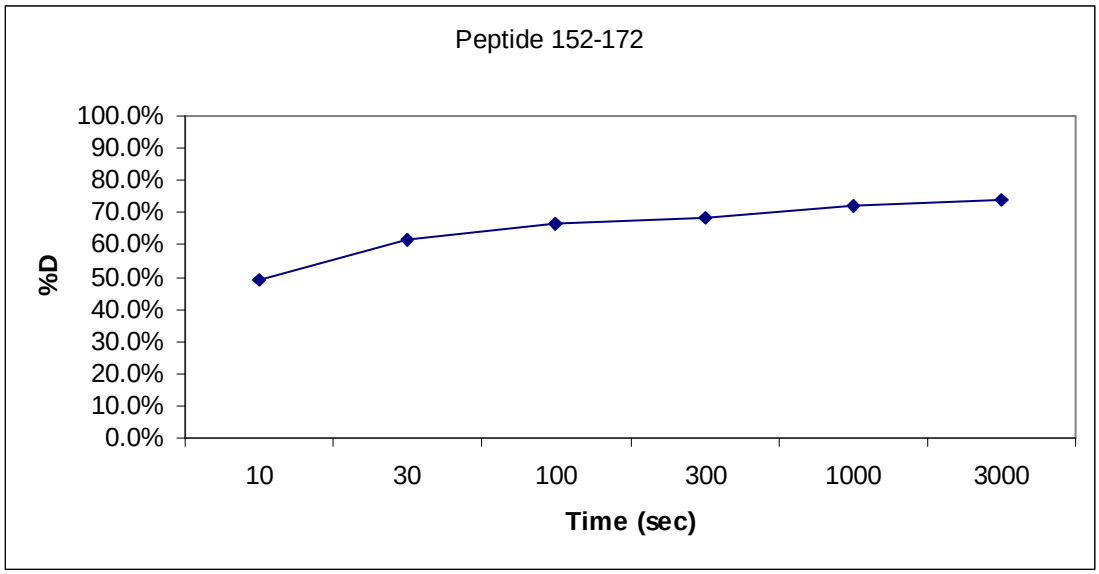
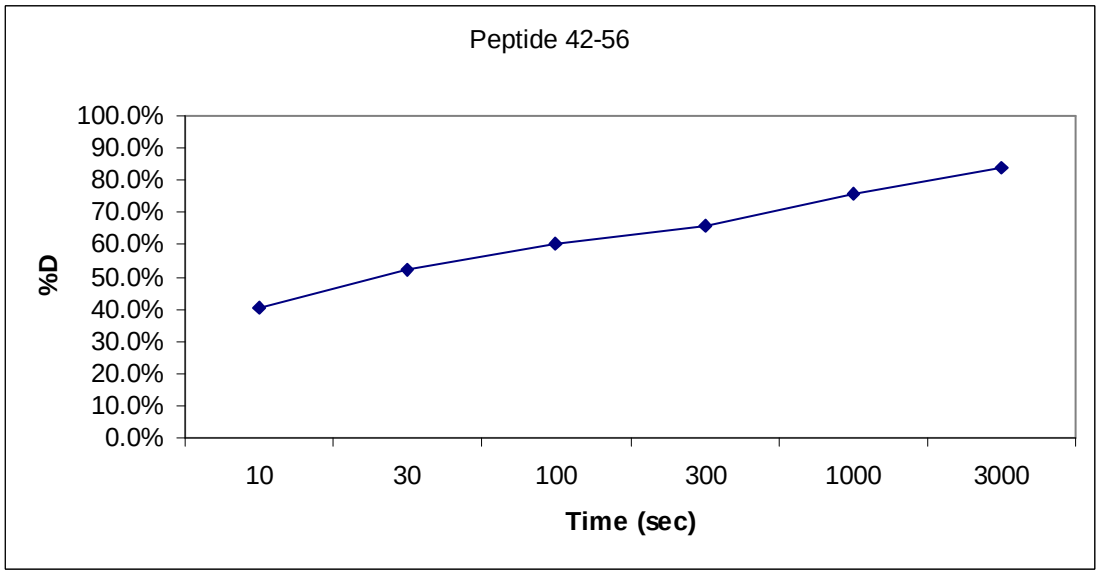
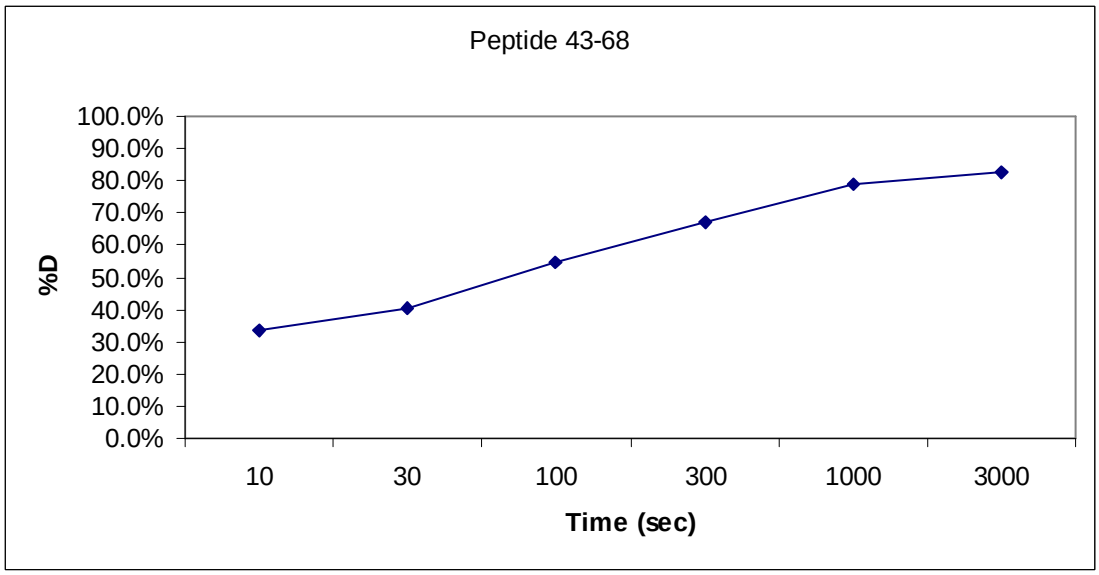


Figure 32: Bar graph showing the percentage deuterium exchange for CLIC1 at pH 7.0 after 10 seconds (rapid exchange). Positioning of secondary structural elements along the primary sequence is shown above the graph with strands represented by black lines and helices represented by red lines.


Peptide 152-172
100.0%
90.0%
80.0%
70.0%
60.0%
50.0%
40.0%
30.0%
20.0%
10.0%
0.0%
%D
10
30
100
300
1000
3000
Time (sec)


Peptide 42-56
100.0%
90.0%
80.0%
70.0%
60.0%
50.0%
40.0%
30.0%
20.0%
10.0%
0.0%
%D
10
30
100
300
1000
3000
Time (sec)


Peptide 43-68
100.0%
90.0%
80.0%
70.0%
60.0%
50.0%
40.0%
30.0%
20.0%
10.0%
0.0%
%D
10
30
100
300
1000
3000
Time (sec)

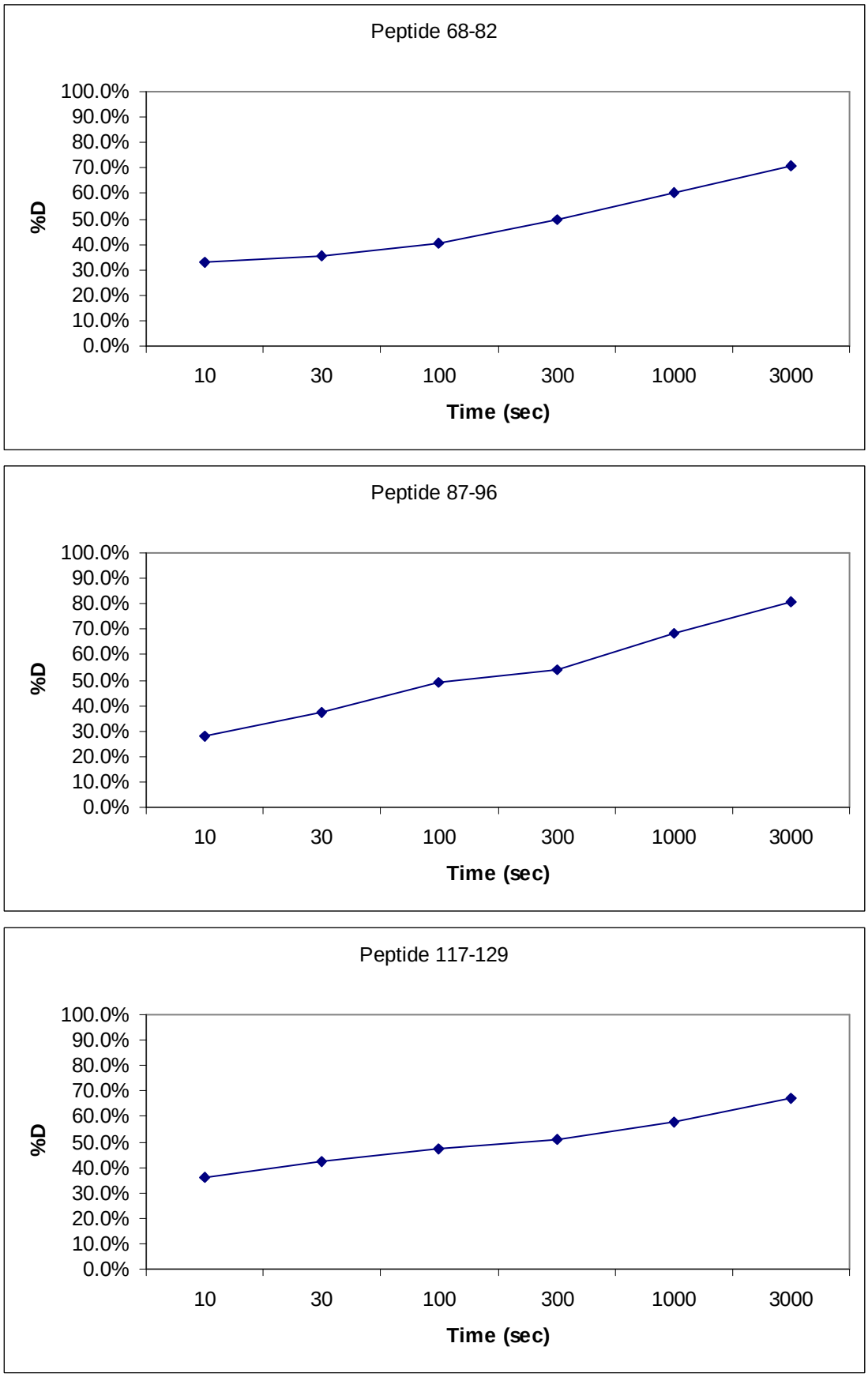


Figure 33: Representative accumulation graphs for high percentage deuterium exchanging peptides in CLIC1 at pH 7.0. Graphs show percentage deuteration over time for specific peptide fragments.

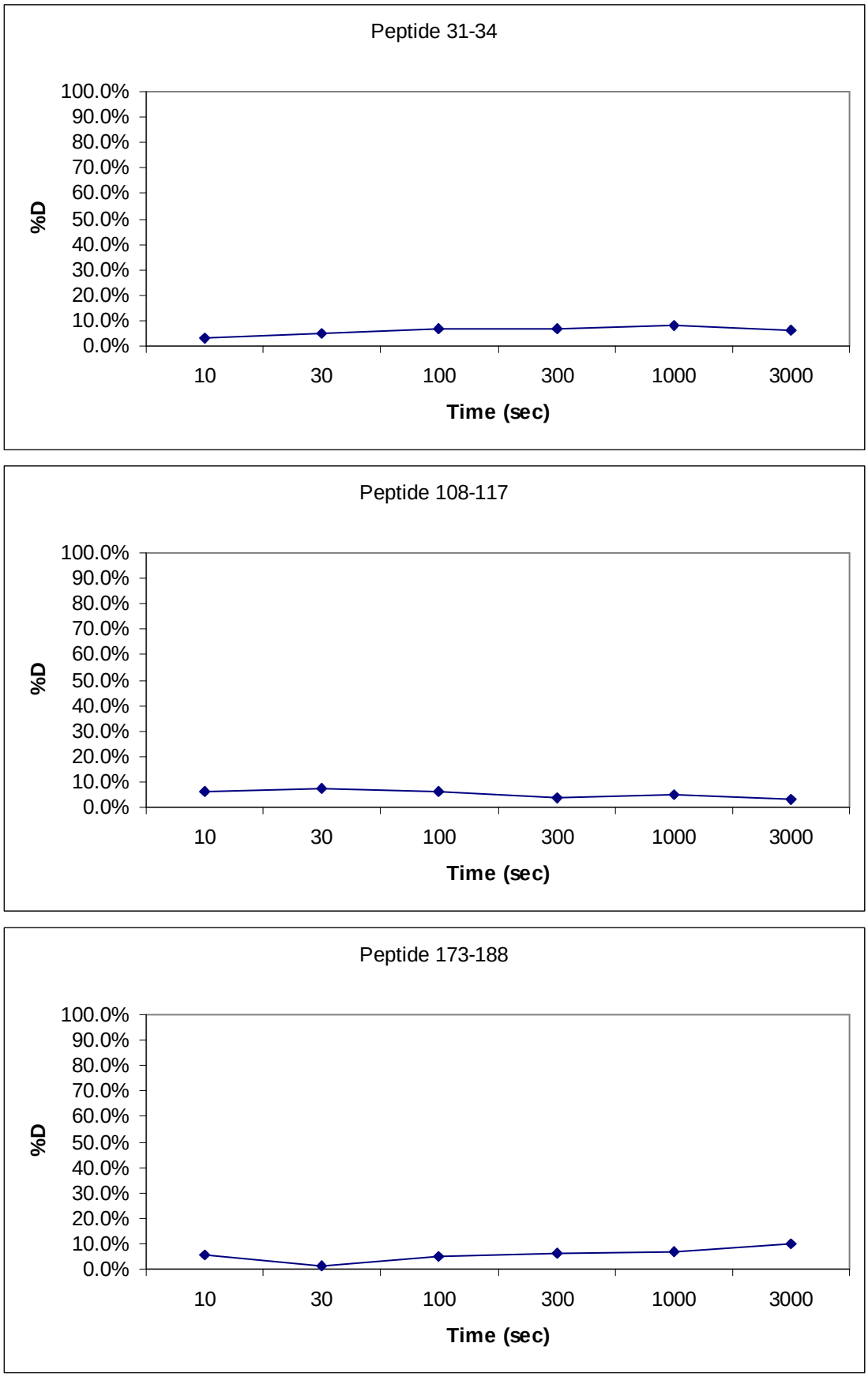
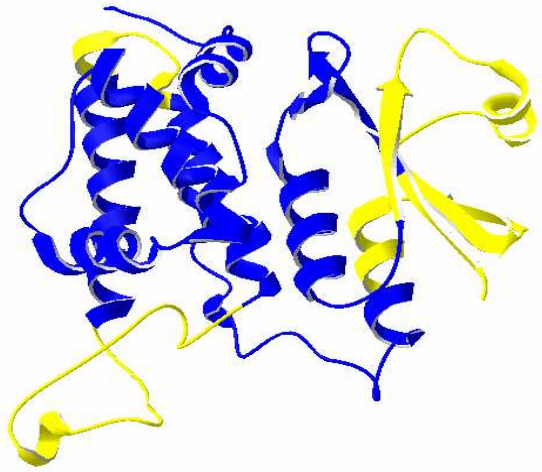
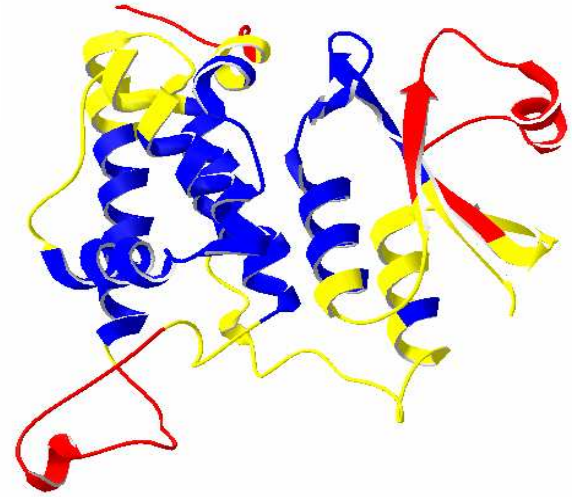


Figure 34: Representative accumulation graphs for low percentage deuterium exchanging peptides in CLIC1 at pH 7.0. Graphs show percentage deuteration over time for specific peptide fragments.

A.



B.



C.

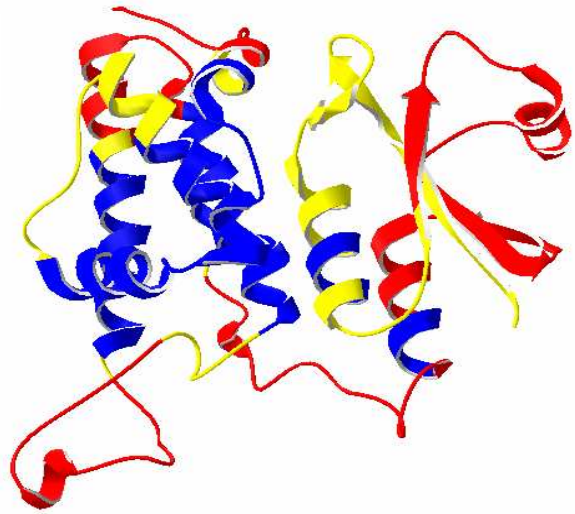


Figure 35: Ribbon diagrams showing the degree of deuterium content incorporated at 3 different time points for CLIC1 at pH 7.0.

The level of deuteration of each peptide after 10 sec (A), 300 sec (B) and 3000 sec (C) is coloured according to the following scheme: blue < 33%; yellow 33 – 67%; red > 67%. The images were generated with Swiss PDB viewer (Guex and Peitsch, 1997) using the PDB file 1k0m (Harrop *et al.*, 2001).

3.4.2.3 HXMS of CLIC1 at pH 5.5

The amide hydrogen exchange patterns of CLIC1 at pH 7.0 and pH 5.5 were measured and the difference in deuteration levels analysed. Changing buffer pH changes hydrogen exchange rates of proteins even if structure is unchanged by the pH difference. In general, it has been observed that a 1 pH unit decrease slows exchange by approximately 10 fold (Bai *et al.,* 1993). The difference between samples at pH 7.0 and pH 5.5 is 1.5 pH units, so the exchange is expected to be 31-fold slower ($10^{1.5}$ = 31) at pH 5.5 than pH 7.0. Any regional change that is significantly different than 31 fold probably reflects structural changes. Therefore, due to the approximately 30 fold difference in exchange rates between the two pH sample sets the 10 sec time point of the pH 7.0 sample was compared with the 300 sec time point of the pH 5.5 sample, and similarly the 100 second time point of the pH 7.0 sample compared with the 3000 second time point of the pH 5.5 sample. For statistical and clarification purposes the time points for the pH 5.5 samples were extended to include 900, 9000, 30000 and 90000 seconds.

Deuterium exchange of CLIC1 peptides at pH 5.5 was sub-localised (Figure 36) by analysis of overlapping peptides and manual adjustment of deuterium positioning as explained in section 2.2.14. The overall global deuteration levels were similar to pH 7.0. Table 3 shows the matching peptides at the two pH conditions and the corresponding percentage deuterium incorporated. This similarity in structure indicates that CLIC1 does not form a molten globule at pH 5.5 in the absence of lipid vesicles. Closer inspection, however, reveals specific regions that are affected by the pH change. These subtle structural and dynamic changes would not be detected by CD or fluorescence experiments. Only identical peptide fragments were used for comparison between pH 7.0 and pH 5.5 and the results indicated an excellent correlation between the data sets (Table 3). Figure 37 shows a bar graph comparing the rapid exchange regions of the protein at pH 7.0 and pH 5.5. Significant differences in percentage deuterium exchange between CLIC1 at pH 7.0 and pH 5.5 were mapped onto the CLIC1 crystal structure (Figure 38). Significant increases in rapid exchange based on percentage and number of deuterium exchange for the pH 5.5 sample were noted for peptides 11-32 (helix 1 region) and 68-82 (strand 4 and helix 3 region), indicating that these regions have become more flexible or mobile at pH 5.5 (Figure 39). As much as a 20 % (~ 4 deuteriums) difference in deuterium exchange for the peptide 11-32 was noted. For the peptide 68-82 as much as 18 % (~ 2.5 deuteriums) more deuterium exchange was noted at the lower pH. Peptide 173-184 (helix 6) was

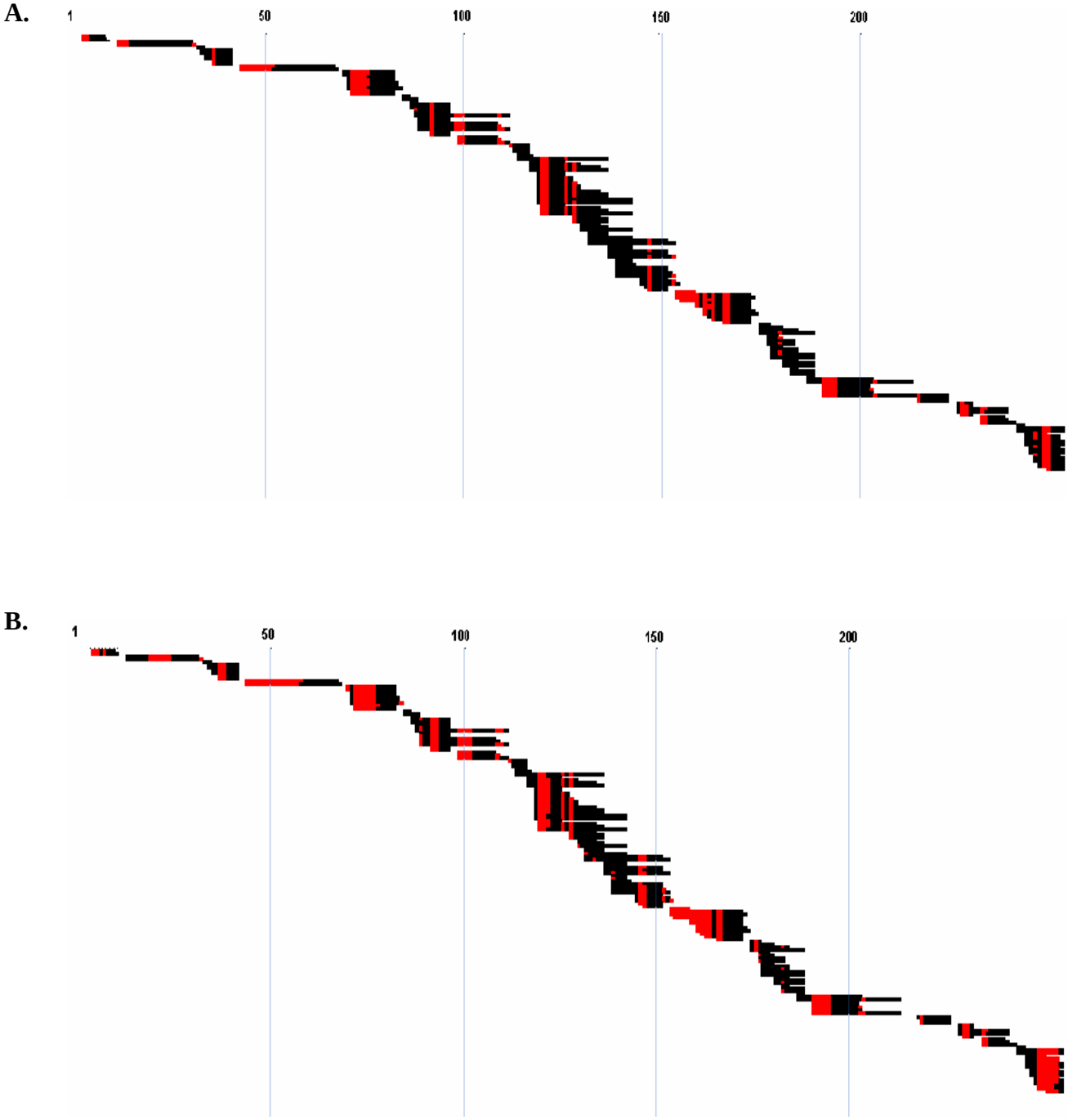


Figure 36: Sub-localisation of the deuterium levels of CLIC1 at pH 5.5 after on-exchange at 0° C. Sub-localisation refers to the prediction of deuterium position within peptide fragments. Manual adjustment of deuterium (red) position within a peptide fragment (black) is based on analysis of overlapping peptides. Deuterium position is manually adjusted to align with overlapping peptides. Sub-localisation of deuterium exchange at (A) 300 seconds and (B) 3000 seconds are shown.

pH 7.0

Peptide fragment	Time point	
	10sec	100sec
2 -10	33.9%	45.4%
11 -30	9.0%	22.3%
11 -30	9.1%	21.5%
31 -34	3.2%	7.1%
33 -41	8.6%	25.0%
35 -41	19.6%	43.7%
68 -82	31.3%	41.8%
68 -82	33.2%	40.3%
69 -82	35.0%	40.7%
69 -83	31.6%	33.7%
83 -86	-3.2%	-4.1%
85 -96	17.5%	36.5%
86 -108	16.9%	34.6%
87 -96	27.8%	49.0%
87 -96	26.5%	50.5%
87 -108	17.9%	38.3%
87 -111	22.5%	39.0%
90 -96	27.2%	51.8%
90 -96	24.9%	43.0%
97 -108	13.6%	37.0%
97 -109	19.1%	39.8%
97 -111	24.7%	41.6%
115 -134	21.6%	28.7%
115 -136	17.8%	25.7%
117 -125	35.3%	49.7%
117 -129	35.9%	47.5%
117 -129	35.5%	49.6%
117 -134	24.0%	30.7%
118 -134	32.1%	31.9%
126 -134	15.1%	6.1%
126 -136	5.9%	7.3%
135 -151	1.9%	10.3%
135 -151	-0.9%	5.2%
137 -142	1.1%	1.1%
137 -151	4.0%	9.3%
137 -151	4.4%	12.2%
143 -151	8.1%	27.5%
152 -172	49.0%	66.6%
152 -174	46.3%	66.7%
153 -172	45.7%	63.5%
155 -172	39.0%	59.3%
157 -172	29.7%	48.8%
158 -172	26.5%	46.1%
159 -172	27.4%	44.0%
159 -172	24.8%	43.4%
159 -174	19.2%	33.4%
164 -172	16.3%	17.1%
164 -172	22.4%	21.0%
173 -177	4.9%	10.8%

pH 5.5

Peptide fragment	Time point	
	300sec	3000sec
2 -10	34.5%	39.2%
11 -30	15.2%	27.4%
11 -30	15.4%	29.0%
31 -34	6.7%	13.3%
33 -41	10.9%	22.6%
35 -41	14.9%	26.8%
68 -82	28.9%	35.6%
68 -82	30.5%	35.5%
69 -82	31.7%	40.7%
69 -83	27.6%	34.2%
83 -86	4.0%	8.4%
85 -96	17.9%	27.5%
86 -108	16.3%	31.3%
87 -96	25.9%	40.4%
87 -96	28.2%	43.9%
87 -108	15.3%	28.4%
87 -111	21.2%	31.6%
90 -96	26.5%	59.1%
90 -96	28.6%	40.3%
97 -108	15.0%	29.9%
97 -109	21.2%	31.9%
97 -111	24.4%	35.5%
115 -134	21.8%	25.7%
115 -136	19.3%	23.6%
117 -125	35.4%	41.7%
117 -129	37.7%	41.3%
117 -129	37.3%	36.8%
117 -134	24.0%	24.6%
118 -134	25.7%	30.7%
126 -134	12.1%	17.3%
126 -136	8.3%	6.6%
135 -151	5.8%	8.9%
135 -151	3.2%	7.4%
137 -142	1.3%	0.1%
137 -151	3.9%	9.2%
137 -151	4.1%	9.8%
143 -151	13.8%	25.7%
152 -172	50.9%	64.8%
152 -174	51.6%	44.3%
153 -172	47.3%	58.4%
155 -172	42.9%	46.7%
157 -172	30.1%	37.4%
158 -172	30.9%	40.1%
159 -172	26.5%	36.7%
159 -172	26.6%	35.5%
159 -174	20.8%	28.5%
164 -172	18.3%	11.7%
164 -172	12.3%	9.4%
173 -177	5.5%	13.8%

pH 7.0	Time point		**pH 5.5**	Time point	
Peptide fragment	10sec	100sec	Peptide fragment	300sec	3000sec
173 -188	5.4%	5.2%	173 -188	-3.9%	-1.4%
175 -183	3.8%	4.4%	175 -183	0.9%	3.0%
176 -184	3.5%	4.1%	176 -184	0.7%	2.8%
176 -188	0.4%	0.2%	176 -188	0.6%	2.5%
176 -188	1.2%	0.9%	176 -188	1.7%	1.5%
179 -184	0.5%	5.0%	179 -184	-18.3%	-5.4%
179 -188	5.6%	5.6%	179 -188	-3.8%	-4.2%
181 -184	-6.6%	-6.7%	181 -184	2.5%	5.4%
181 -188	1.1%	-0.2%	181 -188	2.9%	-0.3%
189 -203	31.9%	47.3%	189 -202	29.6%	36.5%
189 -203	27.8%	43.0%	189 -203	33.2%	38.8%
189 -213	16.7%	23.8%	189 -213	18.1%	18.1%
189 -213	17.2%	23.8%	189 -213	19.0%	19.4%
214 -219	23.1%	25.3%	214 -219	25.4%	20.7%
214 -219	29.7%	31.4%	214 -219	31.2%	27.0%
214 -228	12.1%	14.8%	214 -228	15.0%	24.0%
215 -219	23.4%	20.1%	215 -219	31.3%	23.7%
220 -230	9.7%	16.2%	220 -230	7.7%	19.5%
229 -232	4.2%	13.8%	229 -232	12.6%	10.7%
229 -241	19.7%	47.6%	229 -241	21.0%	44.7%
231 -241	24.0%	55.8%	231 -241	25.0%	50.8%
231 -241	23.6%	54.8%	231 -241	25.7%	54.2%
232 -241	27.6%	64.1%	232 -241	29.7%	62.4%
233 -241	29.3%	64.9%	232 -241	31.3%	64.5%

Table 3: Comparison of percentage deuteration of matching peptides at pH 7.0 and pH 5.5. The 10 second time point for pH 7.0 is compared to the 300 second time point for pH 5.5 when the effect of pH on deuteration rate is factored in (approximately 30 fold slower at pH 5.5). Similarly, the 100 second time point for pH 7.0 is compared to the 3000 second time point for pH 5.5.

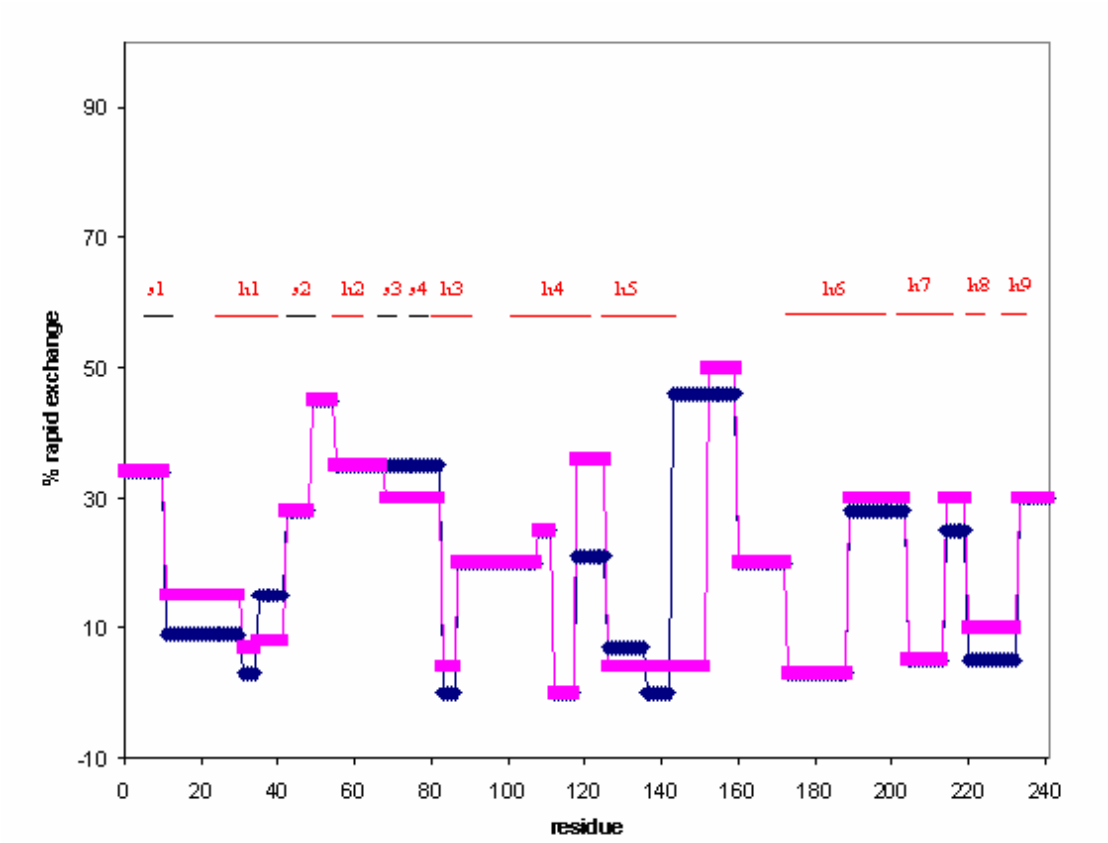


Figure 37: Bar graph showing percentage rapid deuterium exchange for CLIC1 at pH 7.0 (blue) and pH 5.5 (pink).

Overlay of the rapid exchange for pH 7.0 (10 sec) and corresponding time for pH 5.5 (300 sec)**.** Positioning of secondary structural elements along the primary sequence is shown above the graph with strands represented by black lines and helices represented by red lines.

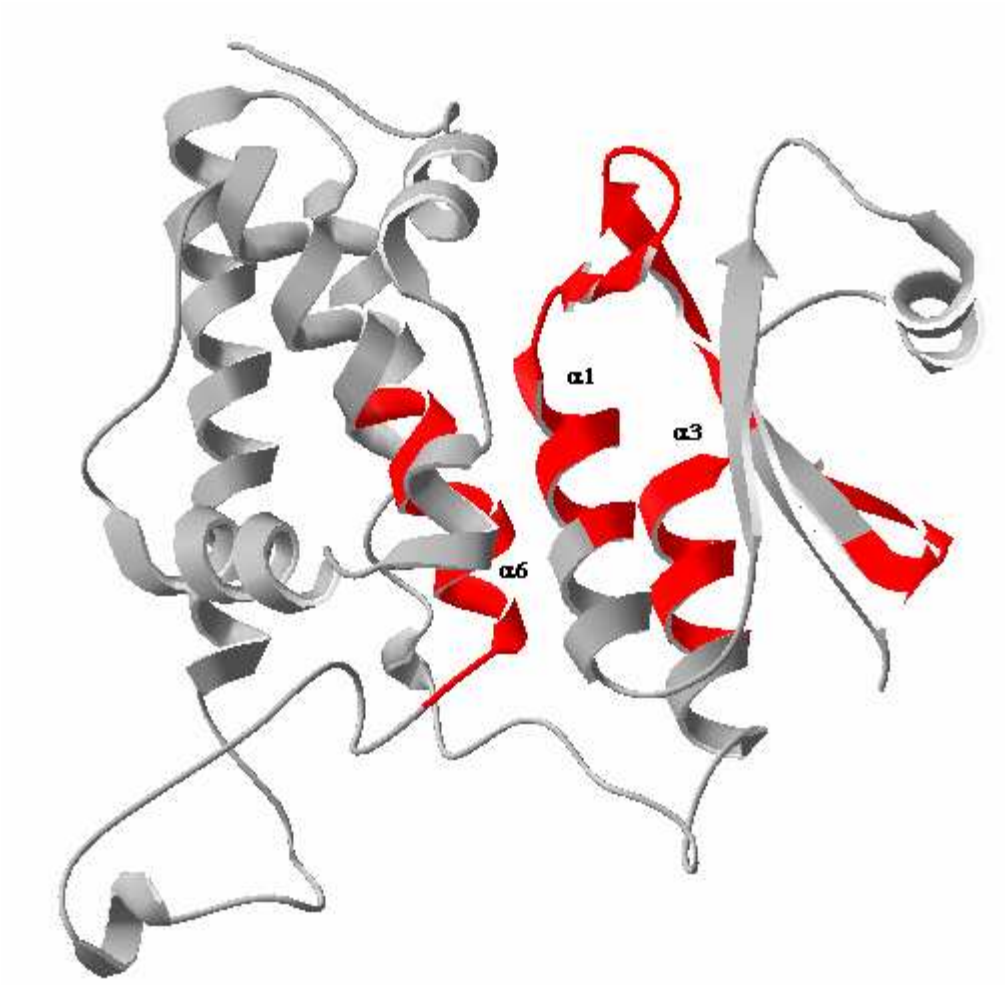
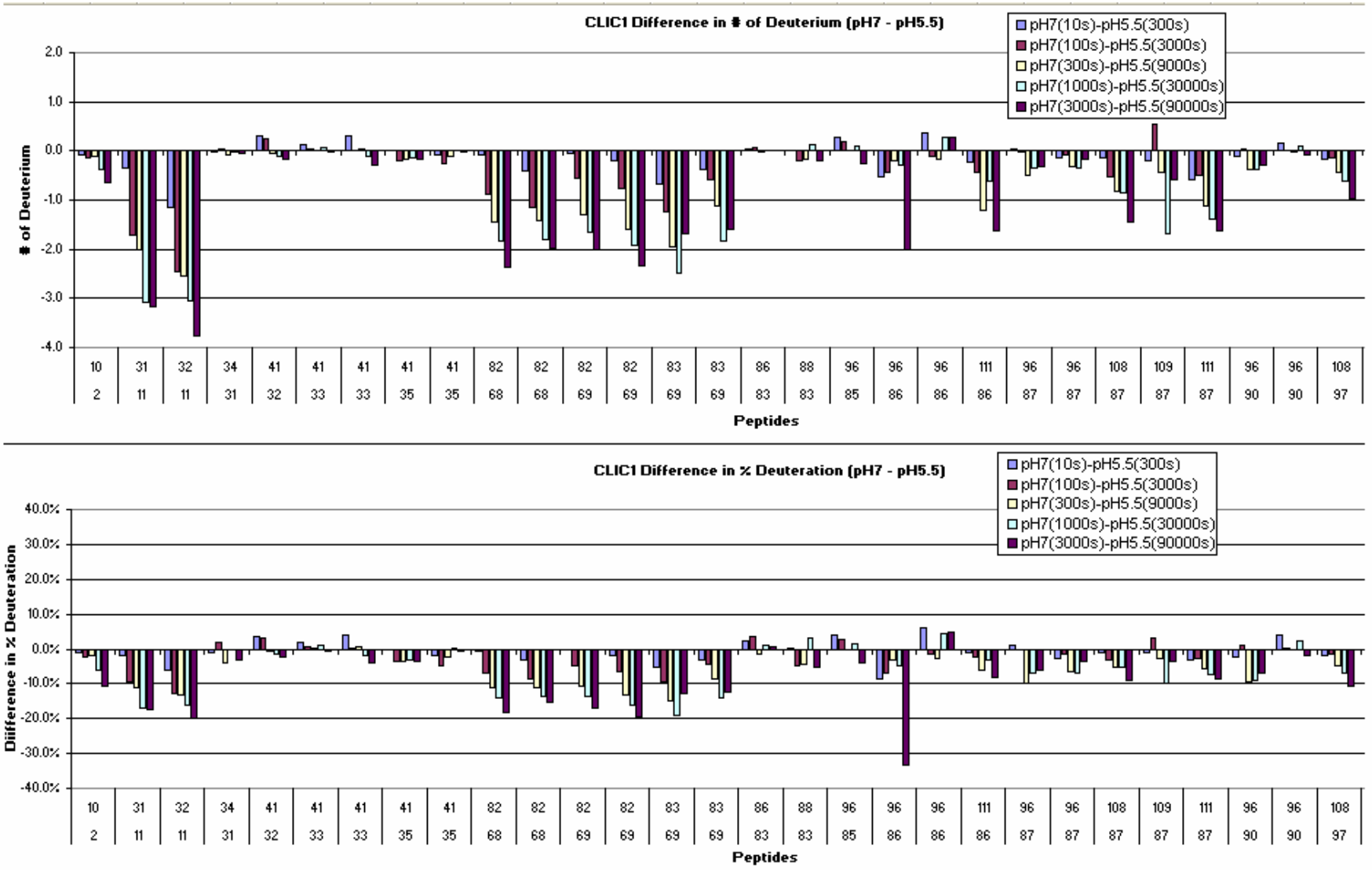


Figure 38: Ribbon representation of CLIC1 crystal structure showing regions affected by a drop in pH conditions.

Based on percentage and number of deuterium exchange for matching peptides of CLIC1 at pH 7.0 and pH 5.5. The regions that are more flexible at lower pH are indicated in red. The image was generated with Swiss PDB viewer (Guex and Peitsch, 1997) using the PDB file 1k0m (Harrop *et al.*, 2001).

A.


CLIC1 Difference in # of Deuterium (pH7 - pH5.5)
pH7(10s)-pH5.5(300s)
pH7(100s)-pH5.5(3000s)
pH7(300s)-pH5.5(9000s)
pH7(1000s)-pH5.5(30000s)
pH7(3000s)-pH5.5(90000s)
# of Deuterium
2.0
1.0
0.0
-1.0
-2.0
-3.0
-4.0
10 31 32 34 41 41 41 41 41 82 82 82 82 83 83 86 88 96 96 96 111 96 96 108 109 111 96 96 108
2 11 11 31 32 33 33 35 35 68 68 69 69 69 69 83 83 85 86 86 86 87 87 87 87 87 90 90 97
Peptides
CLIC1 Difference in % Deuteration (pH7 - pH5.5)
pH7(10s)-pH5.5(300s)
pH7(100s)-pH5.5(3000s)
pH7(300s)-pH5.5(9000s)
pH7(1000s)-pH5.5(30000s)
pH7(3000s)-pH5.5(90000s)
Diiifference in % Deuteration
40.0%
30.0%
20.0%
10.0%
0.0%
-10.0%
-20.0%
-30.0%
-40.0%
10 31 32 34 41 41 41 41 41 82 82 82 82 83 83 86 88 96 96 96 111 96 96 108 109 111 96 96 108
2 11 11 31 32 33 33 35 35 68 68 69 69 69 69 83 83 85 86 86 86 87 87 87 87 87 90 90 97
Peptides

B.

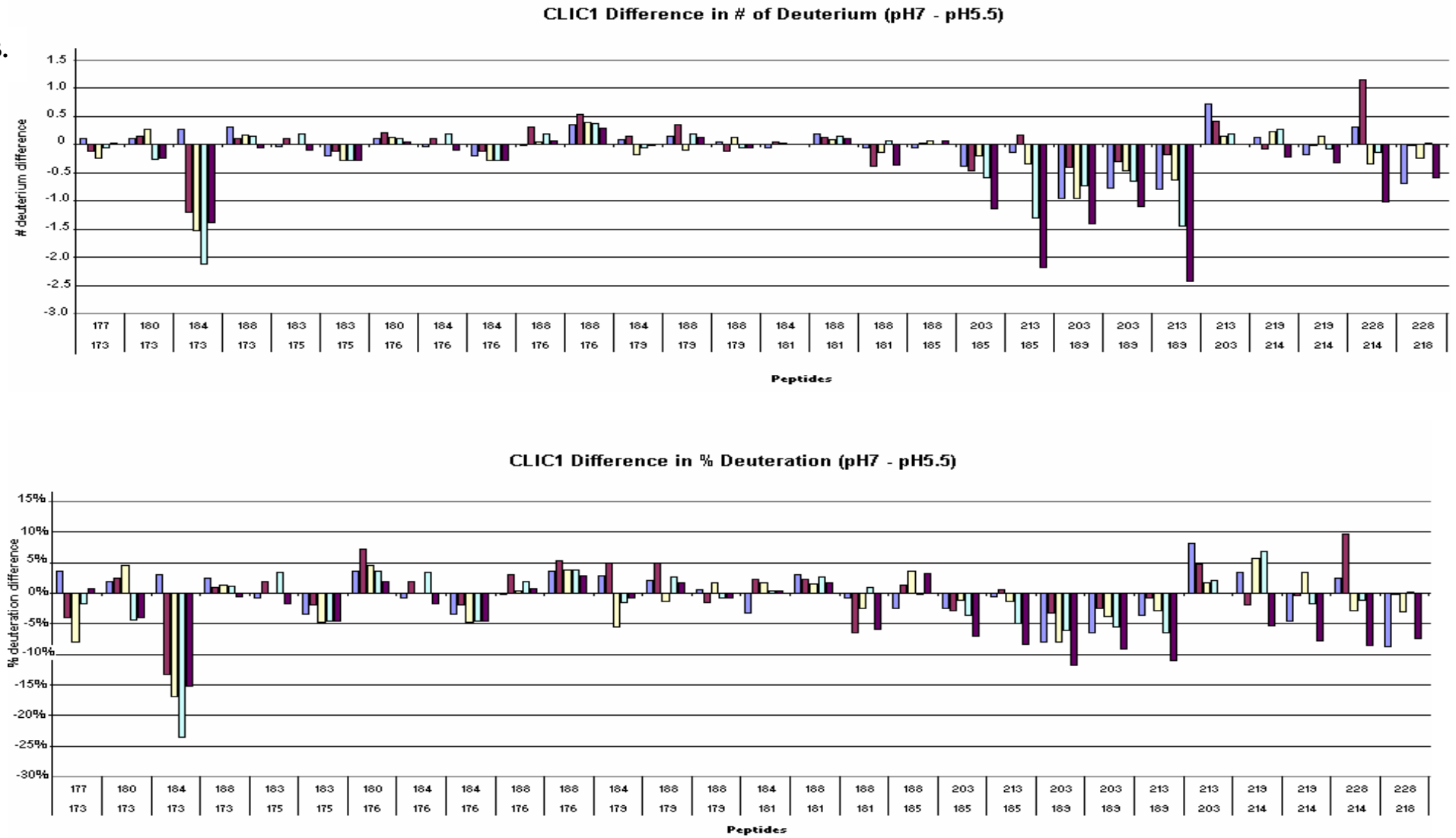


Figure 39: Graph indicating difference in number and percentage of deuterium bound to representative matching peptides at pH 7.0 and pH 5.5

Differences for corresponding time points were analysed. A difference greater than 1.5 deuteriums is considered significant. (A) Shows representative domain 1 peptides in the region of 1-108 (B) Shows representative domain 2 peptides in the region of 173-228.

also more flexible at lower pH exhibiting a 24 % (~ 2 deuteriums) increase in deuterium exchange for the corresponding 1000 second time point. No other significant difference in deuteration between the two pH conditions was observed. Because the hydrogen/deuterium exchange reaction is catalysed by hydroxide ion above pH 4 it is important to note that amide N-H groups that are in an anionic region of the protein will have decreased exchange due to Columbic repulsion of the catalyst. If a carboxylate residue is more fully protonated at lower pH then the region around it may display more robust exchange due to the loss of anionic character in the region.

3.5 Thermodynamics of Ligand Binding

Noncovalent binding of GSH to CLIC1 was investigated by titrating 127 μM of reduced CLIC1 at pH 7.0 with 100 mM reduced glutathione (GSH). The resulting titration profile indicated enthalpically unfavourable interactions with saturation not being reached at a final concentration of 15 mM GSH. This kind of binding isotherm represents weak binding and is consistent with previous preliminary studies by Harrop and co-workers (2001). They were not able to detect any noncovalent binding of GSH to CLIC1 up to 10 mM GSH, thus indicating that the dissociation constant is greater than 10 mM. Further studies titrating 5 μM reduced CLIC1 at pH 7.0 with 200 mM GSH still did not achieve saturation up to a final concentration of 35 mM GSH (see Appendix, Figure B).

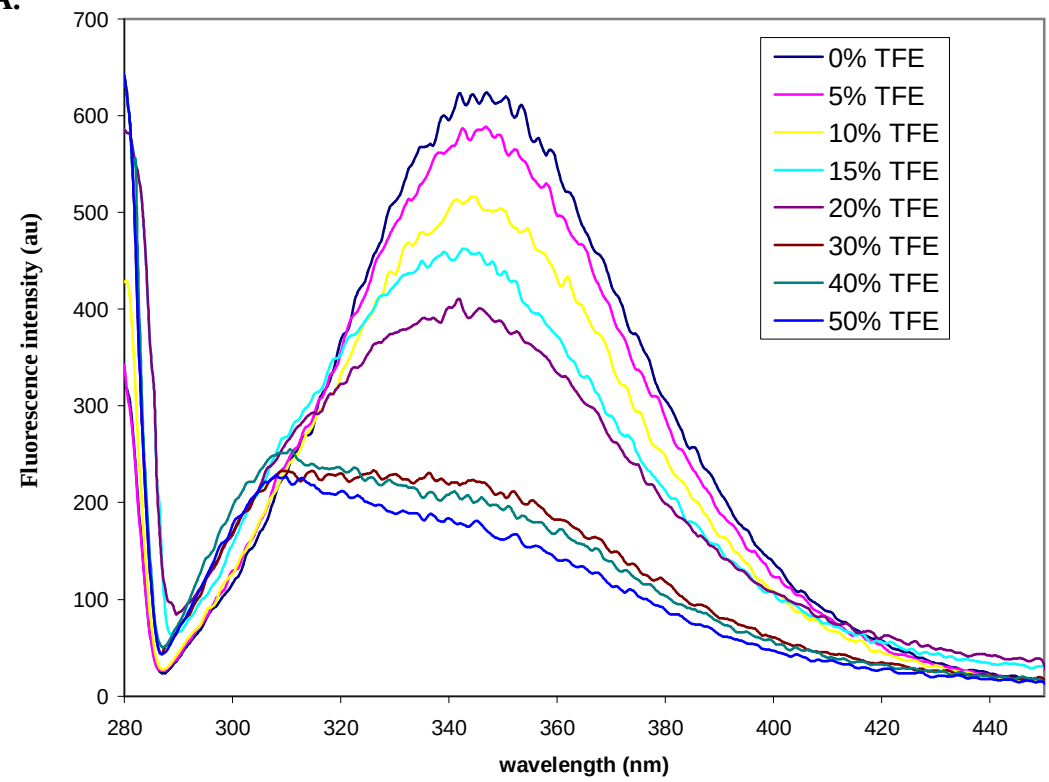
IAA is an indanyloxyacetic acid derivitave that is known to inhibit reconstituted CLIC1 with an apparent IC_{50} of approximately 9 μM (Tulk *et al.*, 1998). It has also been shown that 50 μM IAA significantly reduces CLIC1-mediated chloride efflux in "tip-dip" and planar bilayer experiments (Tulk *et al.*, 2002; Singh and Ashley, 2006). The thermodynamics of IAA binding to CLIC1 was investigated in order to clarify whether the inhibitory effects were due to binding of the molecule to CLIC1 or other effects created when IAA is added to CLIC1. IAA was made up to its maximum soluble concentration of 560 μM and was titrated to 134 μM of reduced CLIC1 at pH 7.0 in 8 μl increments. The resulting isotherms show very weak and noisy exothermic signals (see Appendix, Figure C) indicating that IAA at these concentrations binds CLIC1 very weakly, if at all.

3.6 CLIC1 Interaction with Membrane Model Systems

3.6.1 Effects of membrane-mimetic trifluoroethanol

Because of the similarity in properties between TFE and the hydrophobic interior environment of the membrane, TFE is considered as a membrane-mimetic solution and is widely used as a membrane model system (e.g. Mak *et al.*, 2001). In this study, the effect of varying concentrations of TFE on the secondary and tertiary structure of CLIC1 were investigated. Two μM CLIC1 at pH 7.0 was incubated with 0 – 50 % TFE for 10 minutes and then analysed using fluorescence spectroscopy and far-UV CD. Fluorescence spectra were obtained by exciting the sample at 280 nm and reading emission from 280 nm – 450nm (Figure 40A). TFE is known to progressively quench tryptophan fluorescence so the fluorescent data primarily served to identify aggregation for the far-UV CD data. Fluorescence data also assisted in providing an indication of any tertiary structural changes occurring. CLIC1 in 5% and 10% TFE (vol/vol) showed little or no change in secondary structure. The fluorescence spectrum for CLIC1 in 5 % TFE showed a slight decrease in intensity but the emission maximum was unchanged at 345 nm. For CLIC1 in 10 % TFE the fluorescence spectrum showed a 20 % drop in intensity and a small shift in emission maximum to lower wavelength, indicating a change in the tryptophan environment. Significant amounts of aggregation were noted when incubating CLIC1 with 15 % and 20 % TFE. This was observed by the cloudy solution formed when incubated at these concentrations and by the high fluorescence intensity emission at 280 nm. Interestingly, when the TFE concentration was increased to 30 %, 40% and 50% no evidence of aggregation was present. The helical content was drastically increased when CLIC1 was incubated with these TFE concentrations reaching a maximum helical increase of 37 % when incubated with 40 % TFE (Figure 41). The fluorescence spectra emission intensities were greatly diminished but this is probably due to the known quenching effects of TFE on tryptophan. To test whether the effects of TFE on CLIC1 were reversible, 4 μM CLIC1 incubated with 10 % TFE was diluted by half to give 2 μM CLIC1 with 5 % TFE. The resulting spectrum (Figure 40B), however, did not correspond to the spectrum of 2 μM CLIC1 incubated with 5 % TFE, indicating that the effects were not reversible. Urea-induced equilibrium unfolding experiments were attempted using CLIC1 in 30 % TFE. However, the protein was prone to aggregation even when low concentrations of TFE were used.

A.



B.

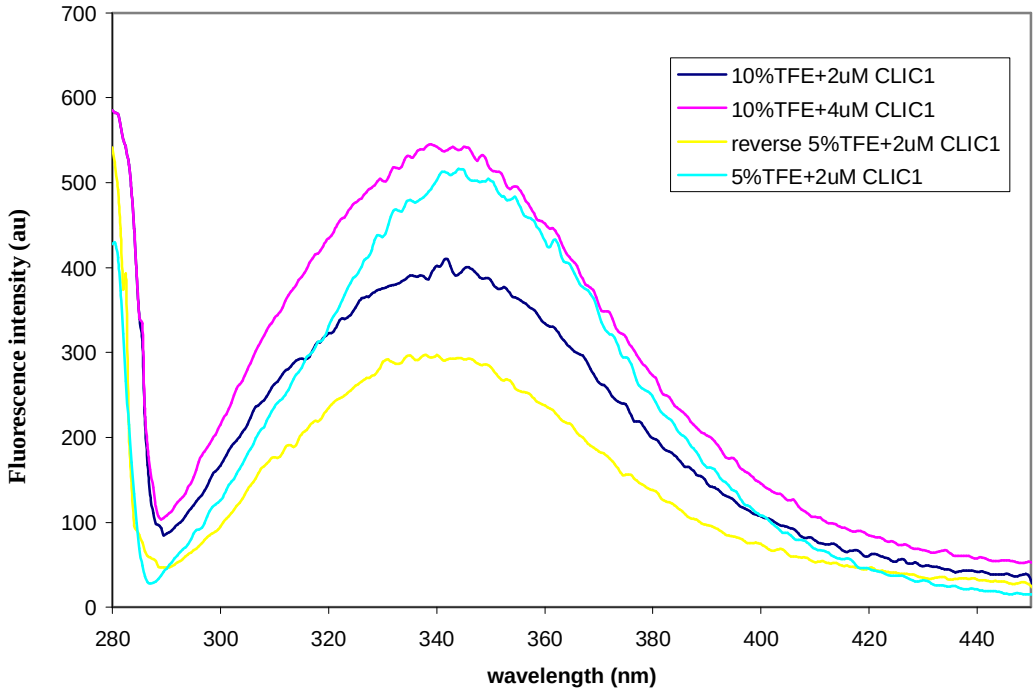


Figure 40: Fluorescence spectra of CLIC1 with varying concentrations of TFE

A. 2 µM CLIC1 was incubated with varying concentrations of TFE (0 – 50 %) and samples were excited at 280 nm.

B. Reversibility studies of CLIC1 incubated with TFE were performed by diluting 4 µM protein in 10 % TFE by half resulting in 2µM CLIC1 in 5 % TFE. The spectra indicate that the process is not reversible.

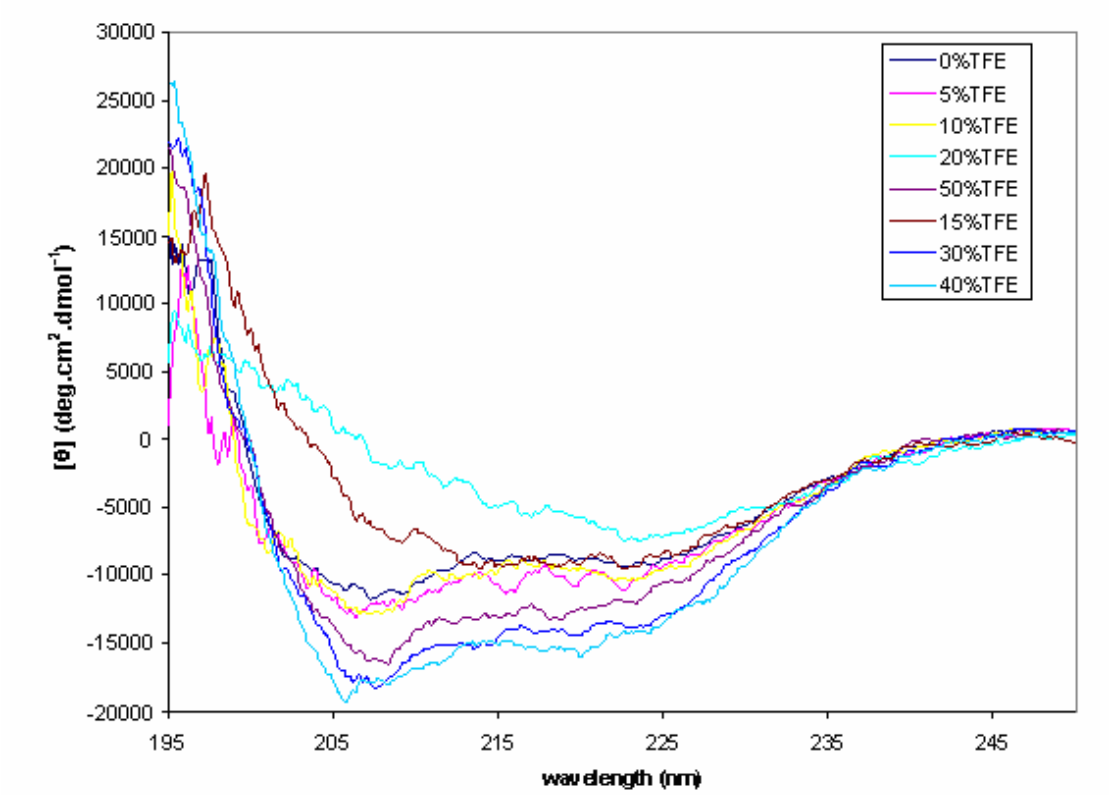


Figure 41: Far-UV CD spectra of CLIC1 incubated with varying concentrations of TFE.

5 μM CLIC1 was incubated with 0 – 50 % TFE and the ellipticity from 250 nm –195 nm was analysed. With 15% and 20% TFE the protein appears to be aggregating. For all other samples the helical content gradually increases with increasing TFE concentration. In 40 % TFE, the ellipticity peak at 208 nm has decreased to –18 mdeg compared to –12 mdeg for CLIC1 in the absence of TFE.

3.6.2 Cholesterol-containing Liposomes

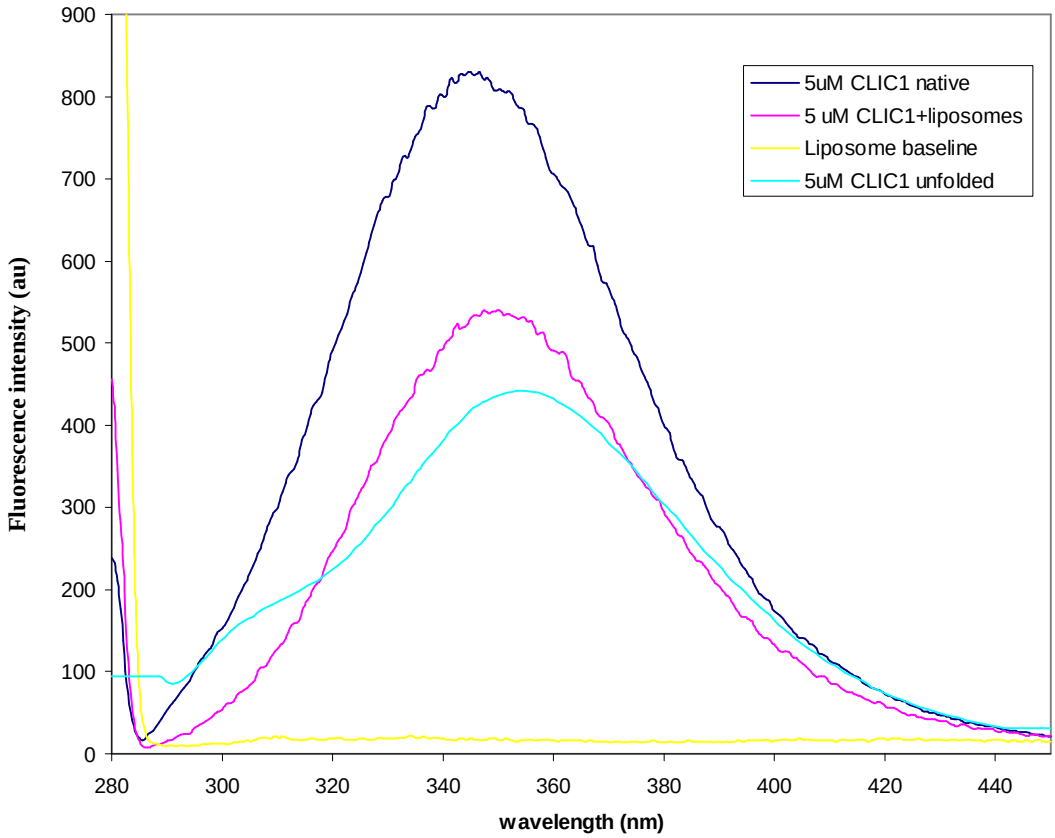
Sterile pre-liposome formulation was purchased from Sigma and prepared by adding 1 ml of protein storage buffer (50 mM sodium phosphate, pH 7.0). After vortexing and sonication in an ultrasonic water-bath for 45 minutes, a homogenous mixture of small unilaminar vesicles (SUV) was obtained. The liposome preparation was composed of approximately 52 % L-α-phosphatidylcholine β-oleoyl-γ-palmitoyl (POPC), 6 % L-α-phosphatidyl-DL-glycerol dioleoyl (DOPG), and 42 % cholesterol. This particular composition was also chosen because it yields negatively charged vesicles. The anionic characteristics best mimic the charge found at the membrane surface of intracellular organelles and the plasma membrane (van der Goot *et al.*, 1991).

3.6.2.1 Structural effects

The effect of liposomes on CLIC1 fluorescence was monitored by exciting the protein at 280 nm. The fluorescent properties of the lone Trp indole ring of 5 μM CLIC1, pH 7.0, incubated overnight with cholesterol-containing liposomes containing a total lipid concentration of 134 μM showed a red shift in emission maximum (Figure 42A). Native CLIC1 exhibits an emission maximum at 345 nm, while unfolded CLIC1 (using 8 M urea) has a maximum emission peak at 355 nm. When CLIC1 is incubated with cholesterol-containing liposomes the emission peak is at 350 nm and shows a decrease in fluorescence intensity. This is indicative of a partially unfolded CLIC1 structure with the lone tryptophan more exposed to solvent. It appears that the anionic, cholesterol-containing liposomes induce a structural re-arrangement of CLIC1 that may be adsorbed to the liposome surface but the protein is unable to penetrate and insert itself into the liposome. If CLIC1 is indeed binding to the liposomes, the proportion of bound to unbound CLIC1 is unknown.

Far-UV CD was used to assess any changes in secondary structure that may be occurring as a result of incubating CLIC1 at pH 7.0 with cholestrol-containing liposomes. Data were corrected for any contribution by free liposomes. The spectrum of CLIC1 incubated with liposomes shows no change in ellipticity pattern compared to native CLIC1 (Figure 42B).

A.



B.

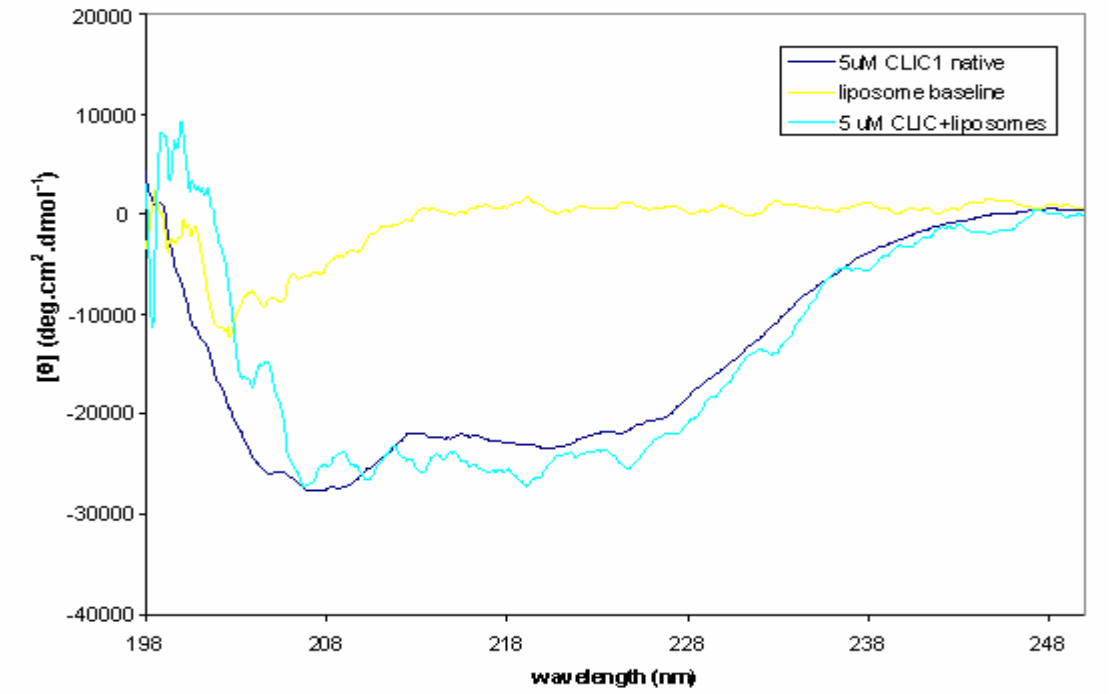


Figure 42: Fluorescence and far-UV CD spectra of CLIC1 incubated with cholesterol-containing liposomes

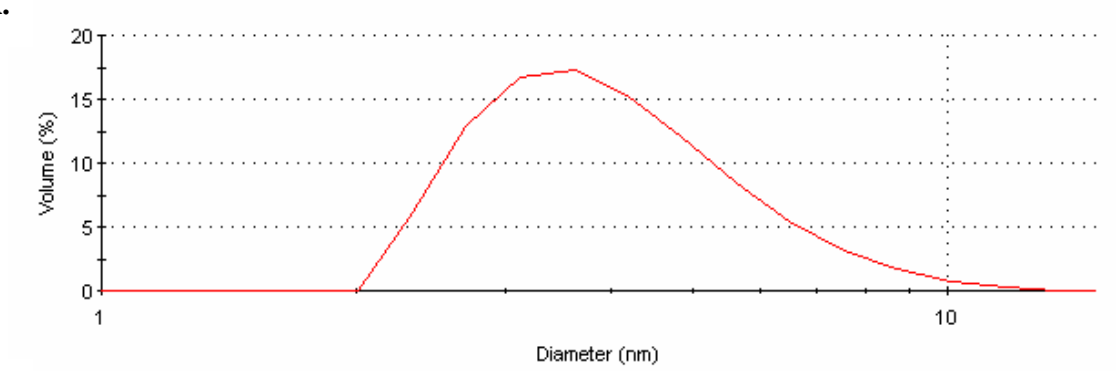
A. 5µM CLIC1 incubated with liposomes (pink) was excited at 280 nm and exhibited a slight red-shift to 347 nm and decrease in intensity.
B. No change in secondary structure was observed for 5 µM CLIC1 incubated with liposmes

The average hydrodynamic diameter of the sonicated cholesterol-containing liposomes was determined by dynamic light scattering (DLS) methods. The diameter of pure liposomes was determined at 75 nm (± 2.7) with a poly dispersity index (PDI) of 0.332 (Figure 43B). This diameter correlates well with the expected size of SUV. The hydrodynamic diameter of CLIC1 was found to be 6.4 nm (± 0.2) with a PDI of 0.240 (Figure 43A). This value is slightly higher than expected based on calculations done on the crystal structure (approx. 5 nm) but may be due to highly flexible nature of CLIC1 that would increase its hydrodynamic volume. This data correlates well with HPLC experiments that also showed CLIC1 to have a higher than expected hydrodynamic volume. It was interesting to note that when DLS was used to analyse CLIC1 incubated with liposomes the hydrodynamic diameter of the liposomes was found to be 100 nm (± 4.9) with a PDI of 0.230 (Figure 44A).

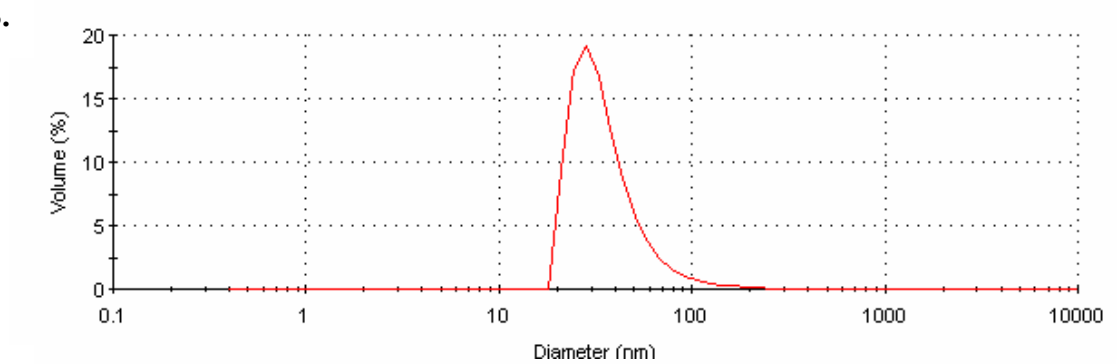
3.6.2.2 Isothermal Titration Calorimetry

The binding properties of CLIC1 at pH 7.0 and pH 5.5 with POPC/DOPG/cholestrol liposomes were studied using ITC. The total heats produced while injecting small aliquots of liposome dispersions in the protein solution at constant temperature 25°C were registered. Measurement of these heats allows very accurate determination of the thermodynamic profile of the molecular interaction. At 25°C the heat of dilution of the liposome dispersion from the syringe into the calorimeter cell containing only buffer was less than –0.05 μcal/sec and was subtracted from the raw ITC data. Optimisation of the experimental conditions to produce useable data (signal > 0.2μcal/sec) included varying the CLIC1 protein concentration in the sample cell from a range of 13 μM – 206 μM, and varying the volume of liposomes injected from 5 μl – 15 μl. After sampling a variety of conditions a useable signal was only obtained for 93 μM CLIC1 titrated with 7 μl and 15 μl injections of liposomes at pH 7.0 and pH 5.5, respectively. The signals obtained were relatively weak ranging from –0.23 μcal/sec to –0.43 μcal/sec but were nevertheless measurable and ran to saturation. The exothermic heat signals are indicative of enthalpically favourable interactions taking place. However, the weak signals and hyperbolic pattern of the isotherms show that the interaction is not very strong at pH 7.0 or pH 5.5.

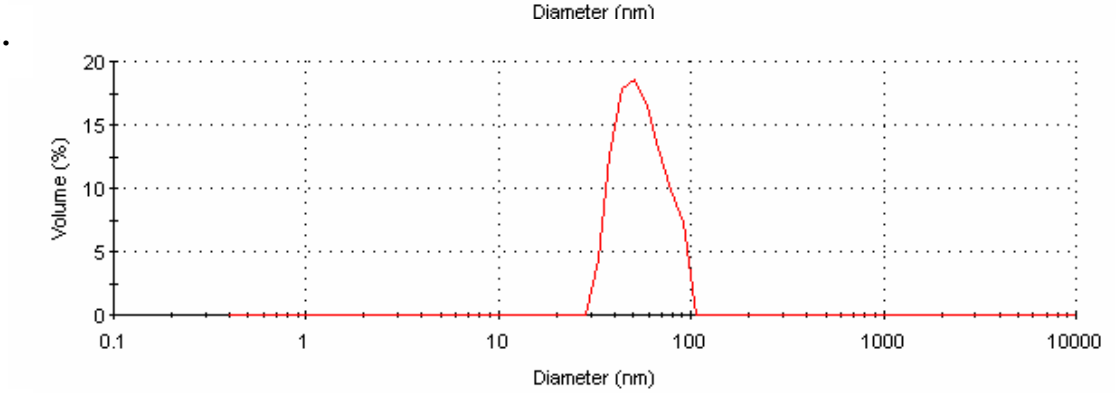
A.



B.



C.



D.

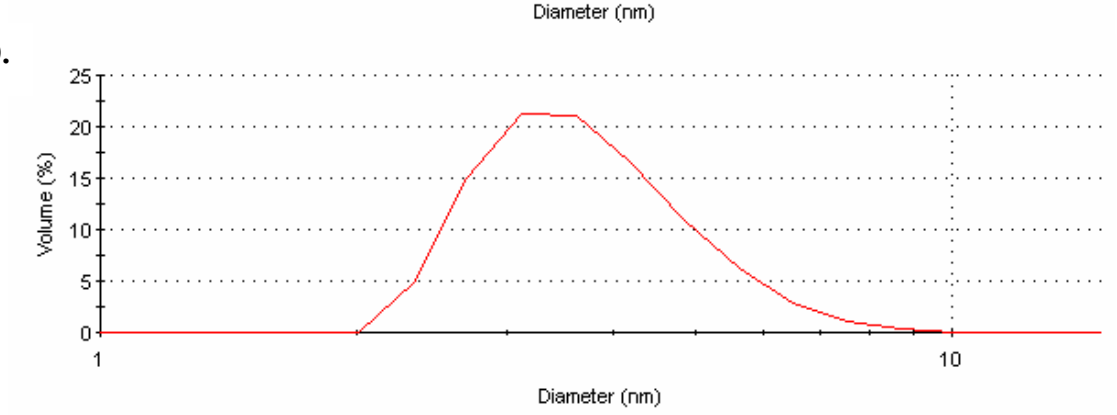


Figure 43: Size distribution by volume using dynamic light scattering of CLIC1, liposomes and micelles. Representative graphs show the distribution of predicted size of samples containing (A) 5 µM CLIC1, (B) 8.3 mM POPC/DOPG/cholesterol SUV, (C) 12.9 mM asolectin SUV and (D) 37.3 mM sarkosyl micelles. The predicted diameter was taken as an average of 5 runs.

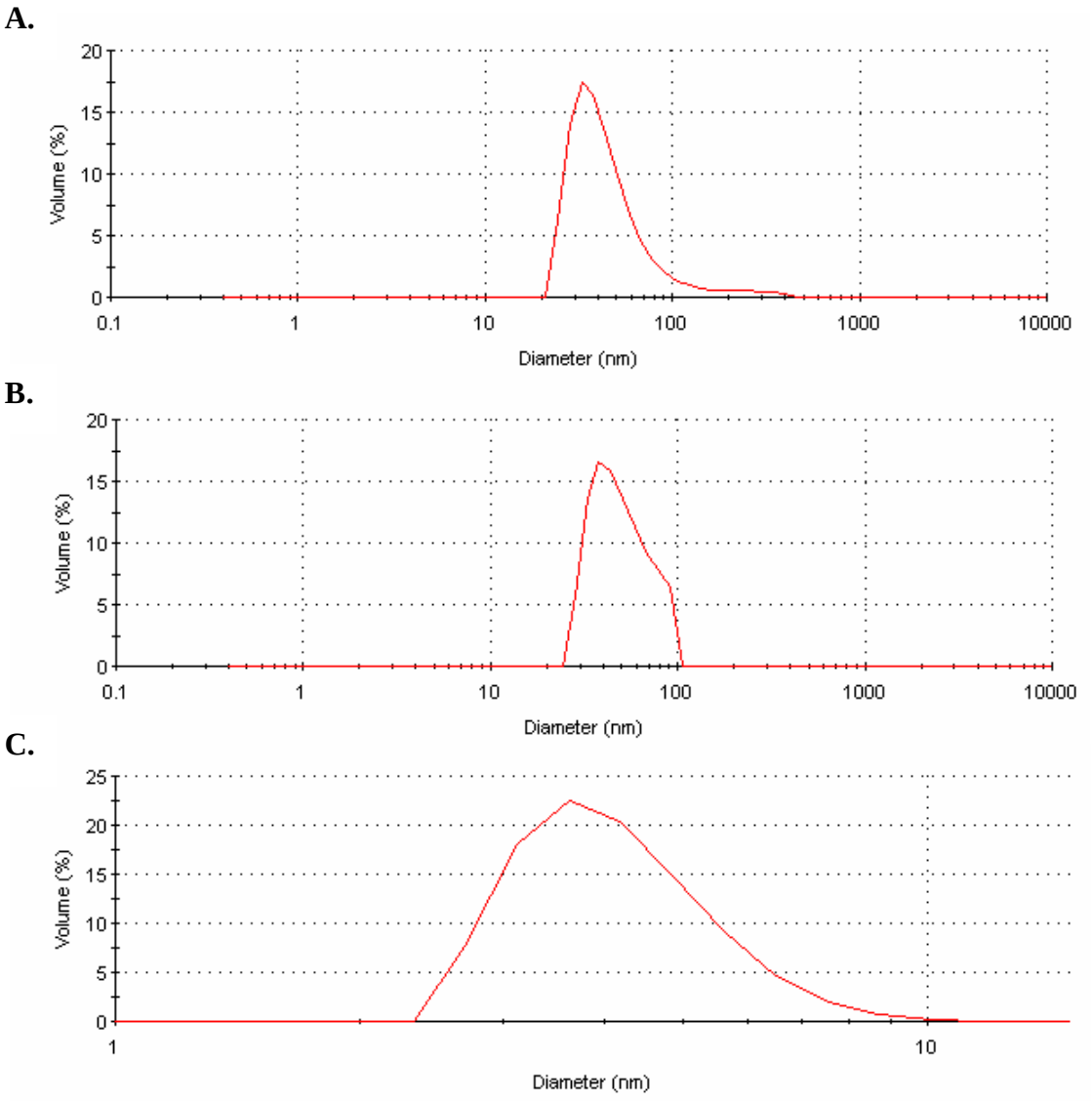


Figure 44: Size distribution by volume using dynamic light scattering of liposomes and micelles incubated with CLIC1. Representative graphs show the distribution of predicted size of samples containing 5 µM CLIC1 incubated with (A) 8.3 mM POPC/DOPG/cholesterol SUV, (B) 12.9 mM asolectin SUV and (C) 37.3 mM sarkosyl micelles. Samples were incubated for 1 hour and the predicted diameter was taken as an average of 5 runs.

Figure 45 shows the ITC data for 93 μM CLIC1 at pH 7.0 titrated with 7 μl injections of SUV (16.6 mM total lipid concentration) with weak initial endothermic heats for the first 4 injections followed by exothermic heats until saturation is achieved (~20 – 25 injections). The data fitted best to a single-site binding model. Figure 46 shows that 93 μM CLIC1 at pH 5.5, titrated with 15 μl injections of liposomes (8.3 mM total lipid concentration), does not exhibit the initial endothermic heats observed at pH 7.0. Exothermic heat signals reached saturation after approximately 12 injections. When the protein concentration was increased from 93 μM to 206 μM the initial endothermic heat signals were more pronounced at pH 7.0 (Figure 47B). The exothermic heats that followed were weaker than those observed using lower concentrations of CLIC1. A comparison of the isothermal profiles of 206 μM CLIC1 at pH 7.0 and pH 5.5 show larger exothermic heats for CLIC1 at pH 5.5 (Figure 47A) than at pH 7.0. This indicates a more enthalpically favourable interaction between CLIC1 and liposome at lower pH.

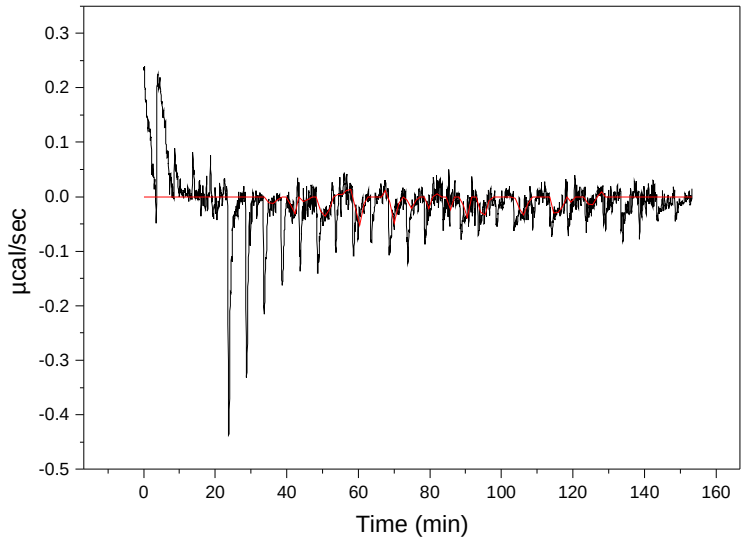
3.6.3 Asolectin Liposomes

3.6.3.1 Structural effects

The tryptophan fluorescence of 5 μM CLIC1 incubated overnight with asolectin containing a total lipid concentration of 140 μM was monitored (Figure 48A). No evidence of strong CLIC1 interaction with asolectin vesicles was noted. The spectrum for CLIC1 incubated with asolectin showed a drastic decrease in intensity and a red shift in emission maximum from 347 nm to 354 nm. Circular dichroism in the far-UV range was performed to monitor any changes in secondary structural content that may be occurring as a result of CLIC1 interaction with asolectin vesicles. Although the contribution of asolectin resulting in a somewhat noisy CD signal it appears as though the spectral pattern of CLIC1 incubated with asolectin vesicles remained essentially unchanged (Figure 48B). Data below 215 nm was too noisy and thus could not be used for analysis.

To determine the size of the prepared asolectin vesicles a pure sample was subjected to scattering by monochromatic light and the scattered light intensity was measured at a scattering angle of 90°. The results indicated a hydrodynamic diameter of 102 nm

A.



B.

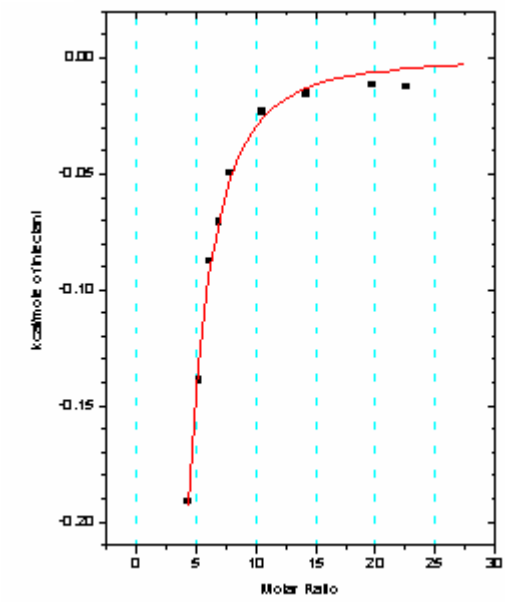
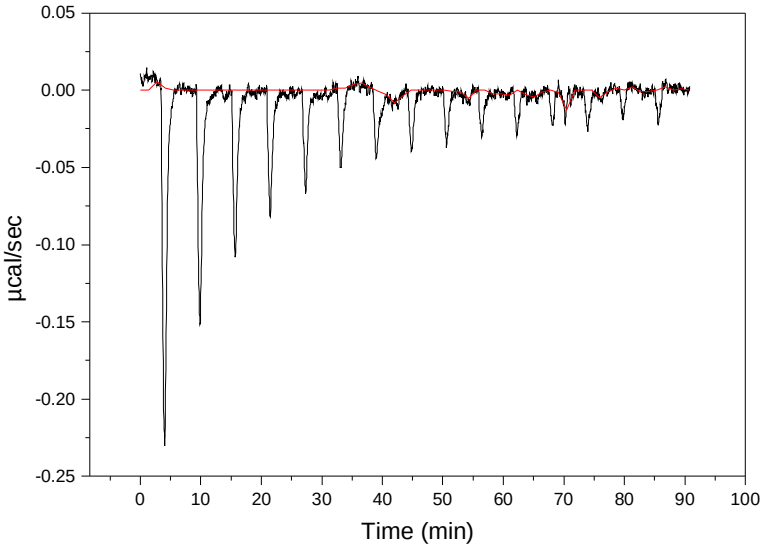


Figure 45: A representative calorimetric profile of the interaction of cholesterol-containing liposomes with CLIC1 at pH 7.0.

Panel A shows the heat effects associated with the 7 µl injections of liposomes into the ITC sample cell containing 93 µM CLIC1 at pH 7.0. Panel B shows the binding isotherm (corrected for heats of dilution) corresponding to the exothermic portion of the data in Panel A. The solid line through the data represents the best fitted curve obtained using ORIGIN software.

A.



B.

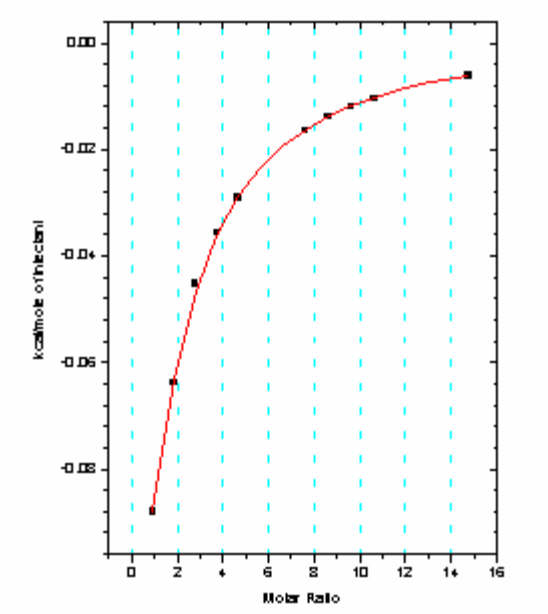
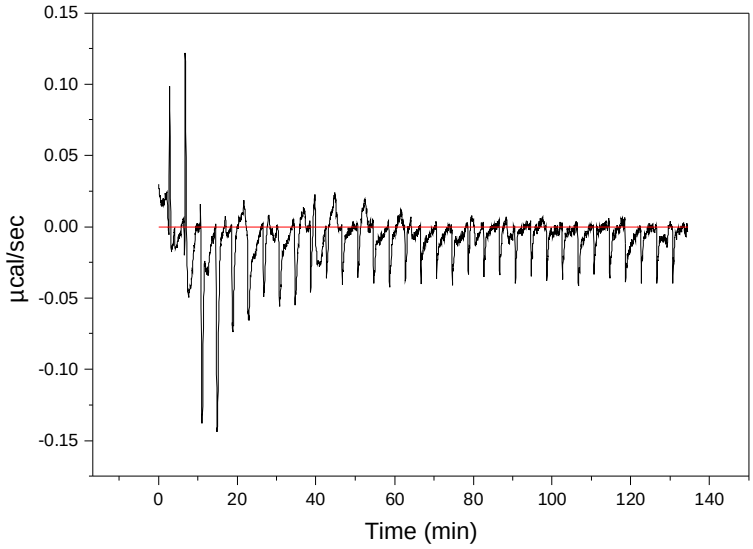


Figure 46: A representative calorimetric profile of the interaction of cholesterol-containing liposomes with CLIC1 at pH 5.5.

Panel A shows the heat effects associated with the 7 µl injections of liposomes into the ITC sample cell containing 93 µM CLIC1 at pH 5.5. Panel B shows the binding isotherm (corrected for heats of dilution) corresponding to the data in Panel A. The solid line through the data represents the best fitted curve obtained using ORIGIN software.

A.



B.

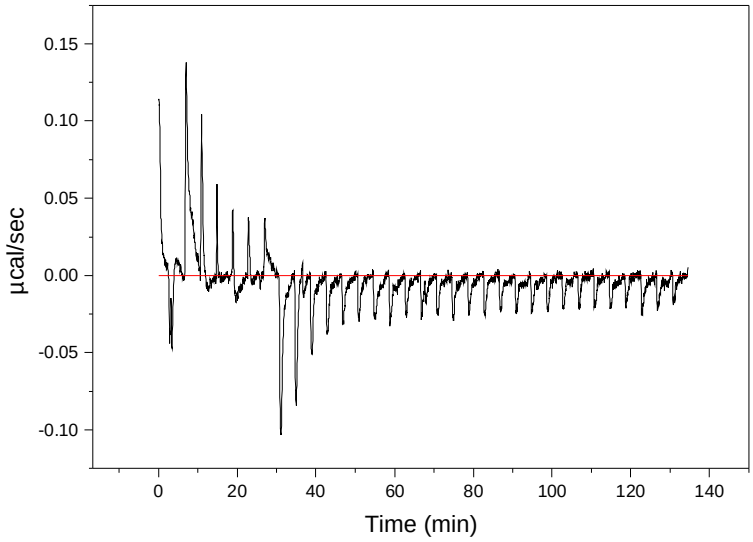
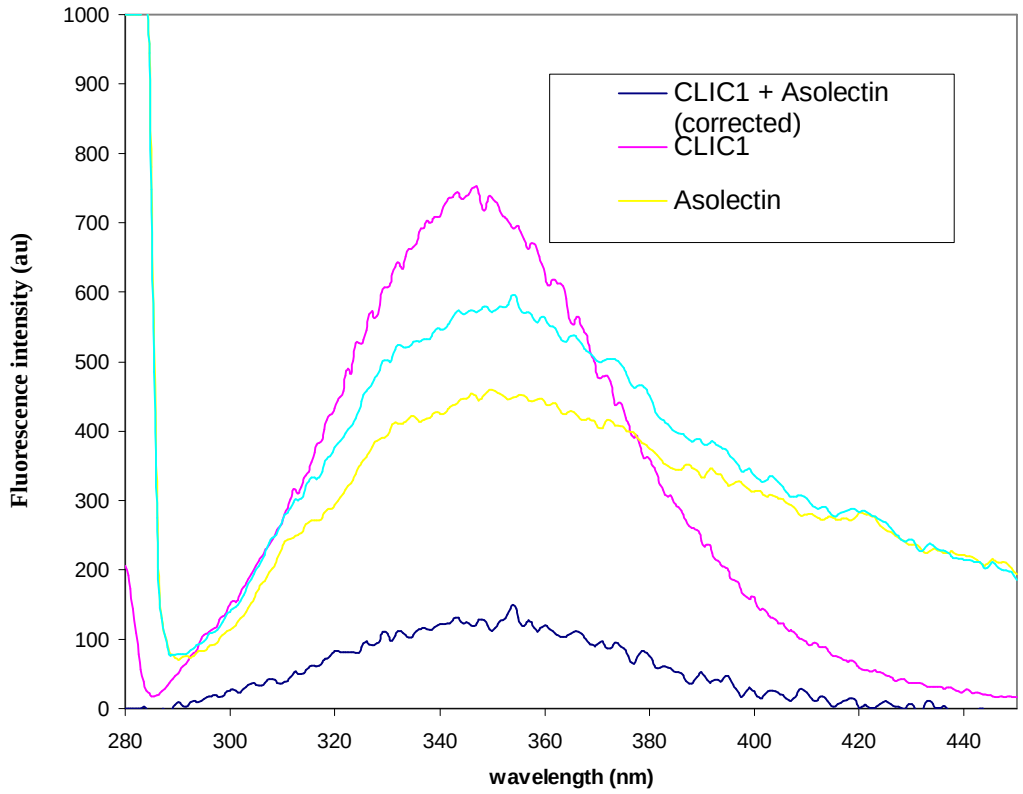


Figure 47: Calorimetric titration profile for high concentrations of CLIC1 titrated with cholesterol-containing liposomes.

Panel A shows the heat effects associated with the 7 µl injections of liposomes into 206 µM CLIC1 at pH 5.5, while panel B shows represents 206 µM CLIC1 at pH 7.0.

A.



B.

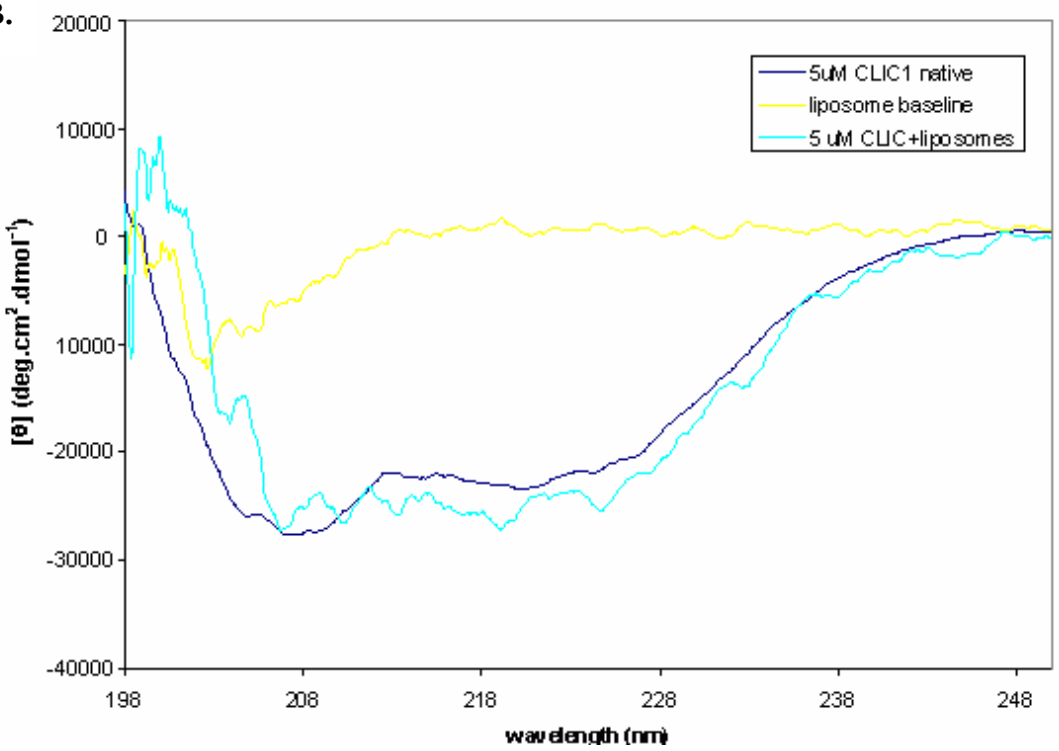


Figure 48: Fluorescence and Far-UV CD spectra of CLIC1 incubated with asolectin vesicles.

A. 5 µM CLIC1 was incubated with asolectin vesicles and excited at 280 nm. The asolectin vesicles exhibited fluorescent properties and data was corrected for this. A slight red-shift to 247 nm and decrease in intensity was observed.

B. Far-UV CD signal was noisy below 215 nm but 5 µM CLIC1 incubated with asolectin vesicles (pink) appears to superimpose with 5 µM native CLIC1 (light blue) from 250 nm – 215 nm. Data was corrected for the asolectin vesicles blank (yellow).

(±1.0) for the asolectin vesicles with a PDI of 0.239 (Figure 43C). When 5 μM CLIC1 was incubated with the asolectin vesicles no significant change in the vesicle size (98.1 nm ± 0.7) was observed (Figure 44B). A change in the hydrodynamic diameter of the vesicles is expected if the protein is adsorbing to or oligomerizing on the vesicle surface.

3.6.3.2 Thermodynamic effects

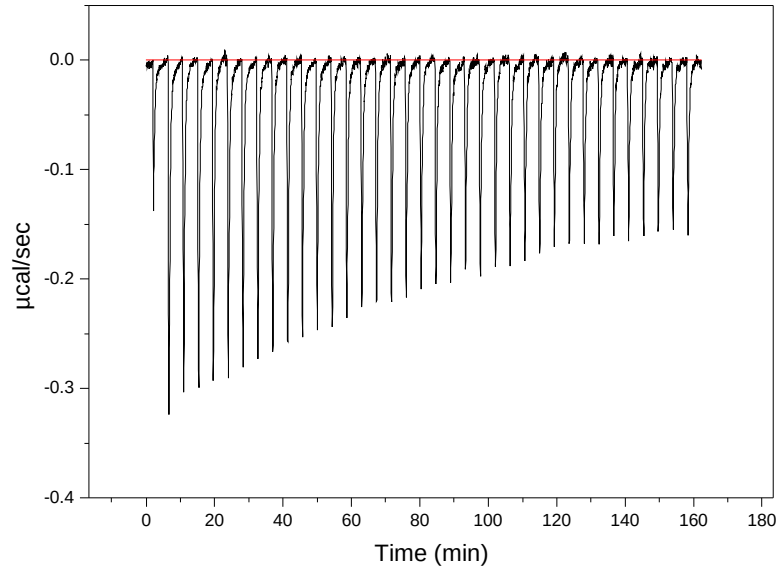
As with the POPC/DOPG/cholesterol liposomes, it appears that CLIC1 does not readily insert into asolectin vesicles. The ITC profiles (Figure 49) show relatively large and measurable exothermic heats (~ -0.32 μcal/sec and -0.54 μcal/sec for pH 7.0 and pH 5.5, respectively) but do not fully reach saturation, even after heat of dilution effects (see Appendix, Figure D) are corrected for.

3.6.4 Detergent Micelles

3.6.4.1 Structural effects

CLIC1 was incubated for 1 hour with varying concentrations of sarkosyl above the critical micellar concentration (CMC). The fluorescence emission spectra of 5 μM CLIC1 incubated with micelles was excited at 280 nm and showed a blue-shift in emission maximum with a decrease in emission intensity (Figure 50A). When 5 μM CLIC1 was incubated with 10.3 mM sarkosyl a shift from 347 nm to 342 nm was noted. This blue-shift pattern is indicative of the proteins lone tryptophan moving to a more non-polar environment and may represent CLIC1 insertion into the micelle or a structural change resulting in the tryptophan becoming more buried within the protein itself. In order explain the decrease in emission intensity when CLIC1 is incubated with micelles an investigation into the quenching effects of sarkosyl on tryptophan fluorescence was undertaken. Fluorescence spectra for 5 μM NATA incubated with micelles showed a decrease in fluorescence emission providing evidence for a quenching effect of micelles on tryptophan fluorescence (Figure 51). Any observed decrease in fluorescence emission intensity observed for CLIC1 incubated with micelles can thus be attributed to this quenching effect. However, no shift in emission maximum was noted when NATA was mixed with micelles suggesting that any shift observed for CLIC1 with micelles was a result of the protein inserting into the micelle, positioning the lone tryptophan residue within the non-polar hydrophobic

A.



B.

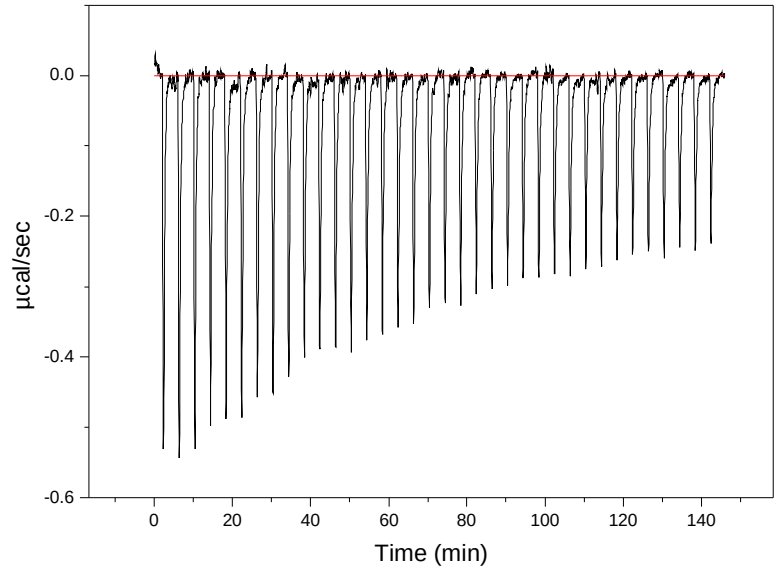
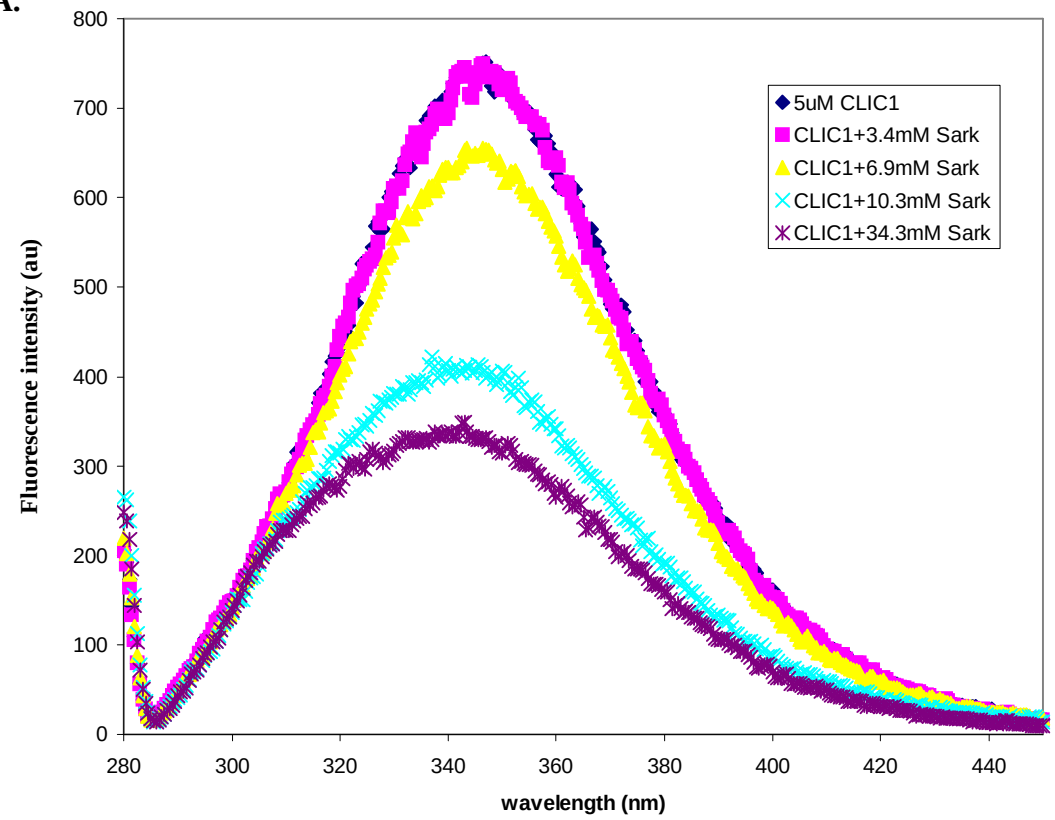


Figure 49: Calorimetric titration profile of the interaction of asolectin vesicles and CLIC1 at pH 7.0 and pH 5.5.

Panel A represents CLIC1 at pH 7.0 (102 µM) while panel B represents CLIC1 at pH 5.5 (104 µM). Neither reaction ran to saturation.

A.



B.

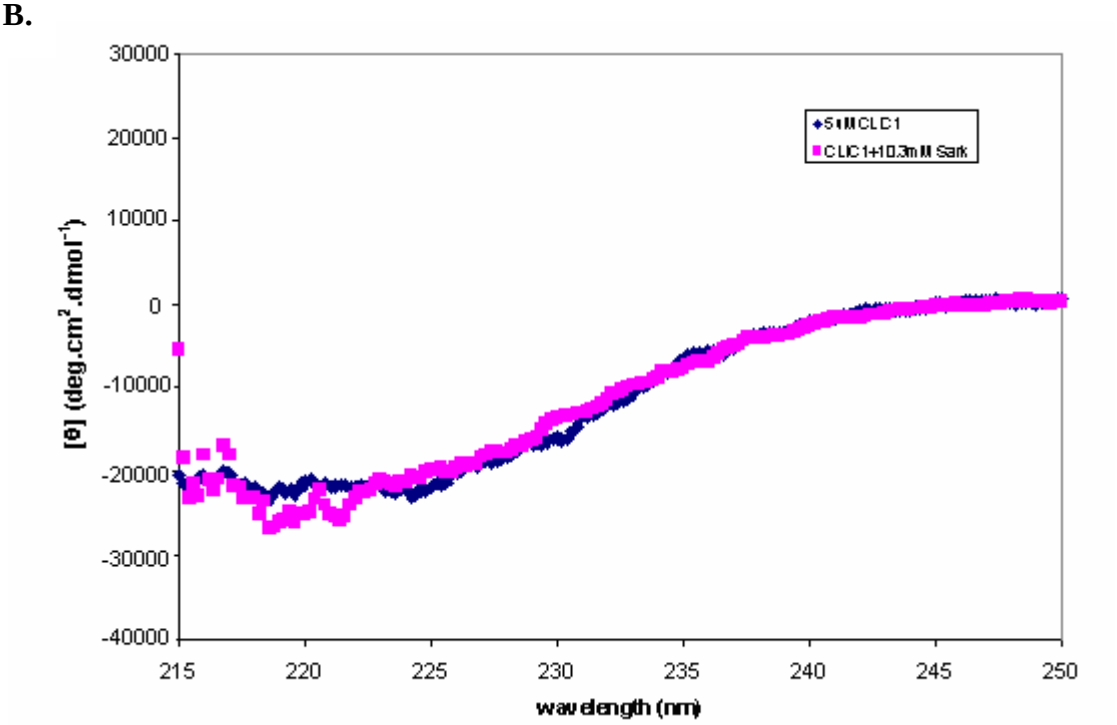


Figure 50: Fluorescence and Far-UV CD spectra of CLIC1 incubated with sarkosyl micelles.

Panel A shows the fluorescence spectra of 5 µM CLIC1 incubated with varying concentrations of sarkosyl and excited at 280 nm. The emission maxima are blue-shifted and the intensity is diminished as the concentration of sarkosyl is increased. Panel B shows the superimposable far-UV CD spectra for 5 µM CLIC1 incubated with micelles (10.3 mM sarkosyl) and 5 µM native CLIC1.

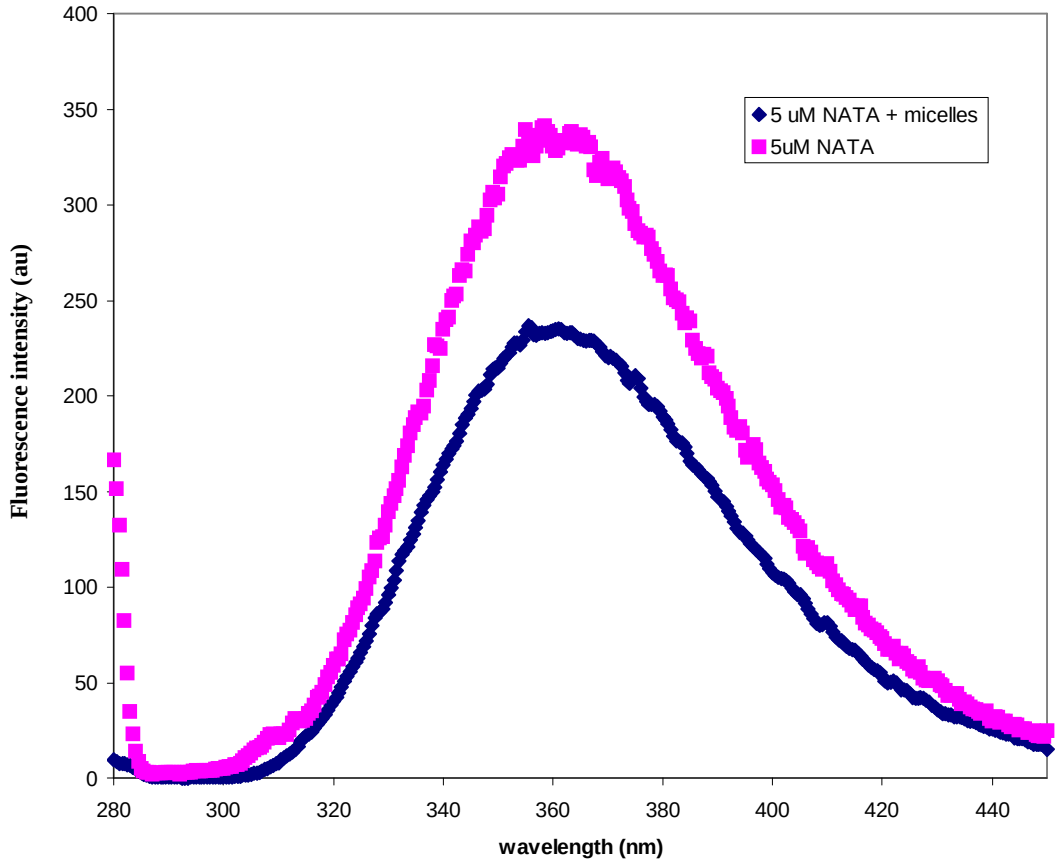


Figure 51: Fluorescence spectra showing the effect of sarkosyl micelles on NATA.

Micelles made up from 10.3 mM sarkosyl were incubated with 5 µM NATA and excited at 280 nm. A diminished fluorescence intensity was evident when the micelles were added to NATA (blue) compared with 5 µM NATA on its own (pink). This indicates a quenching effect of sarkosyl micelles on tryptophan fluorescence.

core. The other possibilities are that the tryptophan is becoming more buried within the protein itself, due to structural changes induced by the micelles, or at the interface of CLIC1 and the surface of the membrane.

Far-UV CD spectra for 5 μM CLIC1 incubated with micelles (10.3 mM sarkosyl) for 1 hour resulted in a noisy signal below 215 nm and data in this range could not be used for comparison with free CLIC1. Spectral data from 250 nm – 215 nm, however, appeared to be superimposible for free CLIC1 and micelle-associated CLIC1 (Figure 50B) indicating that no significant change in secondary structural content was occurring as a result of CLIC1 interaction with micelles. It must be noted, however, that the proportion of inserted/associated to uninserted/unassociated CLIC1 is unknown. If the ratio of inserted/associated CLIC1 to uninserted/unassociated CLIC1 is small, then the signal might not show any associated changes in structure.

The hydrodynamic diameter for the micelles formed by 10 % sarkosyl (343 mM) was determined to be 4.6 nm ± 0.4 (PDI = 0.119) (Figure 43D). This diameter is indicative of small, tightly associated micelles with a low aggregation number. This correlates well with the low CMC value obtained experimentally using ITC (see section 3.6.4.4). The larger hydrodynamic diameter obtained for free CLIC1 (6.6 nm ± 0.2) suggests that it is possible for CLIC1 to completely traverse the micelle. Indeed, DLS shows that when CLIC1 is incubated with micelles the hydrodynamic diameter of the micelles increases from 4.6 nm (± 0.4) to 5.2 nm (± 0.1) (Figure 44C). This increase in diameter may be a result of portions of the inserted protein “sticking out” of the micelle and thus increasing the reported hydrodynamic diameter of the micelles.

3.6.4.2 Thermodynamic effects

Sarkosyl CMC

The critical micellar concentration (CMC) for sarkosyl was experimentally determined by ITC methods. This value is crucial in order to ensure experiments are

performed using fully formed micelles that will mimic membrane structure and not detergent monomers. The CMC of a detergent can be experimentally determined by titrating small aliquots of the detergent into aqueous solution and measuring the resulting heat signals.

Two µl injections of 10 % sarkosyl (343 mM) were titrated into buffer (50 mM sodium phosphate, pH 7.0) at 25 ºC. The raw data obtained from the calorimetric experiments were collected and integrated using ORIGIN software. The sigmoidal graph obtained from plotting enthalpy against sarkosyl concentration was fitted and analysed using the programme SigmaPlot version 7.00 (Jandel Corporation). The midpoint of the sigmoidal graph represents the CMC value and was found to be 2.7 mM for sarkosyl (Figure 52). This is the concentration were sarkosyl monomers begin to aggregate or oligomerise to form micelles. The relatively low CMC value for sarkosyl indicates that its monomers readily interact to form micelles. The enthalpy change (ΔH) value for sarkosyl micellisation was –460 kcal/mol, while the change in Gibbs free energy (ΔG) for the demicillisation process was 3.5 kcal/mol. The high exothermic enthalpy value is indicative of an enthalpically favourable reaction to form tight and compact micelles. Another parameter obtained was $T\Delta S$ of demicellisation (456.5 kcal/mol) at 25° C.

pH 7.0

To correct for heat of dilution effects, control experiments were performed by replicating the exact conditions of each experiment but not including protein in the sample cell (i.e. micelles into buffer) (Figure 53). The control data was subtracted from the raw data to obtain the corrected heat of the interaction between the protein and micelles.

In order to gain insight into the thermodynamic properties of CLIC1 interacting with membrane systems at neutral pH, and to serve as a reference experiment for comparative reasons, a thermodynamic study of CLIC1 at pH 7.0 with micelles was performed. 10 % sarkosyl was injected in 4 µl increments to 115 µM CLIC1 (Figure 54). The first injection of any ITC experiment is usually excluded from analysis. The following 4 injections show an endothermic pattern. Since the concentration of sarkosyl in the sample cell is only greater than the CMC value after 3 injections these

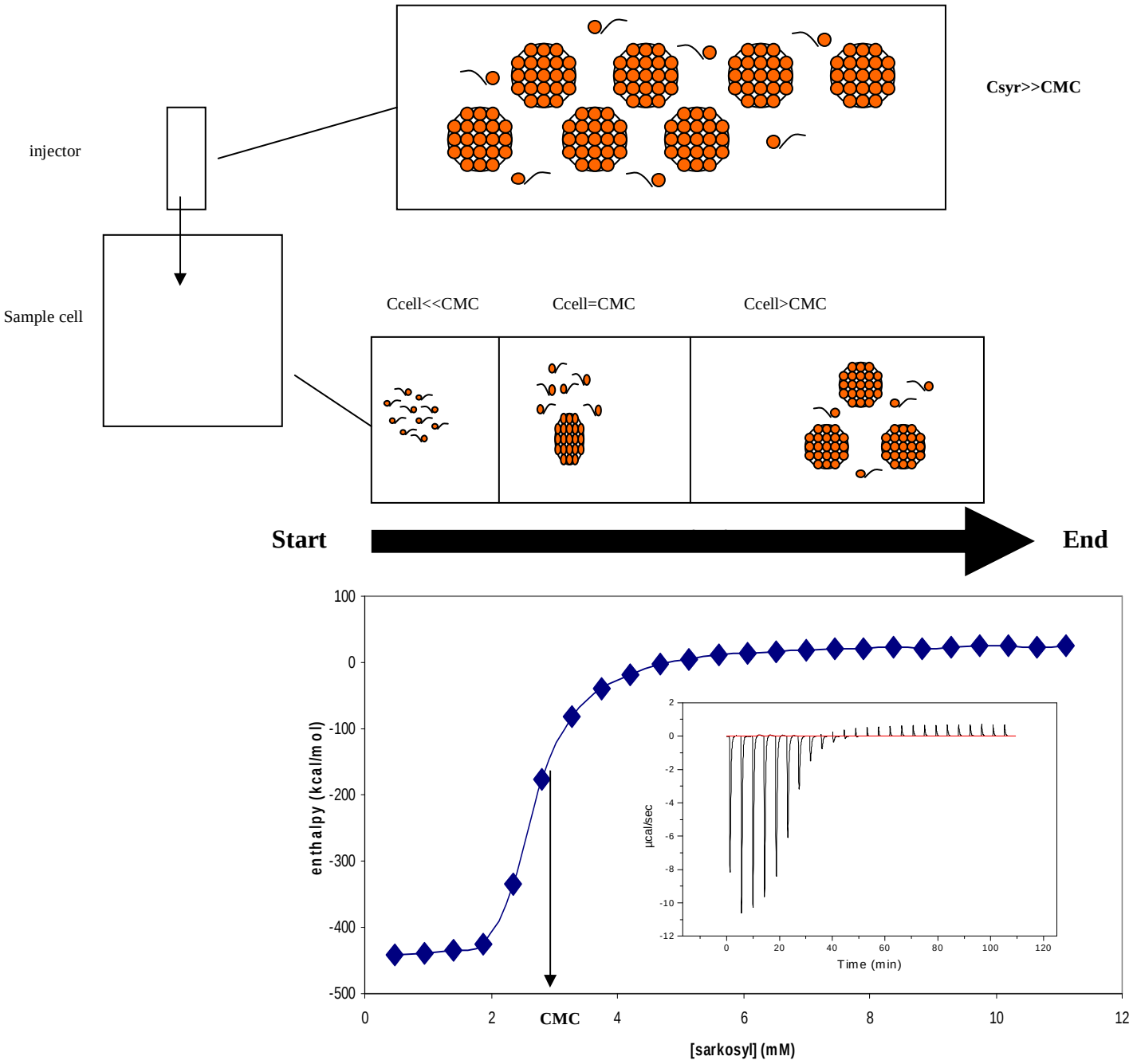


Figure 52: Schematic showing micelle formation and determination of sarkosyl CMC.

The schematic above the start/stop arrow represents the ITC sample cell and injector with a high concentration of sarkosyl being titrated into buffer. Below the start/stop arrow is the calorimetric titration profile used to determine the CMC value for sarkosyl. The detergent was titrated in 2 µl increments into buffer at 25° C and the resulting heat effects monitored (inset). Data was then fitted and the CMC value was determined by the midpoint of the sigmoidal plot.

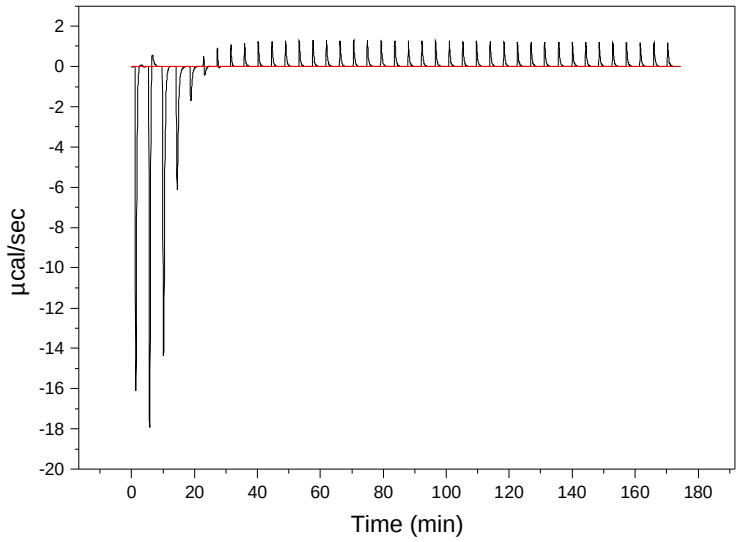
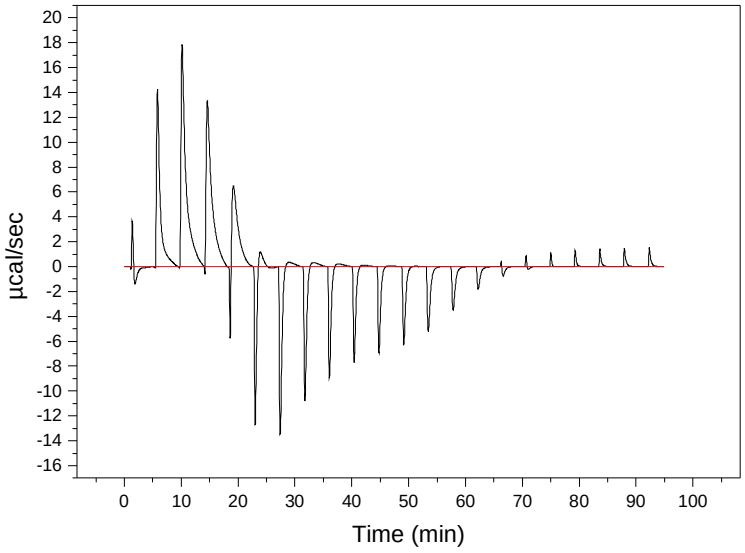


Figure 53: Heat of dilution effects for sarkosyl into buffer at 25° C
4 µl injections of 10% sarkosyl were titrated into buffer in order to determine the heat of dilution pattern and to enable correction of the raw data. The exact conditions of experiments using protein were replicated.

A.



B.

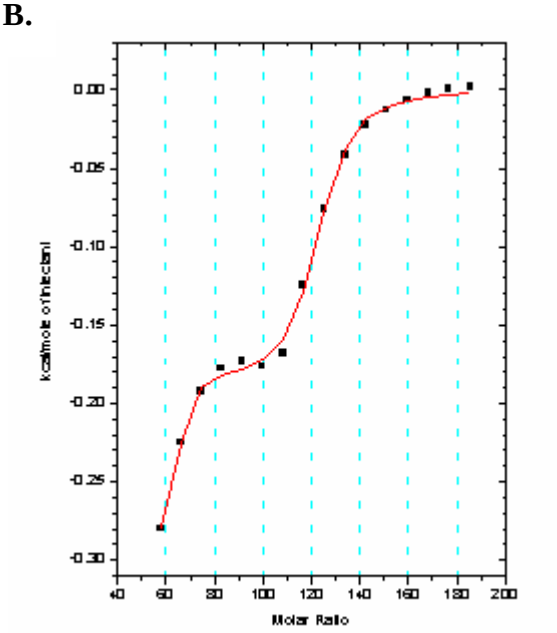


Figure 54: A representative calorimetric profile of the interaction of sarkosyl micelles with CLIC1 at pH 7.0.

Panel A shows the heat effects associated with the 4 µl injections of micelles into the ITC sample cell containing 115 µM CLIC1 at pH 7.0. Panel B shows the binding isotherm (corrected for heats of dilution) corresponding to the data in Panel A. The solid line through the data represents the best fitted curve (2 binding site model) obtained using ORIGIN software.

initial heats cannot be used for analysis since they may be as a result of sarkosyl monomers interacting with the protein. The heats obtained from the fourth injection onwards, however, represent the energetics of the association of CLIC1 with micelles.

A small initial endothermic contribution is followed by strong exothermic signals that reach saturation after approximately 20 injections. The exothermic data were fitted to a 2-binding site model. ΔH_1 and ΔH_2 for the interaction of CLIC1 at pH 7.0 were –0.186 kcal/mol and –0.294 kcal/mol, respectively. ΔG_1 and ΔG_2 were –5.47 kcal/mol and –9.14 kcal/mol, respectively, while ΔS_1 and ΔS_2 were 0.018 kcal/mol and 0.030 kcal/mol, respectively.

Reverse titration

In this experiment, the calorimeter cell contained micelles (34.3 mM sarkosyl) and small aliquots of CLIC1 were injected. A typical result is shown in Figure 55. In each step, 3 µl of a 60 µM CLIC1 solution was injected into a suspension of anionic micelles. The reaction is exothermic, and the heat of reaction is approximately -3 µcal per injection as derived from the integration of the titration peaks. In a control experiment, protein was injected into buffer. The heat of reaction was small (-0.05 µcal/inj) and was subtracted from the raw data.

Reduced glutathione

The effect of reduced glutathione (GSH) on CLIC1 membrane interaction was investigated by pre-incubating CLIC1 (pH 7.0) with 2 mM GSH and performing an identical ITC experiment to that for CLIC1 in the absence of GSH. This relatively low concentration of GSH was selected for this experiment in order to directly compare results with another study (Tulk *et al.,* 2002), which found that 2 mM GSH inhibited CLIC1 channel activity. The raw data (Figure 56) indicated that 2 mM GSH had little or no effect on the thermodynamics of CLIC1 interaction with the micelles and the parameters obtained after fitting the data further validated this. The exothermic data was fitted to a 2-binding site model. Thermodynamic parameters remained largely unchanged compared with experiments using CLIC1 at pH 7.0 in the absence of any ligand or inhibitor. ΔH_1 and ΔH_2 for the interaction of CLIC1 treated with 2 mM GSH were –0.198 kcal/mol and –0.285 kcal/mol, respectively. ΔG_1 and ΔG_2 were –5.29

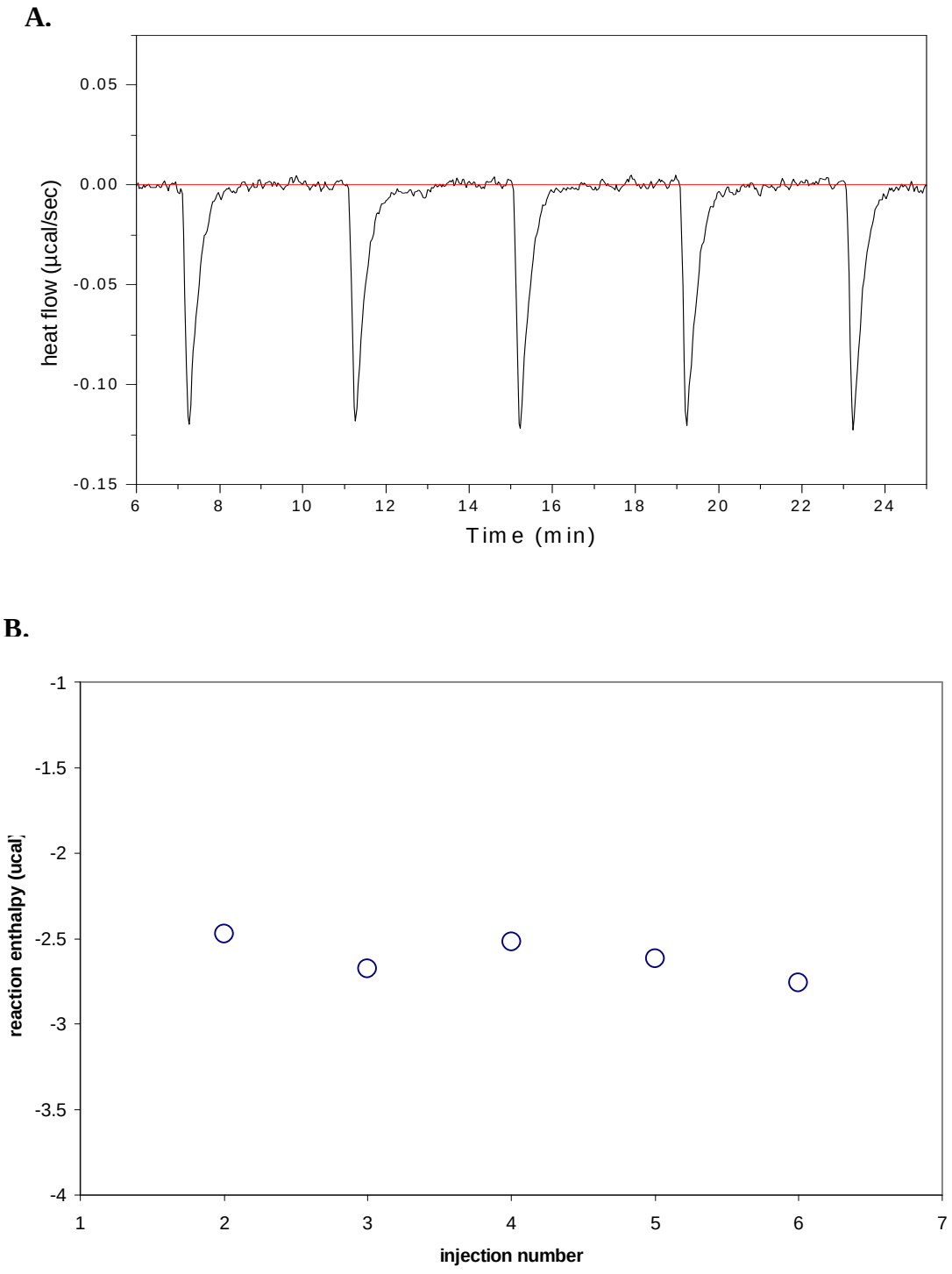
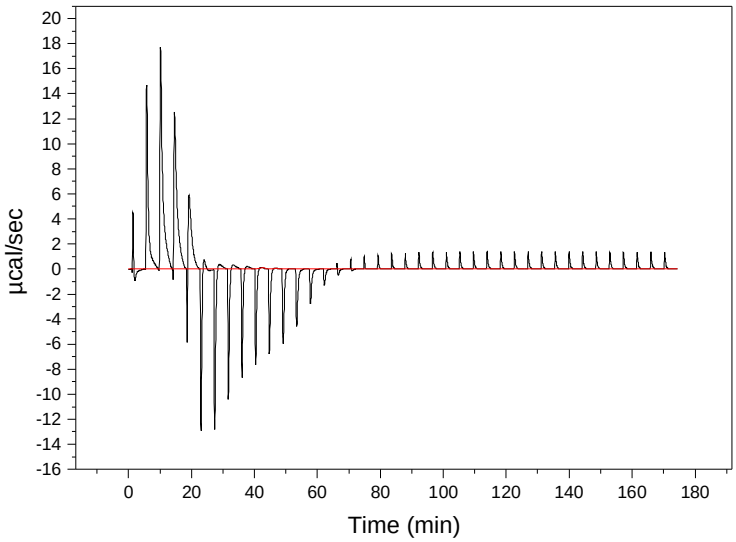


Figure 55: Reverse titration calorimetry of sarkosyl micelles with CLIC1.
3 µl Aliquots of protein solution (60 µM) were titrated to micelles (34.3 mM sarkosyl) in the reaction cell. Temperature was set to 25° C. Panel A shows the calorimeter tracing with downward peaks denote exothermic reactions. The heat per injection as evaluated from the areas underneath the tracing is shown in panel B.

A.



B.

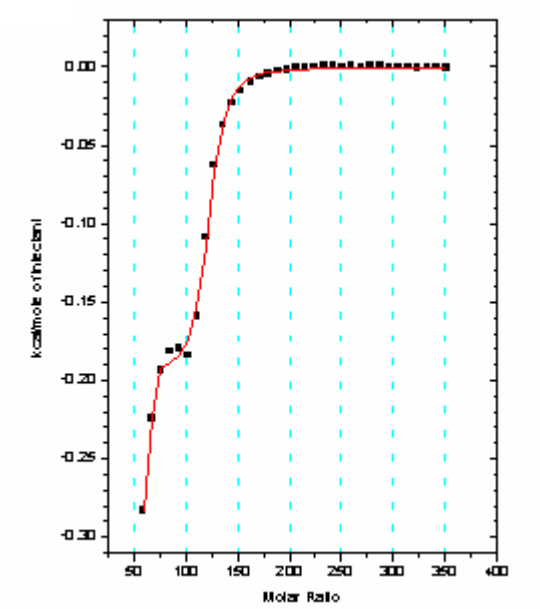


Figure 56: A representative calorimetric profile of the interaction of sarkosyl micelles with CLIC1 incubated with glutathione.

Panel A shows the heat effects associated with the 4 µl injections of micelles into the ITC sample cell containing 113.4 µM CLIC1 incubated with 2 mM GSH at pH 7.0. Panel B shows the binding isotherm (corrected for heats of dilution) corresponding to the data in Panel A. The solid line through the data represents the best fitted curve (2 binding site model) obtained using ORIGIN software.

kcal/mol and –10.45 kcal/mol, respectively, while ΔS_1 and ΔS_2 were 0.017 kcal/mol/K and 0.034 kcal/mol/K, respectively.

IAA

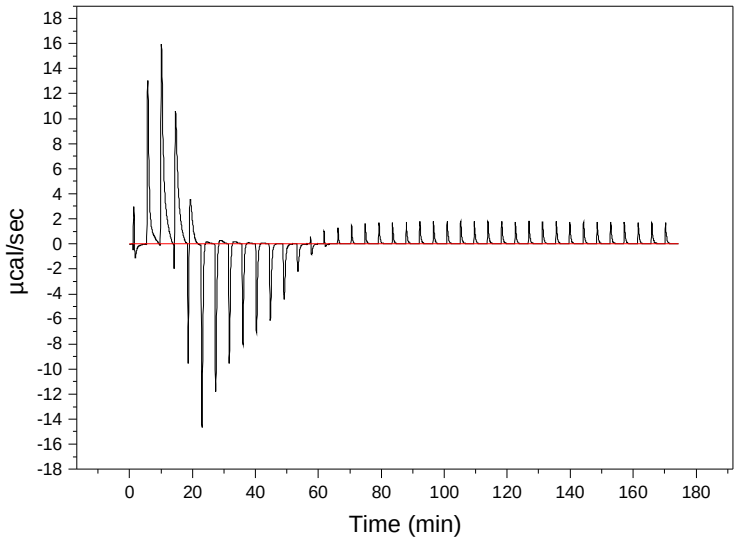
In order to further investigate the role of IAA as a CLIC1 channel blocker, ITC was performed on CLIC1 (pH 7.0) pre-incubated with 100 μM IAA and micelles. The thermodynamic profile of the interaction between CLIC1 with IAA and micelles did not show any significant differences to that of the reference experiment (Figure 57). The thermodynamic parameters obtained after fitting the data also indicated that IAA had no effect on CLIC1 interaction with micelles. Thermodynamic parameters remained largely unchanged compared with experiments using CLIC1 at pH 7.0 in the absence of any ligand or inhibitor

NEM

In order to investigate the role of CLIC1 cysteine residues on membrane insertion thermodynamics, N-ethylmaleimide (NEM) was used to chemically modify the protein and specifically the cysteine residues. NEM reacts with sulfhydryl groups in proteins with considerable specificity (Gregory, 1955). The effect of attaching the relatively bulky thiol-reactive reagent to the proteins accessible cysteine residues was investigated in the context of CLIC1-micelle interaction, since the cysteine residues of CLIC1 have been reported to play an important role in channel formation and functioning (Tulk *et al.*, 2002; Littler *et al.*, 2004; Singh and Ashley, 2006).

Firstly, a DTNB (Ellman's reagent) assay (Sedlak and Lindsay, 1968) was performed on CLIC1 in order to determine the amount of free or solvent accesible sulfhydryl groups relative to the total cysteine residues in the proteins primary amino acid composition. By titrating 6 μM CLIC1 with 250 μM 5,5'-dithiobis(2-nitrobenzoate) (DTNB) and monitoring the release of the nitrothiobenzoate anion using absorbance spectroscopy at 412 nm, the number of accessible sulfhydryl groups to solvent was determined. The concentration of sulfhydryl groups present was calculated by dividing the absorbance at 412 nm by the extinction coefficient for DTNB (13600 $M^{-1}cm^{-1}$). According to the CLIC1 sequence and structure a total of 6 cysteine residues exist, 3 of which are in domain 1, and 3 in domain 2. The DTNB assay performed on unfolded CLIC1 verified this indicating a total of 6 free thiols. For

A.



B.

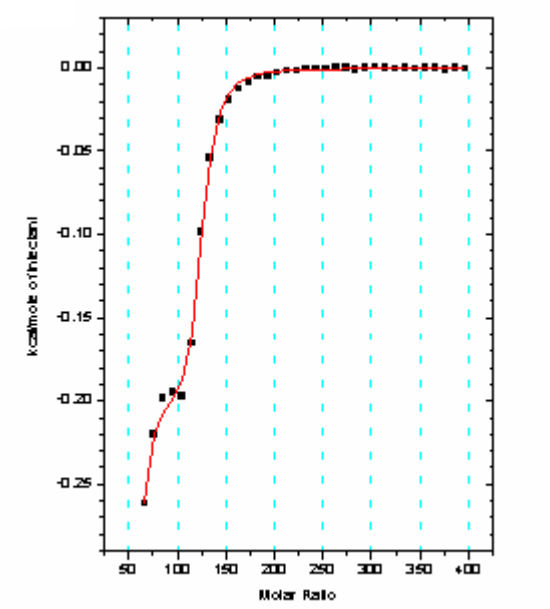


Figure 57: A representative calorimetric profile of the interaction of sarkosyl micelles with CLIC1 incubated with IAA.

Panel A shows the heat effects associated with the 4 µl injections of micelles into the ITC sample cell containing 100 µM CLIC1 incubated with 100 µM IAA at pH 7.0. Panel B shows the binding isotherm (corrected for heats of dilution) corresponding to the data in Panel A. The solid line through the data represents the best fitted curve (2 binding site model) obtained using ORIGIN software.

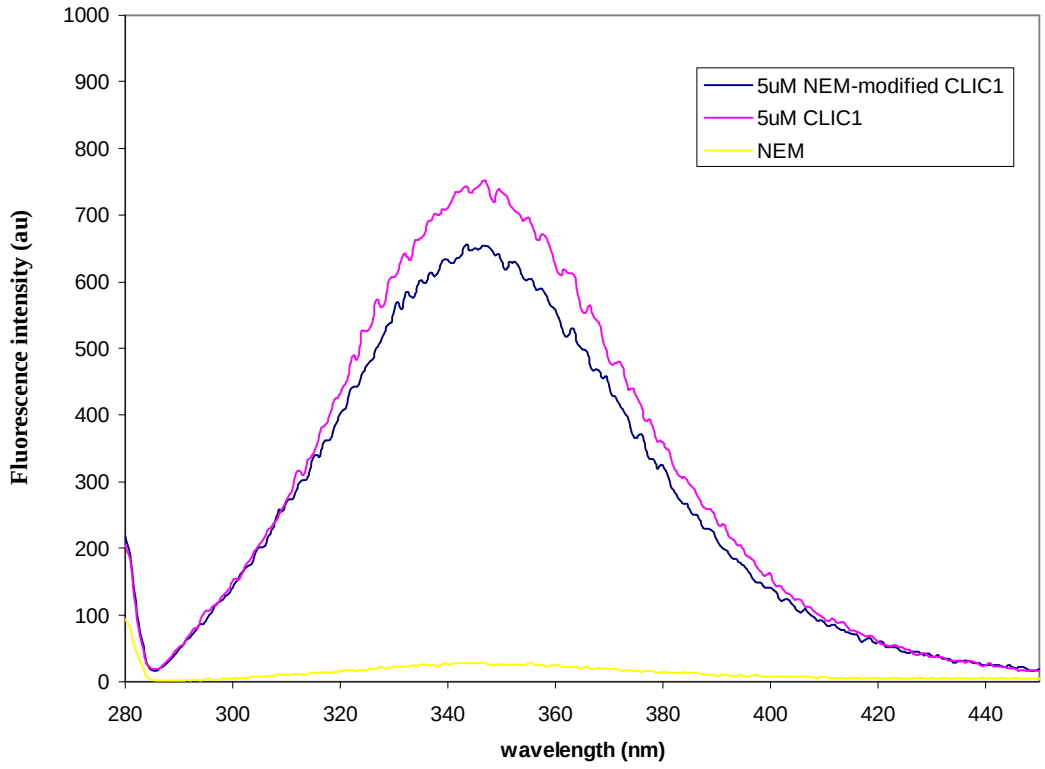
native/folded CLIC1 a total number of 4 sulfhydryls were determined indicating that this is the number of exposed cysteines for the folded protein. Two cysteine residues are therefore buried in the CLIC1 structure.

The secondary and tertiary structures of the NEM-modified protein (Figure 58) were not significantly altered based on fluorescence and far-UV CD analysis. The thermodynamics of NEM-modified CLIC1 interacting with micelles was investigated using ITC (Figure 66A). 45 μM of the NEM-modified protein at pH 7.0 was titrated with 4 μl injections of sarkosyl micelles under the same conditions used in the pH 7.0 reference study. Interestingly, the thermodynamic profile was similar to that obtained when micelles were injected into buffer containing no protein (heat of dilution control experiment, see Figure 53). This indicates that no interaction was occurring between NEM-modified CLIC1 and micelles. Once the signal was corrected for the heat of dilution effects, a net profile showing no heat gain or loss is evident. The endothermic signals once saturation was achieved were, however, notably larger than those for the heat of dilution control experiment. Fluorescence spectra also indicated that the NEM-modified protein had not inserted into the micelle since no shift in emission maximum was observed (Figure 59B).

pH 5.5

The pH dependence of CLIC1 insertion into lipid bilayers has been established in previous CLIC1 experiments (Warton *et al.*, 2002). In order to investigate the effects of pH on the thermodynamics of CLIC1 interaction with micelles, an ITC experiment was performed using the exact conditions as the reference experiment (pH 7.0) but using CLIC1 at pH 5.5. The protein sample was extensively dialysed against buffer adjusted to pH 5.5 and the 10 % sarkosyl solution was made up in pH 5.5 buffer. All data was corrected for heat of dilution effects resulting from micelles mixing with buffer at pH 5.5 (see Appendix, Figure E). The CMC value for sarkosyl did not change at the lower pH conditions. When CLIC1 (pH 5.5) at a concentration of 68 μM was titrated with 4 μl injections of 10 % sarkosyl a reduction in the initial endothermic contribution was evident when compared with experiments at pH 7.0 (Figure 60). Fewer injections resulted in endothermic peaks, with the large exothermic enthalpies beginning after 4 injections. Despite using a much lower protein concentration at pH 5.5 (68 μM) than for the reference experiment at pH 7.0

A.



B.

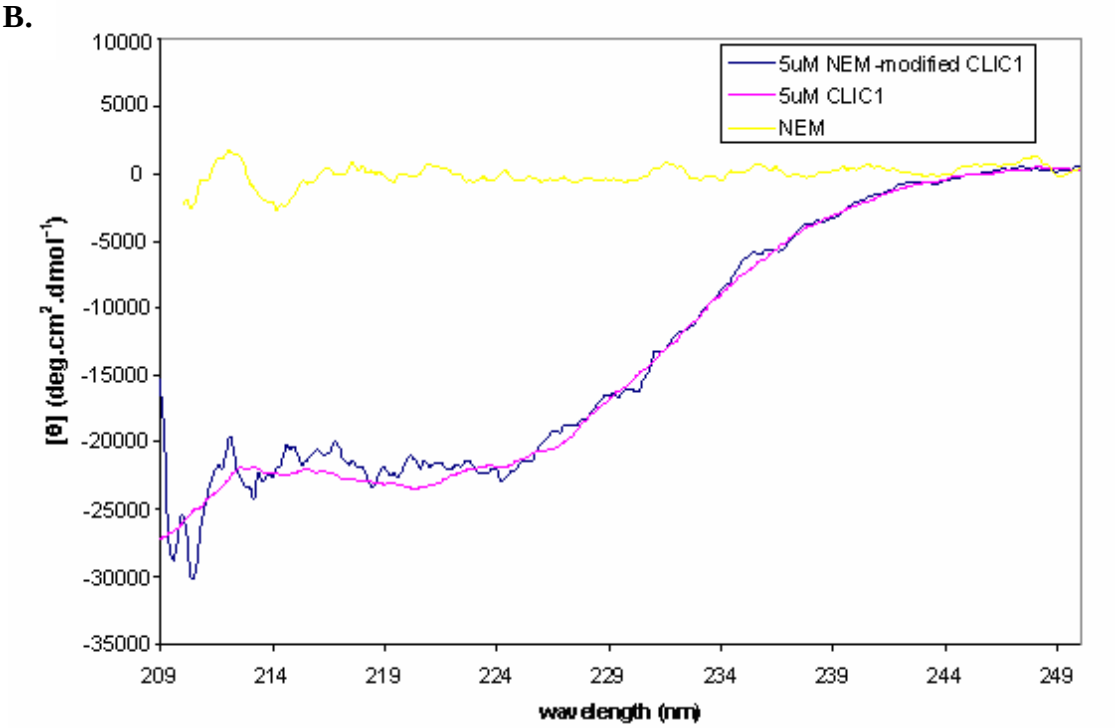
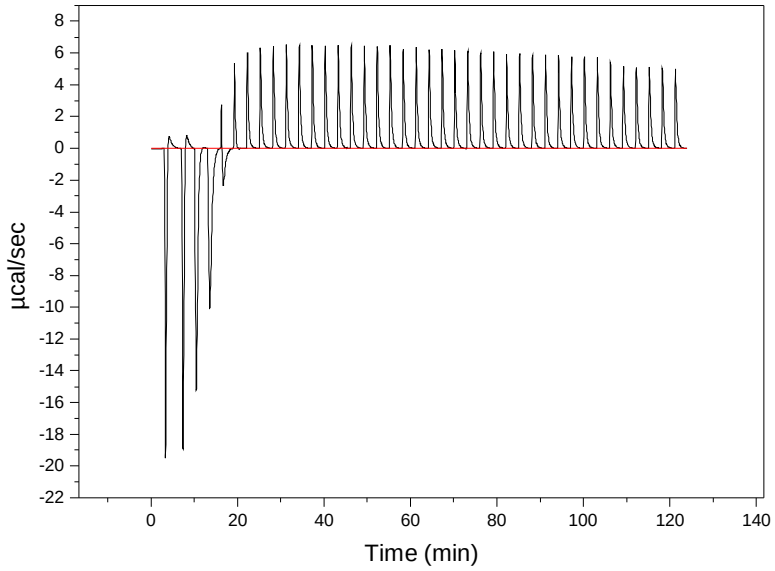


Figure 58: Fluorescence and Far-UV CD spectra of NEM-modified CLIC1.
Panel A shows the fluorescence spectrum for 5 µM NEM-modified CLIC1 (blue) excited at 280 nm. There is no significant change in tertiary structure near the tryptophan environment compared with native CLIC1 (pink). Free NEM fluorescence is shown in yellow. Panel B shows the far-UV CD spectrum for 5µM NEM-modified CLIC1 (blue) is superimposable with the native form of the protein (pink), indicating no change in secondary structural content. Free NEM is shown in yellow.

A.



B.

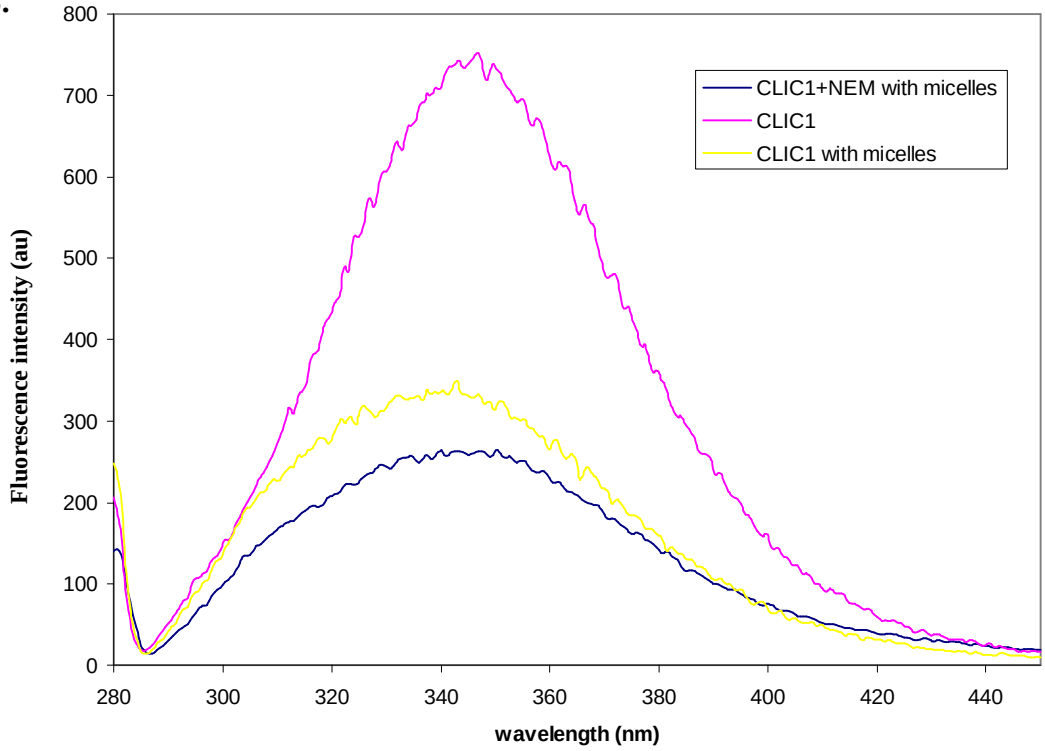
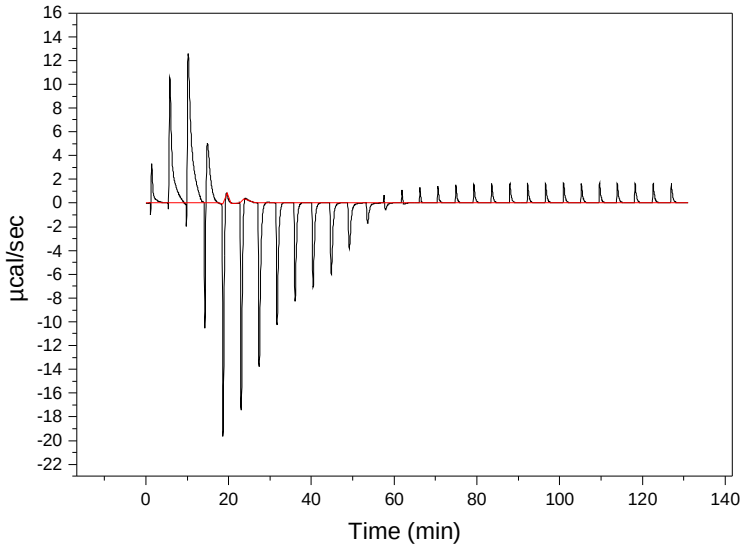


Figure 59: Thermodynamic trace and fluorescent properties of NEM-modified CLIC1 interacting with sarkosyl micelles.

Panel A shows the thermodynamic trace when 45 µM NEM-modified CLIC1 is titrated with 4 µl injections of sarkosyl micelles. Once the heat of dilution effects are corrected for the net result indicates no interaction (heat) occurring. Panel B shows the fluorescence spectra for 5 µM CLIC1 (pink), 5µM CLIC1 inserted into micelle (yellow) and 5 µM NEM-modified CLIC1 incubated with micelles (blue). For CLIC1 inserted into micelles a characteristic blue-shift is observed, while for NEM-modified CLIC1 incubated with micelles this shift does not occur.

A.



B.

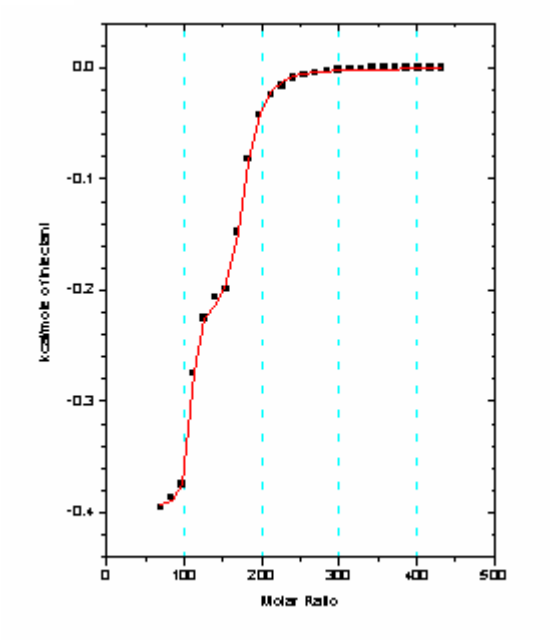


Figure 60: A representative calorimetric profile of the interaction of sarkosyl micelles with CLIC1 at pH 5.5.

Panel A shows the heat effects associated with the 4 µl injections of micelles into the ITC sample cell containing 68 µM CLIC1 at pH 7.0. Panel B shows the binding isotherm (corrected for heats of dilution) corresponding to the data in Panel A. The solid line through the data represents the best fitted curve (2 binding site model) obtained using ORIGIN software.

(115 μM) the maximum magnitude of the exothermic heat produced was greater and, therefore, enthalpically more favourable at the lower pH (~ -20 μcal/sec) than that at neutral pH (~ -13 μcal/sec). The exothermic portion of the calorimetric titration profile exhibited a decrease in the exothermic heat of binding after each successive injection. The reaction is, therefore, characterised by a series of negative peaks representative of a favourable enthalpy change. Thermodynamic parameters obtained for CLIC1 at pH 5.5 interacting with micelles show a different ΔH_2 value (-0.394 kcal/mol) compared with pH 7.0 (-0.294 kcal/mol). ΔS_1 (0.169 kcal/mol/K) and ΔS_2 (0.291 kcal/mol/K) were also larger at pH 5.5 than at pH 7.0.

3.7 Bioinformatics

3.7.1 Transmembrane region prediction and hydropathy plots

In order to identify possible transmembrane regions of CLIC1, sequence analysis using transmembrane prediction programs was undertaken. TMpred (Hofmann and Stoffel, 1993) is a program that makes a prediction of membrane-spanning regions and their orientation. The algorithm used is based on the statistical analysis of a database of naturally occurring transmembrane proteins and predictions are made using a combination of several weight-matrices for scoring. For the CLIC1 sequence only one region (residue 29 – 46) was predicted to form a transmembrane helix in an outside-to-inside orientation. The DAS (dense alignment surface) transmembrane prediction server (Cserzo *et al.,* 1997) was also used to identify possible transmembrane regions in the CLIC1 sequence. The only transmembrane region identified by the algorithm used in this program was residue 30 – 40 (Figure 61).

Early CLIC1 hydrophobicity analysis was only used to help identify possible transmembrane regions (Valenzuela *et al.,* 1997). In this study the hydrophobicity patterns of CLICs, GSTs and thioredoxin superfamily members were investigated and compared using hydrophobicity plots (Kyte and Doolittle, 1982; Fauchere and Pliska, 1983) (Figure 62). For the CLIC proteins the highest level of hydrophobicity was observed at the region corresponding to residues 25 – 40 (CLIC1 numbering). This

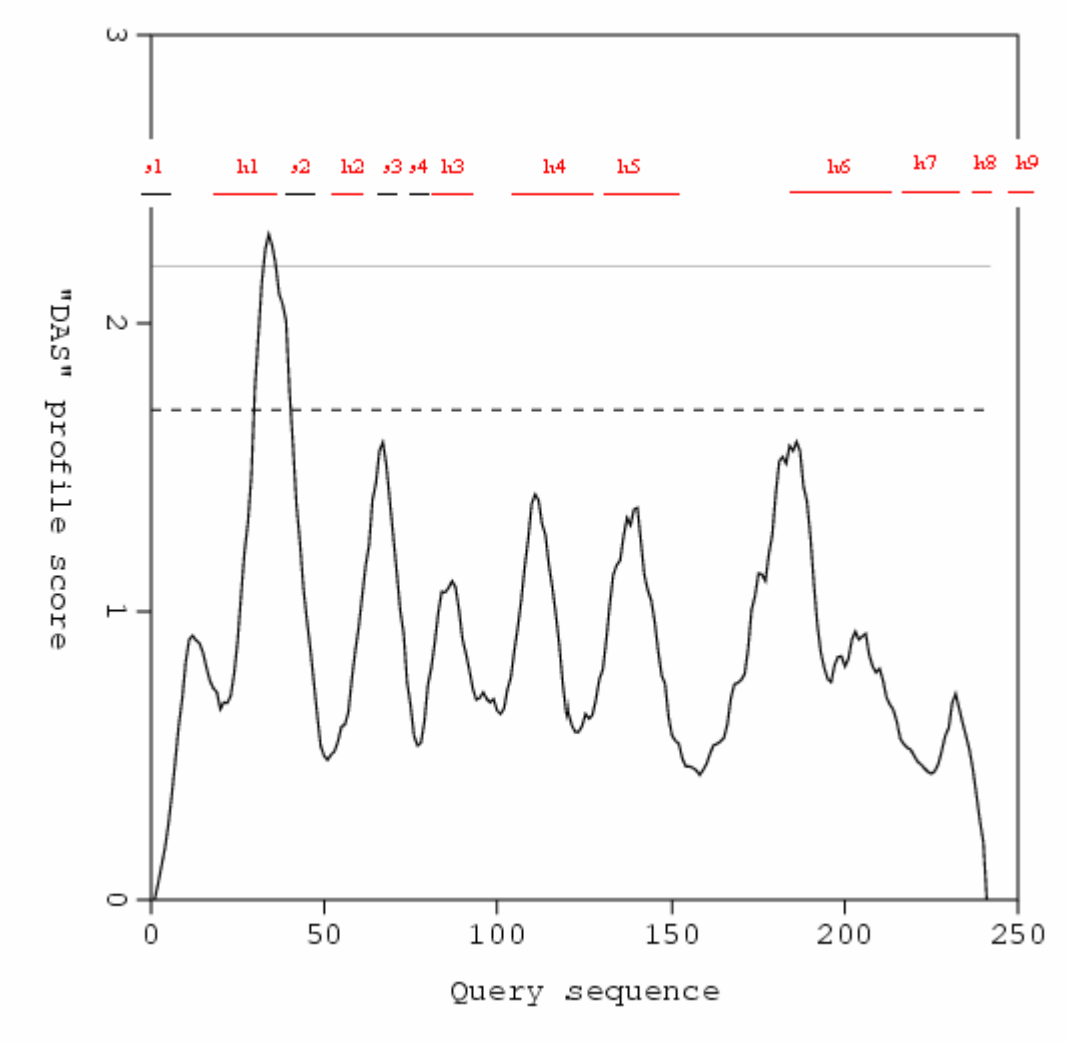


Figure 61: CLIC1 transmembrane prediction graph using Dense Alignment Surface (DAS) method.

Based on the "DAS" profile score only residues 30 – 40 of the CLIC1 sequence are predicted to form the transmembrane region of the integral membrane protein. Dashed line indicates loose cut-off and solid line indicates strict cut-off points. Positioning of secondary structural elements along the primary sequence is shown above the graph with strands represented by black lines and helices represented by red lines.

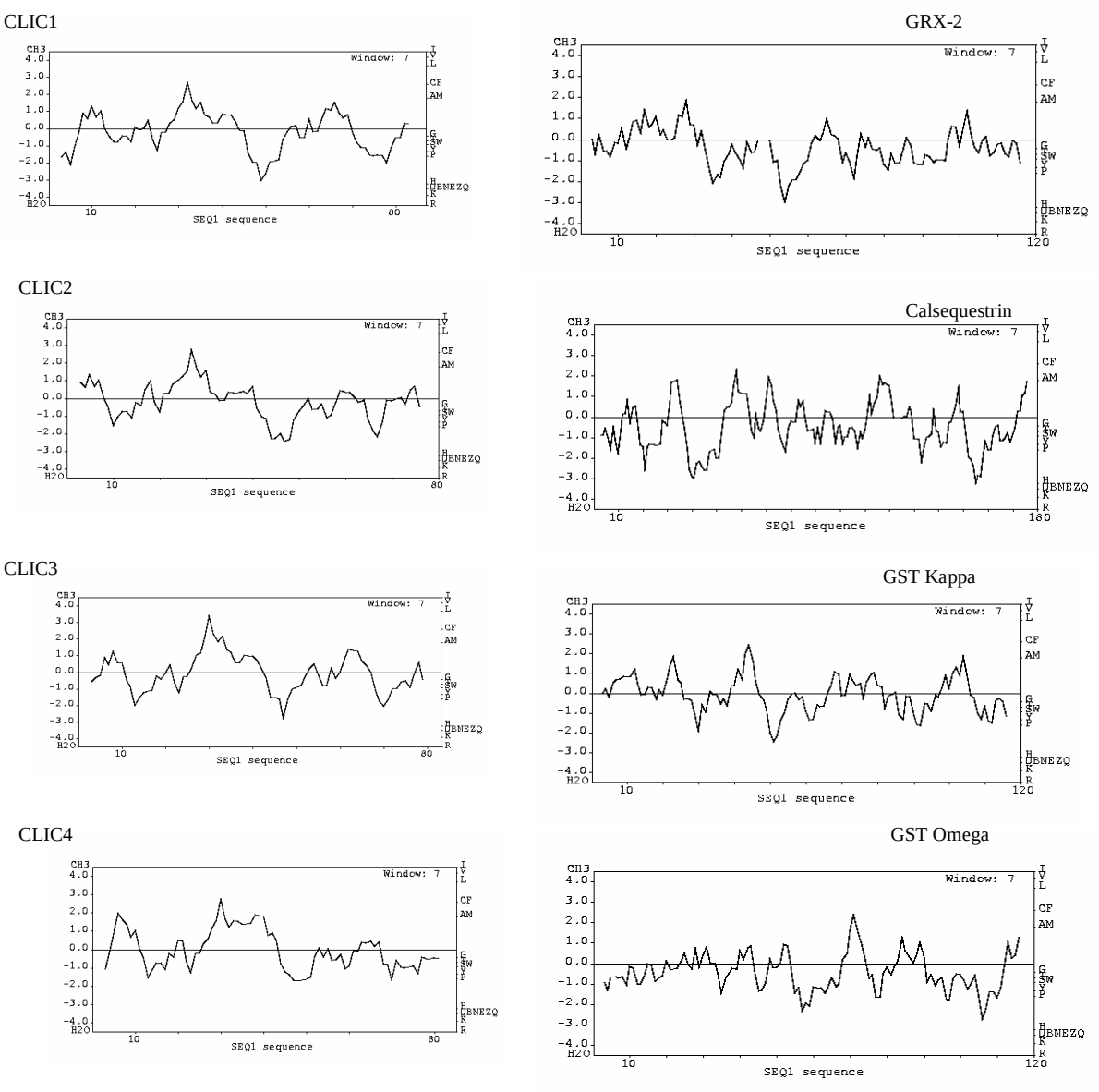


Figure 62: Hydropathy plots of thioredoxin-fold domains of selected CLIC, GST and thioredoxin family members.

Distribution of hydrophobicity conserved in CLICs with regions corresponding to residues ~25 – 40 showing high levels of hydrophobicity followed by a hydrophilic "dip". Plots were generated using the Kyte-Doolittle algorithm (Kyte and Doolittle, 1982).

highly hydrophobic region was immediately followed by a highly hydrophilic dip observed in the plots. This hydrophobicity pattern was distinct for all the CLIC family members and this distribution of hydrophobic/hydrophilic residues may be conserved to enable CLIC functioning in the form of a channel. Comparison of the hydrophobicity plot with another structurally similar monomeric GST family member, Grx-2, does not show similar patterns in hydrophobicity. Furthermore, Omega class GST (which has high structural similarity to CLIC1) shows no high hydrophobicity in the corresponding region.

3.7.2 Sequence alignments showing charge conservation

Sequence alignments of the thioredoxin superfamily and GST family with the CLICs (Figure 63) reveals a conserved feature of the proposed transmembrane region (P25 – V46). This region contains many positively charged residues, but no negatively charged residues for the CLICs. Furthermore, a grouping of positively charged residues occurs at the end of the proposed transmembrane region for all the CLIC proteins.

3.7.3 Helix propensities using AGADIR

Helix propensities of CLIC, GST and thioredoxin superfamily members were analysed using the AGADIR algorithm, which is based on helix-coil transition theory that explicitly considers specific interactions occurring in helices devoid of tertiary interactions (Lacroix *et al.*, 1998). The propensity of certain regions in the amino acid sequence to form helices can provide valuable information about formation and stability of secondary structural elements should the protein undergo some form of structural re-arrangement. This “hidden” information would not be obvious in the quaternary structure of soluble CLIC1 but can be uncovered by analysis of the primary sequence. Certain regions that have a high helical propensity may not be allowed to take on a helical form because of constraints placed upon it in the 3-dimensional folded structure orientation. Certain changes in environment may, however, induce structural changes that would then allow those regions exhibiting high helical propensities to form a helix. Helix propensity analysis using AGADIR shows a high helical propensity for the proposed transmembrane region (α1 and β2) for CLIC1, and in fact the entire CLIC family (Figure 64). Helical propensities for representatives of the GST family are shown in Figure 65. Only the Kappa class GST exhibited high helical propensity at the α1 and β2 region. In the thioredoxin

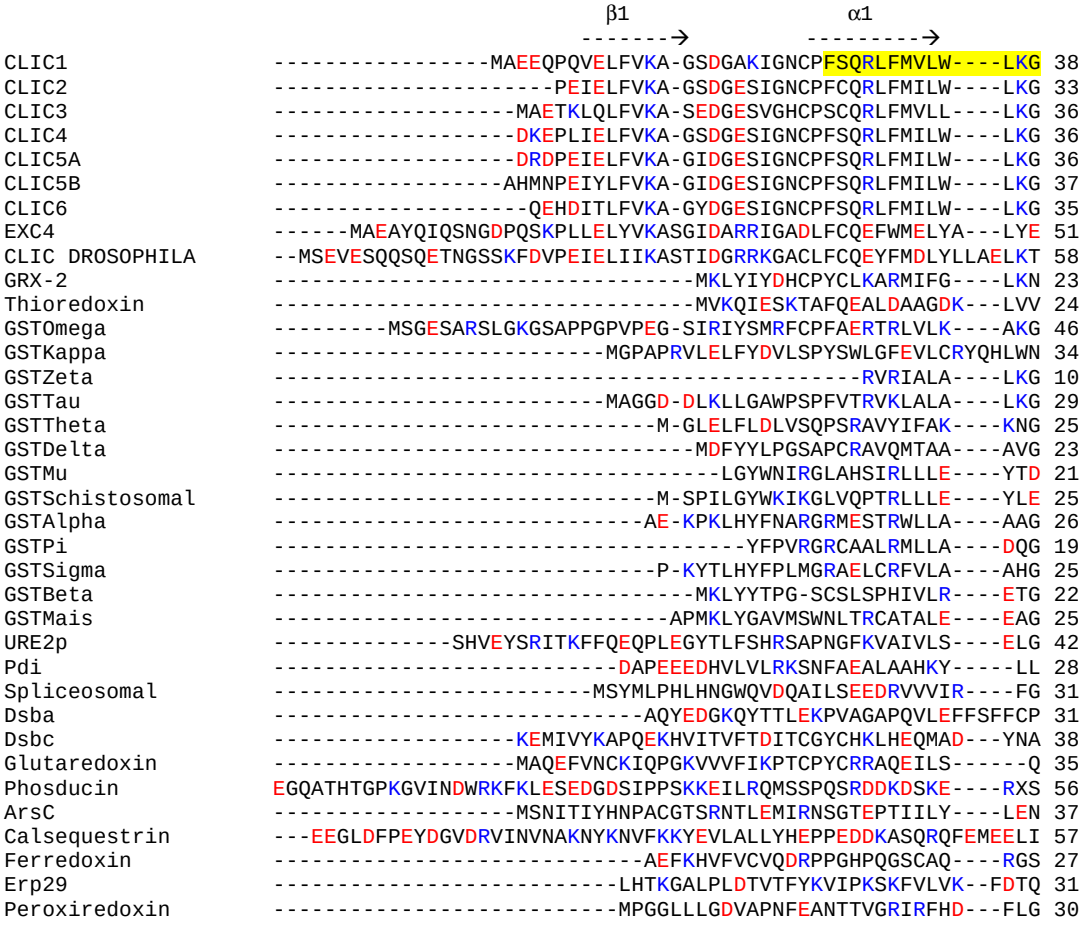


Figure 63: Sequence alignments of thioredoxin-fold domains in CLIC, GST and thioredoxin families indicating residue charge. Positively charged residues are shown in blue and negatively charged residues in red. The proposed transmembrane region of CLIC1 is highlighted in yellow.

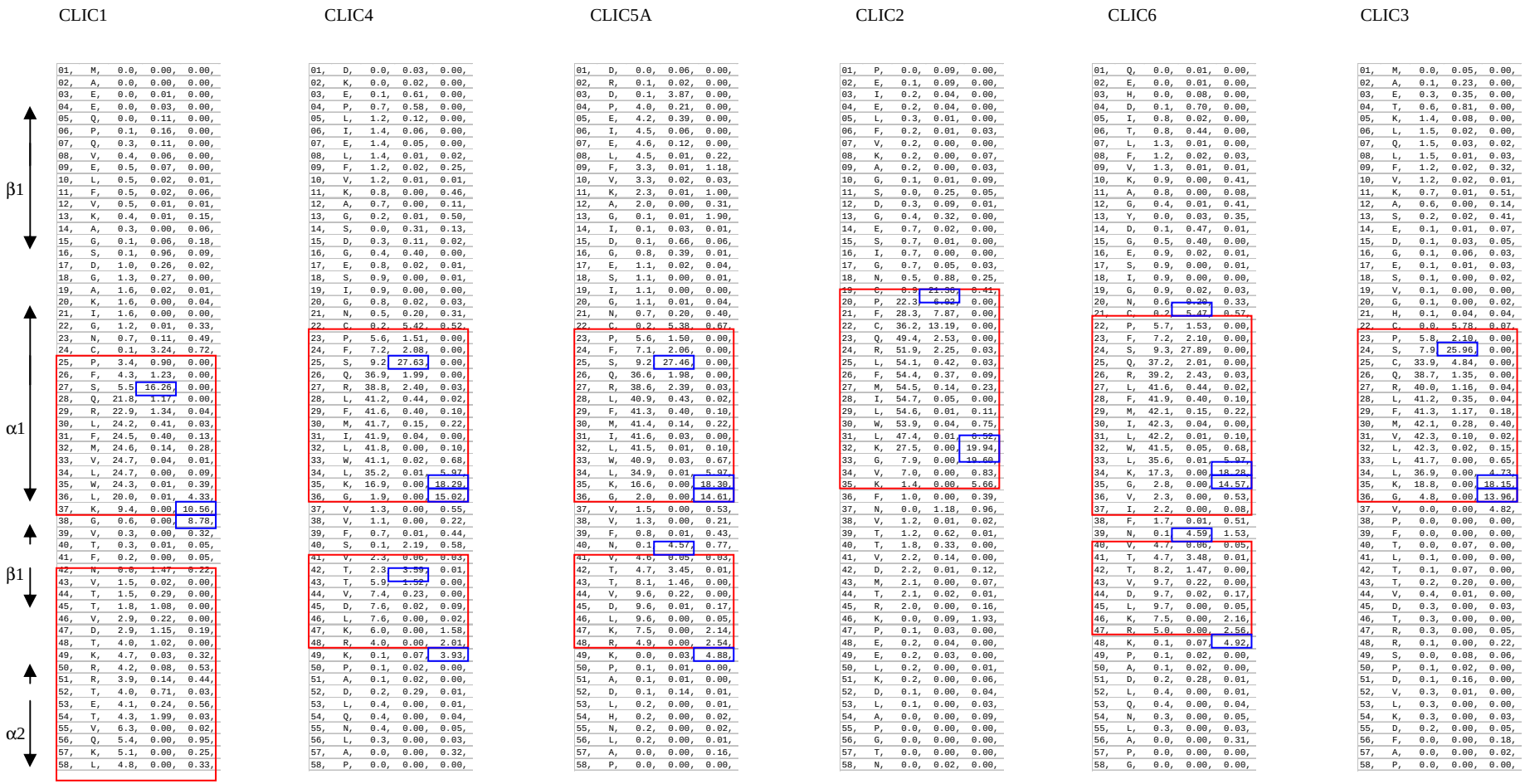


Figure 64: Helical propensities and capping motifs by AGADIR sequence analysis of the CLIC family of proteins.
Regions showing high helical propensities are boxed in red. Residues showing high N-capping or C-capping characteristics are boxed in blue. Data was generated by analysing the protein sequence using the AGADIR algorithm (Lacroix *et al.*, 1998)

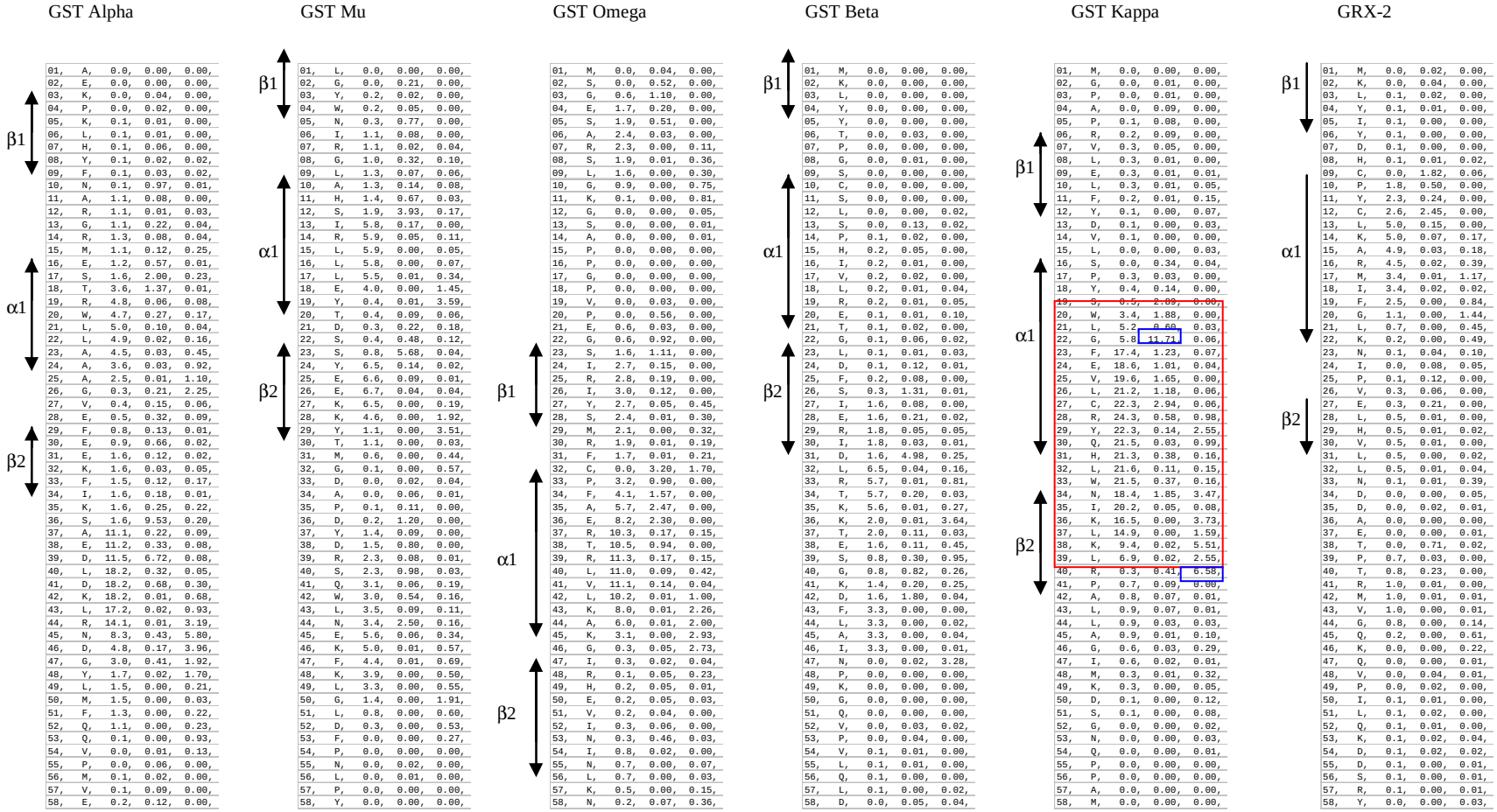


Figure 65: Helical propensities and capping motifs by AGADIR sequence analysis of representatives of the GST family of proteins. Regions showing high helical propensities are boxed in red. Residues showing high N-capping or C-capping characteristics are boxed in blue. Data was generated by analysing the protein sequence using the AGADIR algorithm (Lacroix *et al.*, 1998)

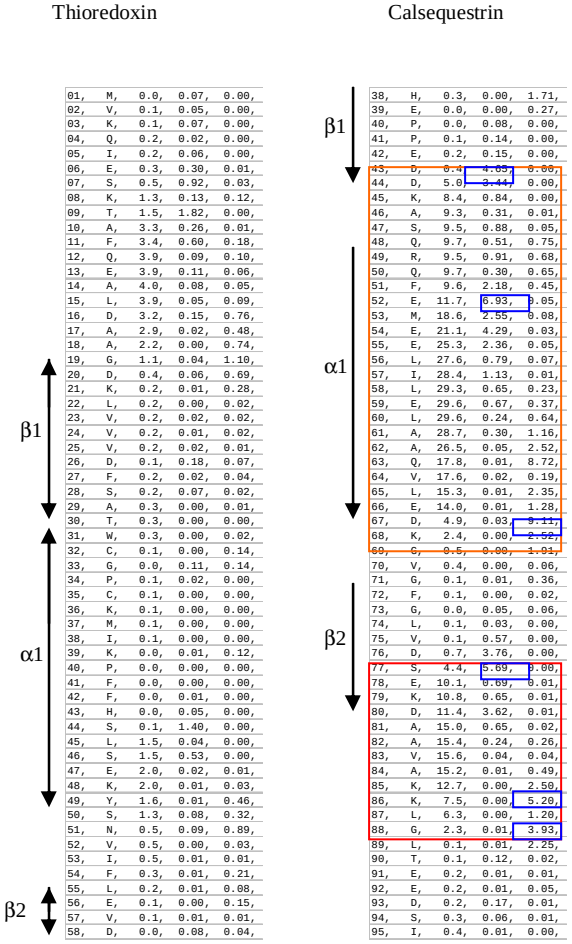


Figure 66: Helical propensities and capping motifs by AGADIR sequence analysis of representatives of the thioredoxin superfamily.
Regions showing high helical propensities are boxed in red. Residues showing high N-capping or C-capping characteristics are boxed in blue. Data was generated by analysing the protein sequence using the AGADIR algorithm (Lacroix *et al.*, 1998).

superfamily the only member to show high helical propensity in the corresponding region was calsequestrin. AGADIR analysis of representatives from the thioredoxin superfamily are shown in Figure 66.

3.7.4 Phosphorylation sites and signalling motifs

A search was done using the CLIC1 amino acid sequence to identify possible motifs that may be involved in signalling (Table 4). The program ProSite (Stamler *et al.*, 1997) was used and revealed 5 possible N-myristoylation sites, 3 protein kinase C phosphorylation sites and 6 Casein kinase II phosphorylation sites. One N-glycosylation site at residue 42 and one cAMP phosphorylation site at position 49 were also noted. Both GST and CLIC families have known associations with protein kinases (Qian *et al.,* 1999; Edwards and Kapadia, 2000; Nishizawa *et al.,* 2000; Cho *et al.,* 2001). Previous studies examining the possible role of phosphorylation regulating CLIC1 activity, only involved using protein kinase A and found that it had no effect on valinomycin-dependent chloride efflux (Tulk *et al.,* 2002). The possibility that CLIC1 channel activity could be regulated by other protein kinases could provide the basis for future studies.

Two putative nuclear localisation sequences were also found to exist at positions 49 – 51 (KRR) and 192-195 (KKYR). The KRR motif is found just after the proposed transmembrane region (a1 - β2) in the N-terminal domain, while the KKYR motif is found at the end of helix 6 in the C-terminal domain. For target importin / karyopherin proteins to bind the nuclar localisation sequences on CLIC1 the folded protein may have to partially unfold or rearrange to utilise this nuclear import machinery.

3.7.5 Surface area determination

Exposed and buried surface area was determined for CLIC1 using the molecular modelling program NACCESS (Lee and Richards, 1971) and compared with another monomeric GST, namely Glutaredoxin-2 (Grx2). The surface areas were modelled using co-ordinates from the CLIC1 (Harrop *et al.,* 2001) and Grx2 (Xia *et al.,* 2001) structures. The entire protein was first modelled and then the two domains were modelled individually. This enabled calculation of the buried surface area at the domain interface. The total accessible surface area calculated for CLIC1 was 12 350 Å with 3 528 Å (29 %) being polar and 7 174 Å (58 %) non-polar. For Grx2, the total accessible surface area of 9 898 Å was made up of 3 000 Å (30 %) polar surface and 5983 Å (61 %) non-polar surface. Although the proteins contain equal percentages of

Table 4: Signalling and phosphorylation sites of CLIC1.
The CLIC1 sequence was scanned for all possible signalling and phosphorylation sites using the ProSite program (Stamler *et al.*, 1997)

SITE TYPE	CLIC1 RESIDUE NUMBER	RECOGNITION SEQUENCE
N-myristoylation site	15-20	GSDGAK
	18-23	GAKIGN
	38-43	GVTFNV
	132-137	GLLKAL
	170-175	GNELTL
Protein Kinase C phosphorylation site	27-29	SQR
	48-50	TKR
	77-79	TNK
	163-165	SQR
N-glycosylation site	42-45	NVTT
Casein Kinase II phosphorylation site	44-47	TTVD
	155-158	TSAE
	156-159	SAED
	174-177	TLAD
	198-201	TIPE
	222-225	TCPD
cAMP- and cGMP-dependent protein kinase phosphorylation site	49-52	KRRT
Nuclear Localisation sequence	49-51	KRR
	192-195	KKYR

polar and non-polar surface area, CLIC1 appears to have a larger total accessible surface area indicating that it is not as tightly packed and perhaps more flexible than Grx2.

Domain 1 of CLIC1 has 18 % more accessible surface area than domain 1 of Grx2, while domain 2 only has 14 % more.The surface area buried at the domain interface of CLIC1 is 2 427 Å and 2284 Å for Grx2. This translates to 16 % of the domains surface area being buried in CLIC1 and 19 % in Grx2.

CHAPTER 4. DISCUSSION

4.1 Structure and stability of CLIC1 in the absence of membrane

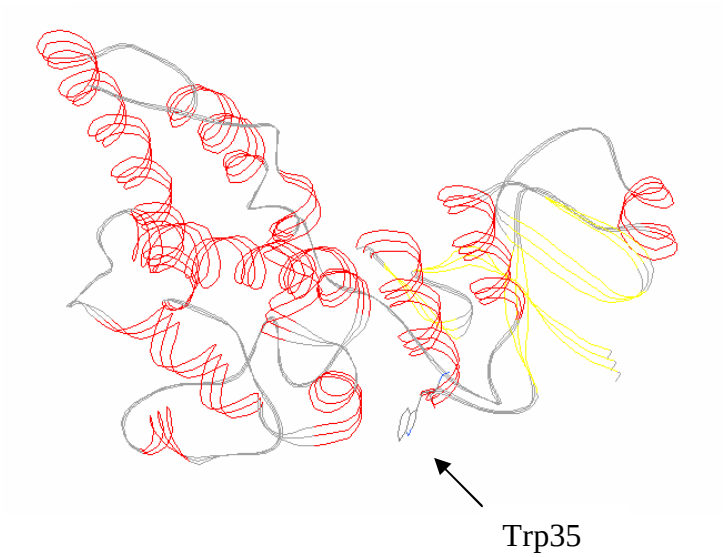
4.1.1 Redox effect on CLIC1

Previous studies have suggested that the functioning and activity of CLIC1 may be regulated by redox processes (Tulk *et al.*, 2002; Littler *et al.*, 2004; Singh and Ashley, 2006). In the cytoplasm, where conditions are strongly reducing, soluble CLIC1 is likely to be in its reduced form. However, reactive oxygen species (e.g. H_2O_2) or reactive nitrogen species (e.g. NO), which are known to be cellular signalling molecules (Klatt and Lamas, 2000; Stamler *et al.*, 1997), are likely to alter the resting state of soluble CLIC1. The present study investigates and compares the properties and characteristics of reduced, non-reduced and oxidised forms of CLIC1.

It appears that there is a slight difference in the tertiary environment of the tryptophan of reduced and non-reduced forms. However, the secondary structure of all forms remains unaffected. The increase in alpha helical content observed in the CLIC1 dimer crystal structure (Littler *et al.*, 2004) would probably be undetectable by far-UV CD analysis since the reduced monomeric form is highly alpha helical to begin with. Although the crystal structure of dimeric CLIC1 was solved at 1.4 Å (Littler *et al.*, 2004) no basic fluorescence or far-UV circular dichroism characterisation of this form has been done. The present study confirms the similarities of the tryptophan environment of monomeric and dimeric CLIC1 observed in their crystal structures (Figure 67).

The unfolding kinetics of reduced CLIC1 monomer appears to be much slower than that of other GST family members (Wallace *et al.*, 1998). CLIC1 exhibits an unfolding time constant of 17.4 minutes while glutaredoxin-2 (Grx2), which is also a monomeric structural homologue of the GST family, unfolds with a time constant of 1.3 minutes under the same conditions (Gildenhuys, PhD unpublished results). This indicates that CLIC1 is a relatively stable monomeric protein in its reduced state at pH 7.0. The buried surface area at the domain interface, as determined by NACCESS

A.



B.

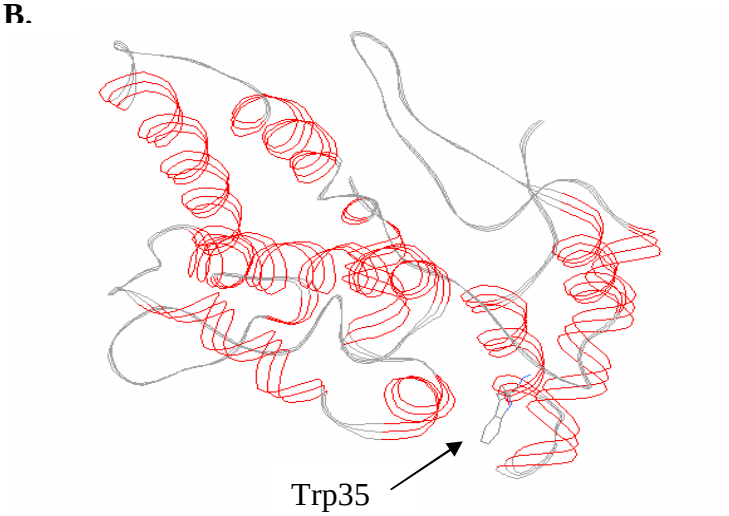


Figure 67: Ribbon representations showing orientation of Trp35 in oxidised and reduced CLIC1 forms.

Comparison of the orientations of the lone tryptophan residue in reduced CLIC1monomer (A) and oxidised CLIC1 monomer (B). Images were generated from the crystal structures of CLIC1 monomer using the PDB code 1k0m(Harrop *et al.*, 2002) and CLIC1 dimer using the PDB code 1rk4 (Littler *et al.*, 2004) with Swiss-PDB viewer (Guex and Peitsch, 1997).

(Lee and Richards, 1971), was 2427 Å for CLIC1 and 2284 Å for Grx2, indicating a similar domain interface for the two proteins. Therefore, the slower unfolding rate observed for CLIC1 cannot be attributed to a more closed domain interface that could stabilise the protein and affect the unfolding rate. The high stability may be a built-in mechanism to prevent CLIC1 from spontaneously unfolding/rearranging in the cytoplasm until the necessary signal occurs. This signal may very well be that coming from reactive oxygen species during cell stress, causing the oxidation of CLIC1. It has been shown in this study that the oxidised form of CLIC1 unfolds at a much faster rate than that of reduced CLIC1 indicating that oxidised CLIC1 is less stable and will therefore be able to unfold or rearrange easier to form a membrane-insertion competent form.

CLIC1 completely refolds in 400 seconds (6.7 minutes), which is much quicker than the time the protein takes to unfold (17.4 minutes). This slow unfolding and fast refolding pattern is indicative of the strong co-operative interactions that keep the reduced protein in its stable form at pH 7.0. The other monomeric member of the GST family, Grx2, takes longer to refold (181 seconds) than it does to unfold (141 seconds) (Gildenhuys, PhD unpublished results)

It appears that the monomeric form of CLIC1 is stabilised by increasing salt concentrations. This is probably due to increased electrostatic or hydrophobic interactions caused by the charging of ionisable residues at high sulphate concentrations. This is not apparent for the oxidised dimeric form of CLIC1 and may be due to the protection of the regions affected by the coming together of the two monomeric subunits to form the dimer.

4.1.2 pH effects on CLIC1

Low pH appears to play a role in promoting membrane insertion by either inducing a molten globule state and/or in making a part of the protein more hydrophobic by neutralizing acidic residues. For so-called amphitropic or dual-form proteins like CLIC1 that exist in soluble and membrane associated forms, a study of the effect of pH on the structure and dynamics of the protein is crucial since the protein will be moving from a neutral pH in the cytoplasm to a more acidic pH at the membrane surface. This lower pH at the membrane surface is due to the anionic lipids on the surface of the membrane causing a negative surface potential, which in turn increases

the proton concentration near the surface and effectively lowers the local pH near the membrane surface (McLaughlin 1989, Menestrina *et al.,* 1989, van der Goot *et al.,* 1991). As the soluble form of CLIC1 approaches the membrane it will move into a micro-environment with a lower pH and thus the effects of this pH change on the protein need to be analysed. Furthermore, a decrease in the pH of the cytosol during the initial phases of apoptosis has been reported (Matsuyama *et al.,* 2000) that may be a signal for soluble CLIC1 to insert into the membrane. The membrane insertion process of other pore-forming proteins, like colicin A, has been explained using membrane-pH dependance (Muga *et al.,* 1993). Colicin A was shown to form a molten globule state at low pH, which reduces the energy barrier required in unmasking the hydrophobic hairpin for membrane insertion.

Fluorescence studies performed on CLIC1 at pH 7.0 and pH 5.5 show a slight change in the environment of the lone tryptophan. A slight red-shift in the emission maximum suggests that the tryptophan residue (Trp32) is more exposed to solvent at the lower pH. Because CLIC1 only has one tryptophan reporter the tertiary structural changes observed could be localised to the α1 helix region where Trp32 is situated. Warton and co-workers (2002) found no significant change in fluorescence properties when they compared CLIC1 at pH7.0 and pH 6.0. However, the pH that was selected to represent “low pH” in that particular study was slightly higher than that of this study. Furthermore, the discrepancy may be due to an inadequate incubation time of CLIC1 at the low pH. For this study, CLIC1 was kept at pH 5.5 overnight, after which the experiments were performed. The fluorescence emission data obtained here indicate a minor change in the tryptophan exposure to solvent and its orientation.

Far-UV CD analysis of CLIC1 at pH 7.0 and pH 5.5 indicates that there are no significant changes in the proportions of secondary structural elements in this pH range. This result is consistent with previous studies on CLIC1 at low pH that showed no major alteration in secondary structure (Warton *et al.,* 2002).

Although ANS binds to the subunit interface of dimeric members of the GST family (Sayed *et al.,* 2002; Dirr *et al.,* 2005) it does not appear to bind to the monomeric member Grx-2 (Wallace, unpublished results). ANS binding studies performed at pH 7.0 and pH 5.5 (McIntyre, PhD unpublished results) indicate no significant hydrophobic surface exposure for CLIC1 at these pH conditions. This rules out the

formation of a molten globule for CLIC1 at pH 5.5, since a hallmark of a molten globule state is its ability to bind ANS (Semisotnov *et al.*, 1991).

The absence of any gross structural change and the lack of molten globule formation for CLIC1 as it moves from pH 7.0 to pH 5.5 argues for either subtle structural or dynamical changes in solution that are undetectable by CD and ANS binding experiments, or the requirement of other factors such as lipids for its pH-dependent solution-to-membrane conformational change.

Amide hydrogen exchange techniques are unparalleled in their ability to probe sub-molecular protein dynamics. This information can be used to refine inferences drawn from high resolution structural studies such as x-ray crystallography, and can provide unique insights when structural information is unavailable for environmental specific conditions (e.g. pH). Enhanced methods of deuterium exchange-mass spectrometry (DXMS) were used to analyse CLIC1 dynamics and structure at pH 7.0 and pH 5.5. It was important to study the structural dynamics and stability of CLIC1 as it occurs in its soluble form in the cytoplasm at neutral pH because this would provide insight into which regions of the protein are most likely to unfold or rearrange in order to form the membrane-insertion competent form, based on stability and flexibility. Comparisons with other GST family proteins may provide information about the evolution of the thioredoxin fold. Furthermore, the only high resolution structural information on the soluble form of CLIC1 was solved at pH 5.0 and at 4°C (Harrop *et al.*, 2001) and may therefore not accurately resemble CLIC1 as it occurs in the cytoplasm. HXMS at pH 5.5 was performed in order to provide important information on the structural changes that are occurring as CLIC1 approaches the membrane. If pH is indeed the trigger for CLIC1 to convert from soluble to integral membrane form analysis of the structural dynamics at low pH are crucial in establishing possible models for the membrane-insertion mechanism. This work represents the first time hydrogen-exchange mass spectrometry has been used to gain valuable insight into the structural dynamics of any CLIC family member, wildtype monomeric GST or any monomeric member of the thioredoxin superfamily for that matter.

In the crystal structure determined for redox-induced transition of CLIC1 (Littler *et al.*, 2004) the α2-loop region differs between each independent molecule where its conformation appears to be dominated by crystal packing interactions. This is also

apparent for one of the molecules in the assymetric unit of the first CLIC1 crystal structure (Harrop *et al.,* 2001). Thus, the α2-loop region is likely to be only partially ordered in solution with high degrees of flexibility.

This region may form the base of the transmembrane segment of the CLIC1 channel (see section 4.2.4) and the flexibility of this region could be required for correct pore orientation. The peptide from residue 43 – 68, which correlates to the α2 region of the protein structure, shows 32 % deuteration within the first time point (10 sec) and accumulates progressively to 81 % deuteration after 3000 seconds. This steep slope in the accumulation graph indicates that this region is flexible. The crystal structure of the oxidised dimeric CLIC1 form shows that the most apparent structural change between the soluble monomer and oxidised dimer is related to the α2 region (Littler *et al.,* 2004). It seems the α2 region is a central structural element for the redox-controlled structural transition that is proposed to represent the membrane docking form (Littler *et al.,* 2004*)*. The structural flexibility of this region observed here by DXMS analysis may reflect that the intrinsic conformational susceptibility of the α2 region could play a role in the initial step of the structural transition of soluble CLIC1 to membrane insertion-competent form. The flexibility of the domain linker, which essentially serves as a hinge connecting the two domains, may be necessary for changes in the relative orientation of the two domains that is likely to occur when CLIC1 converts from soluble to integral-membrane form.

In order to provide some structural insight into the deuteration levels observed overall, the DXMS data was mapped onto the CLIC1 crystal structure (Harrop *et al.,* 2001) showing regions exhibiting high, intermediate and low exchange rates (Figure 24). The results indicate that domain 2 is more stable than domain 1, with the thioredoxin-fold showing relatively high levels of flexibility. It is therefore more probable that the thioredoxin-fold domain is the region that undergoes structural rearrangement or unfolding to form the insertion-competent form that can insert into the membrane. It has been proposed previously that the region 25 – 46 forms the transmembrane segment of CLIC1 (Valenzuela *et al.,* 1997; Littler *et al.,* 2004; Singh and Ashley, 2006). Our DXMS data support this. At pH 7.0 the only regions in domain 1 that appear to be stable and completely protected from deuterium exchange are short segments of helix 1 and helix 3. The interactions between these two

structurally adjacent regions appear to be the stabilizing factor in the otherwise flexible thioredoxin domain.

Although the majority of domain 2 shows low deuterium exchange patterns, indicating that this domain is relatively very stable, the region corresponding to the C-terminal portion of the negatively charged loop is very flexible. It is interesting to note that the N-terminal portion of the loop (residues 130-153) shows low deuterium exchange and probably serves as a stable hinge for the flexible loop. As can be expected, the end portion of the α9-helix at the protein's C-teminus is very flexible (residues 231-236).

Amide hydrogen/deuterium mass spectrometry has recently been used to study the structural dynamics of another member of the GST family (Codreanu *et al.,* 2005; Thompson *et al.,* 2006). The class Mu enzyme, rGSTM1-1, is dimeric. However, its individual subunits are made up of a N-terminal thioredoxin-fold domain and a C-terminal α-helical domain similar to the arrangement found in the monomeric GST family member CLIC1. Thompson and co-workers (2006) demonstrated that a double mutation at the proteins dimer interface resulted in a dissociation to a monomeric enzyme that was native-like. A comparison of the dynamics and stability of the rGSTM1-1 monomer with CLIC1 could provide insight into the evolution and functioning of the monomeric GSTs, and more specifically CLIC1.

The HXMS experiments done on the Mu-class GST (Thompson *et al.,* 2006) were performed under slightly different conditions compared with CLIC1. The protein/D_2O solution was incubated at 25°C for the various time points before quenching. This is at a higher temperature to the 0°C that was used for CLIC1. It is expected that this would have caused an increase in the rate of deuterium binding and so the two experiments are unfortunately not directly comparable. The relative stability of the two domains within each protein can, however, be compared. Peptides completely protected from deuterium throughout the entire length of the experiment indicate the most stable regions of the protein and possible folding nucleation sites. For Mu-class GST the only regions showing no exchange over 480 minutes were short peptides 19-21, 97-100 and 158-163. For CLIC1 the peptides completely shielded form deuterium were residues 31 –34, 83 –86, 108 – 117, 135-142, 173 – 188 and 204 – 213. This

indicates a substantially greater amount of stable/protected regions, especially in domain 2, for CLIC1 compared to the Mu-class GST.

It has been previously speculated that since the N-terminal domain of CLIC1 has evolved from the thioredoxin superfamily, it seems unlikely that it will unfold readily to form a membrane-interacting domain (Cromer *et al.,* 2002). The HXMS data shown here provides evidence that the thioredoxin fold in CLIC1 has indeed evolved into a dynamic/flexible domain capable of rearrangement in order to fulfil a new function, namely, membrane insertion and channel formation. The plasticity of the CLIC1 N-terminal domain was noted by Harrop and co-workers (2001) when two different conformations were observed for the crystal structure. The *cis*/*trans* conformation of Proline 91 had an effect on the orientation of helix 1 and helix 3, indicating that the domain is somewhat plastic and may be susceptible to structural alterations as part of its function *in vivo* (Harrop *et al.,* 2001). The ability of the thioredoxin-fold domain of CLIC1 to rearrange was also shown by Littler and co-workers (2004) with the formation of an entirely α-helical domain when exposed to hydrogen peroxide and forcing the formation of an intra-domain disulphide bond (Cys24 – Cys59). The resulting altered conformation of the N-terminal domain is unstable in solution due to a large exposed hydrophobic surface (Littler *et al.,* 2004).

To date, the evolutionary history of the GST C-terminal domain has remained a mystery. For CLIC1 it appears that this entirely α-helical domain may represent the nucleation site for the protein due to the high stability of this region. Furthermore, the stability of domain 2 in CLIC1 may be necessary to keep the GST fold stable as a monomer.

Although the conformational change from solution to membrane has been shown to be pH dependent (Warton *et al.,* 2002) it appears that an acid-induced molten globule conformation is not what mediates the change from soluble to integral membrane form. Under conditions that favour the solution conformation (pH 7.0), the free energy of unfolding (ΔG) has been determined to be 9.8 kcal.mol^{-1}, while under conditions that favour a membrane conformation (pH 5.5), ΔG was 3.9 kcal.mol^{-1} (McIntyre, PhD unpublished results). This indicates that at pH 5.5 the solution conformation of CLIC1 is destabilised. However, it does not form a molten globule

commonly thought to be necessary for proteins that switch from soluble to membrane form. The presence of a negatively charged membrane or an electrostatic potential across the membrane may be necessary to trigger the conformational switch by interacting with the less stable form at pH 5.5. The absence of molten globule formation at pH 5.5 might have evolved to protect CLIC1 from intracellular proteases as it undergoes the conformational change essential for its activity.

From the comparison of the DXMS data for CLIC1 at pH 7.0 and pH 5.5 it can be concluded that parts of the α1, α3 and α6 helices of CLIC1 become more flexible at lower pH. No other significant difference in deuteration between the two pH conditions was observed. As CLIC1 approaches the membrane and enters into a lower pH micro-environment certain structural changes occur that may be necessary to trigger the association/ insertion of CLIC1 into the membrane. The exact behaviour of a given protein at low pH is a complex interplay between a variety of stabilizing and destabilizing forces. Non-specific repulsions between similarly charged residues (electrostatic forces) may be affected by a change in pH. A change in the proteins net charge leads to more charge repulsions along the protein surface and destabilises the protein. Typically, as the pH approaches the proteins p*I* value the net charge of the protein should be zero thereby minimizing any repulsive surface charge contacts. The effect of pH can, however, vary for proteins with similar p*I* values based on their different amino acid compositions. The individual p*K*a values for amino acid side chains are a crucial factor when considering the effect of pH change. Acid or negatively charged residues with low p*K*a values like aspartic acid and glutamic acid form specific charge contacts with basic or positively charged amino acids like arginine, lysine and histidine. These electrostatic contacts are known as salt-bridges and can provide an energy contribution of up to 15 kcal/mol/ion pair (Kumar and Nussinov, 1999). When pH conditions drop and approach the low p*K*a values of the acidic residues a disruption or weakening of any salt-bridge contact may occur.

DXMS data at pH 5.5 shows the region in helix 1 becomes more flexible, possibly by disruption of the salt bridge formed between Glu81 in helix 3 with Arg29 in helix 1 (Figure 68). This disruption might occur as the p*K*a (4.25) of the negatively charged glutamate residue is approached as the pH environment is lowered. There is also a salt bridge formed between Lys37 of helix 1 and Glu85 in helix 3. Both Arg29 and Lys37 are highly conserved in the CLICs but not other GST-like proteins. The same position

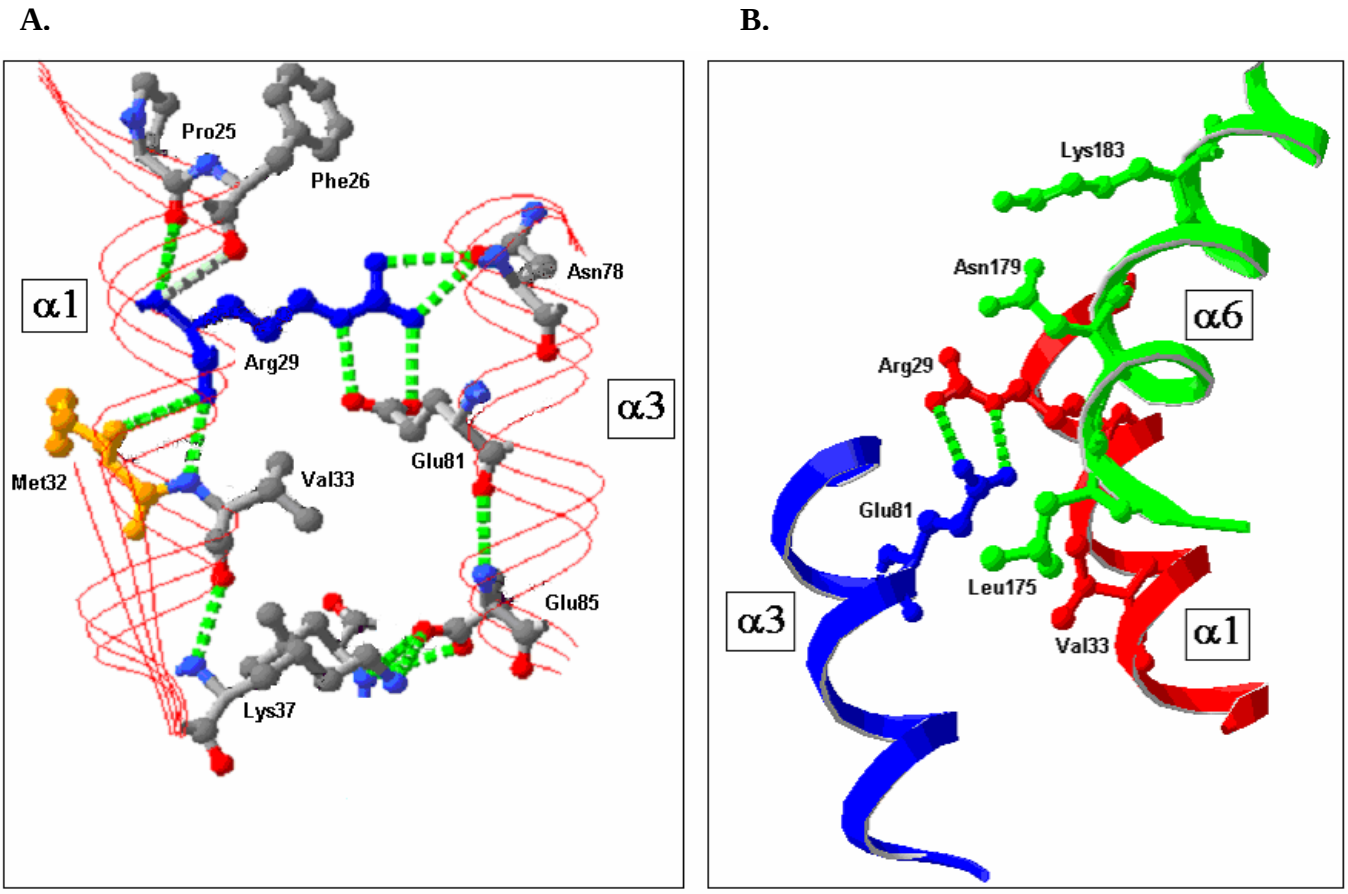


Figure 68: Graphic representations of CLIC1 residues affected by a drop in pH conditions.

(A) Amino acid side chains shown in ball-and-stick format. Met32 side chain shown in orange and Arg29 side chain shown in blue. Hydrogen bonds represented by dashed green lines. (B) Interactions between helix 1 (red), helix 3 (blue) and helix 6 (green). The images were generated with Swiss PDB viewer (Guex and Peitsch, 1997) using the PDB file 1k0m (Harrop *et al.*, 2001).

in the GSTs has hydrophobic residues. Since salt bridges are affected by pH it is very likely that these two positions play an important role and if they "uncouple" at lower pH it is likely that you get the "loosening"/flexibility in helix 1 and helix 3. A low pH environment may also result in a weakening of the double salt-bridge contacts formed between Glu85 in helix 3 and Leu96 that is found in the domain linker region. This linker could serve as a hinge point if interactions are disrupted, allowing the thioredoxin domain to move away from domain 2, rearrange and insert into the membrane. The dependence of the conformation of α1 and α3 on the domain linker region was reported by Harrop and co-workers (2001). A second molecule in the asymmetric unit of the crystal structure indicated that when Pro91 in the domain linker region was in the trans orientation, it resulted in an alternative conformation of the α1 and α3 helices (Harrop *et al.*, 2001).

Helix 6 in domain 2, which also becomes more flexible at lower pH, has inter-domain contacts with helix 1 and helix 3. The side chain of Arg29 of helix 1 is positioned very close to the side chain of Asn179 of helix6. Similarly, the side chain of Glu81 of helix 3 is in close proximity with the side chain of Leu175 in helix 6. A hydrogen bond exists between Asn179 and Leu175, so a weakening of one interaction across the domain interface may result in a co-operative disruption. It is interesting to note that the only region in domain 2 to be affected by a drop in pH, helix 6, is a region that is predicted to form a transmembrane helix in the CLICs because of significant hydrophobicity, as judged by hydrophobicity plots. The DXMS data shows that helix 6 becomes more flexible at pH 5.5. If this helix becomes exposed it could play a role in interacting with the membrane. Certain co-operative interactions across the domain interface may be weakened as the pH environment is lowered and the charge of the acidic residues becomes more neutral. This disruption across the domain interface may result in the proposed transmembrane regions becoming more loose and accessible to solvent. Inter-domain hydrophobic contacts with helix 1 and helix 3 may be disrupted as the pH environment is lowered, since the contacts between helix 1, helix 3 and helix 6 seem to be co-operative. An initial disruption in the salt bridge between Glu81 and Arg29 may result in a co-operative disruption between contacts within and across the domain interface. Arg29 forms two hydrogen bonds with Met32 that could be disrupted by the weakened interaction between Arg29 and Glu81. Inter-domain cooperativity was also noted by H/D exchange studies on the rGSTM1-1 mutant that produced a stable monomer (Thompson *et al.*, 2006). A static core of

interactions between the two domains provided a molecular basis for domain cooperativity. No amide exchange for the entire duration of the experiment for regions corresponding to helix 1 and helix 4 in domain 1 and helix 6 in domain 2 suggests that these stable regions, which are in close proximity to each other across the domain interface, constitute a cooperative link (Thompson *et al.,* 2006).

Mutational studies performed on Met32 in CLIC1 (Stoychev, PhD unpublished results) show that disruption of the inter-domain 'lock-and-key' motif significantly destabilised the protein. The M32A CLIC1 mutant also showed the same three-state unfolding pathway with formation of an intermediate observed for equilibrium unfolding of CLIC1 at pH 5.5 (McIntyre, PhD unpublished results). The accumulation of this intermediate indicates a loss in cooperative folding and thus highlights the crucial role of Met32 in the cooperative folding of CLIC1.

The interesting similarities in stability between the M32A mutant and native CLIC1 at pH 5.5 seem to indicate that Met32 is a key residue effected by a drop in pH. The cooperative interactions between Arg29, Met32, Glu81 and Glu213 may be a target for any signal to trigger the radical structural re-arrangement necessary for soluble CLIC1 to insert into the membrane. The disruption of key interactions across the domain interface may result in the proposed transmembrane region becoming more loose and accessible to solvent.

The structure of the integral membrane form of CLIC1 remains unknown. Future studies involving DXMS analysis of CLIC1 inserted into liposomes may provide some insight on this structure. However, the technique presents some complications that must first be overcome in order to optimise conditions for DXMS analysis of proteins in lipid bilayers.

4.1.3 CLIC1 sequence and structure analysis

The region predicted to form a transmembrane helix for CLIC1 based on sequence analysis was from residue 30 to 40.This predicted segment corresponds to the helix 1 and β-strand 2 regions of CLIC1. Sequence analysis of other CLIC proteins has also identified this region (Cys24 – Val46 for CLIC1 numbering) as a putative transmembrane helix (Valenzuela *et al.,* 1997; Edwards *et al.,* 1999; Qian *et al.,* 1999; Berryman and Bretscher, 2000). Experimental support for this hypothesis also comes

from proteinase K digestion studies on CLIC4 (Duncan *et al.,* 1997) and GFP-tagging studies on a *Caenorhabditis elegans* CLIC-like protein (Berry *et al.,* 2003). Previously, it seemed unlikely that region Cys24 – Val46 might form a transmembrane helix in the channel state because of the GST-like monomer structure (Harrop *et al.,* 2001), which would require an unfolding of the N-domain on membrane insertion. Recent studies involving the transition to dimeric form (Littler *et al.,* 2004) indicate that such an unfolding is indeed possible. The information on CLIC1 stability obtained by HXMS studies (see section 3.4.2.2) further validates this by indicating that the thioredoxin-domain is more likely to unfold and rearrange than the highly stable C-terminal domain.

Sequence alignments of the thioredoxin superfamily and GST family with the CLICs (Figure 63) reveals a conserved feature of the proposed transmembrane region (P25 – V46). This region contains many positively charged residues and no negatively charged residues for the CLIC family of proteins. This would be an essential feature of a pore that transports the negatively charged chloride ion across the membrane. Furthermore, the conserved positively charged motif (K49 – R51 in CLIC1) found at the end of the putative transmembrane region, may be a "plug" to stop the transmembrane region from inserting further into the negatively charged lipid membrane. The "positive inside rule" (von Heijne, 1986) states that regions with a higher content of positively charged residues tend to remain on the side from where insertion is occurring. The membrane dipole potential provides a higher energetic barrier to positively charged residues than to negatively charged residues (Flewelling and Hubbell, 1986).

Analysis of the proposed transmembrane region of CLIC1 in the crystal structure (Harrop *et al.,* 2001) shows that Arg29 and Lys37 line one face of the helix. The central 10 amino acids (Leu30 – Val39) are all non-polar, with the exception of Lys37. This predominantly hydrophobic region is flanked on either side by more polar residues. Polar and aromatic residues at the helix ends interact favourably with the interfacial region of the membrane to "anchor" it (Chamberlain *et al.,* 2004). This pattern is typical for transmembrane helices (Sakai and Tsukihara, 1998).

A comparison of the hydrophobicity patterns for the sequences of CLICs, GSTs and thioredoxin superfamily members was undertaken. For the CLIC proteins the highest level of hydrophobicity was observed at the region corresponding to residues 25 – 40 (CLIC1 numbering). This highly hydrophobic region was immediately followed by a highly hydrophilic dip observed in the plots. Analysis of the hydrophobicity plots of all the GST and thioredoxin superfamily members could not detect similar hydrophobicity patterns for the corresponding region within the thioredoxin-fold indicating that the hydrophobic properties of the CLIC proteins are unique and conserved and may play a crucial role in the proteins ability to insert into membranes.

Helix propensity analysis shows a high helical propensity for the proposed transmembrane region (α1 and β2) for CLIC1, and in fact the entire CLIC family. The loosening of the proposed transmembrane region at low pH may very well represent a mechanism by which the α1 helix and β2 strand region become more exposed to solvent and fulfil their high propensity for helical formation. This extended helical hairpin structure may then be hydrophobically driven to insert into the membrane. It is also interesting to note that the AGADIR helix propensity analysis for the entire GST and thioredoxin superfamily revealed only CLICs to show this high helical propensity at the corresponding α1/β2 region with strong N-capping and C-capping properties. Exceptions were GST Kappa class and calsequestrin, both of which have been implicated in membrane interaction (Wang *et al.*, 1998; Ladner *et al.*, 2004). The Omega class GST and glutaredoxin-2 proteins, which have very similar folds and topology to CLIC1, do not show this peculiarly high helical propensity at the corresponding regions. Even thioredoxin, from which the N-terminal domain of CLIC1 is thought to have evolved from, does not exhibit any high helical propensities in the corresponding regions. Only CLIC2 and CLIC3 did not show high helical propensity at the β2 region. Interestingly, the ability of these CLIC members to form channels has yet to be shown. The high helical propensity of α1 and the "masked" helical propensity of β2 may play a crucial role in the mechanism for CLIC1 membrane insertion.

The type of amino acid residue found at the N-terminal and C-terminal end of a helix has a major effect on the stability of the entire helix (Serrano and Fersht, 1989). These residues are referred to as N-capping or C-capping residues and play an important role

in the folding and stability of α-helices (Scholtz and Baldwin, 1992; Wan and Wilner-White, 1999). Based on AGADIR analysis, strong N-capping and C-capping motifs were identified for CLIC1. The N-cap residue for helix 1 is Serine 27, while the C-cap residue is Lys37. These residues are strictly conserved in the CLIC family. N-capping motifs are also found at Asn42 (CLIC1 numbering) where high helical propensity is noted in the β2-region for CLICs (except CLIC2 and CLIC3). The highly conserved Lysine residue at the C-terminal end of β2 was predicted to form a C-capping motif of CLIC4, CLIC5 and CLIC6 but not CLIC1. The fact that these residues exhibit strong helix capping characteristics and are either strictly or highly conserved in the CLIC family (but not other proteins utilizing the thioredoxin fold) indicates that they may play a crucial role in the proteins functioning in integral membrane form.

Although N-capping motifs have previously been reported for GSTs at helix 6 (Aceto *et al.*, 1997) and helix 9 (Dirr *et al.*, 2005) in domain 2, this is the first time N-capping properties have been observed for regions in the thioredoxin-fold domain of GSTs. An N-cap residue (Serine 12) and C-cap residue (Tyr19) in helix 1 was noted for Mu-class GST. This may serve as a platform for future studies involving GST stability. The high helical propensity prediction for the α1/β2 region of Kappa GST also indicated Lys21 and Arg40 as possible N-cap and C-cap residues, respectively. It has been previously hypothesised that Kappa GST binds to membranes as part of its function (Ladner *et al.*, 2004). The strong N-capping and C-capping properties observed for many of the CLICs in the region of α1 and β2 may be an important feature for the protein families ability to form stable and functional channels.

Surface area determination of CLIC1 and comparisons with Grx-2 show that CLIC1 appears to have a larger total accessible surface area indicating that it is not as tightly packed and perhaps more flexible than Grx2. Despite clues from the CLIC1 crystal structure (Harrop *et al.*, 2001) indicating that this increased surface area may be due to the flexible negatively charged loop region in domain 2, it appears that domain 2 of CLIC1 contributes more to the difference in surface area observed between the two proteins. The slightly higher percentage value for Grx2 buried surface area at the domain interface indicates the domain interface is in a more closed orientation than the more open domain interface of CLIC1. This corresponds well with the hypothesis

that the CLIC1 domain interface is somewhat plastic and may be susceptible to structural alterations as part of its function *in vivo* (Harrop *et al.*, 2001).

4.2 Interaction of CLIC1 with membrane models

4.2.1 TFE

Trifluoroethanol (TFE) is a co-solvent known to enhance the helical content of peptides which display intrinsic helical properties (Rohl *et al.*, 1996; Kumaran and Roy, 1999). TFE interacts with hydrophobic regions on the protein by displacing helix-helix contacts in the bundle conformation. In other words, TFE replaces helix-helix interactions with helix-TFE interactions. The preferential aggregation of TFE molecules around peptides induces a stabilizing effect. The coating displaces water, thereby removing alternate hydrogen-bonding partners and providing a low dielectric environment that favours the formation of intra-peptide hydrogen bonds (Roccatano *et al.*, 2002). Because of the similarity in properties between TFE and the hydrophobic interior environment of the membrane, TFE is considered as a membrane-mimetic solution and is widely used as a membrane model system (e.g. Mak *et al.*, 2001).

These results indicate that CLIC1 has a tendency to drastically increase its helical content when exposed to a lower dielectric constant, hydrophobic environment like that found in the membrane core. The CLIC1 structure and sequence appears to have a high helical propensity when exposed to membrane-like environments, and would probably take on a highly α-helical structure once it has inserted into the membrane. The folding of CLIC1 once it inserts into the membrane would likely take on an entirely α-helical transmembrane structure based on the high helical propensity of the protein observed in this study when in a membrane-mimetic environment.

This could imply that once CLIC1 structure is rearranged in the membrane core it may not have the ability to revert back to its soluble form.

4.2.2 Liposomes

The structural and thermodynamic properties of CLIC1 incubated with anionic liposomes of different lipid composition was investigated in order to establish whether the protein inserts into this membrane model system and what structural changes are occurring. The role of pH in the interaction of CLIC1 with liposomes was also investigated. Liposomes containing cholesterol (POPC/DOPG/ holesterol) and liposomes not containing cholesterol (asolectin) were studied with CLIC1 at pH 7.0 and pH 5.5.

Cholesterol is a planar, tetracyclic hydrocarbon (sterol) compound. It is thought to rigidify membrane structure by breaking up van der Waals interactions and close packing of phospholipid tails that make membranes more fluid. It decreases membrane permeability by strengthening the hydrophobic packing interactions of the constituent lipids. The dependence of CLIC1 activity on vesicle phospholipid and cholesterol composition was investigated by Tulk and co-workers (2002). The results indicated that cholesterol-containing membranes significantly reduced the amount of CLIC1-mediated chloride efflux and therefore had an inhibitory effect on CLIC1 channel formation or functioning. Other functional studies on CLIC1 using similar electrophysiological experiments used membranes containing 10 % - 17 % cholesterol (Warton *et al.*, 2002; Singh and Ashley, 2006). One of those studies could only obtain reproducible ion channel activity using membranes that contained cholesterol (Singh and Ashley, 2006). In an attempt to clarify the contradictory data, basic characterisation and thermodynamics of CLIC1 incubated with cholesterol-containing liposomes were undertaken.

A common and useful method for the detection of protein binding to membranes is fluorescence spectroscopy. Data acquired from tryptophan fluorescence studies can be used to gain qualitative insight into the environment of the fluorophore upon interaction with lipids. The change in intrinsic protein fluorescence, particularly for proteins with one or low number of tryptophan residues, can be readily interpreted based on the sensitivity to the polarity of the surrounding solvent (Duzgunes *et al.*, 2003). When a partially buried tryptophan residue of a protein moves to a more polar solvent or environment, the solvent molecules can reorient dipoles around the excited state of the fluorophore such that the energy of the excited state is minimised and the emission wavelength is shifted to a higher wavelength (Lakowicz, 1999). This is

typical of a protein that is unfolding or re-orientating so that the tryptophan residue is becoming more exposed to aqueous solvent. On the other hand, when a tryptophan group moves to a more non-polar environment, like that found in the membrane, there would be a shift to a more blue emission wavelength. Fluorescent detection of protein inserting into phospholipid membranes using intrinsic protein-associated fluorophores and emission wavelength shift is well documented for other amphitropic proteins such as annexin V (Meers and Mealy, 1993).

The red-shift in fluorescence emission maximum observed when CLIC1 is incubated with the POPC/DOPG/cholesterol liposomes indicates that the protein is partially unfolding when it comes into contact with the anionic liposome membrane. The negative charge at the membrane surface has previously been shown to denature proteins (Endo and Schatz, 1988). The membrane induced destabilisation or partial unfolding of CLIC1 may be the initial trigger necessary for the conversion of soluble CLIC1 to integral membrane form *in vivo*. With the specific lipid composition of the liposomes used in this study however, it does not appear that CLIC1 inserts into the cholesterol-containing liposome since we expect the lone tryptophan to become buried in the liposome interior and exhibit a blue-shift in fluorescence emission maximum.

Far-UV CD analysis of CLIC1 incubated with the cholesterol-containing liposomes show no significant change in secondary structural content of the protein. It can thus be concluded that although CLIC1 partially unfolds or re-arranges in the presence of anionic cholesterol-containing liposomes, it retains all of its secondary structure. Identical results were obtained with CLIC1 at pH 5.5. The increase in size observed by dynamic light scattering of CLIC1 incubated with the POPC/DOPG/cholesterol liposomes may be attributed to oligomerisation of CLIC1 and adsorption to the liposome surface or fusion of the liposomes in the presence of CLIC1 protein.

In the literature, the majority of experimental evidence for CLIC1 insertion into membranes and channel formation has been extrapolated from electrophysiological studies measuring chloride efflux from supposed CLIC1-mediated channels (Tulk *et al.,* 2000; Tulk *et al.,* 2002; Warton *et al.,* 2002; Littler *et al.,* 2004; Singh and Ashley, 2006). Although this information is useful for the functional aspect of CLIC1 channels, specific information on the process of membrane interaction, insertion and

channel formation is lacking from the scientific literature. The association/insertion of CLIC1 into membranes has not been demonstrated directly by quantitative analysis of the thermodynamics involved. In the present study the thermodynamics of CLIC1 interacting with lipid vesicles was investigated.

Although the small thermodynamic signals indicated that CLIC1 was not inserting into the cholesterol-containing liposomes, representative thermodynamic profiles were obtained for comparison of CLIC1 interacting with the liposomes at pH 7.0 and pH 5.5. At neutral pH the initial endothermic (enthalpically unfavourable) heats observed may be a result of CLIC1 partially unfolding or rearranging when coming into contact with the liposomes. The structurally altered form may then be able to favourably (enthalpically) interact and associate with the membrane (exothermic heat signals). At pH 5.5 the lack of any initial endothermic heats may be due to CLIC1 being in a membrane association competent form at pH 5.5. From the binding and thermodynamic parameters obtained it appears CLIC1 at pH 5.5 binds more tightly and favourably to the POPC/DOPG/cholesterol liposomes than CLIC1 at pH 7.0. The more negative change in enthalpy (ΔH) value at pH 5.5 (-5.583 kcal/mol) compared to pH 7.0 (-0.895 kcal/mol) indicates a more enthalpically favourable interaction with membrane for CLIC1 at pH 5.5. At pH 7.0 the free energy of binding (ΔG) value was calculated to be 5.623 kcal/mol while at pH 5.5 ΔG was –4.567 kcal/mol. The negative value for ΔG at pH 5.5 is indicative of a spontaneous reaction compared with pH 7.0. Less disorder was evident at pH 5.5 based on the more negative change in entropy (ΔS) value at pH 5.5 (-0.0034 kcal/mol/K) compared to pH 7.0 (0.0159 kcal/mol/K). This may be as a result of ordering of the membrane or intra-lipid interactions within the liposome. A low or negative ΔS value is also indicative that hydrophobic interactions do not dominate the binding process (Dimitrova *et al.*, 2002). Entropy losses are anticipated when protein binds to membrane since the mobility of the protein as well as undulations of the lipid membrane are significantly reduced due to protein adsorption.

Protein conformational change, surface adsorption, membrane insertion and membrane partitioning are all usually accompanied by changes in the heat content of the system. The driving forces for protein adsorption and binding are hydrophobicity,

electrostatics, and hydrogen bonding. If the protein and the membrane are both charged, as for CLIC1 and POPC/DOPG/cholesterol liposomes, it would be expected that electrostatic interactions would be dominant. For CLIC1 at pH 7.0 the regions on the protein responsible for this electrostatic attraction may be hidden and a structural rearrangement may be necessary for the regions to become unmasked and thus interact with the membrane. The structural rearrangement induced by lowering the pH value may result in a conformation that can readily interact electrostatically with the charged membrane surface.

From the studies performed with CLIC1 and cholesterol-containing liposomes it appears that the protein only weakly interacts with liposomes with this lipid composition. CLIC1 may electrostatically interact with the negatively charged liposome causing adsorption to the membrane surface. The protein does not, however, appear to traverse or insert itself into the membrane. The process of electrostatic attraction to the liposome is favoured by the conformation adopted by CLIC1 at pH 5.5 compared to that at pH 7.0.

In order to establish whether the lack of CLIC1 insertion into the lipid vesicles was due to the cholesterol content of the liposmes a study was performed using asolectin liposomes that contain no cholesterol. In a study by Tulk and co-workers (2002), investigating the dependence of CLIC1 activity on vesicle phospholipid composition, it was reported that a crude preparation of phospholipid from soybean (asolectin) resulted in the most abundant CLIC1-mediated channel activity. The lipid mixture containing approximately 30 % phosphatidylcholine, 20 % phosphatidylethanolamine and 30 % phosphatidylinositol with the remainder of the phospholipids undefined is also known as asolectin. The lipid composition renders a net negative charge on the surface of the formed vesicles. Based on the reported preference for asolectin by CLIC1 to form functional channels, a study was undertaken to investigate the properties of CLIC1 association with asolectin vesicles.

Fluorescence data shows a blue-shift in emission maximum and a decrease in intensity when CLIC1 is incubated with asolectin liposomes. This increase in emission maximum wavelength is observed when CLIC1 unfolds, so the possibility of CLIC1 unfolding upon interaction with negatively charged asolectin vesicles cannot be ruled out. Data was corrected for free asolectin, which peculiarly exhibited some

fluorescent properties. Far-UV CD analysis indicated no change in secondary structural content as a result of incubation with the cholesterol-free liposomes. These results, like those obtained for the cholesterol-containing liposomes, provide no evidence for CLIC1 insertion. Unlike with the cholesterol-containing liposomes, however, dynamic light scattering studies with CLIC1 and asolectin liposomes indicated that the proteins hydrodynamic size did not increase and that the lipid vesicles remain largely intact.

The thermodynamics of CLIC1 interaction with asolectin vesicles were investigated using isothermal titration calorimetry. The resulting thermodynamic profile observed is indicative of weak binding and probably only reflects a small degree of electrostatic attraction or lipid-induced conformational change on CLIC1. Even though no significant insertion of CLIC1 into the membrane is likely to be occurring, the corrected data once again indicates more enthalpically favourable interactions, probably electrostatic, between CLIC1 and asolectin vesicles at pH 5.5 compared with pH 7.0.

This finding that CLIC1 does not readily or spontaneously insert into asolectin vesicles is consistent with recent results, which showed that CLIC1 failed to form well-defined ion channels and thus produce any ion channel activity when incubated with asolectin bilayers (Singh and Ashley, 2006). It was speculated by Singh and Ashley (2006) that CLIC1 may require specific lipids in order to refold or form oligomers after membrane insertion. The results of this present study, however, indicate that CLIC1 may be weakly associating but not inserting into asolectin vesicles, explaining why no channel activity was observed.

4.2.3 Sarkosyl micelles

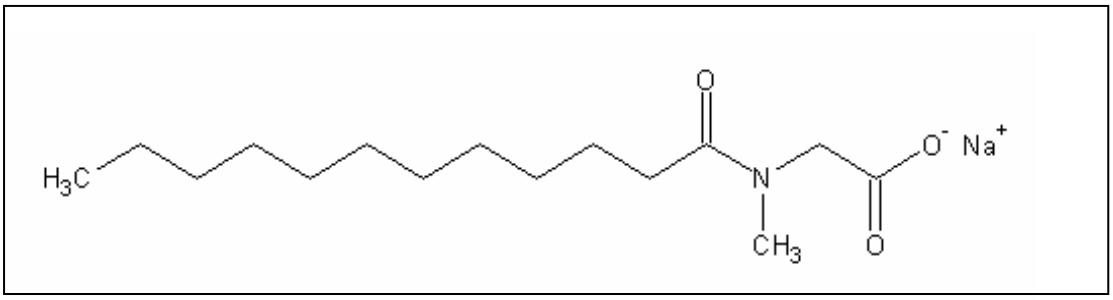
Since CLIC1 did not appear to insert and form channels in the lipid membrane models used (POPC/DOPG/cholesterol liposomes and asolectin vesicles), a simpler membrane model system was considered to compare the effect and role of factors such as pH, ligands, inhibitors and specific residues on membrane insertion. When using lipid vesicles many variables such as lipid composition, cholesterol content, surface charge, vesicle size and vesicle curvature can have an effect on CLIC1 membrane interaction and insertion. In order to eliminate these variables and provide the simplest system, for comparative reasons, detergent micelles were used to better

understand the process of soluble CLIC1 inserting into the hydrophobic membrane core.

Detergent micelles are invaluable tools for mimicking membrane conditions and therefore for studying membrane proteins. Detergents are classically used to solubilize proteins already imbedded in membranes or prone to aggregation and for high-resolution structural analysis (i.e. NMR and X-ray crystallography) of membrane proteins. The fact that detergent micelles are used to reconstitute membrane proteins for three-dimensional structure determination implies that detergent micellar systems should also be suitable for investigations of soluble protein with membranes. Because of the membrane-like properties of the detergent micelle, it provides a simple model for protein-membrane interactions. Using detergent concentrations above the critical micellar concentration (CMC) is crucial in ensuring micellar structures have been formed that will have the polar head of the detergent on the surface and a hydrophobic interior, thus replicating the properties of a lipid bilayer (Figure 69). The balance of the attraction between alkyl chains in the micelle interior and the repulsion of polar head groups determine the CMC and size of the micelle. In general, detergents with longer alkyl chains form larger micelles because stronger repulsion of the head groups are required to terminate micelle growth (Garavito and Ferguson-Miller, 2001). Certain differences in properties do exist between detergent micelles and lipid bilayers, however, both amphoteric compounds provide a polar, often charged interfacial surface and a non-polar hydrocarbon core. Many properties of transmembrane oligomerisation are also conserved between the environments provided by detergent micelles and natural membranes (Russ and Engelman, 1999). Artificially reconstituted proteins generally exhibit lower activity and this may reflect their random orientation in foreign environments, whether lipid or detergent. These systems, however, provide a means for comparative studies in a membrane-mimicking environment. Sarkosyl is an anionic detergent with a chain length of 15 carbons. It was used in this study because the micelles formed would have a negative charge at their surface due to the ionic form of the hydrophilic head group.

When CLIC1 was incubated with 10.3 mM sarkosyl, a fluorescence shift from 347 nm to 342 nm was noted. This blue-shift pattern could be indicative of the proteins lone tryptophan moving to a more non-polar environment and may represent CLIC1 insertion into the micelle. The other possibilities are that the micelles have a structural

A.



B.

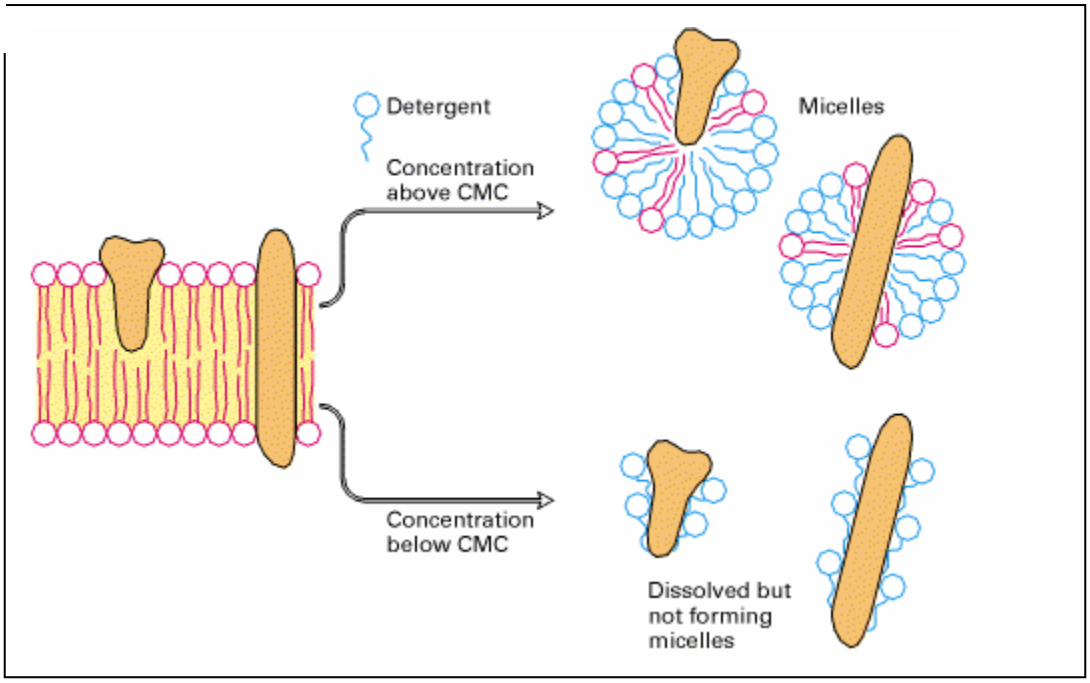


Figure 69: Chemical stucture of sarkosyl and micelle formation with protein insertion.

A. The chemical structure of the anionic detergent N-laurylsarcosine (sarkosyl)
B. Schematic showing micelle formation and protein incorporation. At a concentration higher than its critical micelle concentration (CMC), a detergent solubilises lipids and integral membrane proteins, forming micelles containing detergent and protein. At concentrations below the CMC, many detergents can dissolve membrane proteins without forming micelles by coating the membrane-spanning regions. Since sarkosyl has a low CMC, it is particularly effective in solubilizing integral membrane proteins by forming micelles

.

effect on the protein causing the lone tryptophan to become more buried within the protein itself, or at the protein-membrane interface. The use of fluorescent detection of protein inserting into phospholipid membranes using intrinsic protein-associated fluorophores and emission wavelength shift is well documented (Duzgunes *et al.*, 2003). This method has been used to study the membrane insertion of other amphitropic proteins such as annexin V (Meers and Mealy, 1993).

In order explain the decrease in emission intensity when CLIC1 is incubated with micelles an investigation into the quenching effects of sarkosyl on tryptophan fluorescence was undertaken. Fluorescence spectra for 5 μM NATA incubated with micelles showed a decrease in fluorescence emission providing evidence for a quenching effect of micelles on tryptophan fluorescence. Any observed decrease in fluorescence emission intensity observed for CLIC1 incubated with micelles can thus be attributed to this quenching effect. However, no shift in emission maximum was noted when NATA was mixed with micelles suggesting that any shift observed for CLIC1 with micelles was a result of the protein inserting into the micelle, positioning the lone tryptophan residue within the non-polar hydrophobic core. The possibility that the micelles have a structural effect on the protein causing the lone tryptophan to become more buried within the protein itself cannot, however, be ruled out. No significant change in secondary structural content was occurring as a result of CLIC1 interaction with micelles, as observed by far-UV CD methods.

Dynamic light scattering studies show that when CLIC1 is incubated with micelles the hydrodynamic diameter of the micelles increases from 4.6 nm to 5.2 nm. This increase in diameter may be a result of portions of the inserted protein “sticking out” and thus increasing the reported hydrodynamic diameter of the micelles. This diameter would be indicative of the size of the inserted protein, which when compared to the diameter of free CLIC1 (6.6 nm) would suggest that the inserted form of CLIC1 has a decreased hydrodynamic volume and is assuming a more compact form.

Isothermal titration calorimetry was used to investigate the thermodynamic properties of CLIC1 insertion into micelles. This technique provided a way to compare the roles of pH, ligands, inhibitors and specific residues in CLIC1 membrane insertion. At pH 7.0 the initial endothermic heat signals may represent structural changes occurring to CLIC1 when the protein comes into contact with anionic micelles. The binding

isotherm (corrected for heats of dilution) for the exothermic portion of the experiment fitted best to a 2 binding sites model. The exothermic heats may thus be a contribution of 2 distinct steps, namely, electrostatic adsorption of protein to micelle followed by hydrophobic adsorption or protein insertion into the micelle.

Functional CLIC1 studies have investigated the effect of reduced glutathione (GSH), oxidised glutathione (GSSG), and a known chloride channel blocker, indanyloxyacetic acid-94 (IAA-94) on chloride efflux in order to establish any inhibitory effects these molecules may have on CLIC1 channel functioning (Tulk *et al.*, 2000; Tulk *et al.*, 2002; Singh and Ashley, 2006). The effects of reducing and oxidizing conditions on channel functioning have also been studied (Littler *et al.*, 2004; Singh and Ashley, 2006). The results from these studies are, however, contradictory, making it difficult to draw valuable conclusions. It is also unclear whether the effects observed in the experiments are due to the direct association of the compound to CLIC1 or whether it is a secondary effect caused by a change in environment (i.e. reducing and oxidizing conditions). Isothermal titration calorimetry was used to study the binding properties of GSH and IAA to CLIC1 at pH 7.0 in the absence of micelles initially, and thereafter the effect of these compounds on CLIC1 membrane insertion.

From the ITC data obtained when GSH was titrated to CLIC1 it can be concluded that if reduced GSH does indeed bind CLIC1 it does so very weakly and with a dissociation constant greater than 35 mM. This contrasts with the strong binding of GSH to other GSTs (K_d in μM range) (Wilce and Parker, 1994). Relevant GSH binding may, however, occur in the dimeric form of CLIC1. These results indicate that any effect of reduced GSH on functionality is a result of the creation of a reducing environment and not noncovalent binding of the molecule to CLIC1. Tulk and co-workers (2002) found 2 mM GSH to significantly inhibit CLIC1-mediated chloride efflux, which seems unlikely due to the weak binding of GSH to CLIC1. The effect cannot be attributed GSH creating a reduced environment either since results in that same study showed increasing DTT concentration from 1 to 5 mM yielded higher levels of channel activity. Another possibility is that the binding or effect by GSH on CLIC1 may be different when CLIC1 is inserted in the membrane. Recent contradictory results form Singh and Ashley (2006) show 5 mM GSH to only slightly effect chloride efflux. Isothermal titration calorimetry was not successful in

determining any thermodynamic parameters or the dissociation constant for IAA binding to CLIC1 at pH 7.0. The mechanism by which IAA inhibits chloride channels remains unknown.

The effects of GSH and IAA on CLIC1 membrane insertion were investigated. Results show that 2 mM GSH had no effect on the thermodynamics of CLIC1 interaction with micelles. Previous results claiming that 2 mM GSH has an inhibitory effect on CLIC1 function (Tulk *et al.,* 2002) must thus be attributed to an effect on the CLIC1 channel directly and not to the membrane insertion / interaction process. Similarly IAA did not have any effect on the thermodynamics of CLIC1 membrane insertion process and any inhibitory effects previously noted (Tulk *et al.,* 2002; Singh and Ashley, 2006) are probably as a result of an effect on the formed channels functioning and not from inhibiting the interaction or insertion of the protein into the membrane.

For CLIC1 at pH 5.5, the exothermic data, like those at pH 7.0, fitted to a 2-site binding model. The thermodynamic parameters and enthalpic heat signals indicate a more enthalpically favourable and tighter association for CLIC1 with micelles at the lower pH. Because all data was fitted to a 2-binding site model, two values were obtained for each thermodynamic parameter. A more negative ΔH_2 was noted at pH 5.5 (- 0.394 kcal/mol) compared with pH 7.0 (- 0.294 kcal/mol) indicating a more enthalpically favourable reaction at the lower pH value. Higher values for ΔS_1 and ΔS_2 were noted for pH 5.5 (0.169 and 0.291 kcal/mol, respectively) compared with 0.018 and 0.030 kcal/mol at pH 7. This more positive ΔS value indicates more disorder for CLIC1 interacting with micelles at pH 5.5. The stoichiometry (N) of the experiments performed at the different pH values also appears to be significantly different. At pH 7.0, stoichiometry was 59 and 60 for N_1 and N_2, respectively, while for pH 5.5 the values were 71 and 101, respectively. The higher stoichiometric values of CLIC1 at pH 5.5 indicate that the protein interacts with more sarkosyl molecules, and therefore a greater area of the micelle aggregate, than CLIC1 at pH 7.0.

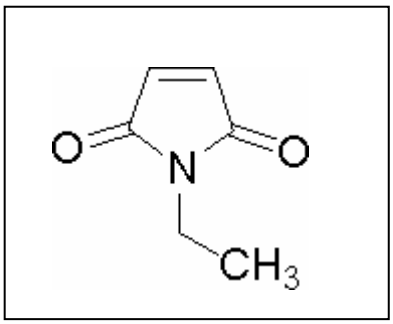
The chemical structure of NEM is shown in Figure 70A. NEM reacts with sulfhydryl groups in proteins with considerable specificity (Gregory, 1955). The effect of attaching the relatively bulky thiol-reactive reagent to the proteins accessible cysteine

residues was investigated in the context of CLIC1-micelle interaction. According to the CLIC1 sequence and structure a total of 6 cysteine residues exist, 3 of which are in domain 1 and 3 in domain 2 (Figure 70B).

The DTNB assay performed on unfolded CLIC1 verified this indicating a total of 6 free thiols. For native/folded CLIC1 a total number of 4 sulfhydryls were determined indicating that this is the number of exposed cysteines for the folded protein and, therefore, the number of NEM molecules bound to CLIC1. Two cysteine residues are therefore buried in the CLIC1 structure.

The NEM-modified proteins tertiary or secondary structure was not compromised or affected. Despite this, however, the attachment of NEM to the proteins exposed cysteine residues resulted in a net effect of no enthalpic signal when brought into contact with micelles. This indicates that the attachment of the relatively bulky reagent to the proteins cysteine residues completely inhibited interaction and insertion with the micelles. This finding emphasises the crucial role of CLIC1 cysteine residues in membrane insertion. Although the role of cysteine residues on CLIC1 channel functioning has been previously investigated (Tulk *et al.*, 2002; Littler *et al.*, 2004; Singh and Ashley, 2006), this represents the first thermodynamic study showing the role of the cysteine residues on direct membrane interaction and insertion. In the electrophysiological (functional) studies of CLIC1, mutagenesis of individual cysteine residues showed Cys24 and Cys59 to play an important role in CLIC1 channel functioning, but not Cys89 (Littler *et al.*, 2004). In another electrophysiological CLIC1 study (Tulk *et al.*, 2002) preincubation with 10 mM NEM dramatically inhibited valinomycin-dependent chloride efflux and it was concluded that the CLIC1 sulfhydryl groups are essential for channel activity. Based on the ITC studies presented here it is now clear that this decreased channel activity was as a result of NEM inhibiting CLIC1 membrane insertion and not because of channel blocking or functioning.

A.



B.

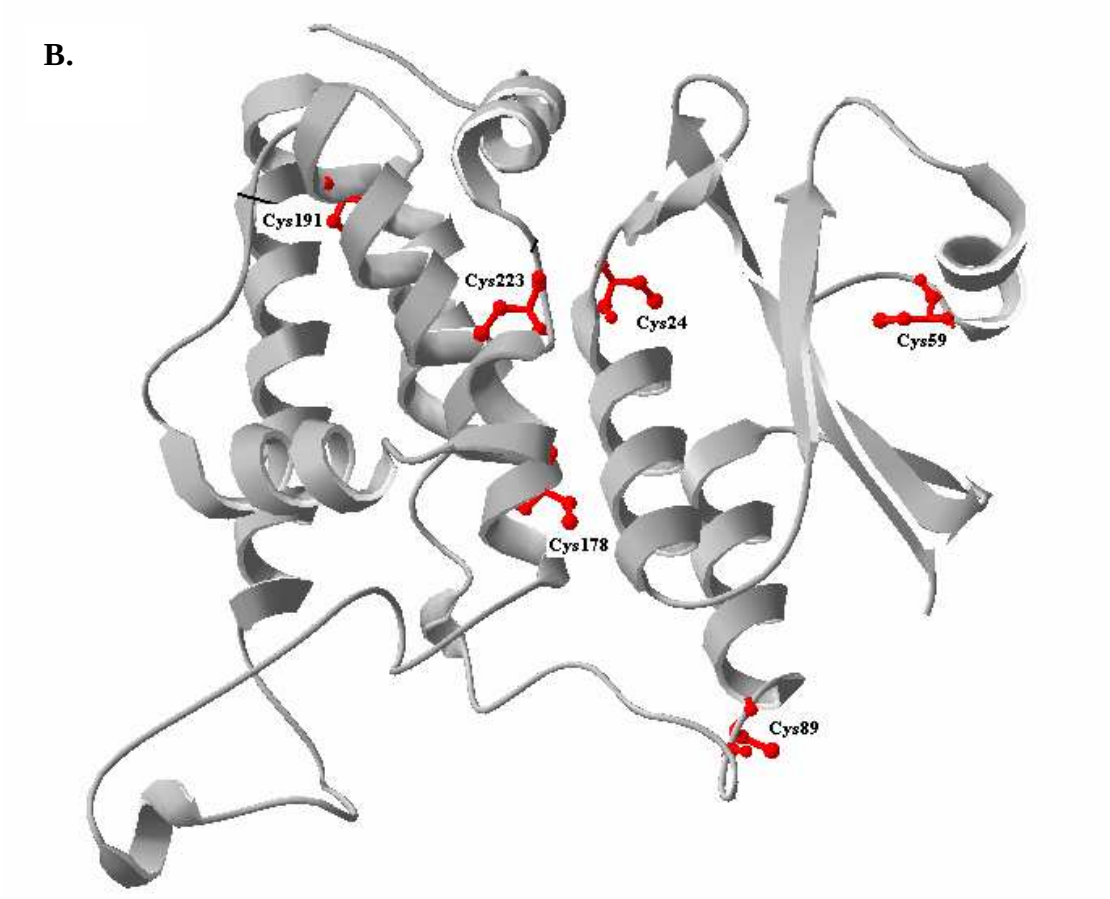


Figure 70: NEM chemical structure and CLIC1 ribbon structure showing cysteine residues.
Panel A shows the chemical structure of the sulfhydryl modifying agent NEM. Panel B shows a ribbon representation of CLIC1 highlighting the distribution of cysteine residues (red). The image was generated with Swiss PDB viewer (Guex and Peitsch, 1997) using the PDB file 1k0m (Harrop *et al.*, 2001).

4.2.4 Model for membrane insertion and channel orientation

Early speculations on CLIC1 membrane insertion (Cromer et al., 2002) suggested that it was unlikely that the N-terminal domain will readily unfold to form a membrane-interacting domain since it has evolved from the thioredoxin superfamily. HXMS and AGADIR helix propensity analysis show that a change in pH may reveal hidden propensities and dynamic structural properties that are not seen in the crystal structure. We propose that the membrane insertion scheme of CLIC1 involves destabilisation of the α1 / β2 region as CLIC1 approaches the membrane and enters into a lower pH environment. This destabilisation results in the region to fulfil its propensity to form a helical hairpin structure. This region then has the ability to insert into the membrane resulting in the N-terminal end going across the membrane and the C-terminal end (domain 2) remaining behind. This is consistent with FLAG-epitope studies done previously (Tonini *et al.,* 2000) showing the N-teminal end of CLIC1 to traverse to the outside of the membrane while the C-terminal end remains on the inside.

The proposed transmembrane region (P25 – V46) shows all the necessary characteristics in terms of length (31 Å) and charge (no negatively charged residues) to form the membrane spanning / pore region of the CLIC1 channel. This, along with the DXMS data showing domain 1 to be more flexible and less stable than domain 2, indicates a high probability that the membrane inserting region is found in domain 1 rather than domain 2 and that the thioredoxin fold has evolved and specialised to adopt the ability for membrane interaction. This evidence, along with GFP-tagging translocation studies in EXC-4 CLIC-like protein (Berry *et al.,* 2003) and mutational studies of residues in the proposed transmembrane region of CLIC1 (Littler *et al.,* 2004; Singh and Ashley, 2006), seem to provide sufficient proof that domain 1, and more specifically region P25 –V46, is responsible for CLIC1 membrane insertion and channel activity. Recently, this region has been shown *in vivo* to be a key determinant of membrane localisation and function of invertebrate CLIC proteins (Berry and Hobert, 2006).

Figure 71 shows a schematic representation of the proposed transmembrane segment and its possible orientation. Since the highest amount of CLIC1 localisation has been reported in the cell nucleus (Valenzuela *et al.*, 1997), a theoretical scheme for CLIC1 functioning *in vivo* may involve a change in nucleoplasm conditions (such as pH or redox changes during cell division), signalling or rearranging the protein to a membrane-insertion competent form. Soluble CLIC1 in the nucleoplasm would then be hydrophobically driven to insert into the nuclear mambrane, where it probably oligomerises to form a channel or pore. The movement of chloride ions can then take place from the cytoplasm into the nucleoplasm. The opening and closing of the pore may be controlled by the redox environment of the N-terminal end of the protein as shown in studies by Singh and Ashley (2006), with Cys24 playing a crucial role. Exposure of the N-terminal end of the channel to oxidising environments would result in the pore being closed possibly due to disulphide bond formation, while a reducing environment would ensure it stays open (Singh and Ashley, 2006).

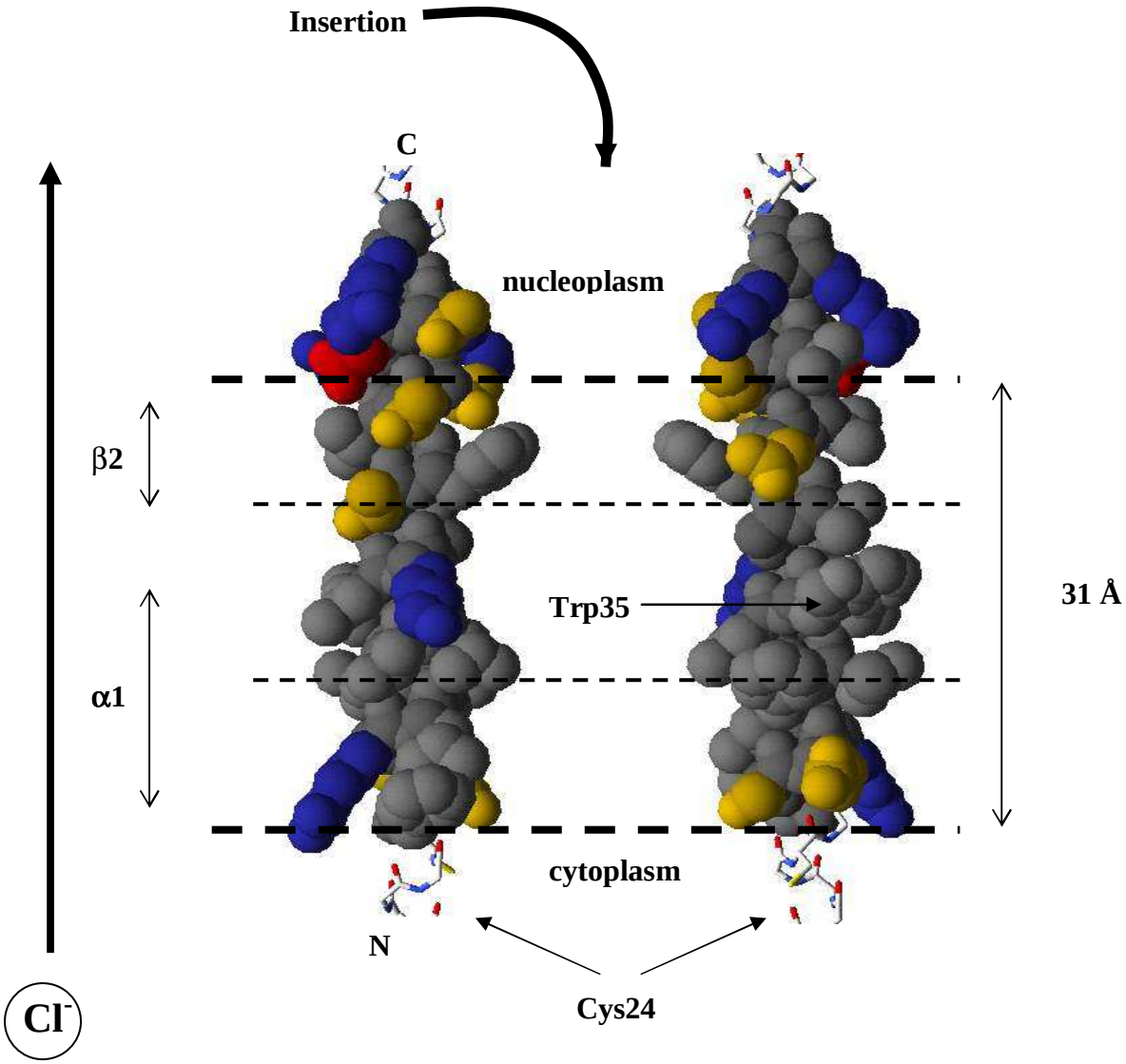


Figure 71: Schematic showing proposed transmembrane segment of CLIC1 and its possible orientation within the membrane.
The proposed model shows region 24 – 46 of two transmembrane segments spanning a typical 30 Å thick membrane and conducting chloride from the N-terminal ends toward the C-terminal end. Insertion is proposed to occur from the nucleoplasmic side with the N-terminal end of the protein inserting through the membrane to the cytoplasmic side. The bold dashed lines indicate the interfacial region of the membrane while the smaller dashed lines represent the boundaries of the hydrophobic core within the membrane. Positive residues are shown in blue, negatively charged residues in red and uncharged residues in yellow. In this model, the lone Trp35 is proposed to lie within the hydrophobic core of the membrane. Cys24 would be positioned at the interfacial region of the membrane, possibly serving a REDOX-controlled gating function.

CHAPTER 5. REFERENCES

Aceto, A., Dragani, B., Melino, S., Allocati, N., Masulli, M., Di Ilio, C. and Petruzzelli, R. (1997) Identification of an N-capping box that affects the alpha 6-helix propensity in glutathione S-transferase superfamily proteins: a role for an invariant aspartic residue. *Biochem J.* **322**, 229-34

Arkin, I.T. and Brunger, A.T. (1998) Statistical analysis of predicted transmembrane alpha-helices. *Biochim. Biophys. Acta.* **1429**, 113-128

Armstrong, R.N. (1997) Structure, catalytic mechanism, and evolution of the glutathione transferases. *Chem. Res. Toxicol.* **10**, 2-18

Anathanasiadis, A., Aderluh, G., Macek, P. and Turk, D. (2001) Crystal structure of the soluble form of equinatoxin II a pore forming toxin from the sea anemone *Actinia equine. Structure* **9**, 341-346

Avanti polar lipids, www.avantilipids.com

Bai, Y., Milne, J.S., Mayne, L. and Englander, S.W. (1993) Primary structure effects on peptide group hydrogen exchange. *Proteins Struct. Funct. Genet.* **17**, 75-86

Bai, M., Zhou, J.M. and Perett, S. (2004) The yeast prion protein Ure2 shows glutathione peroxidase activity in both native and fibrillar forms. *J. Biol. Chem.* **279**, 50025-50030

Banuelos, S. and Muga, A. (1995) Binding of molten globule-like conformations to lipid bilayers: structure of native and partially folded α-lactalbumin bound to model membranes. *J. Biol. Chem.* **270**, 29910-29915

Begley, M.J., Taylor, G.S. Brock, M.A. Ghosh, P. Woods, V.L. and Dixon, J.E. (2006) Molecular basis for substrate recognition by MTMR2, a myotubularin family phosphoinositide phosphatase. *Proc Natl Acad Sci U S A* 103:927-932.

Berry, K.L. and Hobert, O. (2006) Mapping functional domains of chloride intracellular channel (CLIC) proteins *in vivo*. *J. Mol. Biol.* **359,** 1316-33

Berry, K.L., Bülow, H.E., Hall, D.H. and Hobert, O. A (2003) A *C.. elegans* CLIC-like protein required for intracellular tube formation and maintenance. *Science* **302**, 2134-2137

Berryman, M. and Bretsher, A. (2000) Identification of a novel member of the chloride intracellular gene family (CLIC5) that associates with the actin cytoskeleton of placental microvilli. *Mol. Biol. Cell* **11**, 1509-21

Berryman, M., Bruno, J., Price, J., and Edwards, J.C. (2004) CLIC-5A functions as a chloride channel *in vitro* and associates with the cortical actin cytoskeleton *in vitro* and *in vivo. J. Biol. Chem.* **279,** 34794-34801

Black, B.E., Foltz, D.R., Chakravarthy, S., Luger, K., Woods, V.L. Jr. and Cleveland, D.W. (2004) Structural Determinants for Generating Centromeric Chromatin. *Nature* **430,** 578-582.

Board, P.G., Coggan, M., Chelvanayagam, G., Easteal, S., Jermiin, L.S., Schulte, G.K., Danley, D.E., Hoth, L.R., Griffor, M.C., Kamath, A.V., Rosner, M.H., Chrunyk, B.A., Perregaux, D.E., Gabel, C.A., Geoghegan, K.F. and Pandit, J. (2000) Identification, characterisation, and crystal structure of the Omega class glutathione transferases. *J. Biol. Chem.* **275**, 24798-806.

Board, P.G., Coggan, M., Watson, S., Gage, P.W., and Dulhunty, A.F. (2004) CLIC-2 modulates cardiac ryanodine receptor Ca^{2+} release channels. *Int. J. Biochem. Cell Biol.* **36,** 1599-1612

Brudler, R., Gessner, C.R., Li, S., Tyndall, S., Getzoff, E.D. and Woods, V.L. Jr. (2006) PAS Domain Allostery and Light-induced Conformational Changes in Photoactive Yellow Protein upon I(2) Intermediate Formation, Probed with Enhanced Hydrogen/Deuterium Exchange Mass Spectrometry. *J Mol Biol* **363,** 148-160.

Burns-Hamuro, L.L., Hamuro, Y., Kim, J.S., Sigala, P., Fayos, R., Stranz, D.D., Jennings, P.A., Taylor, S.S. and Woods, V.L. Jr. (2005) Distinct interaction modes of an AKAP bound to two regulatory subunit isoforms of protein kinase A revealed by amide hydrogen/deuterium exchange. *Protein Sci* **14,** 2982-2992.

Busenlehner, L.S. and Armstrong, R.N. (2005) Insights into enzyme structure and dynamics elucidated by amide H/D exchange mass spectrometry. *Arch. Biochem. Biophys.* **433**, 34-46

Bychcova, V.E., Dujsekina, A.E., Kleni, S.I., Tiktopulo, E.I., Uversky, V.N. and Ptitsyn, O.B. (1996) Molten globule-like state of cytochrome *c* under conditions simulating those near the membrane surface. *Biochemistry* **35**, 6058-6063

Cartailler, J.P., .Haigler, H.T. and Luecke H. (2000) Annexin XII E105K crystal structure: identification of a pH-dependent switch for mutant hexamerization. *Biochemistry*. **39**, 2475-83.

Cawthern, K.M., Permyakov, E. and Berliner LJ. (1996) Membrane-bound states of alpha-lactalbumin: implications for the protein stability and conformation. *Protein Sci.* **7**, 1394-405.

Chamberlain, A.K., Lee, Y., Kim, S. and Bowie, J.U. (2004) Snorkeling preferences foster an amino acid composition bias in transmembrane helices. *J. Mol. Biol.* **339**, 471-479

Chenal, A., Savarin, P., Nizard, P., Guillain, F., Gillet, D. and Forge V. (2002) Membrane protein insertion regulated by bringing electrostatic and hydrophobic interactions into play. A case study with the translocation domain of diphtheria toxin. *J Biol Chem.* 277, 43425-32

Chenal, A., Vernier, G., Savarin, P., Bushmarina, N.A., Gèze, A., Guillain, F., Gillet, D. and Forge, V. (2005) Conformational states and thermodynamics of α-lactalbumin bound to membranes: a case study of the effects of pH, calcium, lipid membrane curvature and charge. *J. Mol. Biol.* **349**, 890-905

Cho, S.G., Lee, Y.H., Park, H.S., Ryoo, K., Kang, K.W., Park, J., Eom, S.J., Kim, M.J., Chang, T.S., Choi, S.Y., Shim, J., Kim, Y., Dong, M.S., Lee, M.J., Kim, S.G., Ichijo, H. and Choi, E.J. (2001) Glutathione S-transferase mu modulates the stress activated signals by suppressing apoptosis signal regulating kinase1. *J. Biol. Chem.* **276**, 12749-12755

Choe, S., Bennet, M.J., Fujii, G., Curmi, P.M., Kanterdjieff, K.A., Collier, R.J. and Eisenberg, D. (1992) The crystal structure of diphteria toxin. *Nature* **357**, 216-222

Codreanu, G.S., Thompson, C.L., Hackey L.D., Dirr, H.W. and Armstrong, N.R. (2005). Influence of the dimer interface on glutathione transferase structure and dynamics revealed by amide H/D exchange mass spectrometry. *Biochemistry.* **44**, 10605-10612

Cromer, B.A., Morton, C.J., Board, P.G., and Parker, M. (2002) From glutathione transferase to pore in a CLIC. *Eur. Biophys. J.* **31**, 356-64

Cserzo, M., Wallin, E., Simon, I., von Heijne, G. and Elofsson A. (1997) Prediction of transmembrane alpha-helices in prokaryotic membrane proteins: the dense alignment surface method. *Protein Eng.* **6**, 673-6.

Debska, G., Kicinska, A., Skalska, J. and Szewczyk A. (2001) Intracellular potassium and chloride channels: an update. *Acta Biochim Pol.* **48**, 137-44.

Del Mar, C., Greenbaum, E.A., Mayne, L., Englander, S.W. and V.L. Woods, Jr. (2005) Structure and properties of {alpha}-synuclein and other amyloids determined at the amino acid level. *Proc Natl Acad Sci U S A* **102,** 15477-15482.

Derunes, C., Briknarova, K., Geng, L., Li, S., Gessner, C.R., Hewitt, K., Wu, S., Huang, S., Woods, V.L. Jr. and Ely. K.R. (2005) Characterization of the PR domain of RIZ1 histone methyltransferase. *Biochem Biophys Res Commun* **333,** 925-934.

Derunes, C., Burgess, R., Iraheta, E., Kellerer, R., Becherer, K., Gessner, C.R., Li, S., Hewitt, K., Vuori, K., Pasquale, E.B., Woods, V.L. Jr. and Ely. K.R. (2006) Molecular determinants for interaction of SHEP1 with Cas localise to a highly solvent-protected region in the complex. *FEBS Lett* **580,** 175-178.

Dimitrova, M.N., Matsumura, H., Dimitrova, A. and Neitchev, V. (2000) Interaction of albumins from different species with phospholipid liposomes. Multiple binding sites system. *Int. J. Biol. Macro.* **27**, 187-194

Dimitrova, M.N., Matsumura, H., Terezova, N. and Neytchev, V. (2002) Binding of globular proteins to lipid membranes studied by isothermal titration calorimetry and fluorescence. *Colloids and Surfaces* **24**, 53-61

Dirr, H.W., Little, T., Kuhnert, D.C. and Sayed, Y. (2005) A conserved N-capping motif contributes significantly to the stabilization and dynamics of the C-terminal region of class alpha glutathione S-transferases. *J. Biol. Chem.* **280**, 19480-19487

Dulhunty, A., Gage, P., Curtis, S., Chelvanayagam, G., and Board, P. (2001) The glutathione transferase structural family includes a nuclear chloride channel and a ryanodine receptor calcium release channel modulator. *J. Biol. Chem.* **276**, 3319-3323

Dulhunty, A., Haarmann, C., Green, D. and Hart J. (2000) How many cysteine residues regulate ryanodine receptor channel activity*? Antioxid. Redox Signal.* **2**, 27-34.

Duncan, R.R., Westwood, P.K., Boyd, A., and Ashley, R.H. (1997) Rat brain p64H1, expression of a new member of the p64 chloride channel protein family in endoplasmic reticulum. *J. Biol. Chem.* **272,** 23880-23886

Dutzler, R., Campbell, E.B., Cadene, M., Chait, B.T. and MacKinnon, R.(2002) X-ray structure of a ClC chloride channel at 3.0 A reveals the molecular basis of anion selectivity. *Nature.* **415**, 287-94

Duzgunes, N., Bagatolli, L., Meers, P., Oh, Y. and Straubinger, R.M (2003) Fluorescence methods in liposome research, Liposomes 2nd edition. *Oxford University Press*, 105-147

Duzgunes, N., De Ilarduya, C.T., Simoes, S., Zhdanov, R.I., Konopka, K. and Pedroso de Lima, M.C. (2003) Cationic liposomes for gene delivery: novel cationic lipids and enhancement by proteins and peptides. *Curr Med Chem.* **10**, 1213-20.

Edwards, J.C., and Kapadia, S. (2000) Regulation of the bovine kidney microsomal chloride channel p64 by p59fyn, a Src family tyrosine kinase. *J. Biol. Chem.* **275,** 31826-31832

Edwards J.C. (1999). A novel p64-related Cl channel: subcellular distribution and nephron segment-specific expression. *Am. J. Physiol.* **276**, 398-408

Endo, T. and Schatz, G. (1998) Latent membrane perturbation activity of a mitochondrial precursor protein is exposed by unfolding. *EMBO J.* **7**, 1153-1158

Englander, S.W. and Poulsen, A. (1969) *Biopolymers* 379-393

Epand, R.M (1998) Lipid polymorphism and protein-lipid interactions. *Biochim. Biophys. Acta*. **1376**, 353-368

Fauchere, J.L. and Pliska, V.E. (1983) Amino acid hydrophobicity scale. *Eur. J. Med. Chem*. **18,** 369-375

Flewelling, R.F. and Hubbell, W.L.(1986) The membrane dipole potential in a total membrane potential model. Applications to hydrophobic ion interactions with membranes. *Biophys J.* **49**, 541-52.

Friedli, M., Guipponi, M., Bertrand, S., Bertrand, D., Neerman-Arbez, M., Scott, H.S. and Antonarakis, S.E. (2003) Identification of a novel member of the CLIC family, CLIC6, mapping to 21q22.12. *Gene.* **320,** 31-40

Garavito, R.M. and Ferguson-Miller, S. (2001) Detergents as tools in membrane biochemistry. *J. Biol. Chem.* **276**, 32403-32406

Garcia, R.A., Pantazatos, D. and Villareal, F.J. (2004) Hydrogen/deuterium exchange mass spectrometry for investigating protein-ligand interactions. *Assay and drug dev. tech.* **2**, 81-91

Garcia, R.A., Pantazatos, D.P., Gessner, C.R., Go, K.V., Woods, V.L. Jr. and Villarreal. F.J. (2005) Molecular interactions between matrilysin and the matrix metalloproteinase inhibitor doxycycline investigated by deuterium exchange mass spectrometry. *Mol Pharmacol* **67,** 1128-1136.

Garcia-Sáez, A.J., Mingarro, L., Pèrez-Payá, E. and Salgado, J. (2004) Membrane-insertion fragments of Bcl-X_L, Bax and Bid. *Biochemistry* **43**, 10930-10943

Gastinel, L.N., Cambillau, C. and Bourne Y. (1999) Crystal structures of the bovine beta4galactosyltransferase catalytic domain and its complex with uridine diphosphogalactose. *EMBO J.* **18**, 3546-57.

Gazit, E., La Rocca, P., Sansom, M.S. and Shai, Y. (1998) The structure and organization within the membrane of the helices composing the pore-forming domain of Bacillus thuringiensis delta-endotoxin are consistent with an "umbrella-like" structure of the pore. *Proc. Natl. Acad. Sci. U S A.* **95**, 12289-94.

Gregory, R.L. (1955) Colour anomaly, the Rayleigh equation and selective adaptation. *Nature.* **176**, 172-3.

Griffon, N., Jeanneteau, F., Prieur, F., Diaz, J. and Sokoloff, P. (2003) CLIC6, a member of the intracellular chloride channel family interacts with dopamine D(2)-like receptors. *Brain Res. Mol. Brain Res.* **117,** 47-57

Grochulski, P., Masson, L., Borisova, S., Pusztai-Carey, M., Schwartz, J.L., Brosseau, R. and Cygler, M. (1995) *Bacillus thuringiensis* CryIA(a) insecticidal toxin: crystal structure and chemical formulation. *J. Mol. Biol.* **254**, 447-464

Guex, N. and Peitsch, M.C. (1997). Swiss-Model and the Swiss-PDB Viewer: An environment for comparative protein modelling. *Electrophoresis* **18**, 2714-2723

Hamuro, Y., G.S. Anand, J.S. Kim, C. Juliano, D.D. Stranz, S.S. Taylor, and V.L. Woods, Jr. 2004. Mapping intersubunit interactions of the regulatory subunit (RIalpha) in the type I holoenzyme of protein kinase A by amide hydrogen/deuterium exchange mass spectrometry (DXMS). *J Mol Biol* 340:1185-1196.

Hanson, A.M., Qiu, Y., Yeh, N., Blattner, F.R., Durfee, T. and Jin, D.J. (2005) SspA is required for acid resistance in stationary phase by downregulation of H-NS in Escherichia coli. *Mol. Microbiol.* **56**, 719-734

Harrop, S.J., De Maere, M.Z., Fairlie, W.D., Rezstsova, T., Valenzuela, S.M., Mazzanti, M., Tonini, R., Qiu, M.R., Jankova, L., Warton, K., Bauskin, A.R., Wu, W.M., Pankhurst, S., Campbell, T.J., Breit, S.N., and Curmi, P.M.G (2001) Crystal structure of a soluble form of the intracellular chloride ion channel CLIC1 (NCC27) at 1.4Å resolution. *J. Biol. Chem.* **276**, 44993-45000

Heiss, N.S., Poustka, A. (1997) Genomic structure of a novel chloride channel gene CLIC2 in Xq28. *Genomics* **45**, 224-8

Hofmann, K. and Stoffel, W. (1993) TMbase - A database of membrane spanning proteins segments. *Biol. Chem*. **374**,166-172

Hofmann, C., Vanderbruggen, H., Hofte, H., Van Rie, J., Jansens, S. and Mellaert, H. (1988) Speficity of *Bacillus thuringiensis* delta-endotoxins is correlated with the presence of high-affinity binding sites in the brush border membrane of target insect midguts. *Proc. Natl. Acad. Sci. USA.* **85**, 7844-7848

Honig, B.H., Hubbell, W.L. and Flewelling, R.F. (1986) Electrostatic interactions in membranes and proteins. *Annu. Rev. Biophys. Biophys. Chem.* **15**, 163-193

Howell, S., Duncan, R.R., and Ashley, R.H. (1996) Identification and characterisation of a homologue of p64 in rat tissues. *FEBS Lett.*, **390,** 207-210

Hvidt, A. and Linderstrom-Lang, K. (1954) Exchange of hydrogen atoms in insulin with deuterium atoms in aqueous solutions. *Biochem. Biophys. Acta* **4**, 574-575

Iyer, G.H., Garrod, S., Woods, V.L. Jr. and Taylor S.S. (2005) Catalytic Independent Functions of a Protein Kinase as Revealed by a Kinase-dead Mutant: Study of the Lys72His Mutant of cAMP-dependent Kinase. *J Mol Biol* **351,** 1110-1122.

Jentsch, T.J., Stein, V., Weinreich, F. and Zdebik, A.A. (2001) Molecular structure and physiological function of chloride channels. *Physiological Reviews* **82**, 503-568

Johnson, J.E., Xie, M., Singh, L.M., Edge, R. and Cornell, R.B. (2003) Both acidic and basic amino acids in an amphitropic enzyme, CTP:phosphocholine cytidyltransferase, dictate its selectivity for anionic membranes. *J. Biol. Chem.* **278**, 514-522

Kalaria, R.N. (1999) Microglia and Alzheimer's disease. *Curr. Opin. Hematol.* **6**, 15-24.

Klatt, P. and Lamas, S. (2000) Regulation of protein function by S-glutathiolation in response to oxidative and nitrosative stress. *Eur. J. Biochem.* **267**, 4928-44.

Kumar, A.S. and Aronson, A.I. (1999) Analysis of mutations in the pore-forming region essential for insecticidal activity of a Bacillus thuringiensis delta-endotoxin. *J Bacteriol.* **181**, 6103-7.

Kumar, S. and Nussinov, R. (1999). Salt bridge stability in monomeric proteins. *J. Mol. Biol.* **293**, 1241-1255.

Kumaran, S. and Roy, R.P. (1999) Helix-enhancing propensity of fluoro and alkyl alcohols: influence of pH, temperature and cosolvent concentration on the helical conformation of peptides. *J. Pept. Res.* **53**, 284-93.

Kyte, J. and Doolitlle, R.F. (1982) A simple method for displaying the hydropathic character of a protein. *J. Mol. Biol.* **157**, 105-132

Lacroix, E., Viguera AR & Serrano, L. (1998). Elucidating the folding problem of a-helices: Local motifs, long-range electrostatics, ionic strength dependence and prediction of NMR parameters. *J. Mol. Biol*. **284**, 173-191

Ladner, J.E., Parsons, J.F., Rife, C.L., Gilliand, G.L. and Armstrong, R.N. (2004) Parallel evolutionary pathways for glutathione transferases: structure and mechanism of the mitochondria class kappa enzyme rGST K1-1. *Biochemistry* **43**, 352-361

Landolt-Marticorena, C., Williams, K.A., Deber, C.M. and Reithmeier, R.A. (1993) Non-random distribution of amino acids in the transmembrane segments of human type I single span membrane proteins. *J. Mol. Biol.* **229**, 602-608

Laemmli, K.U. (1970). Cleavage of structural proteins during the assembly of the head of bacteriophage T4. *Nature* **227,** 680-685

Lakowicz, J.R. (1983) *Principles of fluorescence spectroscopy*. Plenum Press, New York.

Landry, D., Sullivan, S., Nicolaides, M., Redhead, C., Edelman, A., Field, M., Al-Awqati, Q., and Edwards, J. (1993) Molecular cloning and characterisation of p64, a chloride channel protein from kidney microsomes. *J. Biol. Chem.* **268,** 14948-14955

Lee B. and Richards, F.M. (1971). The interpretation of protein structures: Estimation of static accessibility. *J. Mol. Biol.* **55**, 379-400

Lester, L.B. and Scott, J.D. (1997) Anchoring and scaffold proteins for kinases and phosphatases. *Recent Prog. Horm. Res.* **52**, 409-29

Li, J., Carrol, J. and Eller, D.J. (1991) Crystal structure of insecticidal delta-endotoxin from *Bacillus thuringiensis* at 2.5Å resolution. *Nature* **353**, 815-821

Li, Y., Li, D., Zeng, Z. and Wang, D. (2006) Trimeric structure of the wild soluble chloride intracellular ion channel CLIC4 observed in crystals. *Biochem. Biophys. Res. Comm.* **343**, 1272-1278

Littler, D.R., Harrop, S.J., Fairlie, D., Brown, L.J., Pankhurst, G.J., Pankhurst, S., DeMaere, M.Z., Campbell, T.J., Bauskin, A.R., Tonini, R., Mazzanti, M., Breit, S.N. and Curmi, P.M.G. (2004) The intracellular chloride ion channel protein CLIC1 undergoes a redox-controlled structural transition. *J. Biol. Chem.* **279,** 9298-9305

Littler, D.R., Assaad, N.N., Harrop, S.J., Brown, L.J., Pankhurst, G.J., Luciani, P., Aguilar, M., Mazzanti, M., Berryman, M.A., Breit, S.N. and Curmi, P.M.G. (2005) Crystal structure of the soluble form of the redox-regulated chloride ion channel protein CLIC4. *FEBS J.* **272**, 4996-5007

Lonnerdal, B. and Lien, E.L. (2003) Nutritional and physiologic significance of alpha-lactalbumin in infants. *Nutr. Rev.* **61**, 295-305.

Luecke, H., Chang, B.T., Mailliard, W.S., Schlaepfer, D.D. and Haigler, H.T. (1995) Crystal structure of the annexin XII hexamer and implications for bilayer insertion. *Nature*. **378**, 512-5

Lundbland, R.L. (1995) Techniques in protein modification. *CRC Press.*

Lloyd, S.E., Pearce, S.H., Fisher, S.E., Steinmeyer, K., Schwappach, B., Scheinman, S.J., Harding, B., Bolino, A., Devoto, M., Craig, I.W., Thakker, R.V. (1996) A common molecular basis for three inherited kidney stone diseases. *Nature* **379**, 445-449

Mach, H., Volkin, D.B., Burke, C.J. and Middaugh, C.R. (1995) Ultraviolet absorption spectroscopy in *Methods in molecular biology,* Vol. 40: *Protein stability and folding: Theory and practice* (Shirley, B.A. ed), pp 91-114, Humana Press Inc., Totowa, New Jersey

Mak, P., Szewczyk, A., Mickowska, B., Kicinska, A. and Dubin, A. (2001) Effect of antimicrobial apomyoglobin 56-131 peptide on liposomes and planar lipid bilayer membrane. *Int. J. Antimicrob. Agents* **17**, 137-142

Martin, J.L. (1995) Thioredoxin: a fold for all reasons. *Structure* **3**, 245-250

Matsuyama, S., Llopis, J., Deveraux, Q.L., Tsien, R.Y. and Reed, J.C. (2000) Changes in intramitochondrial and cytosolic pH: early events that modulate caspase activation during apoptosis. *Nat Cell Biol.* **2**, 318-25.

McGeer, P.L. and McGeer, E.G. (1998) Mechanisms of cell death in Alzheimer disease--immunopathology. *J. Neural. Transm. Suppl.* **54**, 159-66.

McLaughlin, S. (1989) The electrostatic properties of membranes. *Annu. Rev. Biophys. Biophys. Chem.* **18**, 113-136

Meers, P. and Mealy, T.R. (1993) Relationship between annexin V tryptophan exposure, calcium, and phospholipid binding. *Biochemistry* **32**, 5411-5418

Melnyk, R.A., Hewitt, K.M., Lacy, D.B., Lin, H.C., Gessner, C.R., Li, S., Woods, V.L. Jr. and Collier, R.J. (2006) Structural determinants for the binding of anthrax lethal factor to oligomeric protective antigen. *J Biol Chem* **281,** 1630-1635.

Menestrina, G., Forti, S. and Gambale, F. (1989) Interaction of tetanus toxin with lipid vesicles. Effects of pH, surface charge, and transmembrane potential on the kinetics of channel formation. *Biophys. J.* **55**, 393-405.

Mosior, M. and Newton, A.C. (1995) Mechanism of interaction of protein kinase C with phorbol esters. Reversibility and nature of membrane association. *J. Biol. Chem.* **270**, 25526-33.

Muchmore, S.W., Sattlen, M., Liang, H., Meadows, R.P., Harlan, J.E., Yoon, H.S., Nettesheim, D., Chang, B.S., Thompson, C.B., Wong, S.L., Ng, S.L. and Fesik, S.W. (1996) X-ray and NMR structure of human Bcl-X_L, an inhibitor of programmed cell death. *Nature* **381**, 335-341

Muga, A., Gonzalez-Manas, J.M., Lakey, J.H., Pattus, F. and Surewicz, W.K. (1993) pH-dependent stability and membrane interaction of the pore-forming domain of colicin A. *J Biol Chem.* **268**, 1553-7.

Myers, K., Somanlath, P.R., Berryman, M. and Visavaraghavan, S. (2004) Identification of chloride intracellular channel proteins in spermatozoa. *FEBS Lett.* **566,** 136-140

Nilius, B. and Droogmans, G. (2003) Amazing chloride channels: an overview. *Acta Physiol. Scand.* **177,** 119-47.

Nishizawa, T., Nago, T., Iwatsubo, T., Forte, J.G., and Urshidani, T. (2000) Molecular cloning and characterisation of a novel chloride intracellular channel-related protein, parchorin expressed in water secreting cells. *J. Biol. Chem.* **275**, 11164-73

Novarino, G., Fabrizi, C., Tonini, R., Denti, M.A., Malchiodi-Albedi, F., Lauro, G.M., Sacchetti, B., Paradisi, S., Ferroni, A., Curmi, P.M., Breit, S.N. and Mazzanti, M. (2004) Involvement of the intracellular ion channel CLIC1 in microglia-mediated β-amyloid-induced neurotoxicity. *The Journal of Neuroscience* **24,** 5322-5330

Oakley, A.J. (2005) Glutathione transferases: new functions. *Curr. Opin. Struct. Biol.* **15**, 1-8

Olson, R. and Gouaux, E. (2002) Crystal structure of the *Vibrio cholerae* cytolysin (VCC) pro-toxin and its assembly into a heptameric transmembrane pore. *J. Mol. Biol.* **350**, 997-1016

Olsen, R. and Gouaux, E. (2005) Crystal structure of the *Vibrio cholerae* cytolysin (VCC) pro-toxin and its assembly into a heptameric transmembrane pore. *J. Mol. Biol.* **350**, 997-1016

Pantazatos, D., Kim, J.S., Klock, H.E., Stevens, R.C., Wilson, I.A., Lesley, S.A. and Woods, V.L. Jr. (2004) Rapid refinement of crystallographic protein construct definition employing enhanced hydrogen/deuterium exchange MS. *Proc Natl Acad Sci U S A* **101,** 751-756.

Pardo-Lopez, L., Gomez, I., Munoz-Garay, C., Jimenez-Juarez, N., Soberon, M. and Bravo, A. (2006) Structural and functional analysis of the pre-pore and membrane-inserted pore of Cry1Ab toxin. *J. Invertebr. Pathol.* **92**, 172-7.

Parker, M.W. and Feil, S.C. (2005) Pore-forming protein toxins: from structure to function. *Prog. Biophys. Mol. Biol.* **88**, 91-142.

Parker, M.W. and Pattus, F. (1993) Rendering a membrane protein soluble in water: a common packing motif in bacterial protein toxins. *Trends in Biochem. Sci.* **18**, 391-395

Parker, M.W., Postma, J.P., Pattus, F., Tucker, A.D. and Tsernoglou, D. (1992) Refined structure of the pore-forming domain of colicin A at 2.4Å resolution. *J. Mol. Biol.* **224**, 639-657

Parker, M.W., Buckley, J.T., Postma, J.P., Tucker, A.D., Leonard, K., Pattus, F. and Tsernoglou, D. (1994) Structure of the *Aeromonas* toxin proaerolysin in its water-soluble and membrane-channel states. *Nature* **367**, 292-295

Plager, D.A. and Nelsestuen, G.L. (1994) Direct enthalpy measurements of the calcium-dependent interaction of annexins V and VI with phospholipid vesicles. *Biochemistry.* **33**, 13239-49.

Poklar, N., Volker, J., Anderluh, G., Macek, P. and Chalikia, T.V. (2001) Acid- and base-induced conformational transitions of equinatoxin II. *Biophys. Chem.* **90**, 103-21.

Qian, Z., Okuhara, D., Abe, M., and Rosner, M.R., (1999) Molecular cloning and characterization of a mitogen-activated protein kinase associated intracellular chloride channel. *J. Biol. Chem.* **274**, 1621-7

Ramsay, G., Prabhu, R. and Freire, E. (1986) Direct measurement of the energetics of association between myelin basic protein and phosphatidylserine vesicles. *Biochemistry* **25**, 2265-2270

Riordan, J.R., Rommens, J.M., Kerem, B., Alon, N., Rozmahel, R., Iannuzzi, M.C., Collins, F.S. and Tsui, L.C. (1989) Identification of the cystic fibrosis gene: cloning and characterization of complementary DNA. *Science* **245**, 1066-1073

Roccatano, D., Colombo, G., Fioroni, M. and Mark, A.E. (2002) Mechanism by which 2,2,2-trifluoroethanol/water mixtures stabilise secondary-structure formation in peptides: a molecular dynamics study. *Proc. Natl. Acad. Sci. U S A.* **99**, 12179-84.

Rohl, C.A., Chakrabartty, A. and Baldwin, R.L. (1996) Helix propagation and N-cap propensities of the amino acids measured in alanine-based peptides in 40 volume percent trifluoroethanol. *Protein Sci.* **5**, 2623-37.

Rothman, J.E. and Lenard, J. (1977) Membrane asymmetry. *Science.* **195**, 743-53.

Russ, W. and Engelman, D.M. (1999) TOXCAT: A measure of transmembrane helix association in a biological membrane. *Proc. Natl. Acad. Sci.* **96**, 863-868

Saito, H., Dhanasekaran, P., Nguyen, D., Deridder, E., Holvoet, P., Lund-Katz, S. and Phillips, M.C. (2004) α-Helix formation is required for high affinity binding of human apolipoprotein A-I to lipids. *J. Biol. Chem.* **279**, 20974-20981

Sakai, H. and Tsukihara, T. (1998) Structures of membrane proteins determined at atomic resolution. *J. Biochem. (Tokyo).* **124**, 1051-9.

Sandvig, K. and Olsnes, S. (1980) Diphtheria toxin entry into cells is facilitated by low pH. *J. Cell Biol.* **87**, 828-32.

Sayed, Y., Hornby, J.A.F., Lopez, M. and Dirr, H.W. (2002) Thermodynamics of ligandin function of human class alpha glutathione transferase A1-1: energetics of organic anion ligand binding. *Biochem. J.* **363**, 341-346

Schendel, S.L., Xie, Z., Montal, M.O., Matsyama, S., Montal, M. and Reed, J.C. (1997) Channel formation by antiapoptotic protein Bcl-2. *Proc. Natl. Acad. Sci.* **94**, 5113-5118

Schlesinger, P.H., Blair, H.C., Tietelboum, S.L. and Edwards, J.C. (1997). Characterization of the osteoclast ruffled border chloride-channel and its role in bone absorption. *J. Biol. Chem* **272**, 18636-18643

Scholtz, J.M. and Baldwin, R.L. (1992) The mechanism of alpha-helix formation by peptides. *Annu. Rev. Biophys. Biomol. Struct.* **21**, 95-118.

Sedlak, J. and Lindsay, R.H. (1968) Estimation of total, protein-bound, and nonprotein sulfhydryl groups in tissue with Ellman's reagent. *Anal. Biochem.* **25**, 192-205.

Semisotnov, G.V., Rodionova, N.A., Razgulyaev, O.I., Uversky, V.N., Gripas, A.F. and Gilmanshin, R.I. (1991) Study of the "molten globule" intermediate state in protein folding by a hydrophobic fluorescent probe. *Biopolymers.* **31**, 119-28.

Serrano, L. and Fersht, A.R. (1989) Capping and alpha-helix stability. *Nature.* **342**, 296-9.

Shanks, R.A., Larocca, M.C., Berryman, M., Edwards, J.C., Urushidani, T., Navarre, J., and Goldenring, J.R. (2002) AKAP350 at the Golgi apparatus. II. Association of AKAP350 with a novel chloride intracellular channel (CLIC) family member. *J. Biol. Chem.* **277,** 40973-40980

Sheehan, D., Meade, G., Foley, M.N. and Dowd, A.C. (2001). Structure, function and evolution of glutathione transferases: implications for classification of non-mammalian members of an ancient enzyme superfamily. *Biochem.* **360**, 1-16

Sigrist, C.J.A., Cerutti L., Hulo N., Gattiker A., Falquet L., Pagni M., Bairoch A., Bucher, P. PROSITE: a documented database using patterns and profiles as motif descriptors. *Brief Bioinform*. **3,** 265-274

Singer, S.J. and Nicolson, G.L. (1972) The fluid mosaic model of the structure of cell membranes. *Science.* **175,** 720-31.

Singh, H. and Ashley, R.H. (2006) Redox regulation of CLIC1 by cysteine residues associated with the putative channel pore. *Biophys. J.* **90**, 1628-38.

Spraggon, G., Pantazatos, D. Klock, H.E.. Wilson, I.A Woods, V.L. Jr. and Lesley, S.A. (2004) On the use of DXMS to produce more crystallizable proteins: structures of the T. maritima proteins TM0160 and TM1171. *Protein Sci* **13,** 3187-3199.

Stamler, J.S., Toone, E.J., Lipton, S.A. and Sucher, N.J. (1997) NO signals: translocation, regulation, and a consensus motif. *Neuron.* **18**, 691-6.

Strange, K., Emma, F. and Jackson, P.S. (1996) Cellular and molecular physiology of volume-sensetive anion channels. *Am. J. Physiol.* **270**, 711-730

Sui, H., Han, B.G., Lee, J.K., Walian, P. and Jap, B.K. (2001) Structural basis of water-specific transport through the AQP1 water channel. *Nature*. **414**, 872-8.

Suzuki, M., Youle, R.J., and Tjandra, N. (2000) Structure of Bax. Coregulation of dimer formation and intracellular localization. *Cell* **103**, 645-654

Tanford, C. (1980) The hydrophobic effect: Formation of micelles and biological membranes (2^{nd} ed.), *Wiley-Interscience*

Thompson, L.C., Walters, J., Burke, J., Parsons, J.F., Armstrong, R.N. and Dirr, H.W. (2006) Double mutation at the subunit interface of glutathione transferase rGSTM1-1 results in a stable, folded monomer. *Biochemistry* **45**, 2267-73.

Thuduppathy, G.R. and Hill, B. (2006) Acid destabilization of the solution conformation of Bcl-X_L does not drive its pH-dependent insertion into membranes. *Protein Science* **15**, 248-57

Thuduppathy, G.R., Craig, J.W., Kholodenko, V., Schon, A. and Hill, B. (2006) Evidence that membrane insertion of the cytosolic domain of Bcl-X_L is governed by an electrostatic mechanism. *J. Mol. Biol.* **359**, 1045-58

Tilley, S.J. and Sabil, H.R. (2006) The mechanism of pore formation by bacterial toxins. *Curr. Opin. Struct. Biol.* **16**, 230-236

Tonini, R., Ferroni, A., Valenzuela, S.M., Warton, K., Campbell, T.J., Breit, S.N. and Mazzanti, M. (2000) Functional characterisation of the NCC27 nuclear protein in stable transfected CHO-K1 cells. *FASEB J.* **14,** 1171-1178

Tulk, B.M., and Edwards, J.C. (1998) NCC27, a homologue of intracellular chloride channel p64, is expressed in brush border of renal proximal tubule. *Am. J. Physiol.* **274,** F1140-F1149

Tulk, B.M., Schlesinger, P.H., Kapadia, S.A., and Edwards, J.C. (2000) CLIC-1 functions as a chloride channel when expressed and purified from bacteria. *J. Biol. Chem.* **275**, 26986-26998

Tulk, B.M., Kapadia, S., and Edwards, J.C. (2002) CLIC1 inserts from the aqueous phase into phospholipid membranes, where it functions as an anion channel. *Am. J. Physiol. Cell Physiol.* **282**, C1103-C1112

Ulmschneider, M.B. and Sansom, M.S. (2001) Amino acid distributions in integral membrane protein structures. *Biochim. Biophys. Acta* **1512,** 1-14

Ulrih, N.P., Anderluh, G., Macek, P. and Chalikian, T.V. (2004) Salt-induced oligomerization of partially folded intermediates of equinatoxin II. *Biochemistry* **43**, 9536-9545

Valenzuela, S.M., Martin, D.K., Por, S.B., Robbins, J.M., Warton, K., Bootcov, M.R., Schofield, P.R., Campbell, T.J., and Breit, S.N. (1997) Molecular cloning and expression of a chloride ion channel of cell nuclei. *J. Biol. Chem.* **272**, 12575-12582

Valenzuela, S.M., Mazzanti, M., Tonini, R., Qui, M.R., Warton, K., Musgrove, E.A., Campbell, T.J., and Breit, S.N. (2000) The nuclear chloride ion channel NCC27 is involved in regulation of the cell cycle. *J. of Physiology* **529,** 541-552

Van der Goot, F.G., González-Manãs, J.M., Lakey, J.H. and Pattus, F. (1991) A 'molten-globule' membrane-insertion intermediate of the pore-forming domain of colicin A. *Nature* **354**, 408-410

Voet, D. and Voet, J.G. (1995) Biochemistry second edition. *John Wiley and sons, inc.*

von Heijne, G. and Blomberg, C. (1979) Trans-membrane translocation of proteins. The direct transfer model. *Eur. J. Biochem.* **97**, 175-181

von Heijne, G. (1986) A new method for predicting signal sequence cleavage sites. *Nucleic Acids Res.* **14**, 4683-90.

von Heijne, G and Gavel, Y. (1988) Topogenic signals in integral membrane proteins. *Eur. J. Biochem.* **174**, 671-678

Wallace, L.A., Sluis-Cremer, N. and Dirr H.W. (1998) Equilibrium and kinetic unfolding properties of dimeric human glutathione transferase A1-1. *Biochemistry* **37**, 5320-5328

Wang, S., Trumble, W.R., Liao, H., Wesson, C.R., Dunker, A.K. and Kang, C. (1998) Crystal structure of calsequestrin from rabbit skeletal muscle sarcoplasmic reticulum. *Nature Struct. Biol.* **5**, 476-483

Warton, K., Tonini, R., Fairlie, W.D., Mathews, J.M., Valenzuela, S.M., Qiu, M.R., Wu, W.M., Pankhurst, S., Bauskin, A.R., Harrop, S.J., Campbell, T.J., Curmi, P.M.G., Breit, S.N., and Mazzanti, M. (2002) Recombinant CLIC1 (NCC27) assembles in lipid bilayers via a pH-dependent two-state process to form chloride ion channels with identical characteristics to those observed in Chinese hamster ovary cells expressing CLIC1. *J. Biol. Chem.* **277**, 26003-26011

Wei, L., Varsanyi, M., Dulhunty, A.F. and Beard, N.A. (2006) The conformation of calsequestrin determines its ability to regulate skeletal ryanodine receptors. *Biophys J.* **91**, 1288-301.

Wilce, M.C.J. and Parker, M.W (1994). Structure and function of glutathione S-transferases. *Biochim. Biophys. Acta.* **1205**, 1-18

Wong, L., Lieser, S.A., Miyashita, O., Miller, M., Tasken, K., Onuchic, J.N., Adams, J.A., Woods, V.L. Jr. and Jennings, P.A. (2005) Coupled Motions in the SH2 and Kinase Domains of Csk Control Src Phosphorylation. *J Mol Biol* **351,** 131-143.

Woods, V.L. and Hamuro, Y. (2001) High resolution, high-throughput amide deuterium exchange-mass spectrometry (DXMS) Determination of protein binding site structure and dynamics: utility in pharmaceutical design. *J. Cell. Biochem. Supp.* **37**, 89-98

Woods, V.L., Sheng, L., Gessner, C., Hewitt, K., Brock, M., Tyndal, S., Martinez, N., Asmus, K. and Arias, L. (2005) DXMS instructional manual for collaborators.

Woody, R.W. (1995) Circular dichroism. *Methods Enzymol.* **246**, 34-71

Xia, B., Vlamis-Gardikas, A., Holmgren, A., Write, P.E. and Dyson, J. (2001) Solution structure of *Escherichia coli* glutaredoxin2 shows similarity to mammalian glutathione S-transferases. *J. Mol. Biol.* **310**, 907-918

Zhang, Z. and Smith, D.L. (1993) Determination of amide hydrogen exchange by mass spectrometry: a new tool for protein structure elucidation. *Protein Sci.* **2**, 522-531

APPENDIX

Figure A: Sequencing results for CLIC1 plasmid DNA

Figure B: Calorimetric titration profile of the binding of reduced glutathione to CLIC1. 5uM CLIC1 was titrated with 41 injections of 7 µl 200mM reduced glutathione. Experiments were performed at 25 ° C.

Figure C: Calorimetric titration profile of CLIC1 titrated with IAA
The exothermic heat effects associated with the 8 µl injections of 560 µM IAA into the ITC sample cell containing 134 µM CLIC1. The experiment was performed at 25 ° C.

Figure D: Heat of dilution effects of asolectin vesicles titrated to buffer

Figure E: Heat of dilution effects of sarkosyl into buffer at pH 5.5

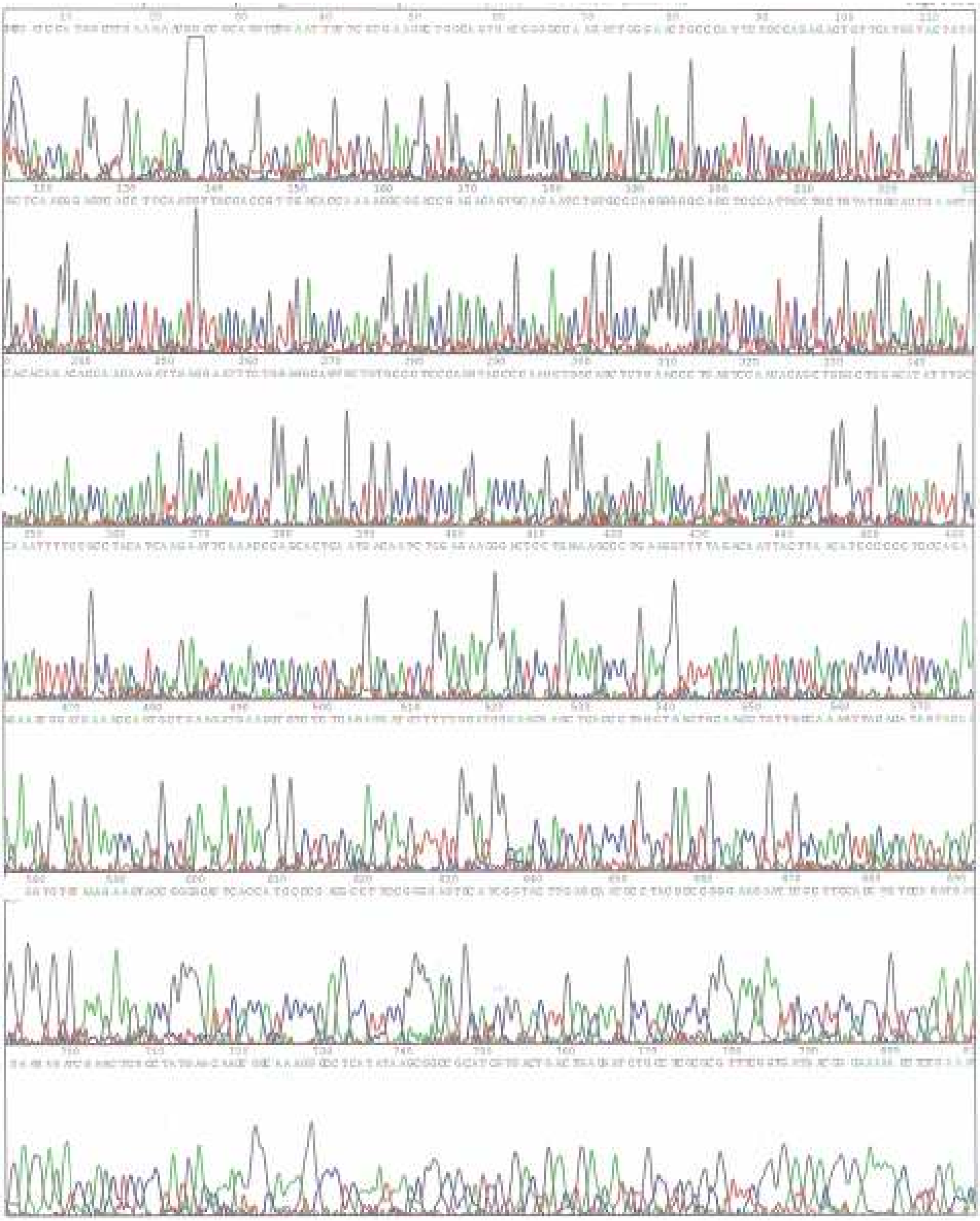


Figure A: Sequencing results for CLIC1 plasmid DNA

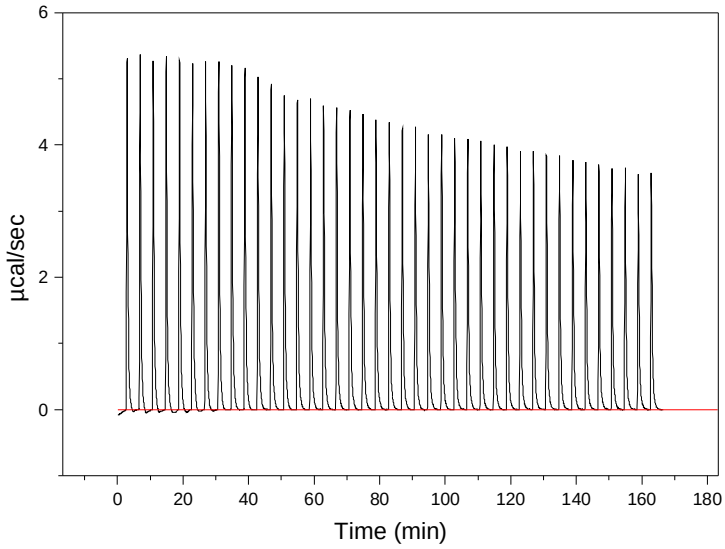


Figure B: Calorimetric titration profile of the binding of reduced glutathione to CLIC1. 5µM CLIC1 was titrated with 41 injections of 7 µl 200mM reduced glutathione. Experiments were performed at 25 ° C.

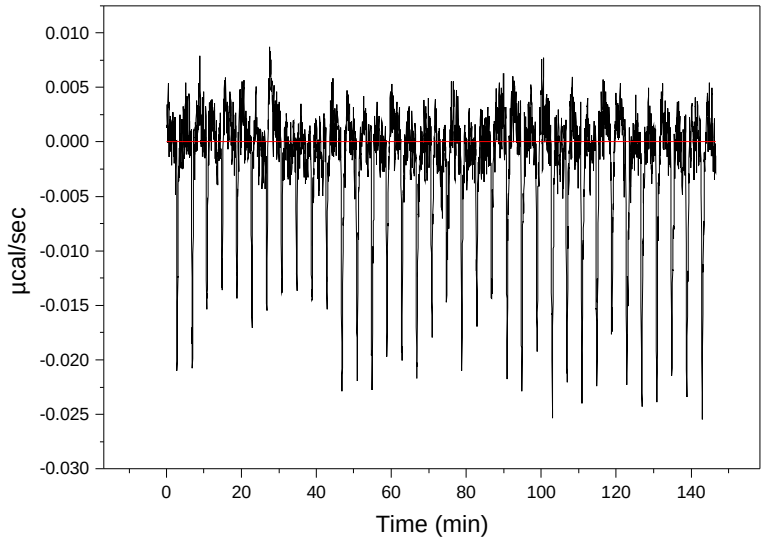


Figure C: Calorimetric titration profile of CLIC1 titrated with IAA

The exothermic heat effects associated with the 8 µl injections of 560 µM IAA into the ITC sample cell containing 134 µM CLIC1. The experiment was performed at 25 ° C.

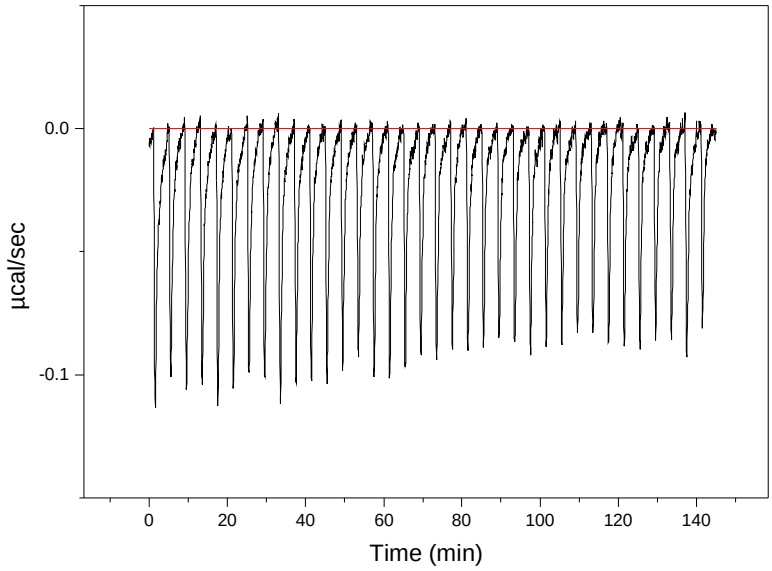


Figure D: Heat of dilution effects for asolectin into buffer

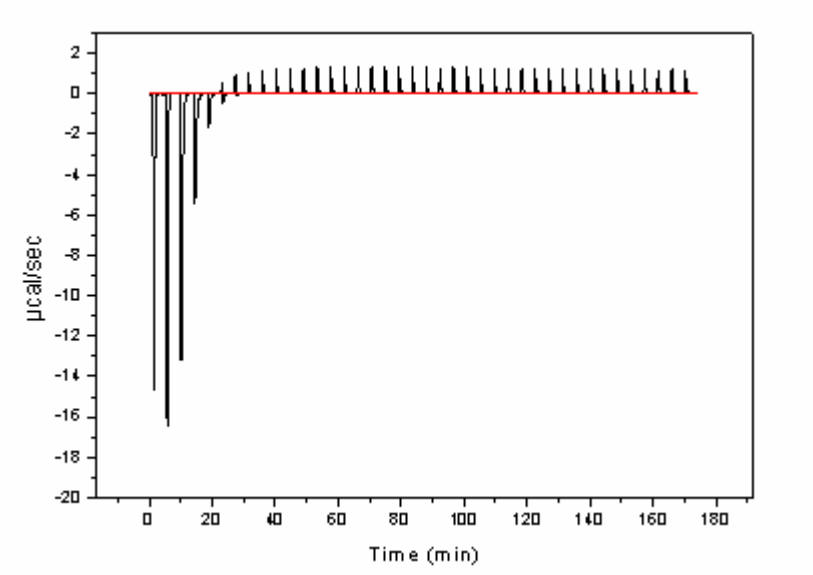


Figure E: Heat of dilution effects of sarkosyl into buffer at pH 5.5